UCGE Reports
Number 20176

Department of Geomatics Engineering

High Sensitivity GPS Performance Analysis in Degraded Signal Environments

(URL: http://www.geomatics.ucalgary.ca/links/GradTheses.html)

by

Glenn D. MacGougan

June 2003

THE UNIVERSITY OF CALGARY

High Sensitivity GPS Performance Analysis in Degraded Signal Environments

by

Glenn D. MacGougan

A THESIS
SUBMITTED TO THE FACULTY OF GRADUATE STUDIES
IN PARTIAL FULFILLMENT OF THE REQUIREMENTS FOR THE
DEGREE OF MASTER OF SCIENCE

DEPARTMENT OF GEOMATICS ENGINEERING

CALGARY, ALBERTA
JUNE, 2003

Abstract

This thesis deals with GPS receiver sensitivity analysis, characterization of interference sources prevalent in degraded signal environments and quantifies measurement availability, signal fading, pseudorange errors, positioning accuracy and position solution availability using an unaided high sensitivity GPS receiver. High sensitivity GPS utilizes total signal dwell times longer than the 20 ms maximum for conventional GPS receivers and results in more signal gain. A description of how this is accomplished is provided. Testing of the high sensitivity GPS receiver involved hardware simulations and extensive field testing in a forest, urban canyons, and in an indoor environment.

The high sensitivity receiver tested, developed by SiRF Technologies Inc., provides more measurements with fewer losses of signal tracking in all environments tested with a signal tracking sensitivity of -186 dBW. Increased tracking capability is highly beneficial in terms of solution availability and increased redundancy for reliability of navigation. However, reliable navigation is a primary concern as interference effects, namely signal cross-correlation, multipath, and echo-only signals, lead to large measurement errors. Navigation accuracy and reliability using a high sensitivity GPS receiver is discussed and recommendations are made for improvements.

Acknowledgements

I owe the completion of this thesis to many and would like to express my gratitude to those that devoted their ideas, time, and patience to it's completion.

- To: Jennifer for her love and support and for keeping me sane and grounded while encouraging me in all of life's endeavors.
- To: My supervisor, Dr. Gérard Lachapelle, for his unwavering support of my research and academic endeavors.
- To: SiRF Technologies Inc. and their staff for providing their expertise and the unaided high sensitivity GPS receivers necessary for this research.
- To: The Natural Science Research Council of Canada (NSERC) and the Alberta Informatics Circle of Research Excellence (iCORE) for their financial support of this research.
- To: All of my fellow students who have listened, criticized, edited, laughed, innovated, and generally made the last two years more fun than I ever expected.
- To: Rocco, the puppy.

Table of Contents

List of Tables

List of Figures

Notation

0.1 Symbols

A	Amplitude
A	Design Matrix
A_r	Antenna Aperture
B	Bandwidth
C_l	Variance-Covariance Matrix Of The Measurements
G	Gain
I_1	Precorrelation In-Phase Code and Carrier Signal
I_2	Precorrelation In-Phase Code Signal
I_3	Post Coherent Correlation In-Phase Signal
I_4	Post Non-Coherent Accumulation Of In-Phase Signal
F	Fading
k	Boltzman's Constant ($1.38066 * 10^{-23} J/K$)
l	Vector Of Pseudorange Measurements
L	Loss Of A Processing Step
L_0	Free Space Loss
L1	GPS Signal Carrier at 1575.42 MHz
L2	GPS Signal Carrier at 1227.60 MHz
M	Number of Non-Coherent Accumulations
N	Length of Coherent Accumulation Time
N_{power}	Noise Power
P	Pseudorange Measurement
P_r	Received Power
P_t	Transmitted Power
Q_1	Precorrelation Quadra-Phase Code and Carrier Signal
Q_2	Precorrelation Quadra-Phase Code Signal
Q_3	Post Coherent Correlation Quadra-Phase Signal
Q_4	Post Non-Coherent Accumulation Of Quadra-Phase Signal
r	Vector Of Least Squares Residuals
R	Radial Distance Between Transmitter And Receiver
SQ_{loss}	Squaring Loss
S_p	Simulator Relative Channel Power
S/W	Ratio Of Strong To Weak Signal
t	Time

T	Temperature
T_{sys}	System Noise Temperature
T_0	Ambient Noise Temperature
T_S	Source (Antenna) Temperature
T_R	Receiver Noise Temperature
w	Measurement Misclosure Vector
ρ	Sample Correlation Coefficient For A Specific Satellite
λ	Wavelength
ρ	Geometric Range
$d\rho$	Orbital Error
dt	Satellite Clock Error
dT	Receiver Clock Error
d_{iono}	Ionospheric Delay
d_{tropo}	Tropospheric Delay
ε_N	Pseudorange Measurement Noise
ε_M	Pseudorange Multipath
$\dot{\phi}$	Doppler Measurement
$\dot{\rho}$	Geometric Range Rate
$d\dot{\rho}$	Orbital Error Drift
$d\dot{t}$	Satellite Clock Drift
$d\dot{T}$	Receiver Clock Drift
$\dot{d_{iono}}$	Ionospheric Delay Drift
$\dot{d_{tropo}}$	Tropospheric Delay Drift
$\varepsilon_{\dot{M}}$	Rate Of Change Of Multipath Delay
$\varepsilon_{\dot{\phi}}$	Doppler Measurement Noise
ω	Residual Frequency Error After Doppler Removal
τ_0	Code-Phase
δf	Frequency Correction
σ_{PLL}	1-Sigma Rule Of Thumb PLL Tracking Threshold
σ_{tPLL}	1-Sigma PLL Thermal Noise
σ_v	1-Sigma Vibration Induced Oscillator Jitter
θ_A	Allan Deviation Induced Oscillator Jitter
θ_E	Tracking Loop Error Due to Dynamic Stress
σ_{FLL}	1-Sigma Rule of Thumb FLL Tracking Threshold
σ_{tFLL}	1-Sigma Thermal Noise Frequency Jitter
F_e	Dynamic Stress Error In The FLL Tracking Loop
c/n_0	Carrier To Noise Density Expressed As A Ratio
ϕ_e	Phase Error
τ	Interval Of Coherent Integration
$\sigma_{Allan}(\tau)$	Allan Deviation For The Interval τ

c	Speed Of Light (299792458.0 m/s)
$s(t)$	Composite Signal Of Direct And Reflected Signals
$p(t)$	Pseudorandom Noise Sequence Of A Specific C/A Code
ω_0	Frequency Of The Direct Signal
α	Relative Power Of The Multipath Signal
δ	Delay Of The Multipath Signal With Respect To The Direct Signal
θ	Phase Of The Multipath Signal With Respect To The Direct Signal

0.2 Abbreviations and Acronyms

AGC	Automatic Gain Control
AGPS	Assisted Global Positioning System
C/A	Coarse Acquisition
C/N_0	Carrier To Noise Density Ratio
CACS	Canadian Active Control Service
CDMA	Code Division Multiple Access
C^3NAVG^{2TM}	Combined Code and Carrier for NAVigation with GPS and GLONASS
CW	Continuous Ware
DLL	Delay Lock Loop
DOP	Dilution of Precision
ERPE	Estimated Relative Pseudorange Error
FCC	Federal Communications Commission
FLL	Frequency Lock Loop
FW	Firmware Version
GPS	Global Positioning System
GLONASS	GLobal Orbiting Navigation Satellite System
HS	High Sensitivity
IF	Intermediate Frequency
IR	Reference In-Phase Carrier Signal
INS	Inertial Navigation System
LAAS	Local Area Augmentation System
LBS	Location-Based-Services
LNA	Low Noise Amplifier
LO	Local Oscillator
LORAN	Long Range Navigation
MEDLL	Multipath Estimation Delay Lock Loop
MET	Multipath Elimination Technique

NCO	Numerically Controlled Oscillator
NF	Noise Figure
NRCAN	Natural Resources Canada
PLL	Phase Lock Loop
PPS	Precision Positioning Service
PRN	Pseudo Random Noise
QR	Reference Quadra-Phase Carrier Signal
RMS	Root Mean Square
RF	Radio Frequency
S/N	Serial Number
SNR	Signal To Noise Ration
SPS	Standard Positioning Service
SW	Software Version
TOA	Time Of Arrival
UTC	Coordinated Universal Time
WAAS	Wide Area Augmentation System
WGS-84	World Geodetic System - 1984

Chapter 1

Introduction

The demand for personal navigation and location-based services is driving research and development of enhanced civilian GPS receivers for use in increasingly difficult operational environments. Receivers with longer signal integration times and external means of acquiring the navigation message are lowering the acquisition and tracking power thresholds to levels at which even indoor operation is possible. The enhanced availability of measurements in environments where signals are highly attenuated benefits solution availability in urban canyons and under heavy foliage. However, interference in such environments can introduce large measurement errors.

GPS signal deterioration occurs by signal masking caused by natural (e.g. foliage) and man-made (e.g. buildings) obstructions, interference due to reflected signals, signal self-interference, jamming, antenna effects, and receiver implementation losses. The impact of any one of these can result in partial to total loss of signal tracking and/or tracking errors, depending on the severity of the effect and the receiver tracking characteristics. Tracking errors, especially if undetected by the receiver firmware, can result in large position errors. Partial loss of tracking results in geometry degradation, which in turn affects position accuracy.

Enhanced sensitivity receivers make measurements in signal conditions where conventional sensitivity receivers falter. The use of measurements acquired using high sensitivity methods in degraded signal environments can however be detrimental to the navigation solution if measurement faults due to signal deterioration are not identified and understood. Thus, there is a need to characterize GPS signal degra-

dation in typical environments where high sensitivity GPS will be used, quantify the effects of prevalent interference sources, and examine methods of fault detection and exclusion to ensure reliable navigation.

1.1 Background

1.1.1 The Drive For Enhanced Signal Tracking Sensitivity

A new emerging world market is evolving from the synergy of wireless communications and personal navigation systems. Location-Based-Services (LBS) are promising investment opportunities offering new conveniences for the public. For example, a cell-phone with a built-in GPS receiver could provide a list of restaurants within a certain proximity, local traffic information, and even local weather information.

In the United States, the primary LBS driver for cellular telephone networks is the E-911 mandate issued by the Federal Communications Commission (FCC), phase II of which was due for implementation by October 2001. This mandate requires caller location to be established in an emergency situation for 67% of mobile calls to within 50 m and 95% of calls to within 150 m for telephone handset-based solutions (FCC, 2000).

Provision of LBS has driven the development of a number of network-based and handset-based technologies that can be used to locate the caller. One of the handset-based technologies being adopted is high sensitivity Assisted-GPS (AGPS). Unlike normal GPS, the receiver does not have to extract the ephemeris or any other data from the GPS satellite data message. This is instead provided over the phone's communication channel from a network-based resource, along with an approximate time and position. This has two major benefits. First, the phone's receiver can make

a more rapid signal acquisition as it already knows the in-view satellite candidates. Second, the receiver can make pseudorange measurements, using a long integration interval, even when the available signal strength is much lower than the carrier-to-noise density ratio, C/N_0, normally needed to read the ephemeris data from the navigation message without error, thus improving sensitivity by as much as 25 dB (Moeglein and Krasner, 1998). AGPS can therefore now be used inside certain buildings or beneath dense foliage (Garin et al., 1999).

An alternate approach allows high sensitivity methods to be used after GPS signals have been acquired under strong signal conditions typically outdoors. These receivers utilize unaided high sensitivity tracking methods and have the advantage of being self contained.

1.1.2 High Sensitivity GPS Methods

The GPS L1 carrier, at 1575.42 MHz, is modulated with the Coarse-Acquisition or C/A code for civilian use. This code repeats every millisecond. This can be used advantageously by a GPS receiver in that the signal can be integrated for extended periods in order to obtain a higher signal to noise ratio (Peterson et al., 1997). Chansarkar and Garin (2000) describes the use of GPS signals at very low power levels using long dwell times. In terms of conventional GPS, this integration can be performed coherently for up to 20 ms. The nominal maximum coherent integration time is due to the navigation bit boundaries. However, longer coherent integration is possible if the navigation bits are known a-priori but this process is still limited by residual frequency errors induced due to signal movement corresponding to satellite motion, local signal movement due to receiver clock instability, and user movement during the integration interval. Non-coherent accumulation, which utilizes the squared output of coherent integration, can be performed for long periods of

time relative to the nominal coherent integration interval as it is insensitive to phase reversal and some residual frequency error during the accumulation period. Using long total dwell times, acquisition and weak signal tracking in degraded environments are possible. A receiver utilizing such long integration methods will hence be referred to as a high sensitivity GPS receiver or HS receiver.

Conventional GPS receivers typically use integration times less than the 20 ms nominal maximum coherent interval and are limited in terms of their operational environments to places with strong signals. Signal masking due to man-made and natural obstructions limit the use of such receivers. HS receivers may be capable of tracking and acquiring signals in some of these environments. The most challenging of which often include indoors, under heavy foliage and in urban canyons. Interference in these environments, such as multipath, can degrade the measurements of the GPS signals. In addition, measurement faults can result from the tracking of false correlation peaks. The ability to provide measurements and positions, when otherwise impossible using conventional tracking, has clear advantages for users in terms of solution availability. However, position degradation will result if measurement faults are included in solution.

1.2 Research Objectives

A newly available unaided HS receiver developed by SiRF Technologies Inc. provides a capability to make measurements in degraded mode GPS environments where conventional GPS receivers typically exhibit frequent losses of signal tracking and or signal acquisition failure. The reason for selecting this model is the availability of the model, together with the capability to record raw measurements and support from SiRF Technologies Inc. This unaided HS receiver differs from an AGPS receiver

in that it must be initialized with time, position, and satellite ephemeris in order to subsequently use longer dwell times. This requires initialization of the receiver in open-sky conditions prior to testing in weak signal environments. As a research tool, this unaided HS receiver allows an assessment of measurement availability in comparison with standard mode GPS. The HS receiver also allows measurements of signal attenuation with respect to the line of sight (LOS) signals in environments where measurements were previously unavailable. However, the pseudorange measurements obtained using HS methods may be degraded due to interference. These effects must be characterized and well understood to facilitate reliable navigation.

The objectives of this thesis are to assess the signal tracking capability of the SiRF HS receiver used and investigate degraded mode signal environments in terms of characterizing measurement availability, any prevalent interference phenomena, pseudorange measurement degradation, signal power degradation, positioning accuracy and solution availability. This entails the design and execution of appropriate field tests, GPS hardware in-the-loop simulations, the development of data processing and analysis techniques, and the synthesis of conclusions and recommendations.

1.3 Literature Review

Investigations into the use of low power GPS signals using long dwell times have been performed by Peterson et al. (1997), Moeglein and Krasner (1998), Garin et al. (1999), Akos et al. (2000), van Diggelen and Abraham (2001), Sudhir et al. (2001), Haddrell and Pratt (2001), and Shewfelt et al. (2001). These investigations have focused on the ability to provide measurements and positions when previously impossible using conventional GPS. Little research regarding prevalent interference sources and characterization of measurement degradation while using HS methods

has been performed. Enge et al. (2001) discusses, to a limited extent, pseudorange multipath and noise using HS GPS in urban canyons and some indoor environments but recognizes that further investigation and development of test metrics are needed. Jahn (2001) discusses signal power degradation modeling for mobile satellite communications. Ma et al. (2001) also discusses signal power degradation modeling using HS GPS as a measurement tool. Both of these studies relied on limited data. Thus, further testing with HS receivers for environmental characterization could enhance models of signal power and measurement degradation.

1.4 Thesis Outline

Chapter 1 provides the necessary background information and establishes the intent of this thesis. Chapter 2 provides an overview of GPS, HS GPS, related interference phenomena in a degraded-mode context, and description of the environments that have traditionally challenged conventional GPS. Chapter 3 describes the methodology and test measures used to assess measurement availability, signal power degradation, pseudorange measurement errors, positioning accuracy, and solution availability in specific degraded-mode environments. A hardware GPS simulation test provides useful insight into the tracking performance of the HS GPS receiver over a wide range of signal power in Chapter 4. Large anomalous pseudorange error effects associated with the use of HS GPS are discussed in Chapter 5. In addition, further hardware simulation testing in Chapter 5 identifies probable sources of the large measurement errors and interference susceptibility. Chapter 6 presents the results of testing in a forest environment. Test results from some urban canyon environments are presented in Chapter 7. Chapter 8 presents results of testing in a residential indoor environment. Chapter 9 provides the conclusions and recommendations for future research.

Chapter 2

High Sensitivity GPS Theory, Error Effects, And Interference Concerns

2.1 Chapter Overview

This chapter provides an overview of GPS and a discussion of high sensitivity GPS theory. Interference effects that concern high sensitivity GPS are also discussed. In addition, an overview of the degraded mode environments that challenge conventional GPS and where HS GPS may be potentially beneficial is provided.

2.2 GPS Overview

GPS is a satellite-based radionavigation system that is well described in textbooks such as Parkinson and Spilker (1996), Kaplan (1996), and Misra and Enge (2001). Currently there are 28 functional GPS satellites in orbit (as of May 24^{th}, 2003, refer to http://www.navcen.uscg.gov/ftp/GPS/status.txt). GPS is a pseudorange (ranging with a time/range bias) based positioning system that uses radio frequency (RF) signals to determine range estimates, based on the time difference between transmission and reception, from each of the satellites. This is sometimes referred to as a time-of-arrival (TOA) ranging method.

GPS satellites generate and transmit two carrier frequencies referred to as L1 and L2 at 1575.42 MHz and 1227.60 MHz respectively. The carriers are modulated using spread spectrum codes and each satellite is identified using a technique called code

division multiple access (CDMA) using pseudorandom noise (PRN) codes. The codes are referred to as the Coarse Acquisition (C/A) code designed for civilians using the Standard Positioning Service (SPS) and the Precise (P) code designed for military users using the Precise Positioning Service (PPS). The precision code is denied to the civilian segment via a technique called anti-spoofing, which modulates an encryption on the P code. The encrypted P code is referred to as the Y code. In addition to spread spectrum code modulation a navigation message is also modulated on the carrier signals.

As high sensitivity GPS relies upon the L1 carrier and the C/A code, the P-code and the L2 signal will not be addressed in this thesis. Table 2.1 provides a summary description of the C/A code modulated on the L1 carrier.

Table 2.1: The Coarse Acquisition Pseudorandom Noise Code

Code	Length (chips)	Length (time)	Modulation Frequency (MHz)	Available Bandwidth (MHz)	Length of One Chip (m)
C/A	1023	1 ms	1.023	20.46	293.0523

GPS signal measurements include, in general, pseudorange, Doppler, and carrier phase (derived by accumulating the Doppler while maintaining phase lock). The L1 C/A code pseudorange and Doppler measurements are of primary use to high sensitivity users. They allow determination of both position and velocity. Carrier phase measurements are used for geodetic grade applications and are thus outside the scope of this thesis.

2.2.1 The Pseudorange Measurement

Range measurements can be based on time differences between transmission and reception with a known signal speed. If the clocks used to measure these time

differences are not synchronized, the resulting range measurement is biased and the measurement is referred to as a pseudorange. GPS pseudorange measurements are useful in determining a user's position in terms of latitude, longitude, and height (all referenced to the WGS84 ellipsoid). However, the receiver's clock difference with respect to the GPS time of the satellites must be solved as well. This amounts to four unknown parameters and thus at least four satellite measurements are necessary to compute a complete position solution.

Single point civilian GPS use relies on pseudorange measurements based on the C/A code which is modulated on the L1 carrier. This code is replicated in the user receiver and correlated with the incoming code to produce a code-phase measurement which, along with some additional information, forms a pseudorange measurement. The equation for this measurement is

$$P = \rho + d\rho + c(dt - dT) + d_{iono} + d_{tropo} + \varepsilon_N + \varepsilon_M \tag{2.1}$$

where P is the pseudorange measurement (m), ρ is the geometric range (m), $d\rho$ is the orbital error (m), dt is the satellite clock error (m), dT is the receiver clock error (m), d_{iono} is the delay due to the ionosphere (m), d_{tropo} is the delay due to the troposphere (m), ε_N is the noise (m), and ε_M is multipath (m).

Orbital error, satellite clock error, and atmospheric delay are common to standard and HS GPS measurements. These effects are spatially correlated and can be reduced by differencing pseudorange measurements with a receiver at a known location or by analytic modeling often based on parameters included in the broadcast navigation message. The receiver clock error is included as an unknown parameter in single point and single difference GPS methods. Noise on the pseudorange measurement depends on the received signal strength and the correlation method used by the receiver. Multipath is the result of reflected signals interfering with the direct line-of-sight signal and is a dominant source of error in GPS methods that utilize the

pseudorange measurement.

2.2.2 The Doppler Measurement

Doppler as a physical phenomena is the rate of change of the range between two points, A and B, or, equivalently, the change in reception frequency due to the relative motion of the transmitter and receiver. This implies that it can be used as a measure to derive the velocity of A with respect to B. In GPS, Doppler is a measurement of the instantaneous phase rate of a tracked satellite's signal. Thus, the velocity of the user with respect to GPS satellites can be determined. However, the GPS Doppler measurement does not only include effects due to motion. The equation for this measurement provides further details and is defined as

$$\dot{\phi} = \dot{\rho} + d\dot{\rho} + c(d\dot{t} - d\dot{T}) + \dot{d}_{iono} + \dot{d}_{tropo} + \varepsilon_{\dot{M}} + \varepsilon_{\dot{\phi}} \tag{2.2}$$

where $\dot{\phi}$ is the Doppler measurement (m/s), $\dot{\rho}$ is the geometric range rate (m/s), $d\dot{\rho}$ is orbital error drift (m/s), $d\dot{T}$ is receiver clock drift (m/s), $d\dot{t}$ is satellite clock drift (m/s), $\dot{d}_{iono}$ is ionospheric delay drift (m/s), $\dot{d}_{tropo}$ is tropospheric delay drift (m/s), $\varepsilon_{\dot{M}}$ is the rate of change of multipath delay and $\varepsilon_{\dot{\phi}}$ is noise. Orbital error drift, satellite clock drift, ionospheric delay drift, and tropospheric delay drift can be reduced by differencing Doppler measurements with a receiver at a known location or by analytic modeling often based on parameters included in the broadcast navigation message. The receiver clock drift is included as an unknown parameter in solving for the user's velocity. Thus, four or more Doppler measurements are used in solving for the user's velocity and clock drift.

2.3 High Sensitivity GPS Theory

Obtaining GPS measurements has, in the past, been limited by the paradigm that using unobstructed line-of-sight signals is the best method. Weak signals whether they are attenuated line-of-sight signals, diffracted signals, multipath signals or echo-only signals were not desirable for use because they may have large associated noise and other errors. The expansion of GPS for location-based services such as E-911 is changing that paradigm. Using weak signals inside, under trees, or through the roof of a car can provide measurements that mean the difference between a position solution or no solution at all.

2.3.1 Weak GPS Signals And The GPS Signal Budget

GPS signals are weak to begin with. A good analogy is that using GPS signals is like listening to a 25 mW baby monitor 400 km away. The following discussion explains just how much signal is received for line-of-sight signal reception.

GPS satellites radiate signals at a power level of 13.4 dBW. The antennas on the satellites are directive with the beam pointed to Earth. The one-sided beam angle is 14.3^o as shown in Figure 2.1.

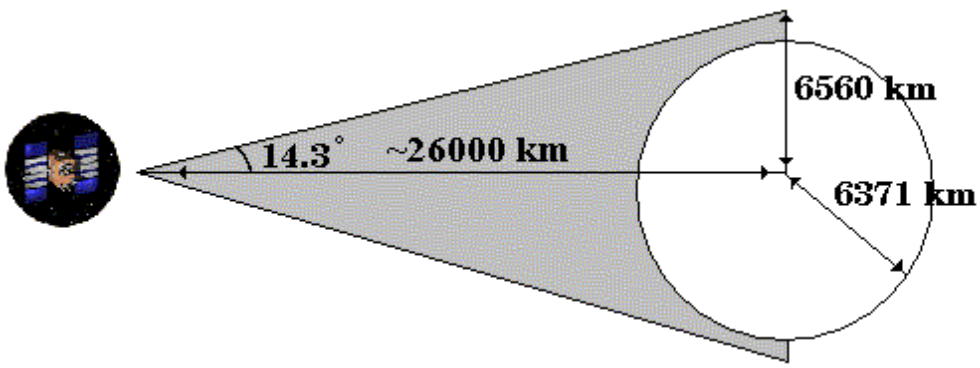

Figure 2.1: Satellite Radiation Pattern

This provides an effective directive gain of 13.4 dB. This amounts to 26.8 dBW of radiated power. However, the distance to the satellites is great and this translates into a significant free space loss. Free space loss is calculated using the following equations.

$$P_r = P_t A_r/(4\pi R^2) \tag{2.3}$$

where

$$A_r = \lambda^2/(4\pi) \tag{2.4}$$

Thus

$$L_0(dB) = 10log(P_r/P_t) = 10log(\lambda^2/(4\pi R)^2) = 20log(\lambda/(4\pi R)) \tag{2.5}$$

where P_r is the received power, P_t is the transmitted power, A_r is the antenna aperture, λ is the wavelength for L1 (approximately 19 cm), R is the radial distance between the transmitting and the receiving antenna, and L_0 is the free space loss. For a satellite at the zenith, approximately 20000 km away, this amounts to 182.4 dB loss. A satellite on the horizon, approximately 26000 km away, has 184.7 dB loss. An example signal budget for C/A code modulated on L1 is given in Table 2.2 for a satellite at the horizon.

Table 2.2: The GPS Signal Budget (Lachapelle, 1998)

SV antenna power (dBW)	13.4
SV antenna gain (dBW)	13.4
User antenna gain (hemispherical) (dB)	3.0
Free space loss (L1) for R = 25092 km (dB)	-184.4
Atmospheric attenuation (dB)	-2.0
Depolarization loss (dB)	-3.4
User receiver power (dBW)	-160.0

The specified received minimum signal strength for L1 C/A code is -160 dBW and is defined in the GPS Interface Control Document (ICD200C, 2000). Fortunately for GPS users, the minimum power is not generally used to transmit the signals. Most

GPS satellites emit signals at 3 to 7 dB higher than the specified minimum with an average power level typically 5.4 dB above the minimum (Spilker, 1996b).

These signals are still very weak compared to the nominal thermal noise floor. The bulk of the GPS signal power, about 90%, is contained within the 2.046 MHz null-to-null bandwidth of the broadcast signal. The noise power within this bandwidth is given by

$$N_{power} = kTB \tag{2.6}$$

where N_{power} is the noise power in watts, k is Boltzman's constant ($1.38066\ x\ 10^{-23}$ J/K), T is the equivalent noise temperature (nominally 273^o K), and B is the bandwidth considered. Within the null-to-null 2.046 MHz bandwidth, the noise power is approximately -141 dBW. Thus, the GPS signal is well below the noise floor and is not visible with a spectrum analyzer even at its spectral peak. Standard mode GPS works because despreading of the signal through correlation reduces the noise bandwidth considered to 1 KHz (for a 1 ms integration time) and the noise power nominally becomes -174 dBW. Line-of-sight signals can then be detected.

All of the above discussion of signal budget assumes a line-of-sight signal. Signal attenuation due to propagation through various materials, multipath interference, and other interference are not considered. The amount of signal attenuation due to signal masking depends on the material, its density, and how much material the signal passes through. High sensitivity GPS receiver manufacturers are aiming for sensitivity levels in the range of -182 dBW to -188 dBW (Ray, 2002). This will allow receiver function at attenuations of 27 to 33 dB with respect to the average typical received power of -154.6 dBW.

2.3.2 Weak Signal Processing

The processing task involved in obtaining measurements from weak signals depends on context. Signal acquisition is difficult. Signal tracking is relatively easy and signal reacquisition is somewhere in between. In order to explain high sensitivity GPS, knowledge of the GPS signal processing steps are necessary.

Figure 2.2 presents on overview of GPS signal processing for both standard and high sensitivity GPS. RF down-conversion, sampling, Doppler removal and coherent integration and accumulation are discussed in detail in Ward (1996) and van Dierendonck (1996). Weak GPS signals are acquired and tracked by using long signal integration times. This is accomplished by coherent correlation and integration and further non-coherent accumulation. To understand weak signal processing, examination of the coherent correlation process and non-coherent integration is useful.

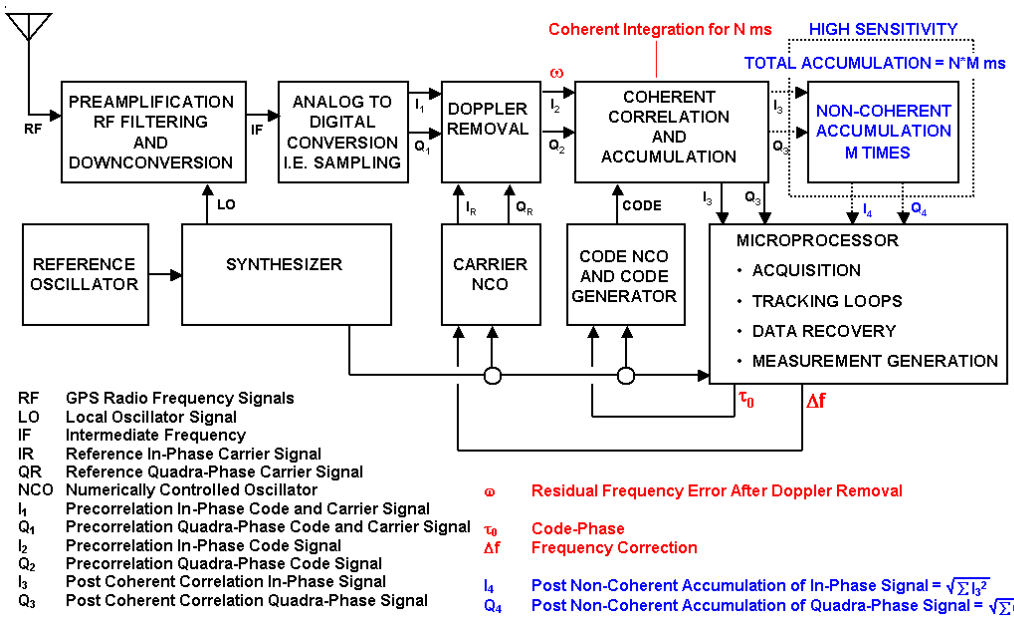

Figure 2.2: Generic Receiver Signal Processing Block Diagram

The result of correlating an incoming signal plus noise with a receiver generated C/A

code signal replica as shown in Figure 2.3, is shown in Figure 2.4 in the case of 1-bit sampling.

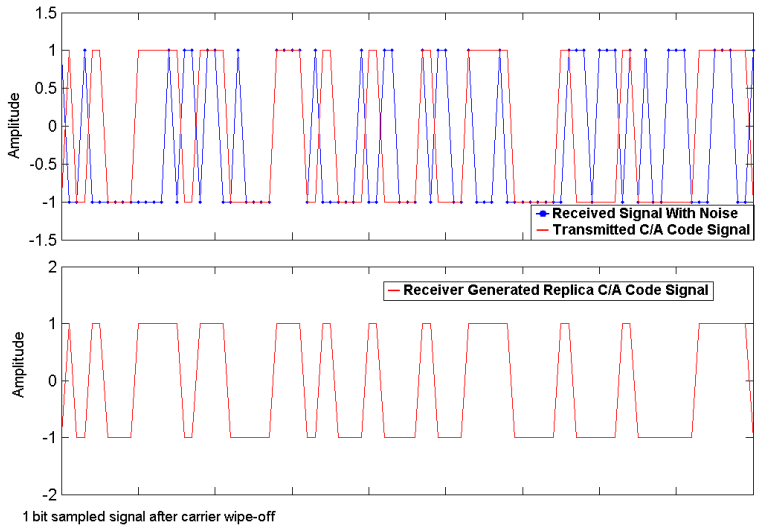

Figure 2.3: Incoming GPS Signal After Carrier Wipe-Off and Receiver Generated C/A Code Signal

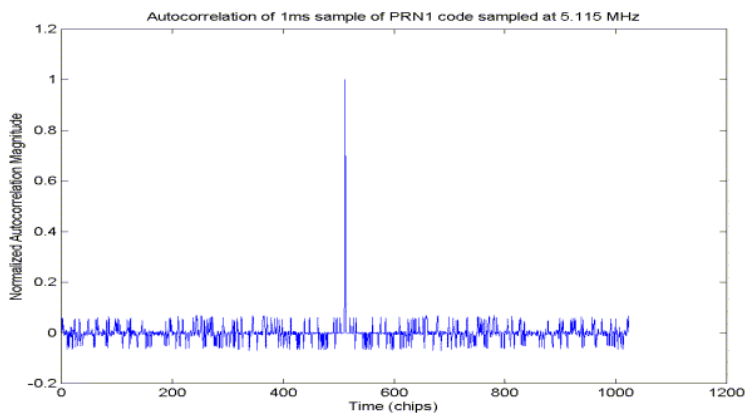

Figure 2.4: C/A Code Correlation

For the L1 C/A code the length of the code sequence is 1 ms. Thus, sequential correlation of multiple 1 ms sequences results in a signal power gain with respect to

the noise amounting to

$$G = 20log\sqrt{N} = 10log(N) \tag{2.7}$$

where G is the gain in decibels and N is the integration time (ms) (van Diggelen, 2001). With N milliseconds of coherent integration the signal power increases by N and the noise power increases by $\sqrt{N}$. This results in a gain of $\sqrt{N}$ in terms of signal to noise ratio (SNR). This is illustrated in Figure 2.5.

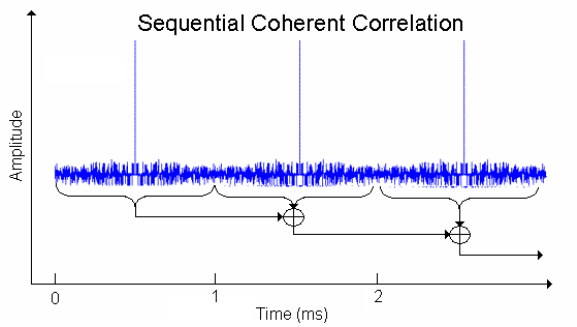

Figure 2.5: Sequential Coherent Correlation

However, every 20 ms there is a possible navigation bit transition which can change the phase of the correlation peak. This 20 ms period limits coherent integration of the GPS signal unless the navigation bits are known a-priori as shown in Figure 2.6.

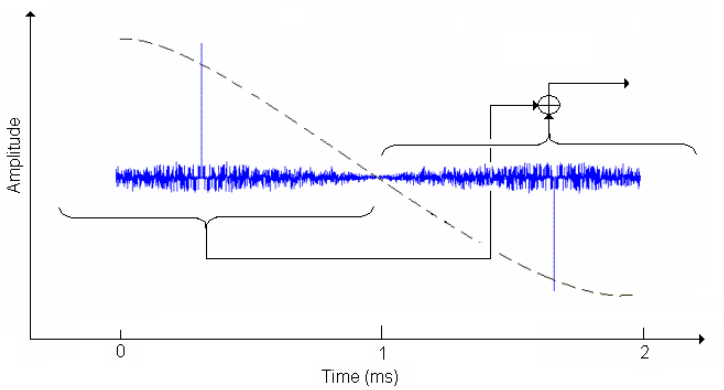

Figure 2.6: Sequential Coherent Correlation Over A Navigation Data Bit Transition

In addition, any residual frequency error after Doppler removal can cause the power in the in-phase component to decrease such that there is no point in further integration. In other words, coherent integration is very sensitive to frequency error. As long as the signal is still tracked (i.e. within the carrier tracking bandwidth of the receiver), a residual frequency error causes the signal power to oscillate between the in-phase and quadra-phase signal components (van Diggelen, 2001). To illustrate this concept, pre-correlation in-phase and quadra-phase sampled data generated in Matlab is shown in Figure 2.7 for the case where there is frequency error and the power clearly oscillates between the two components.

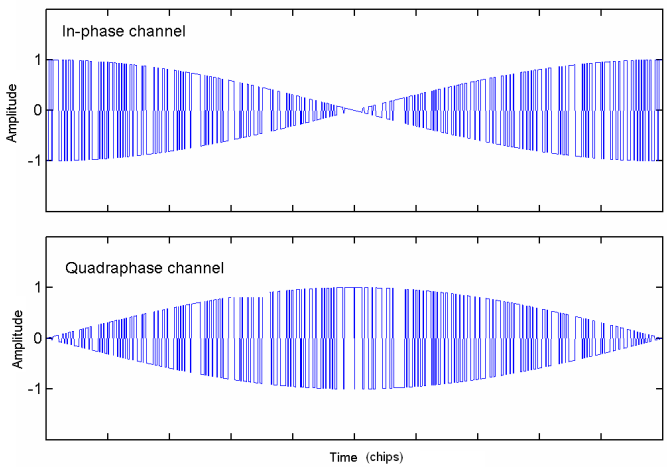

Figure 2.7: In-Phase And Quadra-Phase Signals After Carrier Removal Due To Residual Frequency Error

Thus, coherent integration is also not possible for long periods due to residual frequency errors. Chansarkar and Garin (2000) discuss this concept in detail. Coherent integration is limited by navigation bits and residual frequency errors. Non-coherent integration uses the square root of the sum of squares of the in-phase and quadra-phase signal components after coherent correlation of some interval as shown in

Equations 2.8 and 2.9.

$$I_4 = \sqrt{\sum_1^M I_3^2} \tag{2.8}$$

$$Q_4 = \sqrt{\sum_1^M Q_3^2} \tag{2.9}$$

where I_3 is the accumulated in-phase coherent signal after correlation, Q_3 is the accumulated quadra-phase coherent signal after correlation, I_4 is the accumulated in-phase non-coherent signal, Q_4 is the accumulated quadra-phase non-coherent signal, and M is the number of non-coherent accumulations.

Thus, navigation bits become irrelevant and some residual frequency errors during non-coherent accumulation that are within the carrier tracking bandwidth of the receiver can be tolerated. However, squaring of the signal in non-coherent accumulation also results in squaring of the noise and results in squaring loss. van Diggelen (2001) shows that squaring loss varies with the SNR after coherent correlation as shown in Figure 2.8.

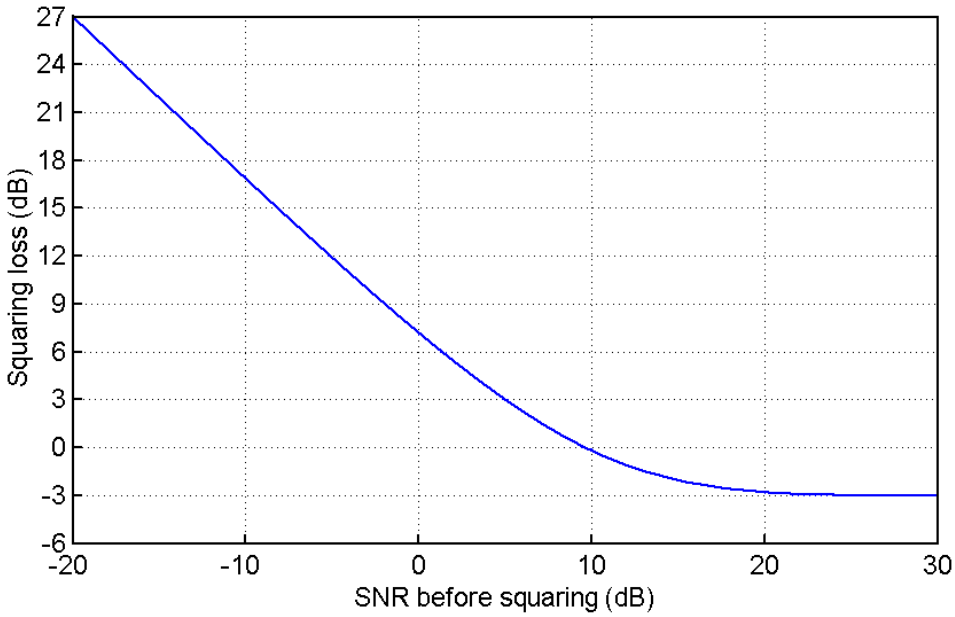

Figure 2.8: Non-Coherent Integration and Squaring Loss (van Diggelen, 2001)

This figure shows that squaring loss is significant if the post coherent correlation SNR is low. Thus, maximal coherent integration prior to non-coherent integration results in less squaring loss.

The total gain using coherent correlation and non-coherent accumulation is given by

$$Gp = 10log(N) + 10log(M) + SQ_{loss} \tag{2.10}$$

where Gp is the processing gain (dB), N is the total coherent integration time in milliseconds, M is the number of non-coherent accumulations of the coherent output, and SQ_{loss} is the squaring loss due to non-coherent accumulation.

The limitations of coherent correlation accumulation are data bit transitions and residual frequency errors. Predicting the data bit transitions and limiting residual frequency errors during coherent correlation is necessary to obtain optimal gain prior

to non-coherent accumulation. This is because reduction of the ensuing squaring loss is paramount to beneficial non-coherent accumulation.

The limitations of coherent correlation are highly dependant on the receiver operating mode. If the receiver is already tracking the GPS signals, the task of maintaining signal tracking under weak signal conditions is much easier than acquisition of weak GPS signals. This is discussed further in the ensuing sections.

2.4 Factors Affecting Weak Signal Tracking And Acquisition

The ability to acquire and track weak GPS signals depends on the capabilities of the receiver to maximize the coherent integration interval prior to non-coherent accumulation while minimizing residual frequency errors during coherent integration. In addition, the design of the receiver must also minimize the impact of thermal noise to maintain signal tracking. The ability to predict the sign of the bits and the timing of the navigation message signal modulation directly affects the ability to perform long coherent integration. Residual frequency errors during coherent integration cause reduction in coherent signal gain and higher squaring loss for non-coherent accumulation. Residual frequency error sources include oscillator instability, and user motion induced Doppler effects. Thermal noise also induces frequency error jitter depending on the carrier tracking loop bandwidth. Thermal noise can often be a dominant source of carrier tracking error, especially for weak GPS signal tracking. All of these issues are discussed in the following subsections.

2.4.1 Frequency Error

The amount of tolerable frequency error during the total dwell time depends on the length of coherent integration and the type of carrier tracking performed. A

frequency lock loop (FLL) and/or a phase lock loop (PLL) are used to perform Doppler removal, as discussed in Ward (1996). Phase lock loops and frequency lock loops, as 1-sigma rule-of-thumb, cannot tolerate phase errors greater than 15^o and 30^o respectively during the total dwell time.

The 1-sigma rule-of-thumb threshold for PLL tracking is given by Ward (1996)

$$\sigma_{PLL} = \sqrt{\sigma_{tPLL}^2 + \sigma_v^2 + \theta_A^2} + \frac{\theta_e}{3} \leq 15^o \tag{2.11}$$

where σ_{tPLL} is the 1-sigma PLL thermal noise (^{o}), σ_v is the one sigma vibration induced oscillator jitter (^{o}), θ_A is the Allan deviation-induced oscillator jitter (^{o}), and θ_e is the tracking loop error due to dynamic stress (i.e. user motion).

For FLL tracking, the 1-sigma rule-of-thumb tracking threshold is given by Ward (1996)

$$\sigma_{FLL} = \sigma_{tFLL} + f_e \leq \frac{30^o}{360^o}\frac{1}{T}(Hz) \tag{2.12}$$

where σ_{tFLL} is the 1-sigma thermal noise frequency jitter (Hz), f_e is the dynamic stress error in the FLL tracking loop (Hz), and T is the length of coherent correlation (s).

2.4.2 Thermal Noise And Tracking Loop Error

The thermal noise for PLL tracking is given by Ward (1996)

$$\sigma_{tPLL} = \frac{180}{\pi}\sqrt{\frac{B_n}{c/n_0}(1 + \frac{1}{2Tc/n_0})} \tag{2.13}$$

where B_n is the carrier loop noise bandwidth (Hz), c/n$_0$ is the carrier to noise density expressed as a ratio ($10^{\frac{C/N_0}{10}}$), and T is the length of coherent correlation (s).

Thermal noise for FLL tracking is given by Ward (1996)

$$\sigma_{tFLL} = \frac{1}{2\pi T}\sqrt{\frac{4FB_n}{c/n_0}(1 + \frac{1}{Tc/n_0})} \tag{2.14}$$

where F is 1 at high C/N_0 and 2 near the tracking threshold. Frequency lock loops are less accurate but are more robust in terms of accommodating noise than phase lock loops.

Increasing the coherent integration time decreases thermal noise jitter. Decreasing the carrier tracking loop bandwidth decreases the amount of thermal noise jitter. However, as will be discussed later on, the carrier tracking loop bandwidth must be large enough to accommodate residual frequency errors.

2.4.3 Oscillator Stability

Oscillator drift during long coherent integration periods causes frequency errors which reduce the gain due to coherent integration. Non-coherent accumulation is tolerant of some frequency error as the power of the signal simply shifts from the in-phase to the quadra-phase accumulated post-correlation component.

The typical frequency standards chosen for GPS receivers are low cost quartz crystal oscillators due to their good short term stability with typical Allan deviation, a statistical measure used to characterize the stability of a frequency standard over a specific time interval, of better than 10^{-10} for intervals of 1 to 20 ms. The 3-sigma phase error during coherent integration is given by Ward (1996)

$$\phi_e = 3\sqrt{T^2 * \sigma^2_{Allan}(\tau)} * c/\lambda * 360^o \tag{2.15}$$

where ϕ_e is the phase error (^{o}), T is the interval of coherent integration (s), $\sigma_{Allan}(\tau)$ is the Allan deviation for the interval τ, c is the speed of light (m/s), and λ is the wavelength of L1 (m). Given an Allan deviation of 10^{-10} for a 20 ms period, this amounts to 3.4^o which is well below the 15^o and 30^o 1-sigma tolerances for PLL and FLL tracking respectively. Assuming three constant Allan deviations for intervals up to 500 ms for three grades of receiver frequency standards, Figure 2.9 shows the

corresponding phase error versus the length of coherent integration. The assumption of constant Allan deviation is pessimistic in this case as the deviation tends to decrease in terms of short term stability (Lachapelle, 1999). The integration intervals of up to 500 ms are reasonable for the integration time of interest for GPS. This time is generally limited by user induced frequency error. Figure 2.9 clearly demonstrates the impact of the oscillator stability for long coherent integration intervals and that an Allan deviation of 10^{-11} or better is highly desirable for integration intervals longer than 500 ms.

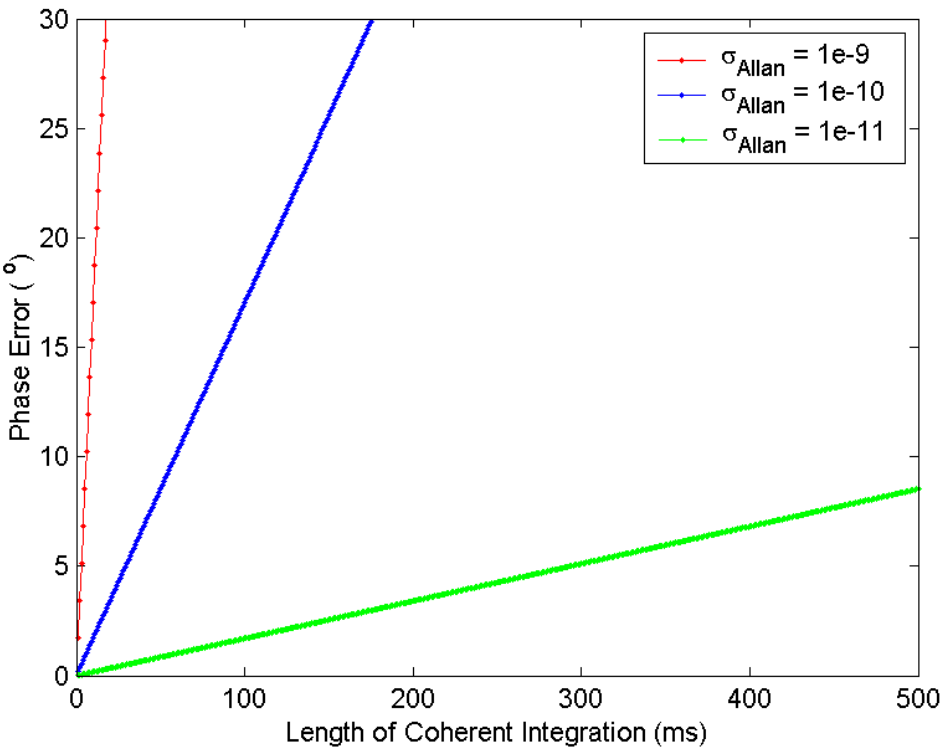

Figure 2.9: Effect of Oscillator Stability on Phase Tracking Assuming Constant Allan Deviation for Non-Coherent GPS Integration Intervals of up to 500 ms

Oscillator drift also affects signal acquisition in the same way as signal tracking in terms of correlation gain; although, the drift should be predictable in a tracking-

mode context. However, the drift causes uncertainty in the Doppler search space which can increase time to acquisition unless the receiver performs some form of massive parallel correlation (correlation of many possible delays and frequency bins (van Diggelen, 2001)) or uses an external aiding source to estimate its clock drift.

Thus, better oscillators result in less loss during coherent-integration, reduced acquisition search space, and better weak signal tracking in general as more 'space' in the jitter budget is available for other jitter sources.

Other factors also influence oscillator stability including vibration, oscillator stress due to user motion, and in some cases temperature.

2.4.4 Motion Induced Frequency Error

User induced frequency error due to motion also reduces gain during coherent integration and limits weak signal tracking. Satellite motion induces a predictable frequency effect and thus does not induce a residual frequency error.

Frequency error due to user motion is also referred to as dynamic stress error. The amount of tolerable dynamic stress error depends on the type and order of the carrier tracking loop, length of coherent integration time, and the noise bandwidth (carrier tracking loop bandwidth).

First order loops are sensitive to velocity stress. Second order loops are sensitive to acceleration stress and third order loops are sensitive to jerk stress. In general, FLL based tracking loops are less sensitive to dynamic stress. For example, a second order FLL based tracking loop has about an order of magnitude better dynamic stress performance than a third order PLL with the same carrier tracking bandwidth (Ward, 1996).

Longer integration time limits the tolerable dynamic stress. The induced frequency error during coherent integration will reduce coherent gain or may cause loss of signal tracking completely.

The bandwidth of the carrier tracking loop limits the amount of thermal noise but must accommodate dynamic stress error if tracking is to be maintained. Thus, the design of the carrier tracking loop must balance thermal noise reduction versus dynamic stress error.

2.4.5 Timing And Navigation Message Prediction

Prediction of the data bits for enabling coherent integration up to 20 ms or for data wipe-off (coherent integration longer than 20 ms by cancelling the sign of the incoming bits) requires precise timing. If a receiver is already tracking enough GPS signals, it will have GPS time and can perform these operations but if the receiver is in acquisition mode timing assistance is necessary. Without timing assistance during acquisition, coherent integration gain is limited, squaring loss is higher during non-coherent accumulation, and longer total dwell time is necessary. Predicting the actual data bits is not exceptionally difficult but a-priori knowledge of the navigation message and timing information is needed. For example, the ephemeris message for each satellite repeats every 30 s and is only updated every two hours. During full tracking, the navigation message is already known and further prediction is relatively simple. During acquisition, assistance data is necessary to provide the navigation message if long coherent intervals are to be used. Syrjärinne (2001) lists the portions of the known bits for navigation message reconstruction available using assistance data (two types of assistance, namely GSM point-to-point and Broadcast assistance, are considered) and this is shown in Table 2.3. The percentage values listed refer to the percentage of bits recovered successfully.

Table 2.3: Bit Prediction Using Assistance Data (Syrjärinne, 2001)

Known bits for subframe reconstruction with GSM point-to-point and broadcast assistance.

Subframe	Known bits (point-to-point)	% (p-t-p)	Known bits (broadcast)	% (b)	Notes
1	300/300	100%	300/300	100%	Clock corrections
2	300/300	100%	300/300	100%	Ephemeris
3	300/300	100%	300/300	100%	Ephemeris
4	300/300	100%	300/300	100%	Almanac for SVs 25-32: pages: 2,3,4,5,7,8,9,10
	60/300[(1)]	20%	60/300[(1)] (300/300)[(3)]	20% (100%)	Reserved pages with SVID 57: pages: 1,6,11,16,21
	60/300[(1)]	20%	60/300[(1)] (300/300)[(3)]	20% (100%)	Reserved pages with misc. SVIDs: pages: 12,14,15,17,19,20,22,23,24
	270/300[(2)]	90%	300/300	100%	Ionospheric and UTC data: page: 18
	60/300[(1)]	20%	60/300[(1)]	20%	NMCT parameters[(4)]: page: 13
	60/300[(1)]	20%	300/300	100%	A-S flags, SV health 25-32: page: 25
5	300/300	100%	300/300	100%	Almanac for SVs 1-24: pages: 1-24
	60/300[(1)]	20%	300/300	100%	SV health 1-24 and almanac time page: 25
Summary: SFs 1,2,3: SFs 1-5: (SFs 1-5:)		100% 89.04% (89.04%)		100% 90.4% (99.36%)[(3)]	

[(1)] Only the words 1 and 2 (TLM and HOW) can be reconstructed.
[(2)] The 10th word cannot be reconstructed since the 14 reserved bits are unknown.
[(3)] Possible future expansion.
[(4)] Unique for each SV and unavailable for unauthorized users.

2.5 High Sensitivity Implementations

In general, high sensitivity methods can be implemented in either aided (AGPS) or unaided modes. In aided mode, high sensitivity receivers rely on assistance data including time, approximate position, satellite ephemerides, and possibly code differential GPS corrections. Massive parallel correlation is necessary to facilitate the complex task of searching for the weaker GPS signals while using long coherent in-

tegration periods and further non-coherent accumulation (van Diggelen, 2001). In unaided mode, the high sensitivity receiver lacks the ability of the aided receiver to acquire weak signals if it has no apriori knowledge. However, if the receiver is initialized with the same assistance data, by acquiring and tracking four or more GPS satellites with strong signals, it has the same functional capability as an assisted GPS receiver so long as it can maintain timing, approximate position, and satellite ephemeris.

There are obvious advantages and disadvantages to both implementations. Aided receivers do not have to continually track the GPS signals and can function in an acquire-when-tasked mode. Aided receivers also have the capability of applying code differential GPS corrections in real-time to reduce orbital, ionospheric, and tropospheric errors. Unaided high sensitivity GPS receivers rely on initialization with strong GPS signals. This limits their operational capability to a tracking mode context. However, no infrastructure is necessary for receiver operation. In addition, there are multiple operational environments that challenge conventional GPS where high sensitivity signal tracking would improve signal availability and therefore solution geometry and the corresponding accuracy. More measurements also provide higher redundancy for reliability testing of the observations.

Differential corrections can be applied in post-mission to an unaided HS receiver measurement. Thus, unaided HS receivers can be used in research that parallels the use of aided HS receivers, subject to the acquisition requirements described above.

2.6 GPS Error Sources And Interference Phenomena

Standard GPS receivers typically use integration times less than the 20 ms maximum coherent interval and are limited in terms of their operational environments to places

with strong signals. Signal masking due to man-made and natural obstructions limit the use of such receivers. HS receivers may be capable of tracking and acquiring signals in some of these environments. The most challenging of which, often include indoors, under heavy foliage and in urban canyons. Interference in these environments, such as multipath, can degrade the measurements of the GPS signals. In addition, blunderous measurements can result from the tracking of false correlation peaks.

The ability to provide measurements and positions, when otherwise impossible using standard tracking, has clear advantages for users in terms of availability. However, position degradation due to increased interference results from the use of the degraded measurements unless detected and mitigated.

GPS error sources are given in Equations 2.1 and 2.2. Error sources are typically due to error in orbital modelling of the satellites, residual ionospheric and tropospheric delays after correction via modelling or using single differences between receivers, satellite clock errors, and multipath.

These observation equations do not include unpredictable error effects due to interference phenomena. High sensitivity GPS measurements are particularly susceptible to the tracking of false correlation peaks due to signal self-interference and echo-only (a reflected signal only) tracking.

The following subsections discuss GPS observation error sources, signal masking, and interference effects.

2.6.1 Satellite Clock Errors

Coefficients for the behavior of the satellite clocks are included in the broadcast navigation message. The correction is generally less than 1 ms and and the broadcast

correction has a typical accuracy of about 5 to 10 ns or equivalently about 1.5 to 3 m in units of length (Cannon, 1999). As the satellite clock error is common to all receivers simultaneously tracking the same satellite, the effect can be removed by single differencing measurements between receivers.

2.6.2 Orbital Errors

Orbital errors are due to errors in the broadcast ephemerides and typically range from 2 to 10 m (Cannon, 1999). Fortunately, orbital errors are spatially correlated for two receivers simultaneously tracking the same satellite and can be reduced by single differencing measurements between the receivers. The remaining differential orbital error is less than 0.5 ppm of the distance between the two receivers in general (Cannon, 1999). Precise orbits can be used in post-mission data analysis and to a limited extent in ultra-rapid real time operation (with external aiding) to reduce orbital error effects. However, the resulting accuracy gain is insignificant in the present context.

2.6.3 Ionospheric Errors

The ionosphere is a large source of range error for GPS users. This region of the atmosphere nominally extends from 50 to 1000 km above the Earth, as shown in Figure 2.10, and contains electrons freed by ionizing radiation from the sun. The free electrons disturb the propagation of RF signals including GPS signals.

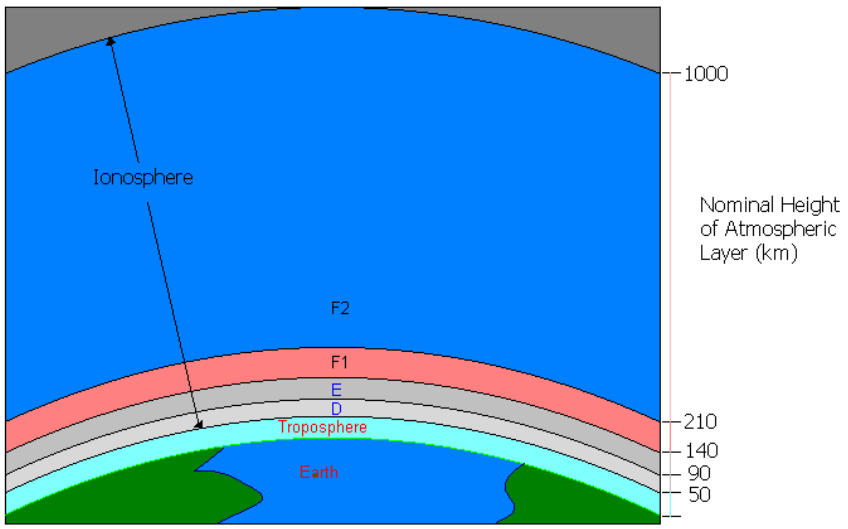

Figure 2.10: The Atmosphere From A GPS Perspective

The ionospheric induced delay can vary from only a few metres at the zenith to many tens of metres at the horizon (Klobuchar, 1996). The ionosphere is a dispersive medium; that is, the refractive index of the ionosphere is a function of the frequency. Therefore, dual frequency GPS users can make use of this property to measure and correct for range and range-rate error effects. Single frequency GPS users rely upon a set of broadcast ionospheric correction coefficients included in the GPS navigation message. As the ionospheric error is spatially correlated, it can be significantly reduced by single differencing between receiver measurements or equivalently by corrections from a nearby reference station.

Other ionospheric effects include Faraday rotation and scintillation. Faraday rotation on electromagnetic signals causes a linearly polarized signal to undergo additional rotation along the plane of its polarization. Since GPS signals are circularly polarized, Faraday rotation has no effect on GPS signals (Klobuchar, 1996). Ionospheric scintillation is caused by electron density irregularities in the ionosphere (Klobuchar,

1996). Scintillation is a rapid variation in the amplitude and/or phase of an RF signal. These variations correspond to high levels of solar and geomagnetic activities. The presence of these irregularities can cause GPS signals to experience phase and amplitude scintillation effects. Receiver carrier tracking bandwidth is usually not designed to accommodate such fast frequency variations and this may result in loss of lock. The frequency of occurrence of such events varies with location and levels of solar activity (Klobuchar, 1996). The frequency of these events is very low and can be detected easily by examining the variations in C/N_0 using a receiver operating with LOS access to the satellites. Thus, scintillation effects are not an issue in the context of this study.

2.6.4 Tropospheric Effects

For GPS purposes, the troposphere can be defined as the region of the atmosphere extending from the Earth's surface to approximately 50 km in altitude. The troposphere is non-dispersive at GPS frequencies. Its contribution to GPS signal degradation is small in terms of attenuation and signal delay.

The tropospheric attenuation of the GPS signal varies with the elevation angle of the satellite. Attenuation ranges from 0.4 dB at the horizon to typically 0.04 dB at the zenith. The attenuation effect is due to oxygen attenuation while effects due to water vapor, rainfall, and nitrogen are negligible at GPS frequencies (Spilker, 1996c).

As the GPS signal is refracted as it travels though the atmosphere, the received signal is delayed. The troposphere can be divided into two components as far as the delay is concerned. These are the dry and wet components. The dry component accounts for the majority (about 80-90%) of the delay effect and can be easily modelled. The dry effect corresponds to a delay of typically 2.3 m at the zenith and varies by less

than 1% over a few hours. On the other hand, the wet component varies by 10-20% over the same period. The magnitude of this delay is relatively smaller, namely 1-80 cm at the zenith. Lower elevation satellite signals have a much larger delay as the tropospheric path length increases. The delay terms for the wet and dry components can increase by up to a factor of ten as the elevation angle decreases. In general, for any satellite signal the tropospheric delay ranges from 2 to 25 m. Fortunately, tropospheric models can typically correct for about 90% of the delay. There are several models that estimate the tropospheric error. Saastamoinen (1972) proposed a constant lapse rate model for troposphere that estimates the delay as a function of elevation. Hopfield (1963) developed separate zenith models for the dry and wet components of the troposphere. This was further extended by Black and Eisner (1984) to include an elevation angle mapping function.

The tropospheric delay should be corrected by about 80-90% through modeling in any single point GPS receiver. In differential GPS, the spatial correlation of the delay between stations is very high and allows for the majority of the effect of the delay to be corrected by differencing. Thus, tropospheric effects are not an issue in the context of this study.

2.6.5 Multipath

Multipath is one of the larger error sources in both single point and differential GPS and is much more probable and significant for HS GPS users. Multipath is the error caused by reflected signals entering the RF front end and mixing with the direct signal. These effects tend to be more pronounced in static receivers close to large reflectors. As shown in Figure 2.11, reflectors of electromagnetic signals could be buildings, metal surfaces, water bodies, the ground, etc. Multipath errors are also specific to a receiver's antenna as each antenna has a different gain pattern.

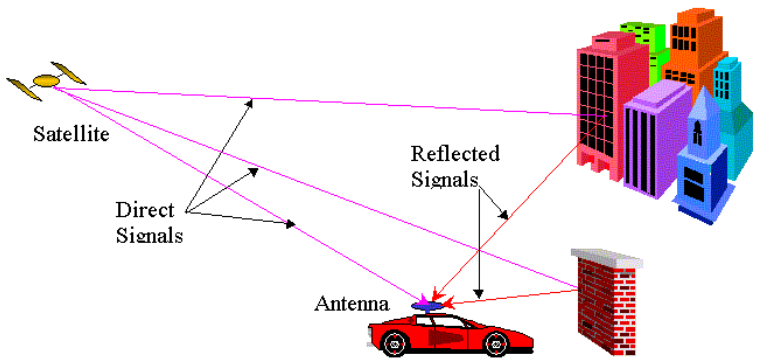

Figure 2.11: Multipath Environment

High sensitivity GPS users will likely be in closer proximity to reflection sources and line-of-sight signals may be weak in relation to the strength of the multipath signal.

The composite multipath signal can be expressed as (Braasch, 1996):

$$s(t) = -Ap(t)sin(\omega_0 t) - \sum_m \alpha_m Ap(t+\delta_m)sin(\omega_0 t + \theta_m) \tag{2.16}$$

where $s(t)$ is the composite signal, A is the amplitude of the direct signal, $p(t)$ is the pseudorandom noise sequence of the specific C/A code, ω_0 is the frequency of the direct signal, α_m is the relative power of the multipath signal, δ_m is the delay of the multipath signal with respect to the direct signal, and θ_m is the phase of the multipath signal with respect to the direct signal.

Code multipath errors depend on the code tracked by the GPS receiver. The C/A code has a maximum possible multipath delay of 1.5 code chips or 450 m. Code multipath errors can be of tens of metres with a maximum error of 150 m and are highly localized and hence cannot be removed through differential techniques (Ray, 2000).

Multipath signals are always delayed compared to the line-of-sight signals because of

the longer travel paths caused by reflection. Multipath can introduce both negative and positive error on the pseudorange measurement depending on the phase of the multipath signal. The direct and reflected signals will superimpose to produce the composite received signal and in turn affect the correlation property of the C/A code. This is illustrated in Figure 2.12 for the case of in-phase multipath.

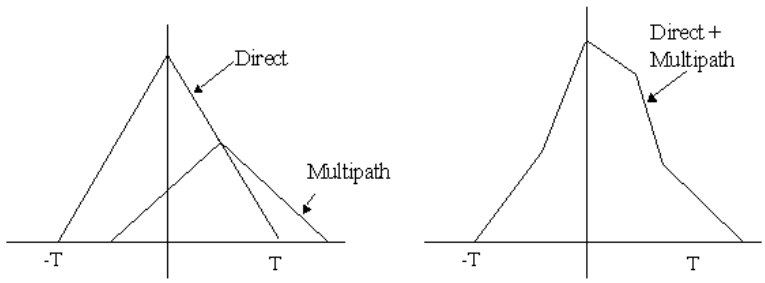

Figure 2.12: Multipath Effect On The Correlation Triangle

The superposition of the direct and the reflected signals can result in positive or negative pseudorange measurement error depending on the relative phase of the reflected signals. Multipath can be significant in magnitude but decorrelates both spatially and temporally. The temporal decorrelation is accelerated on a moving platform. The magnitude of the multipath error depends on the reflector distance and its strength, the correlator spacing and the receiver bandwidth.

Multipath can be classified into diffuse and specular reflection. Diffuse multipath results when the GPS signal gets reflected from rough surfaces and specular multipath results when the GPS signal gets reflected from smooth surfaces like metal surfaces. Multipath affects the code and carrier of the GPS signal in different ways, as described in Ray (2000).

Most multipath mitigation technologies are based on the design of suitable architectures in receivers that can minimize multipath and there are also special antenna

designs such as choke rings and other multipath-limiting antennas, which prevent multipath signals at low elevations from entering the RF section of the receiver.

Figure 2.13 illustrates multipath induced tracking errors encountered by various correlators. The standard correlator has a spacing of 1.0 chip between the early and the late correlators and a precorrelation bandwidth of 2 MHz. In contrast, the Narrow Correlator^{TM} has a precorrelation bandwidth of 8 MHz and a correlator spacing of 0.1 chip between the early and the late correlators (van Dierendonck et al., 1992). From Figure 2.13 it can be seen that the standard correlators are susceptible to substantial multipath errors for C/A code chip delays of up to 1.5 chips, with the most significant C/A code multipath errors occurring at about 0.25 and 0.75 chips (approaching 80 m error for the relative multipath power used to generate this figure). On the other hand, in case of the Narrow Correlator^{TM}, multipath susceptibility peaks at about 0.2 chips (about 10 m error) and remains relatively constant out to 0.95 chips, where it rapidly declines to negligible errors after 1.1 chips. The code multipath error envelope for two other techniques, namely MET^{TM} (Multipath Elimination Technique, (Townsend and Fenton, 1994)) and MEDLL^{TM} (Multipath Estimation Delay Lock Loop, (van Nee et al., 1994)) are also shown in Figure 2.13.

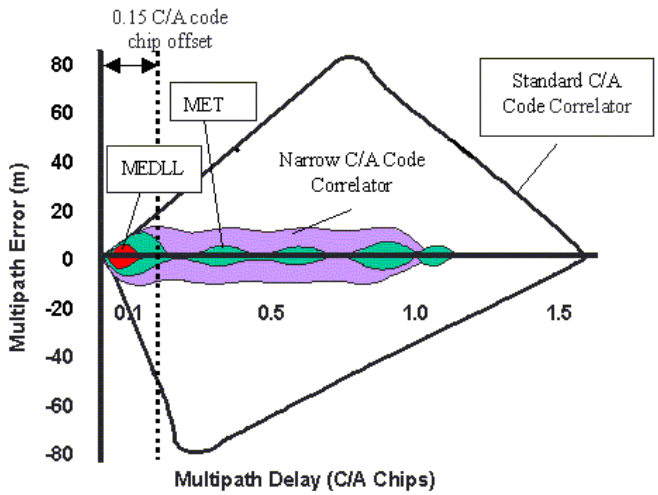

Figure 2.13: Multipath Error Envelope (Ford, 1998)

All correlator-based mitigation techniques are effective for long delay multipath errors but are less effective for short delay multipath. Hence, for a standard correlator with a spacing of 1 chip between early and late correlators, the maximum multipath delay can be 1.5 chips, which translates to 450 m. However, for Narrow Correlator^{TM} with a spacing of 0.1 chips, the maximum delay that can cause multipath error is 1.1 chips, which translates to 330 m.

Narrow correlation is not generally used in acquisition mode as it would require an unnecessary number of code bins to be searched. In tracking mode, narrow correlation requires a higher analog-to-digital sampling rate as it utilizes a higher precorrelation bandwidth. The noise power for both wide and narrow correlation is the same but there is some signal power gain, 0.4 dB, as 10% of the signal power contained in the sidelobes is utilized. Aside from the increased sampling frequency needed, narrow correlation methods might be beneficial for HS GPS in tracking mode.

In summary the maximum code multipath error can be up to $\pm$ 150 m for receivers

with wide correlator spacing (Ray, 2000). A multipath signal delayed by up to 450 metres can affect the pseudorange measurement. Multipath is not a zero mean process (van Nee et al., 1994) but decorrelates temporally and spatially.

2.6.6 Echo-Only Signal Tracking

It is likely that HS receivers will track echo-only signals where there is no possibility for multipath discrimination regardless of the type of correlator used. For example, this situation will arise in an urban canyon with skyscrapers blocking direct satellite signals while strong specular reflections from others building are tracked. The attenuated direct signal may still reach the antenna but if the power of the reflected signal is greater, the receiver will track the echo-only signal. This situation leads to large measurement errors greater than the maximum multipath error of $\pm$ 150 m for wide correlator receivers that will depend only on the echo signal geometry.

2.6.7 Pseudorange And Doppler Measurement Noise

Noise on the pseudorange and Doppler measurements increases as signal power decreases. This is due to increasing thermal noise jitter in the carrier and the code tracking loops. Measurement noise depends on correlation bandwidth (i.e. length of coherent integration), code tracking loop bandwidth, carrier tracking loop bandwidth, and type of correlation method.

The noise power depends directly on bandwidth of the coherent signal integration and can be computed by Equation 2.6 where the bandwidth of integration is $1/N$ and N is the length of the coherent integration (s).

Doppler measurement noise depends on the thermal noise of the carrier tracking loop and thus depends on the correlation bandwidth.

Pseudorange measurement noise depends on the bandwidth of the delay lock loop used in code tracking. It should be noted that this bandwidth can be greatly reduced by a carrier-aided DLL (Ward, 1996). In addition, pseudorange measurement noise depends on the correlation spacing and associated pre-correlation bandwidth. In other words, utilizing narrow correlation techniques significantly reduces pseudorange measurement noise. High sensitivity receivers should utilize narrow correlation techniques to reduce pseudorange measurement noise.

Weaker signals will have higher associated measurement noise in general. This can be characterized by using hardware GPS simulation to perform a signal tracking test whereby the power is lowered to the tracking threshold of the receiver and the measurement noise is characterized.

2.6.8 Self-Interference

The L1 C/A codes are pseudorandom noise codes (PRN codes). In general, noise correlated with noise results only in noise. Thus, as these codes are designed to be noise-like, their mutual interference after the correlation process should be minimal. However, the autocorrelation and cross-correlation properties for the C/A code are not ideal. The C/A codes have the following problems in terms of correlation properties:

- There are small autocorrelation peaks in the periods between maximum autocorrelation peaks (Ward, 1996).
- C/A-codes have a line spectra as a result of a repeating 1 ms long code sequence, and this is responsible for vulnerability to continuous wave (CW) interference (Ward, 1996). A narrow bandwidth coherent carrier tone signal, when overlaying a strong C/A-code spectral line, will correlate with the C/A-code and

may cause distortion of the correlation peak, lead to tracking of a false peak, or result in loss of tracking entirely.

- Since a C/A-code is only 1023 chips long, it has undesirable cross-correlation characteristics even amongst the 32 C/A-code Gold codes chosen for GPS usage. Of the possible C/A-codes that can be generated, the Gold codes have the more desirable cross-correlation properties. The cross-correlation functions have peak levels that reach -24 dB with respect to the autocorrelation peak (Ward, 1996). This is known to result in tracking of false correlation peaks at certain Doppler offsets and signal strength differences between signals (Ward, 1996).

These C/A-code properties can be especially problematic during search and acquisition mode operations. Acquisition of a false correlation peak due to cross-correlation signals or possible CW jamming leads to large measurement error.

High Sensitivity GPS Vulnerability

As HS receivers are expected to function with both low power and nominal power GPS signals, the problems associated with cross-correlation become magnified. It is conceivable that cross-correlation peaks and the true correlation peak could have the same power levels (-24 dB maximum offset as mentioned above). This leads to high probabilities of false correlation peak detection and tracking when using HS methods.

2.6.9 Signal Masking

GPS signals suffer from signal masking due to obstructions, such as buildings and dense foliage as shown in Figure 2.14. Signal masking may cause complete loss of

signal tracking and clearly induces attenuation of the direct signal. The direct signal may not be the strongest signal reaching the antenna. It is likely that echo-only signals are strongest in some cases. Such signal masking could cause large tracking errors.

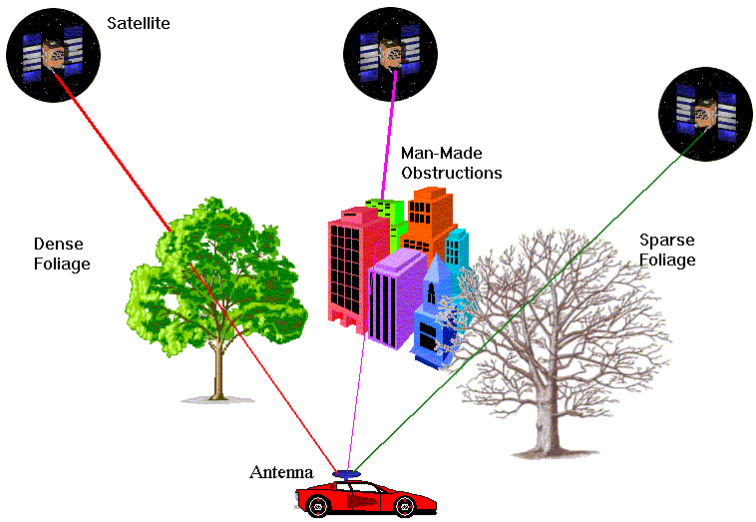

Figure 2.14: Signal Masking

The concept of the Fresnel zone, especially the first Fresnel zone, is used to characterize shadowing and blocking effects, as shown in Figure 2.15. The Fresnel zone is the volume of space enclosed by an ellipsoid, which has the two antennas A and B at the ends of a radio link as its foci. The first Fresnel zone is an ellipsoid defined such that the distance summation of a point C on the ellipsoid to A and B is one wavelength (λ) longer than the direct distance between A and B, and is given by

$$AC + CB = AB + \lambda \tag{2.17}$$

The fading effect is negligible if there are no objects in the first Fresnel zone, and significant otherwise.

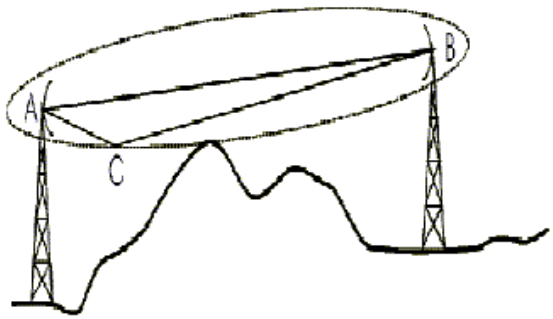

Figure 2.15: Fresnel Zone

According to the Fresnel theory, if the size of an obstacle is big enough to block the first Fresnel Zone, the strength of the diffracted signal arriving at the receiver is considered weak compared with that of the direct signal in the case of no obstacle. In terms of signal path-length, if the first Fresnel Zone is blocked, the diffracted signal will reach the receiver with a path-length longer than the direct signal by at least $\lambda/2$, and with a phase shift of 180^o. In order to avoid diffraction problems, one must ensure that most of the signals that go through the obstacle are stronger than the diffracted signals. As a result, the obstacle must be larger than the first Fresnel Zone in order to totally block this area and decrease the effect of diffraction.

For GPS the first Fresnel zone is very small as the distance to the satellites is great and the wavelength is very small in comparison. Thus, if an object blocks a line-of-sight signal it will most likely block the entire first Fresnel zone and significant fading will occur. Receiving strong signals via diffraction occurs only when the edge of the object is within the Fresnel zone. Thus, measurement errors due to diffraction are very small, less than 1 cm, and are well within the noise of the typical pseudorange measurement.

Thus, received GPS signals that are masked are either attenuated line-of-sight signals, multipath signals, or echo-only signals.

Propagation of GPS Signals Indoors

At a boundary surface between two materials, GPS signals may be reflected, absorbed, and refracted depending on the angle of arrival of the signal and the properties of the material. Material thickness, reflectivity, index of refraction, conductivity, and absorption properties all affect the attenuation of the line-of-sight signal.

Few studies so far have looked at signal propagation effects through different building materials for personal mobile satellite systems in the L-band of the RF spectrum. Vogel et al. (1995) investigated propagation effects for L-band signals at 1618 MHz and S-band signals at 2493 MHz by examining slant path signal fading for buildings using wood frame, concrete, cinder block, and brick construction. Typically only one or two walls affected signal propagation. Signal fades in the wood frame buildings were the smallest with typical fades of 8 to 10 dB. Concrete, cinder block, and brick buildings caused the strongest signal fading with typical fades of 15 to 20 dB.

A recent investigation at the University of Calgary investigated GPS pseudolite signal propagation through gyprock (drywall), plywood, cinder blocks, and an aluminum sheet (Lachapelle et al., 2002). Testing with an aluminum sheet and cinder blocks showed attenuation of the received signal with respect to the line-of-sight signal of more than 20 dB. Signal attenuation for plywood sheets (two sheets, each approximately 2.3 cm thick) was found to be 2 to 3 dB while attenuation for the drywall (two sheets, approximately 1.1 cm thick) amounted to less than 1 dB.

Thus, attenuation in wood frame buildings is expected to be much less than in concrete buildings or buildings with metal roofing.

Masking by Foliage

Foliage attenuation is often characterized as attenuation in dB/m of foliage penetration. The attenuation depends on the nature of the tree, namely its height, the foliage density and the trunk and branch sizes. When a mobile receiver is moving rapidly past intermittent trees, the mean attenuation should be considered instead of attenuation from a single tree. Spilker (1996a) provides comprehensive analysis on foliage attenuation of GPS signals on moving and stationary GPS receivers. Attenuation is primarily due to the wooden tree limbs and trunks with a tree in full foliage only causing 35% more signal attenuation.

2.6.10 Jamming And High Sensitivity GPS

A jammer is an intentional or unintentional signal that directly interferes within the L1 or L2 frequency bands. As high sensitivity GPS uses weak signals, the jammer-to-signal ratio will be higher for the weaker signals and interference may cause loss of signal tracking or large measurement errors. This section provides an overview of GPS signal jamming in general as well as a discussion of weak signal jamming issues.

High sensitivity GPS in principle operates at lower C/N_0 values and thus can tolerate more broadband interference than standard mode GPS when signals are strong. However, if weak signals are utilized the jammer-to-signal ratio will be higher and interference concerns increase.

The various sources of jamming are summarized in the Table 2.4.

Table 2.4: Sources of Jamming Interference (Ward, 1996)

Types of Interference	Typical Sources
Wideband-Gaussian	Intentional noise jammers
Wideband phase/frequency modulation	Television transmitter's harmonics or near band microwave link transmitters overcoming front-end filter of the GPS receiver
Wideband-spread spectrum	Intentional spread spectrum jammers or near-field of pseudolites
Wideband-pulse	Radar transmissions
Narrowband phase/frequency modulation	AM stations transmitter's harmonics or CB transmitter's harmonics
Narrowband-swept continuous wave	Intentional CW jammers or FM stations transmitter's harmonics
Narrowband-continuous wave	Intentional CW jammers or near-band unmodulated transmitter's carriers

Continuous Wave Interference and Sources

Continuous wave (CW) interference generally consists of signals with very narrow bandwidths, occupying less than 100 kHz (Rash, 1997). CW interference often only consists of one tone, i.e. one frequency. CW also implies that the signal is without any kind of modulation. Unmodulated narrow band interfering signals are hence referred to as CW signals.

The GPS C/A-codes are Gold-codes created by a specific combination of registers; they are not optimal codes (i.e. a 'maximum length' codes). This results in a line spectrum in the frequency domain which is susceptible to interference. CW interference may be particularly detrimental, as its peak in the frequency domain may coincide with these local peaks in the GPS L1 spectrum. Figure 2.16 depicts the GPS C/A-code line spectrum and such an interfering CW signal. When this happens, the signal leaks through in the correlation process and causes code measurement

errors or a complete loss of tracking.

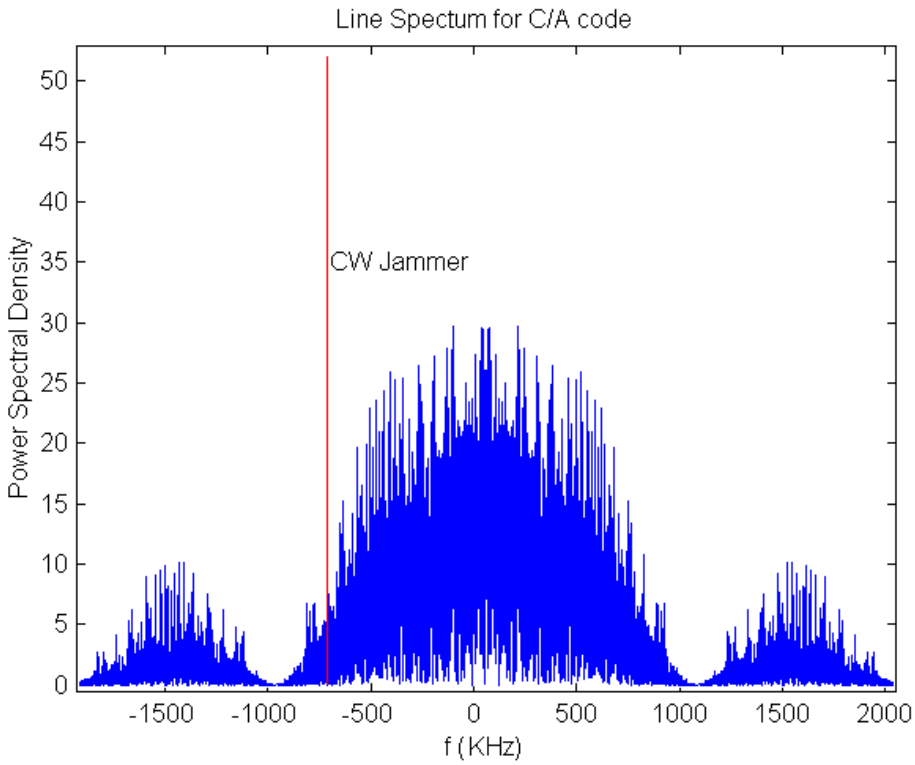

Figure 2.16: The C/A Code Spectrum And A Continuous Wave (CW) Jammer

Figure 2.17 depicts the effect of an in-phase 42 kHz CW Jammer for a 1 ms correlation interval using PRN 01 generated using Matlab. The jammer-to-signal ratio used was 12 dB. Correlation with and without the CW jammer is shown. There is both correlation peak degradation and the possibility of tracking one of the erroneous peaks or loss of tracking completely.

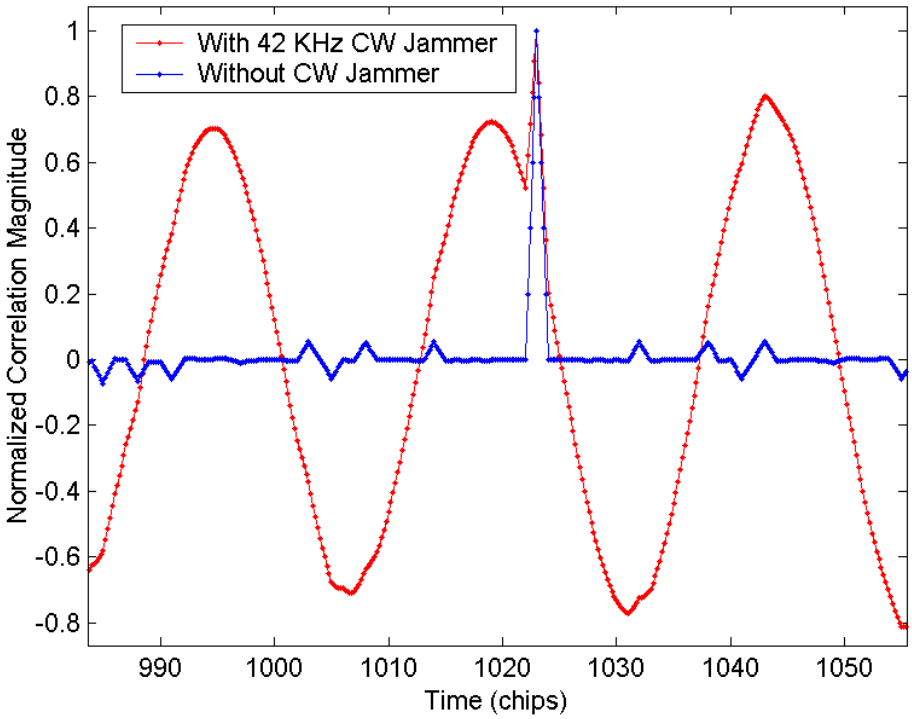

Figure 2.17: Effect Of A CW Jammer On The Correlation Process

CW is hence considered one of the most harmful kinds of interference to civilian GPS. It can be centered around L1, and effectively avoid filtering techniques due to the fact that all the interfering power is located within its narrow bandwidth.

CW interference is also known to trick the PLL tracking loop into locking in on the interfering signal instead of the GPS ranging signals, even after spreading by the correlation process.

Typical sources of CW interference in the GPS spectrum, apart from intentional jammers, are FM stations transmitter's harmonics or near-band unmodulated transmitter's carriers.

High sensitivity receivers are highly susceptible to CW interference when using weak GPS signals as the jammer-to-signal power is high.

Narrowband Interference and Sources

Narrowband interference usually refers to any unwanted signal occupying more than 100 kHz of bandwidth, but less than the entire broadcast spectrum available for C/A code, 20.46 MHz. Of course, what is a narrowband signal will also depend on the bandwidth of the wanted signal. Hence the same signal can be described as both wide and narrow, depending on the GPS receiver: A 5 MHz interfering signal can be regarded as wide if the receiver utilizes a wide correlator design with a 4 MHz pre-correlation filter, and narrow with narrow correlator designs, which have bandwidths of up to 20 MHz.

Generally, narrowband interference is usually centered on one of the GPS frequencies to effectively jam the receiver, but not necessarily so. The center frequency is usually what determines how destructive an interfering CW or narrow band interference signal is.

Unintentional narrowband interference most often arises from spurious signals generated by inadequately shielded electrical equipment. Some narrow band radio links adjacent to GPS frequencies are also known to cause local interference problems.

Wideband Interference and Sources

Wideband interference occupies the entire GPS C/A-code spectrum, covering bandwidths of 20.46 MHz (two-sided) or more (Rash, 1997). As with narrowband interference, wideband interference is regarded as dependant on the bandwidth of the original signal. The lower limit of what is considered wideband hence depends on the receiver pre-correlation filters.

Wideband jammers effectively lower the GPS signal C/N_0 ratio by increasing the noise level. The effect of such jamming varies from increasing the noise on code and carrier measurements to loss of signal tracking and the inability of the receiver to acquire the GPS signals.

Typical sources of wideband interference in the GPS spectrum, apart from intentional jammers, are television transmitter's harmonics or near band microwave link transmitters overcoming the front-end filter of the GPS receiver. Wideband noise from various electrical devices can lower the C/N_0 below a receiver's tracking threshold.

Unintentional in-band (RF signals generated within the GPS frequency band) sources of interference include pseudolite signals, that can sometimes overpower other signal channels and the different C/A codes that can interfere with each other in certain circumstances. Intentional in-band interference is associated with military jamming systems.

Out-of-band interference is typically generated by harmonic frequencies of transmitters outside the GPS frequency band. For example, television channel 66 broadcasts at close to 785 MHz and produces second harmonics centered very close to the L1 frequency, 1575.42 MHz.

The most effective form of wideband interference is called a spoofer. A spoofer is an intentional transmission of a false but strong version of a GPS signal so that it captures the receiver tracking loops and provides devious navigation information. Pseudolites can be considered spoofing signals in some circumstances. Military systems using spoofing are not as much of a threat as jamming because of the high cost of a spoofer versus a jammer.

High Sensitivity GPS Advantage

High sensitivity GPS in principle operates at lower C/N_0 values and thus can tolerate more narrowband and broadband interference than standard mode GPS.

2.7 Overview of Signal Degradation Phenomena in Relation to High Sensitivity GPS

During normal operation (no jamming effects), the signal degradation due to atmospheric attenuation and delay (both tropospheric and ionospheric), free space loss, satellite signal effects, and Doppler shift are clearly common to all methods of GPS signal tracking and acquisition and can usually be dealt with using a differential technique. However, self-interference effects, multipath, echo-only signal tracking, and increased measurement noise have been identified as distinct vulnerabilities in terms of the ability of an HS receiver to provide useful, unbiased measurements when using weak GPS signals.

For a HS receiver, signal reacquisition and tracking under signal masking conditions due to buildings and foliage are expected to improve in relation to standard mode operation.

In general, high sensitivity receivers have better resistance to narrowband and wideband interference than conventional GPS receivers as they inherently operate at lower C/N_0 levels; although, the jammer-to-signal ratio increases as signals become weaker. CW jamming resistance is the same for high sensitivity and conventional GPS. Thus, the potential for jamming of the weak GPS signals used in high sensitivity GPS is higher.

2.8 Degraded Mode GPS Environments

This section provides a brief classification of degraded mode environments that challenge conventional GPS, namely the forest environment, the urban canyon environment, and the indoor environment.

Propagation through the leaves, branches, and tree trunks of a forest environment causes signal attenuation and provides multiple sources of diffuse and specular reflectors. Environmental variables include the thickness of leaves and branches, the height of canopy and density of foliage, wind, humidity and the amount of recent rainfall.

Outdoor environments with large buildings (i.e. downtown environments) are considered urban canyons. They are characterized by signal masking, multipath, and echo-only signals due to skyscrapers and other high-rise buildings. Thus, signal attenuation and strong specular reflections are probable sources of signal degradation. In some cases, signal masking occurs from two directions only. For example, when driving in a city with streets running East-West and North-South, there will often be open sky perpendicular to the direction of travel. Environmental variables include height of buildings, reflective characteristics of buildings walls, orientation of city streets, and construction material used for skyscrapers.

The indoor environment is characterized by varying levels of signal attenuation from all directions with windows and doors sometimes providing clear signal propagation. Environmental variables include the number of building levels, building material types for roofs, walls, floors, and ceilings, the availability of windows for unobstructed signal sources, and the availability of reflected signals.

2.9 Background Summary

HS GPS is an emerging technology that faces the same interference sources as standard mode GPS but in a new context. Multipath, echo-only signals, self-interference, increased measurement noise, and CW jamming are probable sources of HS measurement degradation. These sources are more prevalent in signal environments where standard mode GPS is challenged, namely the forest environment, the urban canyon environment and the indoor environment.

Chapter 3

Test Measures And Methodology

3.1 Chapter Overview

Newly available HS GPS receivers provide the capability to make measurements in degraded mode GPS environments where conventional GPS receivers typically exhibit frequent losses of signal tracking and/or signal acquisition failure. This allows measurement availability in comparison with conventional GPS. In addition, signal attenuation with respect to line-of-sight (LOS) signals and pseudorange measurement degradation in such environments can now be estimated. The use of HS measurements will allow position determination when previously not possible although the position solution may be degraded by poor quality measurements.

Hardware GPS simulation provides a very effective method of assessing the tracking capability of HS receivers in relation to standard mode GPS receivers. In addition, interference susceptibility in terms of signal cross-correlation and CW interference can be assessed.

In order to achieve the proposed objectives of this thesis, the following specific test metrics are proposed: the measurement availability, the fading test measure, the estimated pseudorange error (EPE), and the least squares positioning accuracy and solution availability.

To utilize these test measures, a HS receiver along with a standard mode GPS receiver and a high grade GPS receiver are tested in various degraded mode environments in which each of the test measures are used for environmental characterization. These

environments include a forest, some urban canyon environments, and an indoor environment.

This chapter addresses the test measures utilized and describes the generalized testing methods necessary to facilitate their use.

3.2 Test Measures

The following test measures were developed to characterize measurement availability, positioning accuracy, and signal and measurement degradation:

- Measurement Availability
- Fading
- Estimated Pseudorange Error (EPE)
- Positioning Accuracy, Solution Availability, and Dilution of Precision

Each measure is explicitly defined and discussed in the following sections.

3.2.1 Measurement Availability

Measurement availability is used as a measure of the number of available measurements provided by each test receiver at each epoch. The statistics concerning availability assume that all available measurements provided by each test receiver are usable. That is, they contain no faults that adversely affect the position solution. The task to address the availability of usable measurements is not trivial. Reliability methods can be used to statistically test the measurements for such faults. This is addressed in the sections concerning positioning accuracy, solution availability, and dilution of precision.

3.2.2 Fading

Signal Power Reaching The GPS Receiver

At the typical GPS user's location, the received GPS L1 C/A-code signal power is specified to be at least -160 dBW at 5^o and 90^o elevation angles but will be as much as 2 dB higher at 40^o elevation angles (Ward, 1996). This characteristic is due to the shaped transmit beam pattern on the satellite transmitting antenna arrays. However, the signal power reaching the digital sampling section of a GPS receiver is also dependant upon the gain pattern of the receive antenna used and any ensuing line losses in the RF front end of the receiver. Most GPS antennas have maximum gain at the zenith and minimum gain at lower than 5^o elevation angles.

Carrier-To-Noise Density Ratio

Carrier-to-noise density ratio or C/N_0 is the best measurable value of the signal quality present at the input to a GPS receiver. C/N_0 is an instantaneous measure of the ratio of carrier power present to noise power density measured per Hertz of bandwidth. The nominal noise floor has a spectral density of approximately -204 dB-W/Hz. With minimum guaranteed line-of-sight GPS signal power at -160 dB-W, the nominal C/N_0 level is 44 dB-Hz. Theoretically C/N_0 is irrespective of the receiver used; however, each receiver must compute its value based on the measured signal. These estimators often utilize information measured by the automatic gain control (AGC), the signal-to-noise ratio measurement (SNR), and knowledge of the integration time of measurement. The noise density and carrier power are typically measured post-correlation (van Dierendonck et al., 2002). Thus, receivers with different correlation processes (e.g. 'wide' versus 'narrow') will have differences in C/N_0.

By itself, C/N_0 is not a good estimator of signal power degradation because it is

dependant on the antenna gain pattern and the correlation process used by the receiver. Short term variation in C/N_0 can be used as an estimate of signal degradation but a better estimator of signal power degradation is fading.

Fading

Signal strength degradation is due to two effects. The first effect is the attenuation of the LOS signal due to propagation through a material. This is often referred to as shadowing. The second effect is due to constructive and destructive interference when the GPS signal experiences interference, multipath for example. This effect is generally referred to as fading. However, for the purposes of this thesis fading will refer to both the shadowing effect and the interference fading effect.

The fading test measure is thus a measure of the signal strength degradation and can be measured by differencing a test receiver's carrier-to-noise density ratio data with that from a reference receiver of similar type located nearby with line-of-sight signal reception. Fading can thus be calculated as:

$$F = C/N_0^{reference} - C/N_0^{rover} \tag{3.1}$$

where F is the level of signal fade (dB), $C/N_0^{reference}$ is the carrier-to-noise density ratio at the reference station (dB-Hz), and C/N_0^{rover} is the carrier-to-noise density ratio at the test location (dB-Hz). As C/N_0 is a receiver dependant estimator, it is necessary that the fading calculations are performed with like-type receivers. In addition, like-type antennas (i.e. similar gain pattern) and line losses are needed at the reference station to ensure similar signal conditions. This method assumes that there is no signal power degradation at the reference station due to its local environment. This method also assumes that C/N_0 is a measure that reflects a linear relationship with actual signal power variation with a slope of 1.0.

In some test cases when the reference receiver is not available and the ensuing test period is short (less than 1/2 hr), the signal fading can be calculated by differencing the test period C/N_0 with the nominal C/N_0 value during the LOS warm-up period for each satellite.

Accuracy Of The Fading Test Measure

The assumption is made that the reference station is not affected by any localized signal power degradation effects. However, differences in gain pattern and multipath at the reference station will adversely affect the fading test measure. In an effort to determine the accuracy of the test measure a simple test was devised. Data was collected using like-type HS receivers and antenna combinations with similar line losses on the roof of the CCIT building on the University of Calgary campus. The receivers were offset by about 3 metres. Both antennas had a clear view of the sky above a 5^o elevation angle. By differencing the C/N_0 data from both receivers, statistics concerning the accuracy of the fading test measure were derived.

The antennas were not aligned in terms of azimuth and thus this test assumes that the antenna gain patterns are isotropic (azimuthally independent). The antennas used were NovAtel model 600 antennas. The designer of the NovAtel 600 antenna, Mr. Waldemar Kunysz, provided the information shown in Table 3.1 regarding the consistency of the 600 antenna in terms of azimuthal gain pattern variation.

Table 3.1: Azimuthal Variation Of The NovAtel 600 Antenna

Elevation Angle (^{o})	**Gain Pattern Variation 3σ (dB)**
0	3.0
10	2.2
15	2.0
20	1.9

Figure 3.1 shows the C/N_0 measured by both receivers for PRN13 and the corresponding difference in C/N_0 as well as the satellite's elevation angle. There is a direct correlation between fading variation and elevation. To further investigate this behavior, the C/N_0 data from all satellites was binned into elevation groups and the distributions for each group along with the mean and standard deviation for each group are shown in Figure 3.2. The precision of the fading test measure is reflected in the standard deviation for each elevation group. This varies from 4.4 dB at 2σ for 0 to 15 ^{o} to 1.4 dB at 60 to 75 ^{o}. As each elevation group is very close to zero mean the accuracy of the fading test measure is reflected by its precision.

The test measure degrades with elevation. This is likely due to slight differences in antenna gain pattern and local multipath. The information collected at low elevation angles in degraded mode environments is of key interest for analysis as high elevation satellite signals are often not as affected by environmental interference such as multipath. However, sufficient accuracy is still present for useful analysis of fading data.

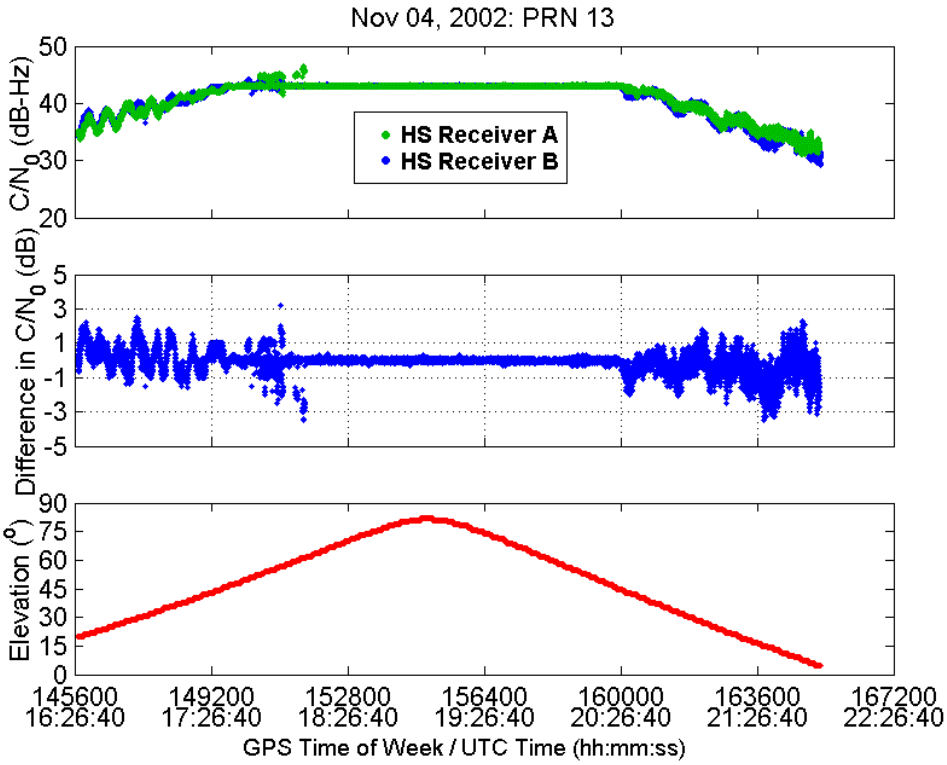

Figure 3.1: C/N_0 And C/N_0 Differences For PRN13 As Function Of Satellite Elevation

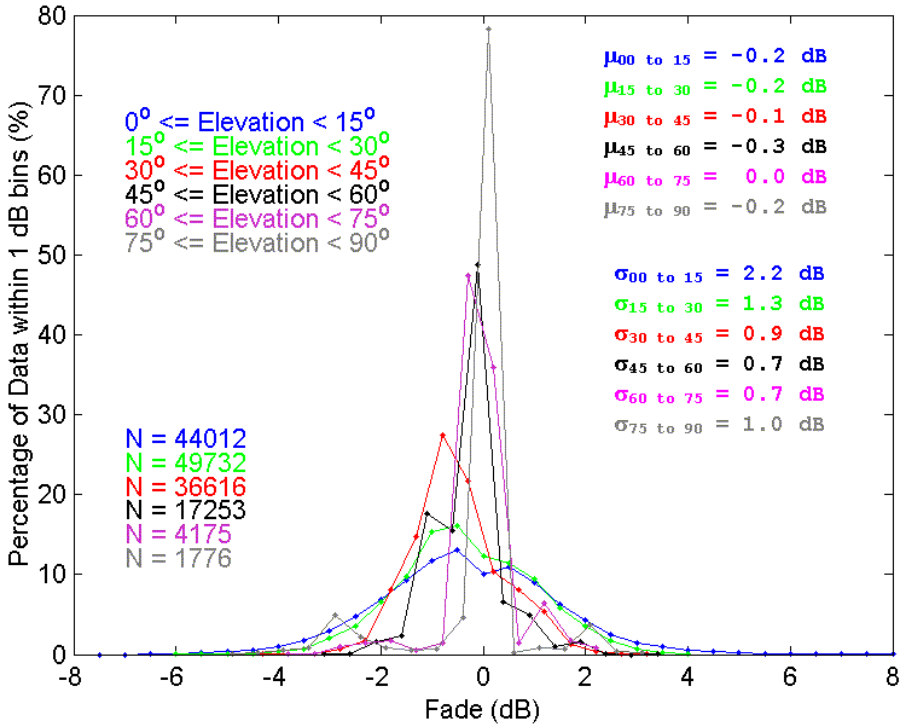

Figure 3.2: Distributions For Open Sky C/N_0 Differences

As C/N_0 is also assumed to be a linear measure estimated by the test receivers, differencing of C/N_0 as a measure of signal fading is dependant upon that assumption. If 1 dB of fading does not correspond to one decibel of C/N_0 difference, this must be accounted for. A hardware simulation signal power tracking threshold test can provide information about the relationship between actual power variation and C/N_0 difference variation. This must be performed in order to use the C/N_0 difference as a fading statistic. This will be addressed further in Chapter 4.

3.2.3 Estimated Pseudorange Error

To determine the extent to which multipath, noise, echo-only signals, and other interference degrade the pseudorange measurements taken at the test site, the test receiver's raw data can be post-processed using estimation techniques in which the errors on the measurement to each satellite are estimated. This test metric is hence referred to as estimated pseudorange error or EPE.

EPE is determined by two methods in this thesis depending on the testing context. For static testing, a Kalman filtering approach is taken, unless otherwise stated, that utilizes the known position and velocity in estimating the EPE values. In kinematic testing, a least squares approach, in which the positions are constrained to known values, is used to estimate the EPE values. This is due to the complexity of the kinematic case as providing continuous truth trajectory information is very difficult. The least-squares approach will be discussed first followed by an explanation of the Kalman filtering estimation method.

Least Squares Approach

The test receiver's raw data can be post-processed using parametric least squares with positions fixed to the known test locations. In addition, single difference corrections from the base station receiver can be utilized to reduce the effect of spatially correlated errors. The residuals of this solution provide a measure of the unmodelled effects left in the measurements. This statistic is relative between satellites as the estimation of the receiver clock bias will absorb some of the unmodelled error effects in each measurement.

This is accomplished using C^3NavG^{2TM}, a software package developed at the University of Calgary. C^3NavG^{2TM} is a C program that processes GPS and/or GLONASS

pseudorange and Doppler data in both static and kinematic modes to determine position and velocity in either single point or differential mode. The program also allows carrier smoothing of pseudoranges, differential positioning, and height fixing.

Epoch-by-epoch GPS pseudoranges can be described by the parametric least squares model (Krakiwsky and Abousalem, 1995):

$$l = f(x), C_l, \tag{3.2}$$

where l is an $nx1$ vector of the pseudorange measurements, x is a vector containing the unknown user position and receiver clock bias, and C_l is the variance covariance matrix of the measurements. The measurement model is described in Equation 2.1. For simplicity, in the following discussion, the receiver clock bias is assumed to be a known value and is removed from x.

This least-squares process is iterative as the measurement model is non-linear and must be linearized. Thus, the estimated unknowns converge with each iteration. This is explained by:

$$\hat{x} = x_0 + \hat{\delta} \tag{3.3}$$

where $\hat{x}$ are the adjusted unknowns, x_0 is the a-priori approximate unknowns, and $\hat{\delta}$ is the estimated iteration correction to the unknown parameters. $\hat{\delta}$ is calculated by:

$$\hat{\delta} = (A^T C_l^{-1} A)^{-1} A^T C_l^{-1} w \tag{3.4}$$

where A is the design matrix, and w is the measurement misclosure. The residuals of the least squares solution

$$\hat{r} = A\hat{\delta} + w \tag{3.5}$$

are minimized in the final solution but if the unknown parameters (concerning position) are well known:

$$C_{\hat{x}} = I * \sigma_x^2, \sigma_x^2 \approx 10^{-12} m^2 \tag{3.6}$$

and

$$C_{\hat{x}} = (A^T C_l^{-1} A)^{-1} \tag{3.7}$$

then

$$\hat{\delta} = C_{\hat{x}} A^T C_l^{-1} w \approx 0 \tag{3.8}$$

thus

$$\hat{x} = x_0 \tag{3.9}$$

and

$$\hat{r} = w \tag{3.10}$$

The misclosure vector is defined by

$$w = l_{predicted} - l_{observed} \tag{3.11}$$

and thus any unmodelled effects in the measurements can be observed in the residuals of a position constrained least-squares filter.

However, since the receiver clock bias is not known and only the position is being constrained, this parameter is still estimated. This makes the EPE statistic somewhat relative between measurements. The simplified measurement equation is

$$P = \rho + cdT + \varepsilon \tag{3.12}$$

where P is the measured pseudorange, c is the speed of light, dT is the receiver clock bias, and ε is the unmodelled range error, and this aids in explaining the relative nature of this EPE statistic. The impact of a 10 m measurement error, with two satellite measurements in solution:

$$P_{SV01} = \rho_{SV01} + cdT + 10m \tag{3.13}$$

$$P_{SV02} = \rho_{SV02} + cdT + 0m \tag{3.14}$$

leads to 5 m of the error averaging into the clock bias while the residuals corresponding to each range will be 5 m each. In addition, any common unmodelled errors are also propagated into the estimation of the receiver clock bias. To limit the effect of large measurement faults distorting the EPE estimates, residuals greater than 150 m are rejected from solution. This is discussed further in a later section entitled 'Large Anomalous Error Effects'.

Kalman Filtering Approach

Kalman filtering can reduce the distortion of the EPE values due to error absorbtion by the receiver clock estimate. This is effectively accomplished by using the estimates of the receiver clock drift to drive the receiver clock estimates.

Kalman filtering is a useful technique for estimating the state of a system given a previous state, an assumed set of system dynamics, and external measurements of the state variables, or functions thereof. The method incorporates the covariance information of both the state variables and the external measurements to provide a statistically optimal estimate. A summary of the equations used in a basic Kalman filter is given in Gelb (1974), and is shown in Table 3.2.

Table 3.2: Summary of Discrete Kalman Filter Equations

System Model	$\underline{x}_k = \Phi_{k-1}\underline{x}_{k-1} + \underline{w}_{k-1}$, $\underline{w}_k \sim N(\underline{0}, Q_k)$	(1) (2)
Measurement Model	$\underline{l}_k = A_k\underline{x}_k + \underline{v}_k$, $\underline{v}_k \sim N(\underline{0}, C_{l_k})$	(3) (4)
Initial Conditions	$E[\underline{x}(0)] = \underline{\hat{x}}_0$, $E[\underline{x}(0) - \underline{\hat{x}}_0)(\underline{x}(0) - \underline{\hat{x}}_0)^T] = Cx_0$	(5) (6)
Other Assumptions	$E[\underline{w}_k \underline{v}_j^T] = 0$, for all j, k	(7)
State Estimate Extrapolation	$\underline{\hat{x}}_k(-) = \Phi_{k-1}\underline{\hat{x}}_{k-1}(+)$	(8)
Error Covariance Extrapolation	$C_{x_k}(-) = \Phi_{k-1}C_{x_{k-1}}(+)\Phi_{k-1}^T + Q_{k-1}$	(9)
State Estimate Update	$\underline{\hat{x}}_k(+) = \underline{\hat{x}}_k(-) + K_k[\underline{l}_k - A_k\underline{\hat{x}}_k(-)]$	(10)
Error Covariance Update	$C_{x_k}(+) = [I - K_kA_k]C_{x_k}(-)$	(11)
Kalman Gain Matrix	$K_k = C_{x_k}(-)A_k^T[A_kC_{x_k}(-)A_k^T + C_{l_k}]^{-1}$	(12)

Where,

M	A matrix or vector
A	Amplitude
M_k	Denotes a matrix or vector at time k
M_{k-1}	Denotes a matrix or vector at time k-1
$\underline{M}$	Denotes a vector
$M(-)$	Denotes a prior estimate
$M(+)$	Denote an updated estimate
$\hat{M}$	Denotes an estimated matrix or vector
$E[]$	Expectation Operator
$\underline{x}$	State vector of estimated parameters
$\underline{w}$	Input (driving) noise vector
$\underline{v}$	Measurement noise vector
$\underline{l}$	Measurements
Φ_{k-1}	Transition Matrix

A_k	Design Matrix
K_k	Kalman Gain Matrix
C_x	Covariance Matrix concerning the state vector
I	Identity Matrix
C_l	Covariance matrix concerning the measurements = $E[vv^T]$
Q_k	Process noise matrix = $E[ww^T]$

The Kalman filter developed to estimate pseudorange errors uses single difference pseudorange and Doppler measurements. Measurements from a nearby reference station using a high quality receiver facilitates these single differences. Using single differencing effectively eliminates satellite clock errors, orbital errors, and atmospheric delays. The resulting measurement equations are described by the following equations.

$$\Delta P = \Delta\rho + c\Delta dT + \Delta\varepsilon_M + \Delta\varepsilon_\phi \tag{3.15}$$

$$\Delta\dot{\phi} = \Delta\dot{\rho} + c\Delta\dot{dT} + \Delta\varepsilon_{\dot{M}} + \Delta\varepsilon_{\dot{\phi}} \tag{3.16}$$

Where,

c	Speed of light (m/s)
	Single difference pseudorange measurement (m)
$\Delta\rho$	Single difference geometric range (m)
ΔdT	Single difference receiver clock offset (m)
$\Delta\varepsilon_M$	Single difference multipath delay (m)
$\Delta\varepsilon_\phi$	Single difference pseudorange noise (m)
$\Delta\dot{\phi}$	Single difference Doppler measurement (m/s)
$\Delta\dot{\rho}$	Single difference geometric range rate (m/s)
$\Delta\dot{dT}$	Single difference receiver clock drift (m/s)
$\Delta\varepsilon_{\dot{M}}$	Rate of change of single difference multipath delay (m/s)
$\Delta\varepsilon_{\dot{\phi}}$	Single difference Doppler noise (m/s)

The transition matrix is based on the following equations:

$$\Delta dT_k = \Delta dT_{k-1} + \Delta d\dot{T}\Delta T \tag{3.17}$$

$$\Delta d\dot{T}_k = \Delta d\dot{T}_{k-1} \tag{3.18}$$

where ΔT is the change in time from T_{k-1} to T_k.

This filter effectively solves for the receiver clock drift while the receiver clock offset is driven by the clock drift and a good apriori estimate. This estimate was obtained by examining and selecting least squares solutions for the first ten epochs of the dataset. It should be noted that the variance of ΔP with respect to $\Delta\dot{\phi}$ is high thereby reducing the amount a large pseudorange measurement error affects the estimate of the receiver clock drift.

The innovation sequences are tested for Doppler measurement blunders while the pseudorange measurements are not rejected unless greater than 150 m. The resultant pseudorange residuals in this filter provide very good estimates of the pseudorange errors.

The process noise concerning the receiver clock drift was chosen by first examining the filter performance in comparison with the least squares method using a hardware simulation test with no error sources. A NovAtel OEM4 receiver was used to perform this testing as it's receiver clock offset is very stable. First, the process noise was set very high to effectively emulate the least squares estimation. The process noise was then lowered in multiple iterations while observing the impact on the receiver clock offset. A more pessimistic value was then selected for use with the SiRF receivers.

Large Anomalous Error Effects

The tracking of a cross correlation peak or a peak due to an echo-only signal leads to very large pseudorange error effects. If such an error occurs, it will distort the EPE

statistics for the other satellite measurements. This is due to the estimate of the single difference clock offset absorbing some error from each measurement. This occurs albeit to a lesser extent even if the receiver clock estimate is driven by the clock drift in the Kalman filtering approach. If one measurement is a large fault, that fault will be averaged into the SD clock offset and the EPE values for the other measurements will adjust as well. In order to reduce the effect of large pseudorange error effects, measurements with EPE values above 150 m (the maximum multipath error) will be rejected from the solution. The number of large measurement fault occurrences relative to the number of EPE estimates will be determined for each satellite and shown in the time series analysis sections. The impact of these measurement faults will also be observed in the positioning accuracy sections of the chapters containing the results of field testing.

3.2.4 HS Fading and EPE Time Series Analysis

The fading, absolute EPE, and elevation values for each satellite are shown in time series figures for the HS receiver in each environment. In addition, the number of large anomalous error effects and the number of EPE estimates for each satellite are shown in these figures.

3.2.5 Positioning Accuracy, Solution Availability, and Dilution of Precision

In order to assess the impact of the pseudorange errors induced in each test, it is necessary to examine the positioning accuracy achievable with the available measurements on an epoch by epoch least-squares basis using C^3NavG^{2TM} in differential mode. This means that all the measurements must be included in the solution. How-

ever, measurement faults do occur and will need to be removed from the solutions if possible. For this reason, epoch by epoch least-squares solutions with fault detection and exclusion enabled are computed as well. This is accomplished by a test of the standardized residuals whereby a measurement is rejected if it exceeds a threshold value of 3.28 and the solution is recomputed. In static and some kinematic testing the height is well known, thus a height fix will be used to improve the ability to detect measurement faults and only the horizontal position domain will be assessed. Dilution of precision, DOP, will be indicated for each solution computed to assess the influence of solution geometry.

The solution availability is desirable for solutions when not adversely affected by poor DOP. Thus, solution availability will be presented for testing when position DOP or PDOP is less than 5.0 and fault detection and exclusion is enabled.

3.3 Testing Methodology

Initial receiver performance characterization and testing is performed using a hardware GPS simulator and is discussed in Chapters 4 and 5. Further performance evaluation is accomplished by extensive field testing. In tests described in subsequent chapters, a HS receiver along with a standard mode GPS receiver and a high grade GPS receiver are taken to degraded mode environments in which each test measure is assessed. All receivers are tested in parallel.

The HS receivers provided need to have approximate position, ephemeris information for each satellite, and an accurate estimation of GPS time before they can fully utilize long integration intervals and provide measurements of low power signals. Thus, testing must begin with a warmup period in open-sky conditions long enough to allow the receivers to obtain this information. Twelve minutes are required to download

the full GPS navigation message. This provides the receiver with enough information to aid in the acquisition of satellite signals and use high sensitivity methods. Thus, a warmup period of 20 minutes should be sufficient to obtain all the information needed. This method of testing is referred to as testing in a tracking-mode context.

A nearby reference station with receivers of similar type using a like-type antenna with similar line-losses is necessary to facilitate the fading test measure and the single difference operations used to compute EPE values.

A GPS/INS system, namely the NovAtel Black Diamond^{TM} system, is used in some of the testing to establish high accuracy test trajectories when possible. Reference trajectories will only be used for EPE calculation if they are deemed to have better than 5 m 3D accuracy at 1-sigma. In addition, the accuracy of the Black Diamond solution will be compared to digital road maps whenever possible to verify solution accuracy.

In all tests, the GPS antenna will not be interfered with by the user. In other words, the impact of user specific signal attenuation due to head shading for example will be minimized.

3.3.1 Parallel Comparison Of Receivers

It is useful in GPS receiver testing, to test a receiver in parallel with an equivalent or higher quality receiver. This allows for effects common to both receivers to be identified and vice-versa. This practice is hereby referred to as parallel comparison of receivers.

In most cases, a specific GPS receiver is tested in parallel with a reference receiver or multiple reference receivers. This setup is shown Figure 3.3 where a signal splitter is used to share the GPS signal with multiple GPS receivers.

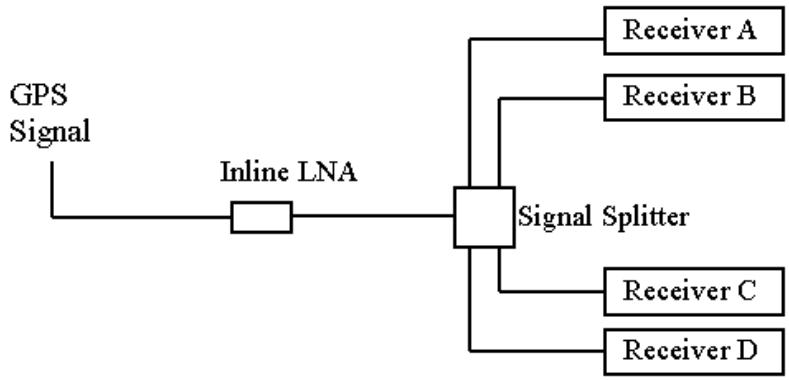

Figure 3.3: Parallel Receiver Comparison

Figure 3.3 shows the use of a common low noise amplifier (LNA). This LNA acts to set the signal conditions to similar values for each receiver. In simulation mode, it simulates the effect of a common antenna. In order to ensure valid comparisons, the signal conditions experienced by each receiver must be very similar. Under field conditions, this is achieved by using a common active antenna. The diagram in Figure 3.4 illustrates the signal processing chain of every GPS receiver.

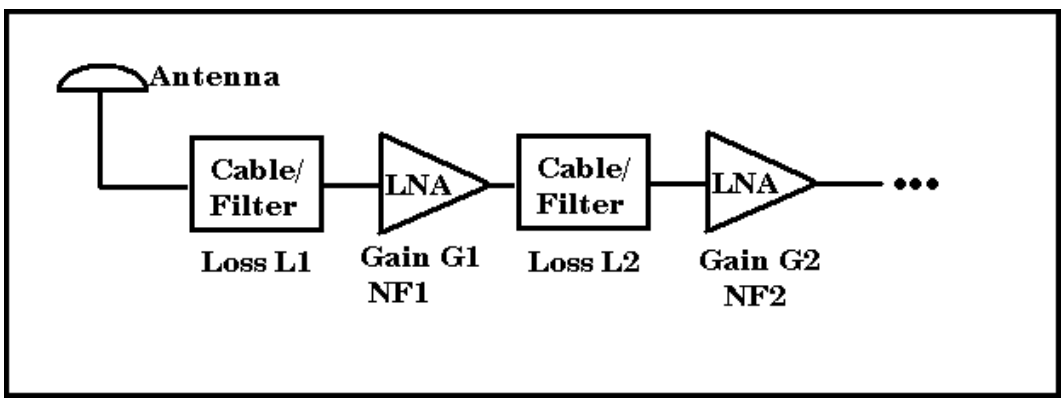

Figure 3.4: GPS Receiver RF Processing Chain

Different receivers have different gains, losses, and noise figures for each step in the

signal processing chain. Often the first filter, gain, and noise figure in the chain are associated with the antenna. The first gain of the RF processing chain is the most important in terms of setting the effective noise for the ensuing processing steps. This is explained mathematically by the Friss Formula shown in Equation 3.19.

$$NF_{system}(dB) = 10log_{10}(1 + \frac{T_{sys}}{T_0}) \tag{3.19}$$

where

$$T_{sys} = T_S + T_R \tag{3.20}$$

and

$$T_R = T_0((L_1NF_1 - 1) + \frac{L_1}{G_1}(L_2NF_2 - 1) + \frac{L_1L_2}{G_1G_2}(L_3NF_3 - 1) + ...) \tag{3.21}$$

where NF_i is the system noise figure (ratio), T_{sys} is the system noise temperature (^oK), T_0 is the Ambient Noise Temperature (290^oK), T_S is the source (antenna) temperature (^oK), T_R is the receiver noise temperature (^oK), G_i is the gain of a processing step (ratio), and L_i is the loss of a processing step (ratio). It can be clearly seen that the ensuing gains and losses are scaled by the first gain of the system.

In the case of hardware simulations, there is no antenna and the source temperature is actually room temperature rather than antenna temperature. This means that the noise level in a simulated environment in general is higher than in the real case. In order to set the effective noise level equally for receivers in a parallel comparison, a high gain must be applied at the first processing stage. This sets the effective noise floor for the system. The noise figures for the individual receivers still have an effect on the noise level but are scaled by that first gain.

The NovAtel 600 antenna has $26 \pm 3\ dB$ gain and a noise figure of 2.5. In simulation, a low noise amplifier with an effective 20 dB gain was used to set the effective noise floor for the receivers.

3.4 HS Performance Characterization using Hardware Simulations

Hardware GPS simulators capable of simulating 8 to 12 GPS satellite signals are available for commercial testing. They allow simulation of complex satellite and vehicle motion and control of signal levels and error sources such as atmospheric delays, orbital perturbations, satellite clock effects, and to some extent multipath.

It is useful to characterize the signal power tracking threshold of the new HS receivers with respect to standard mode GPS receivers. Hardware simulation provides an effective means to test this given the tracking-mode testing constraint associated with the use of the HS receiver.

This test will allow characterization of receiver tracking performance over a range of weak signal conditions. The idea is to allow the test receivers to track nominal signals of equal power for a warmup period of 20 minutes. After this period, the power levels of each channel are reduced by Y dB every Z seconds until the receiver loses track of all satellites.

The results of this test also determine the relationship between actual power variation and C/N_0 variation. This relationship must be used to scale the fading test measure if a one-to-one relationship is not present.

The simulator is also useful in demonstrating the susceptibility of HS receivers to cross-correlation and CW interference effects. This is discussed in Chapter 5.

3.5 Description Of GPS Receiver Tested

A SiRF unaided high sensitivity GPS receiver (HS receiver) and conventional SiRF receivers (ST receiver) were used in testing along with a geodetic grade NovAtel OEM4 receiver.

Both the HS and conventional SiRF receivers utilize the SiRFSTAR IIe chip-set and have the same hardware configuration. Figure 3.5 shows the receiver evaluation kit provided by SiRF Technologies Inc. and Table 3.3 provides descriptive details of the SiRF receivers. The receivers only differ in terms of the amount of dwell time used in signal processing. The conventional receiver utilizes up to 12 ms total dwell time while the high sensitivity receiver has coherent integration and non-coherent accumulation for a total of somewhere between 340 and 800 ms of dwell time. The exact dwell time is proprietary. The chip-set is designed for use in low cost receivers and OEM integration with devices such as cellular phones. The receivers are designed for use with an active antenna (i.e. containing a low noise amplifier) and function well using the NovAtel 600 antenna.

The NovAtel OEM4 receiver is used for comparison purposes in some cases. It is a conventional GPS receiver in that it uses a dwell time less than 20 ms but it is a high quality geodetic grade L1/L2 (3^{rd} order DLL, 3^{rd} order PLL) GPS receiver that provides precise pseudorange measurements using the PAC^{TM} correlation technology, Doppler measurements and carrier phase measurements.

Figure 3.5: The SiRF HS Receiver

The specific details of the SiRF receivers tested are shown in Table 3.3.

Table 3.3: Descriptions of Receivers Under Test

Receiver	**Software Version**	**Description**
SiRF High Sensitivity (SiRFStarIIe [1]LP chipset)	2.0.1A134(HS) May 21	12-Channel L1-only C/A code with carrier aiding **340-800 ms dwell time** Wide correlator 25 ppm [2]VCO 2^{nd} order DLL 2^{nd} order PLL (FLL aided)
SiRF Standard (SiRFStarIIe LP chipset)	2.0.1P00333L1S_1ADS	12-Channel L1-only C/A code with carrier aiding **4 or 12 ms dwell time** Wide correlator 25 ppm VCO 2^{nd} order DLL 2^{nd} order PLL (FLL aided)

[1]LP: Low Power
[2]VCO: Voltage Controlled Oscillator

Chapter 4

High Sensitivity GPS Receiver Sensitivity Performance Characterization Using A Hardware Simulator

4.1 Hardware GPS Simulation

In recent years, advances in simulation technology have contributed to the development of state-of-the-art hardware GPS signal simulators. Spirent Communications Inc. makes the STR-6560 GPS simulator. The simulation system used by University of Calgary comprises of a control computer and two synchronous 12-channel L1-only hardware signal simulation units. This system is shown in Figure 4.1.

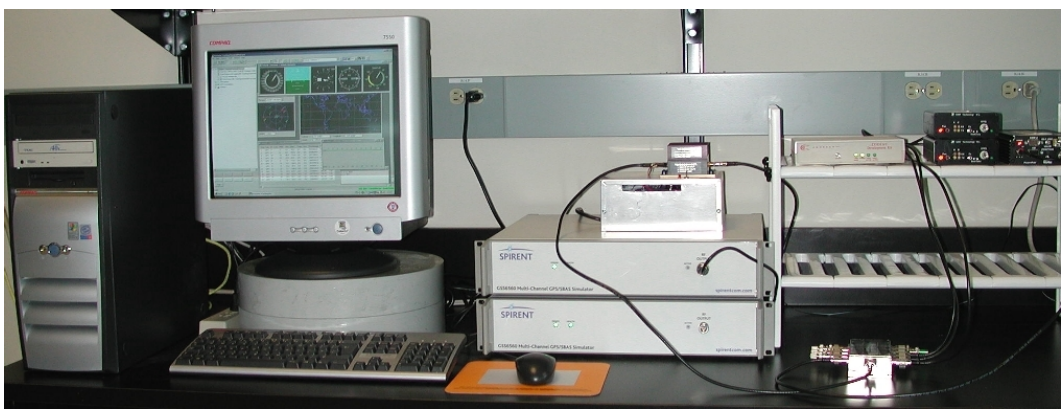

Figure 4.1: Spirent STR-6560 Hardware GPS Signal Simulator

Some of the simulator capabilities are as follows:

- Control of the signal power for each channel

- Complex simulated vehicle trajectories
- Multipath simulation
- Satellite constellation definition and modeling
- Atmospheric effects modeling (Iono/Tropo)
- Vehicle motion modeling for aircraft, cars, and spacecraft
- User supplied motion trajectories
- Antenna gain pattern manipulation
- Pseudorange error ramping
- Terrain obscuration modeling
- ASCII format scenario files (sharable between scenarios)
- Real time data display
- Post mission truth data output

4.2 Simulator Tracking Threshold Test

The simulator allows real-time control of the signal level at ± 20 dB with respect to -160 dBW for each satellite corresponding to one channel of signal output. This power level is referred to as relative channel power. The signal level can be set equally or differently and varied by predefined amounts for all channels. The C/N_0 threshold for tracking weak signals can be determined by lowering the signal level slowly until the receiver is no longer able to track the satellite. In addition, the variation in C/N_0 due to actual signal power variation can be assessed by this test. This is useful in determining if signal power fade, as measured by the fading test measure, has a linear relationship with C/N_0 differences with a slope of 1.0.

4.2.1 Methodology

A test was designed with 10 to 12 satellites in simulation and no orbital, atmospheric or any other errors. Three GPS receivers were tested in parallel as shown in Figure 4.2. The channel power for each satellite was set equally at a relative simulator channel power of 12 dB for a warmup period of twenty minutes. The power was then lowered in 0.1 dB decrements every 5 seconds to -20 dB, the lowest power setting achievable on the simulator. The simulator relative channel power during the test is shown in Figure 4.3. In order to achieve higher levels of signal attenuation, a 9 dB attenuator was inserted prior to the low noise amplifier (LNA). The LNA provides a 30 dB gain while also setting the effective noise floor thus providing similar carrier to noise density signals for each receiver under test. The following 10 dB attenuator provides the LNA with burnout protection while the LNA and following attenuator still effectively simulates the effect of an active GPS antenna. Note that an active antenna or external LNA is required for all the receivers tested for proper receiver function.

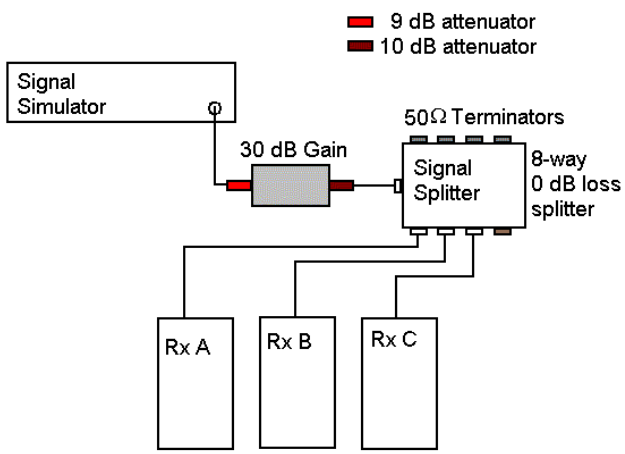

Figure 4.2: Signal Tracking Threshold Test - Test Setup

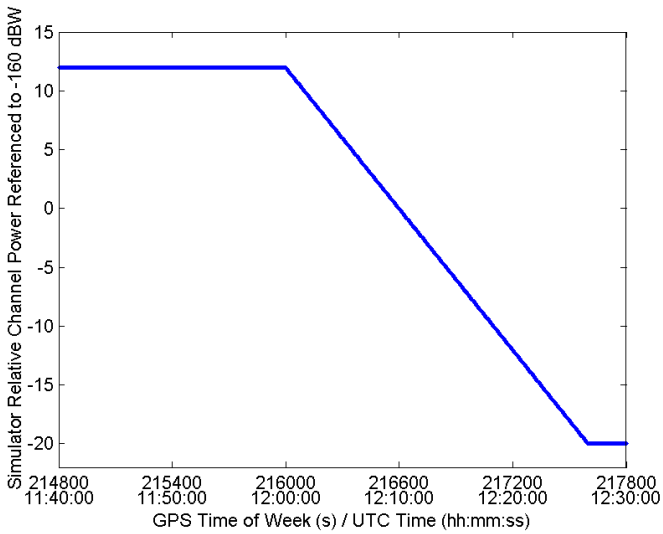

Figure 4.3: Signal Tracking Threshold Test - Simulator Relative Channel Power

Using the method of parallel receiver comparison as discussed in Chapter 3, a HS SiRF was tested along with a NovAtel OEM4, and a standard SiRF receiver. The NovAtel OEM4 is a geodetic-grade 24 Channel L1/L2 receiver used as high grade reference comparison.

4.2.2 Results

The number of satellites tracked by each receiver and the simulator relative channel power is shown in Figure 4.4. The average C/N_0 receiver measurements for all satellites tracked is depicted in Figure 4.5. Raw pseudorange data was extracted at 1 Hz from each receiver and processed with C^3NavG^{2TM}. The receivers' position errors and the relative channel powers are shown in Figure 4.6. The time at which less than 4 satellites were available in solution and the simulator channel powers for each receiver are shown in Table 4.1 along with the receiver measurements of C/N_0. The time at which the last available measurement is taken for each receiver, the

simulator channel power and the approximate C/N_0 are shown in Table 4.2.

As C/N_0 is a biased estimator, a simple estimate that is common to all receivers is useful for comparison purposes in tracking performance. Noise density, derived via Equation 2.6, is

$$N_{density} = kT \tag{4.1}$$

For this simulation test, a pessimistic assumption of a noise temperature at 40^oC or 313^oK results in a noise power density of approximately -203.6 dBW/Hz. As the simulation power is very accurately known, an estimate of the C/N_0 for each receiver can be computed. Thus, an estimate of C/N_0 for each receiver during this simulation is given by

$$C/N_{0estimate} = -160 + S_p - 9.0 -^{-} 203.6 \tag{4.2}$$

where $C/N_{0estimate}$ is the carrier to noise density ratio estimate (dB-Hz), S_p is the simulator relative channel power, -9.0 is the effect of the inline attenuator prior to the low noise amplifier (dB), and -203.6 is the noise power density for the simulation (dBW/Hz).

The HS receiver is able to track signals to close to a C/N_0 of 18 dB-Hz corresponding to between -16 to -17 dB simulator relative channel power or equivalently -185 to - 186 dBW absolute signal power. This is roughly a 13 to 14 dB greater tracking ability in terms of simulator relative channel power when compared to the standard receivers.

Figure 4.6 shows that with the use of measurements for low power signals there is an increase in the measurement noise as reflected in the position domain. Note that HDOP and VDOP values were less than 2 in general except for the last 10 to 60 s of signal tracking for each receiver when DOP values increase quickly as loss of signal lock occurs on each satellite.

To further investigate the noise effects for low power signals, the EPE values (residuals from a position constrained least-squares solution) were computed for the HS receiver. In this case, differential corrections were not needed as no atmospheric, orbital, or satellite clock errors were simulated. The position of the simulated vehicle is always known and thus easy to constrain. The EPE values and statistics for the time interval depicted are shown for ten of the satellites tracked in Figures 4.7 and 4.8. Maximum EPE values are typically around 10 to 25 m; however, a 54 m error effect was observed on PRN03. Note that the DOP values do not have an effect on the EPE values because the positions are constrained.

The functional relationship of absolute signal power versus EPE is shown in Figure 4.9. The measurement noise level increases significantly below -180 dBW.

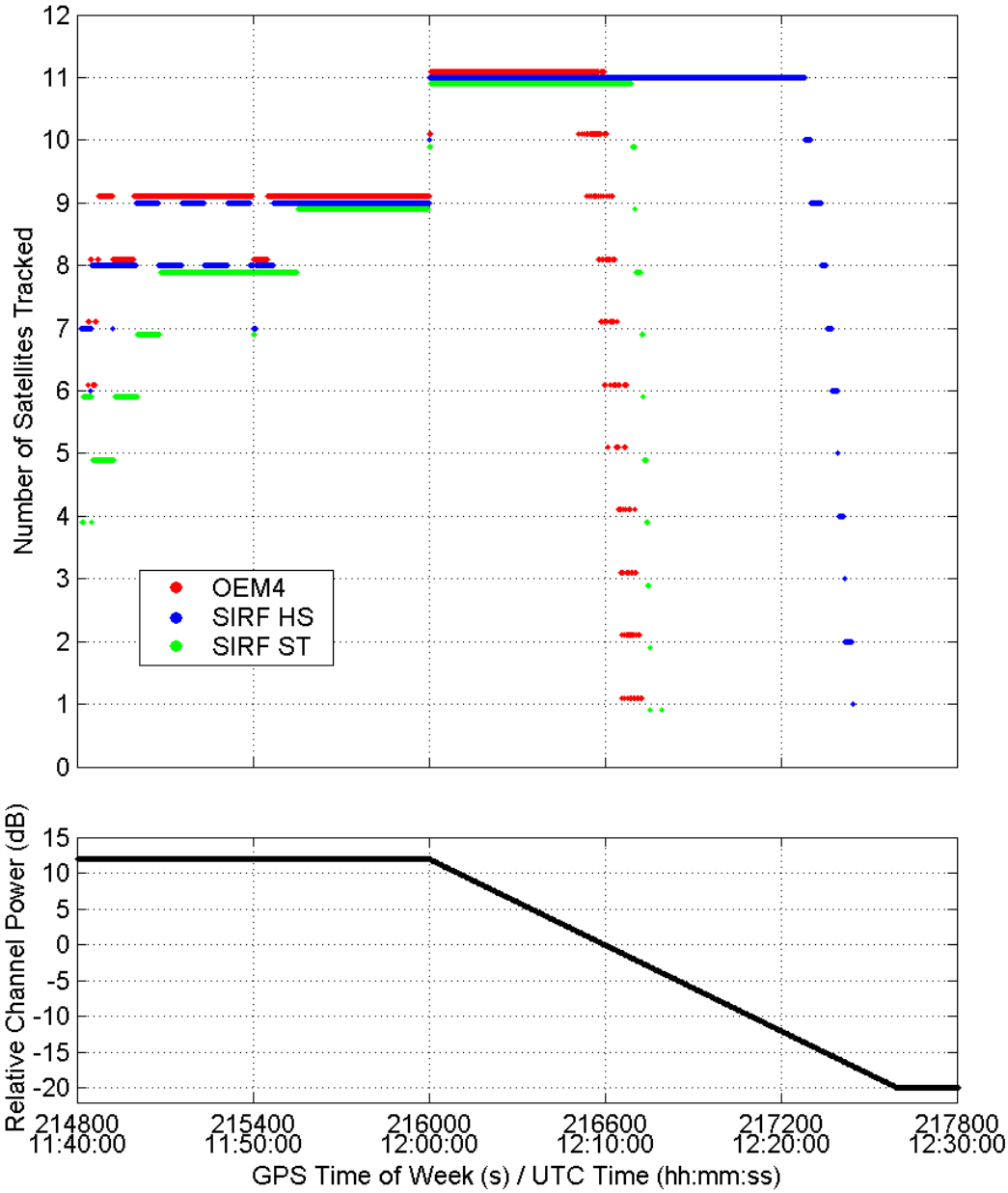

Figure 4.4: Signal Tracking Threshold Test - Availability

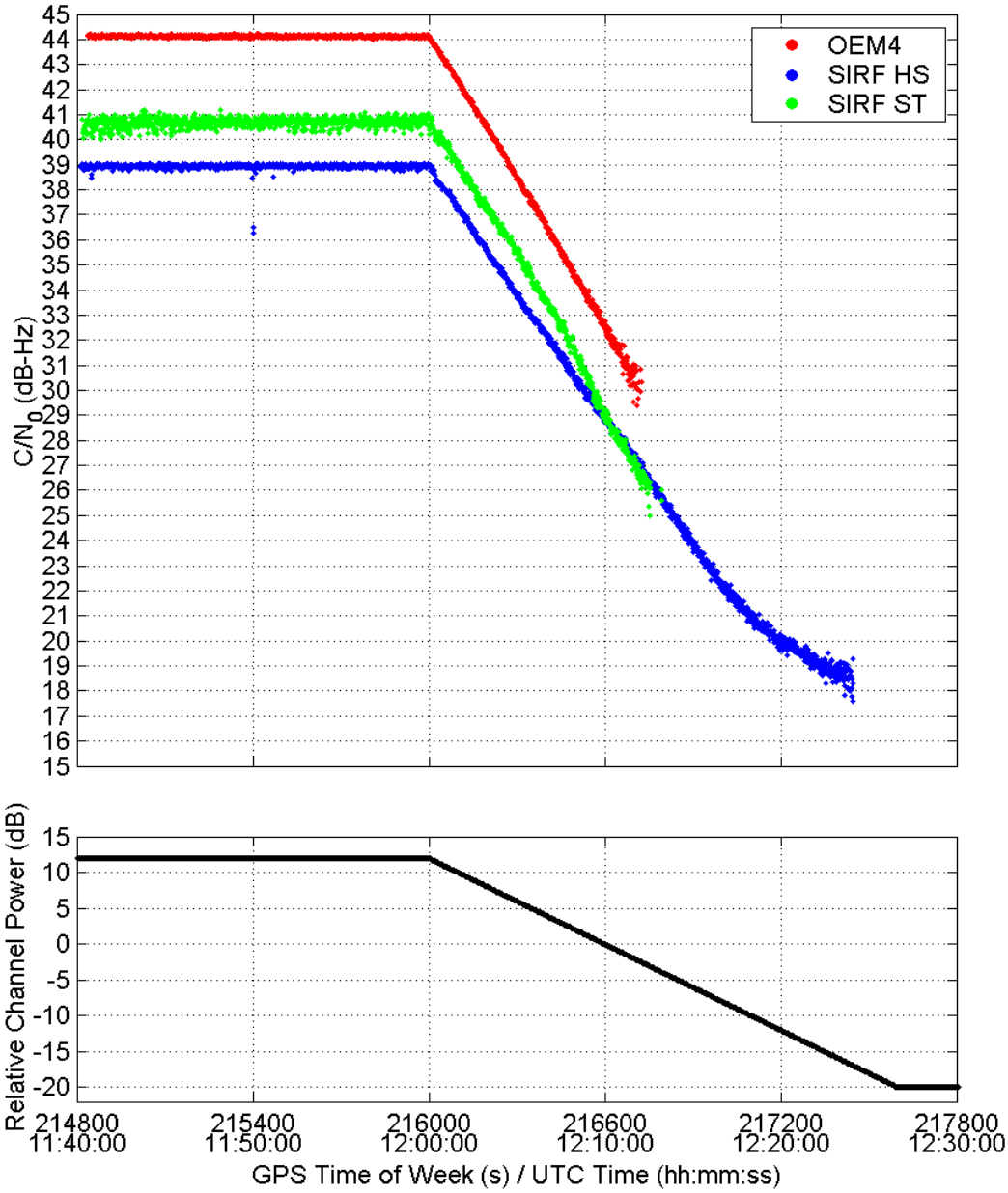

Figure 4.5: Signal Tracking Threshold Test - C/N_0

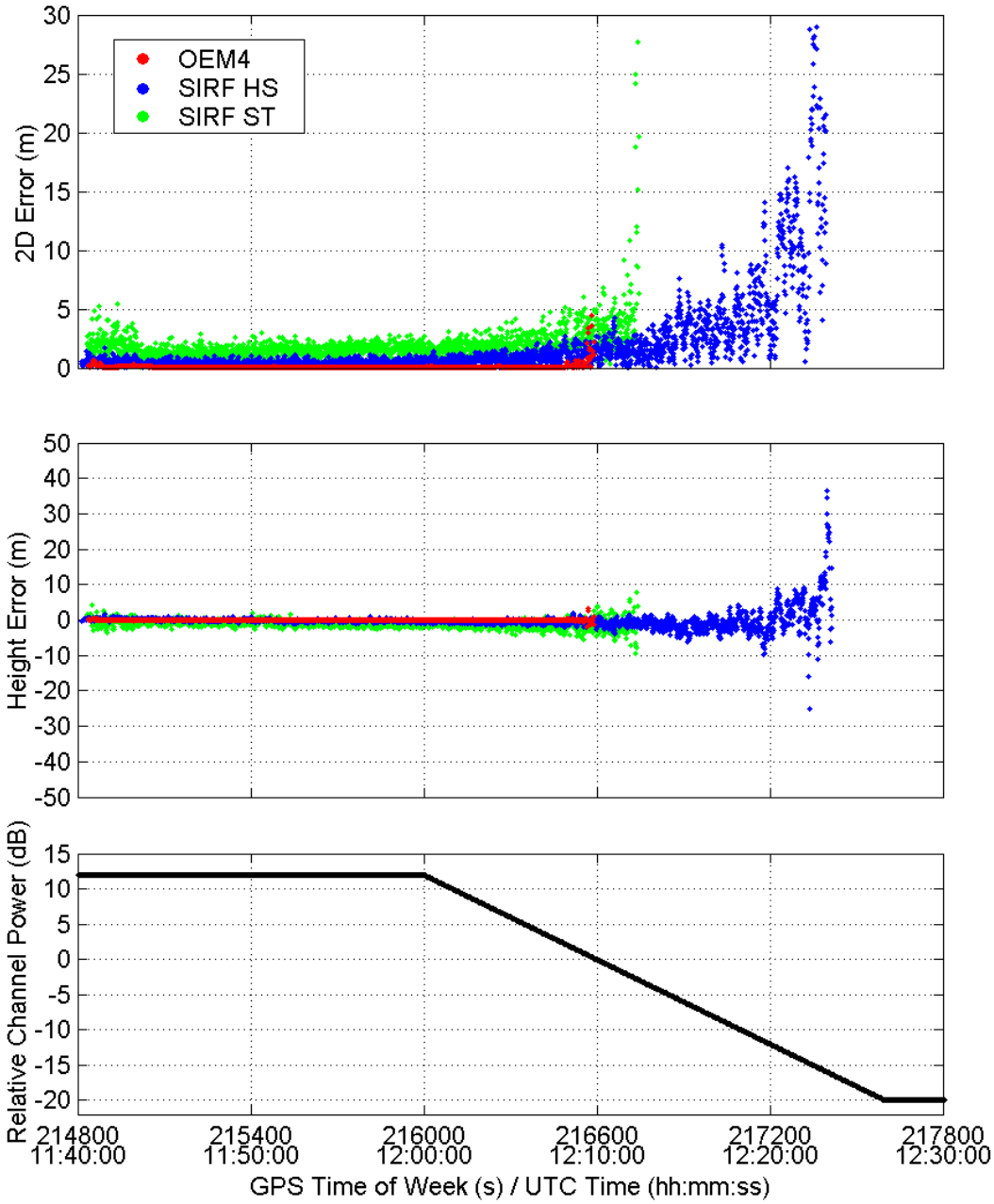

Figure 4.6: Signal Tracking Threshold Test - Position Error

Table 4.1: Tracking Threshold Test - C/N_0 and Simulator Relative Channel Powers For Last 3D Fix (4 SV Solution)

Receiver	GPS Time Of Week (s)	Simulator Channel) Power (dBW)	Receiver C/N_0 (dB-Hz)	Estimated C/N_0 (dB-Hz)
SiRF HS	217415	-185.4	18	18.2
SiRF ST	216745	-172.0	26	31.6
OEM4	216626	-169.6	32	35.2

Table 4.2: Tracking Threshold Test - C/N_0 and Simulator Relative Channel Powers For Last Measurement

Receiver	GPS Time Of Week (s)	Simulator Channel) Power (dBW)	Receiver C/N_0 (dB-Hz)	Estimated C/N_0 (dB-Hz)
SiRF HS	217446	-186.0	18	17.6
SiRF ST	216755	-172.1	24	31.5
OEM4	216725	-171.5	30	32.1

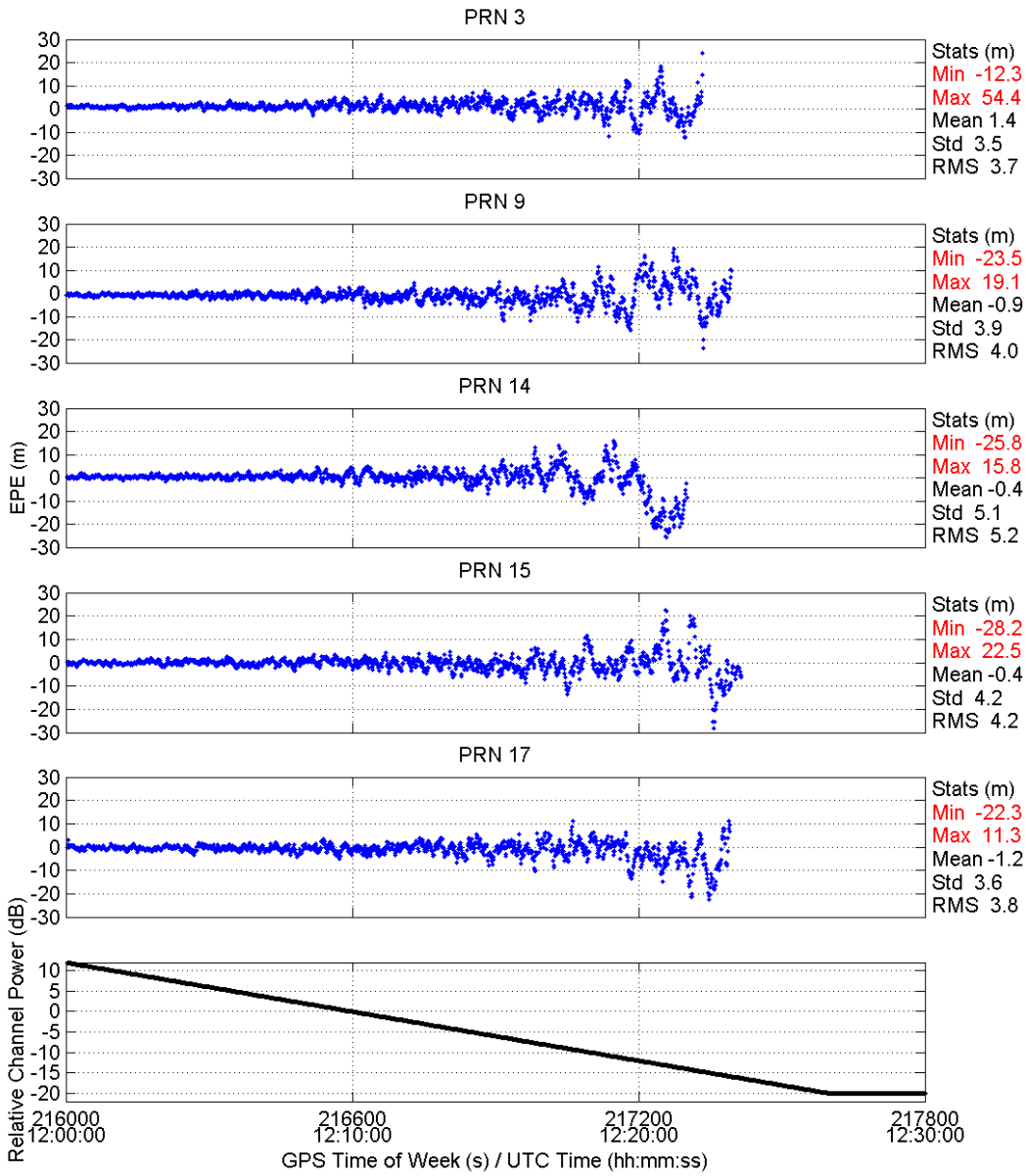

Figure 4.7: Signal Tracking Threshold Test - EPE Values Part I of II

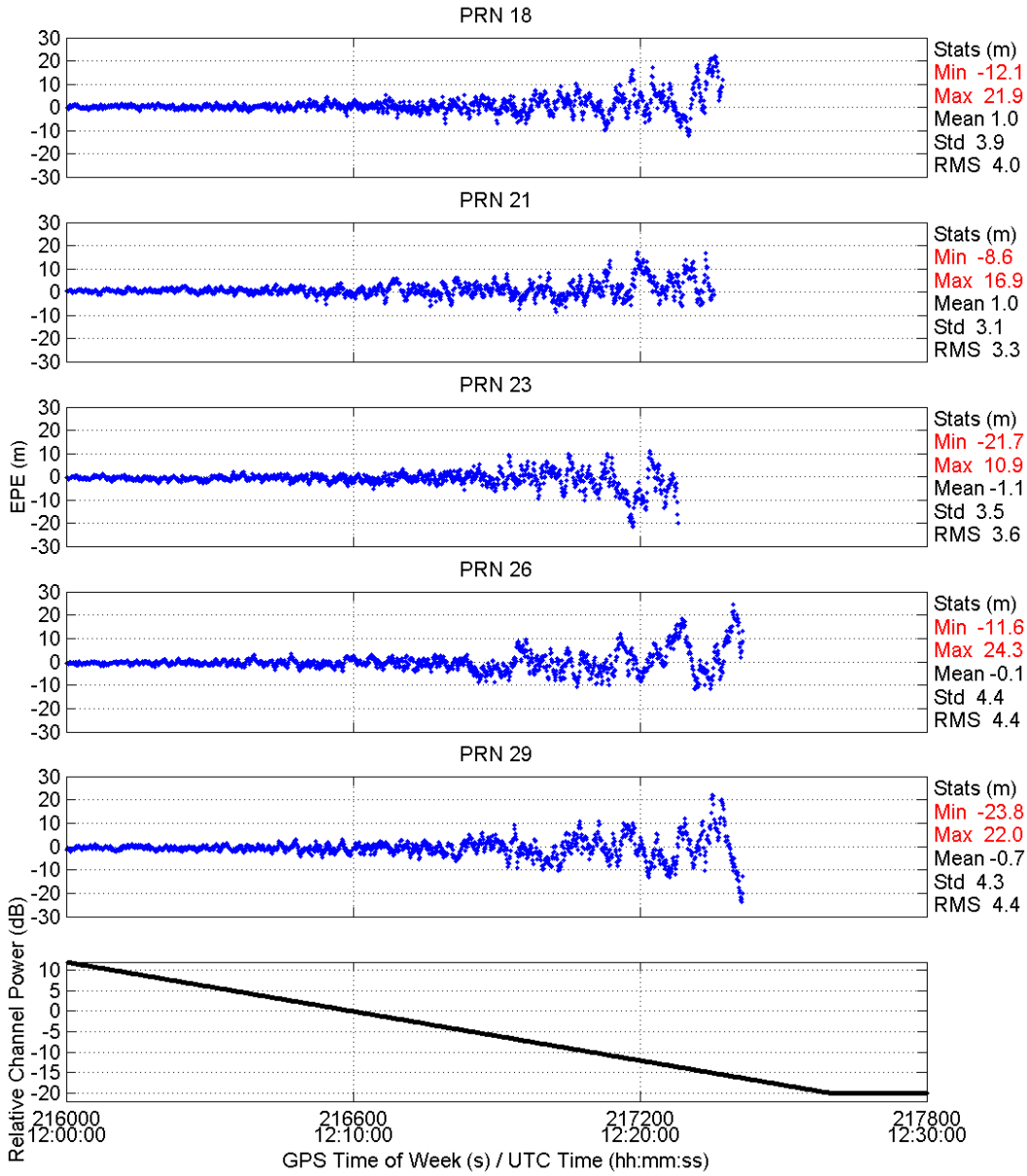

Figure 4.8: Signal Tracking Threshold Test - EPE Values Part II of II

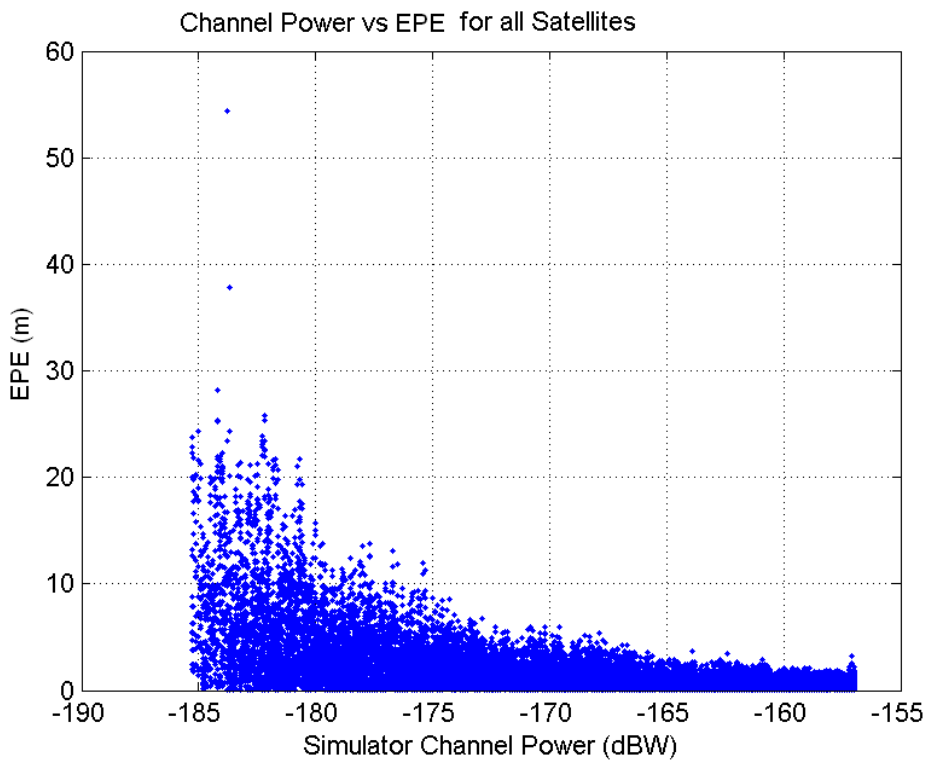

Figure 4.9: Signal Tracking Threshold Test - Simulator Channel Power versus EPE

4.3 Variation Of C/N_0 Estimates With Simulator Relative Channel Power

The simulator outputs signal power relative to -160 dBW. As the noise floor in this test is constant, a decrease of 1 dB of simulator relative channel power should correspond to a decrease of 1 dB-Hz of C/N_0. The results of this test can be analyzed in terms of the variation of C/N_0 due to the variation of simulator relative channel power. This is shown in Figure 4.10 for the SiRF HS, the SiRF ST, and the OEM4 receivers. Lines were fitted to the ST and OEM4 receiver results. The SiRF HS has

some non-linear variation especially at low relative channel powers ($< -10\ dB$). The data closely follows two linear trends, hereby referred to as the 'hockey stick effect'. Thus, the HS data was divided into two sets and a line was fitted for each set. The slopes and y-intercepts for these lines are also shown in Figure 4.10.

The ST and OEM4 receivers have linear C/N_0 relationships to simulator relative channel power with slopes of nearly 1.0. However, the HS receiver clearly does not, especially at low power levels. This means that the fading test measure using HS data must apply a scale factor to compensate for this non-linearity. The following formulas allow C/N_0 differences as estimated by the SiRF HS receiver to provide a reasonably unbiased fading test measure.

$$F = \frac{C/N_0^{reference} - C/N_0^{rover}}{0.83}, for C/N_0^{rover} \geq 21(dB - Hz) \tag{4.3}$$

$$F = \frac{C/N_0^{reference} - 21}{0.83} + \frac{21 - C/N_0^{rover}}{0.35}, for C/N_0^{rover} < 21(dB - Hz) \tag{4.4}$$

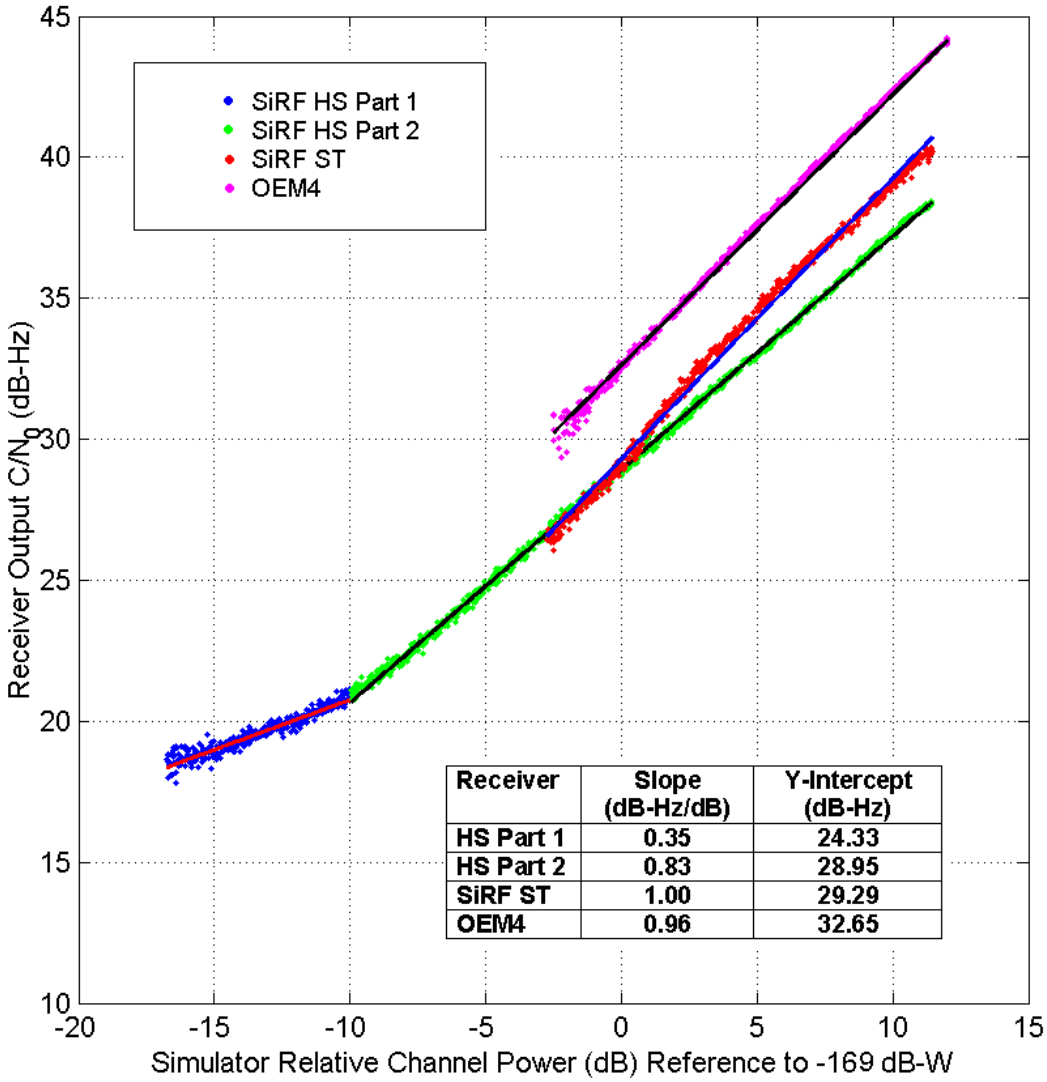

Receiver	Slope (dB-Hz/dB)	Y-Intercept (dB-Hz)
HS Part 1	0.35	24.33
HS Part 2	0.83	28.95
SiRF ST	1.00	29.29
OEM4	0.96	32.65

Figure 4.10: C/N_0 Versus Simulator Channel Power

4.4 Relationship Between C/N_0 For Standard And High Sensitivity SiRF Receivers

During some tests, the fading test measure could not be computed using like receiver estimates of C/N_0 at the base and rover stations for the HS receiver. This could have been due to a large line loss or receiver malfunction. However, the relationship between the C/N_0 estimates as calculated by the SiRF ST and SiRF HS can be calculated using the results of this test. The relationship between the two receivers for line-of-sight signals is linear as can be seen in Figure 4.10. The C/N_0 data at each epoch was matched for both receivers and plotted against each other in Figure 4.11. Thus, the following relationship allows the SiRF ST C/N_0 data to difference the SiRF HS test data to produce the HS fading values as

$$HS_{referenceC/N_0}(dBWHz) = 0.847 * ST_{referenceC/N_0} + 4.35 \tag{4.5}$$

where $HS_{referenceC/N_0}$ is the calculated SiRF HS equivalent C/N_0 based on the SiRF ST reference receiver C/N_0 (dB-Hz), $ST_{referenceC/N_0}$.

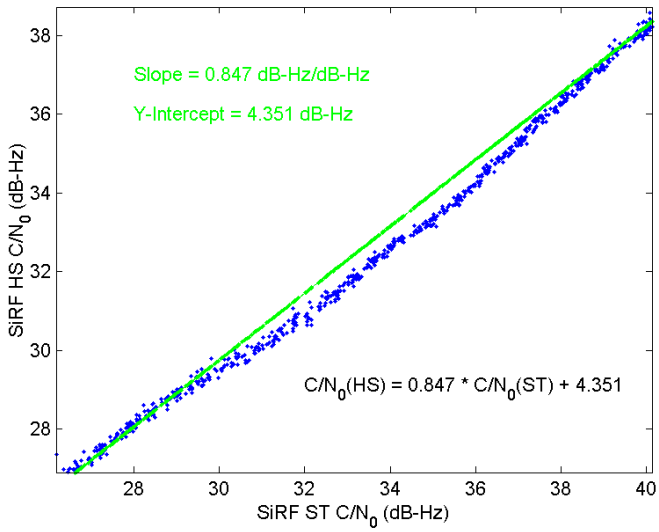

Figure 4.11: C/N_0 Relationship Between SiRF HS And ST Receivers

4.5 Conclusions

The SiRF HS receiver is capable of tracking signals 13 to 14 dB lower than a standard GPS receiver. Signals with C/N_0 as low as 18 dB-Hz, with simulator channel powers of -186 dBW, as measured by the HS receiver were tracked. In addition, the pseudorange measurements taken close to the tracking threshold of the HS receiver are clearly more noisy. Typical maximum EPE values of up to 25 m were observed and a 54 m maximum error effect was observed for one satellite.

The SiRF HS receiver does not provide an unbiased fading test measure as its estimate of C/N_0 does not vary with a linear relationship with actual signal power variation with a slope of 1.0. However, the relationship can be modelled and the SiRF HS C/N_0 differences can still provide a unbiased fading test measure.

Chapter 5

Observed Signal Cross-Correlation Effects and Interference Testing

5.1 Chapter Overview

In Chapter 2, signal cross-correlation, CW interference, multipath, and echo-only interference concerns were identified. This chapter provides details of large measurement degradation effects that were observed in the environments tested, specifically due to signal cross correlation effects. In addition, hardware GPS simulations were performed to isolate and identify the probable sources of these effects.

5.2 Observed Signal Cross-Correlation Errors

In most of the field tests performed very large pseudorange error effects were observed. Effects greater than 150 m and up to the kilometre level were observed.

Analysis of EPE values computed using position-constrained least squares during the forest testing showed two different very large error effects. In one case, the pseudorange error ramped from a nominal value up to 3 to 5 km over periods of about one or two minutes. This effect is shown in Figure 5.1. Measurements of satellites 7, 8, and 11 exhibit these large ramping error effects. These errors also influence the EPE values for the other satellites to a lesser extent due to the receiver clock bias absorbing and spreading some of this large error. In a second case, as shown in Figure 5.2, errors of similar if not greater magnitude occur but during

acquisition or reacquisition. The ramping effect is not seen in Figure 5.2 but instead large instantaneous errors are observed after brief losses of signal tracking, notably for satellites 8 and 9.

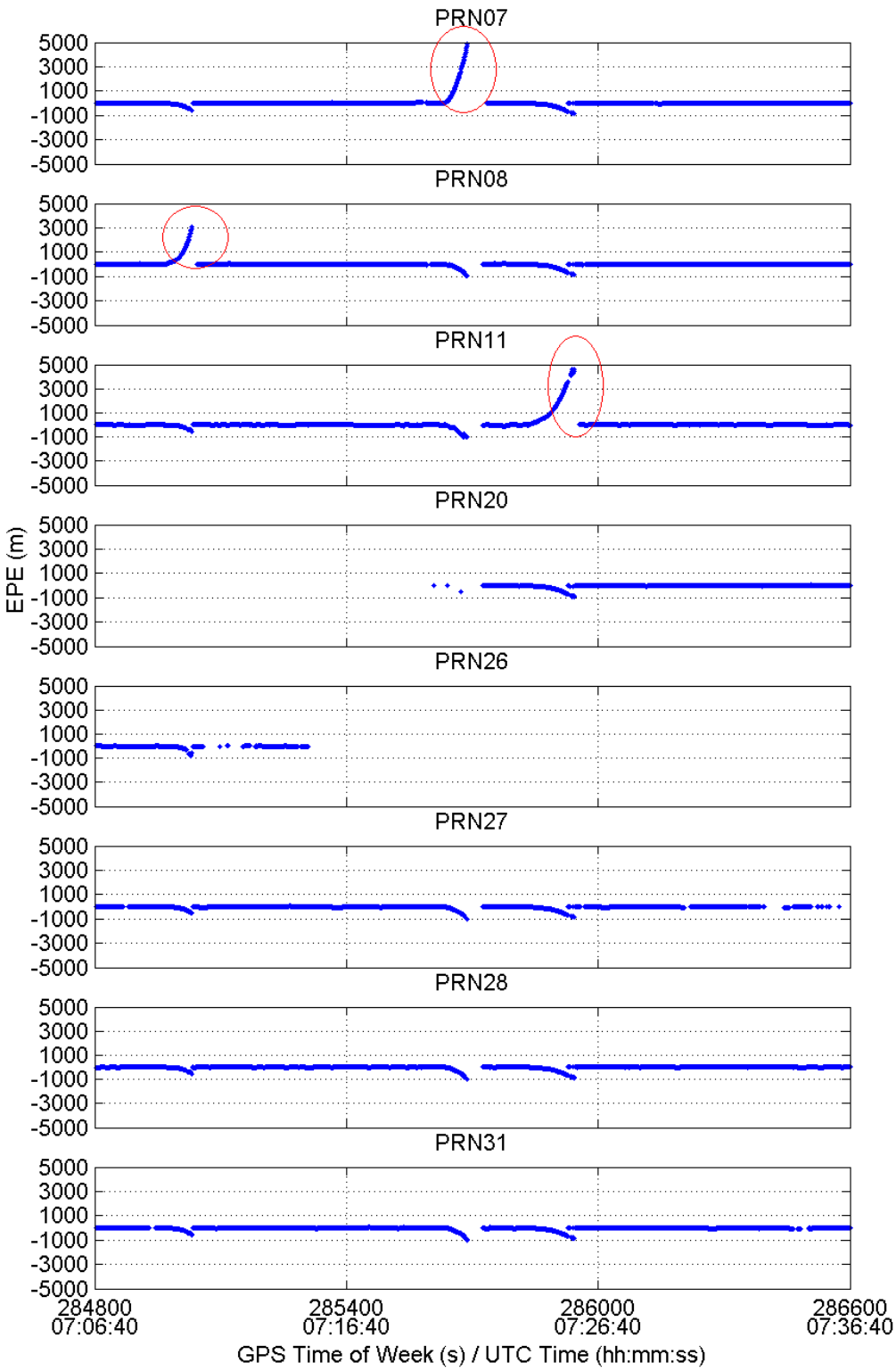

Figure 5.1: Large Ramping Pseudorange Errors During Static Forest Testing

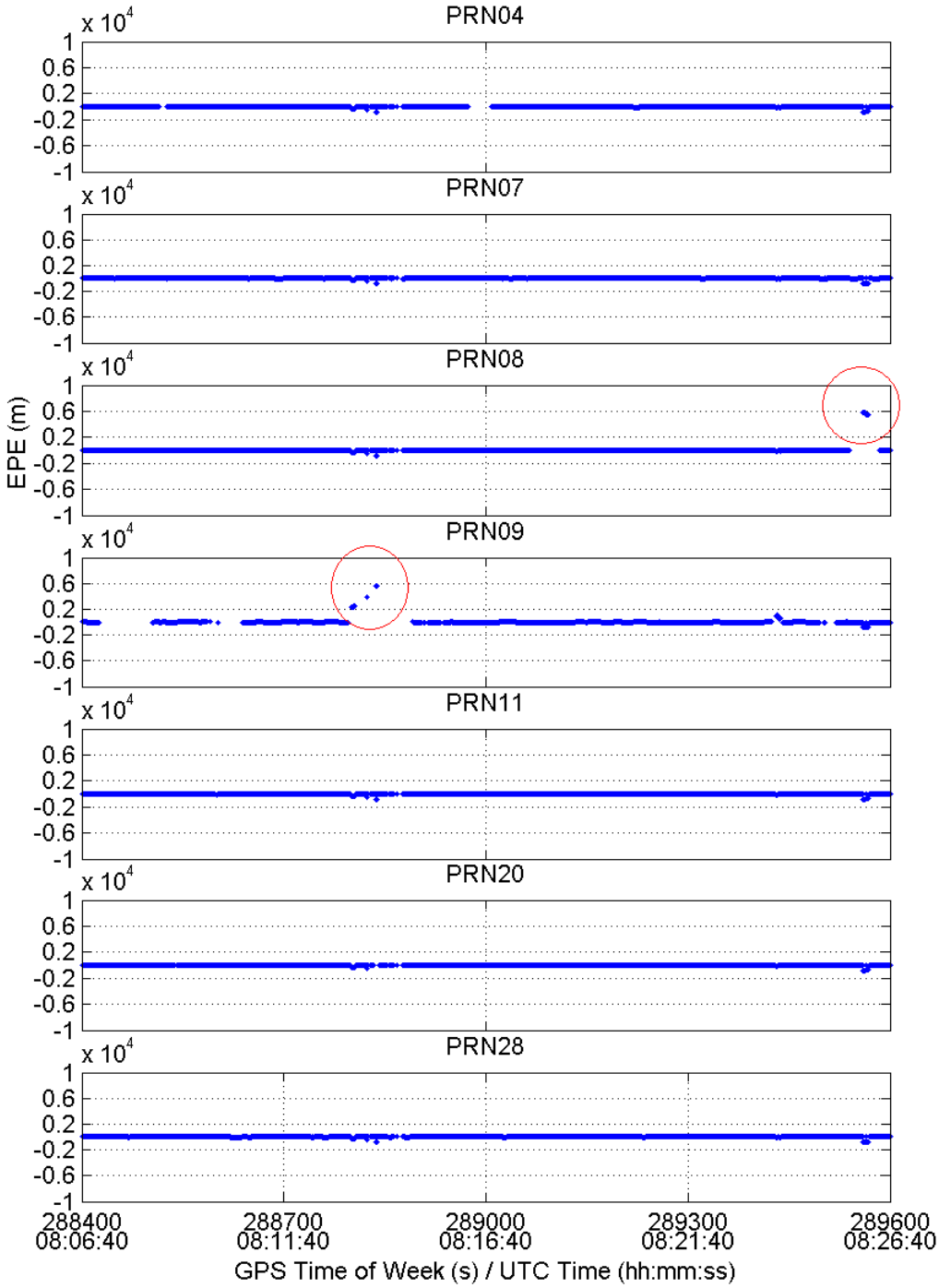

Figure 5.2: Large Pseudorange Errors Upon Reacquisition/Acquisition During Static Forest Testing

Probable causes for these errors are tracking of cross-correlation peaks, or tracking of a peak due to CW jamming. However, since these error effects were observed in several environments, it is very unlikely that CW jamming is the source of this error. False reacquisition or acquisition of the correlation peak is probable for the second observed effect. This is expected to some extent as the probability of false detection at lower signal powers is much higher (Chansarkar and Garin, 2000). Chapter 2 discussed signal self interference, namely signal cross correlation. The cross-correlation functions have peak levels that reach -24 dB with respect to the autocorrelation peak (Ward, 1996). This is known to result in tracking of false correlation peaks at certain Doppler offsets and signal strength differences between signals. This is the most likely cause of both error sources.

The fading and EPE values for PRN07 during a ramping event are shown in Figure 5.3. The same values for satellite 9 during a reacquisition event are shown in Figure 5.4. The high fading values of 15 to 20 dB during the error events support the reasoning that the interference effect is due to cross-correlation.

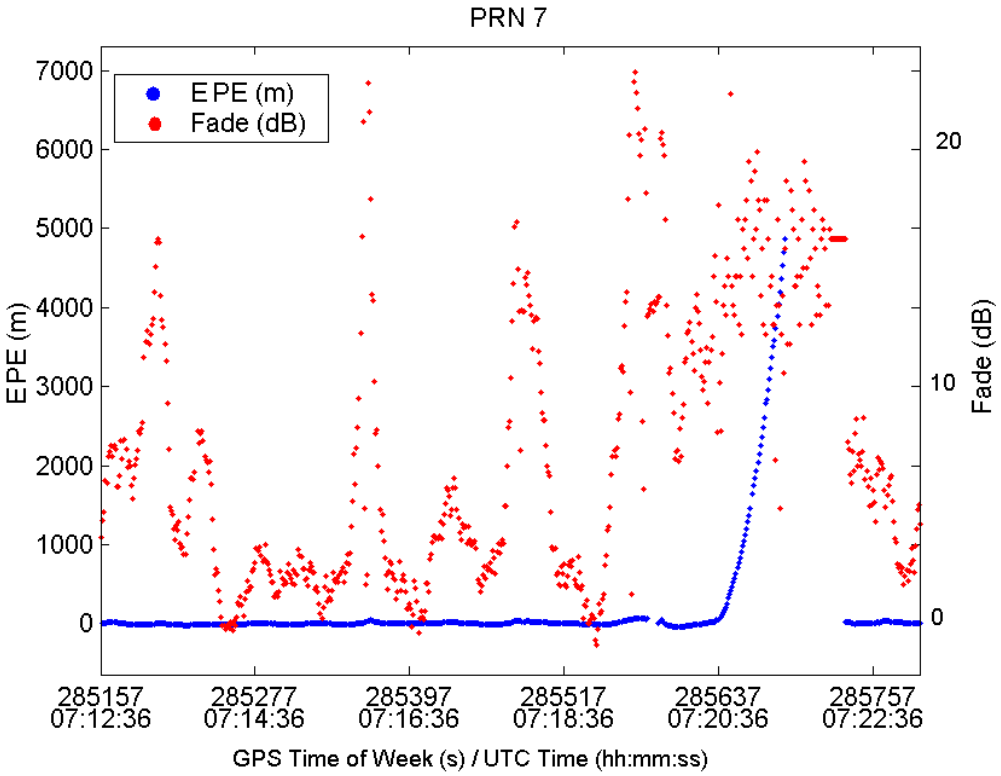

Figure 5.3: Large Ramping Pseudorange Error And Associated Fading During Static Forest Testing

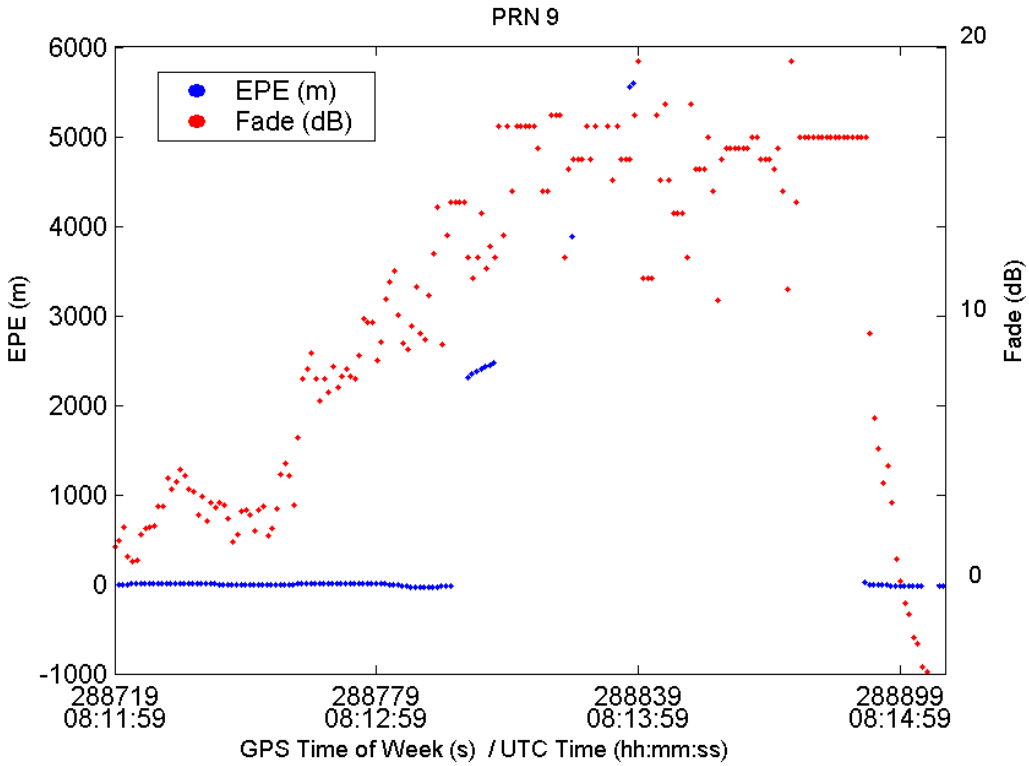

Figure 5.4: Large Pseudorange Errors And Associated Fading Upon Reacquisition/Acquisition During Static Forest Testing

5.3 Hardware GPS Signal Cross-Correlation Simulation

In order to confirm that the very large error effects are due to signal cross correlation, a hardware GPS simulation was performed using the Spirent STR-6560 simulator. A simulation was devised with a 9-satellite constellation based on a real YUMA almanac for the week including October 8, 2002. The hardware setup is shown in Figure 5.5. All satellites were given fixed signal power levels of 15 dB relative channel power referenced to -169 dBW for a warmup period of 20 minutes to allow the receiver to obtain all the necessary information for high sensitivity methods. Following the

initialization period, the relative power level on channel 1, corresponding to PRN02, was lowered to -15 dB and varied sinusoidally with an amplitude of 2 dB and a period of 60 s. The intent was to vary the signal power for PRN02 such that it goes above and below the tracking threshold of the receiver. Thus, tracking of a cross-correlation peak is probable upon reacquisition when the power is raised.

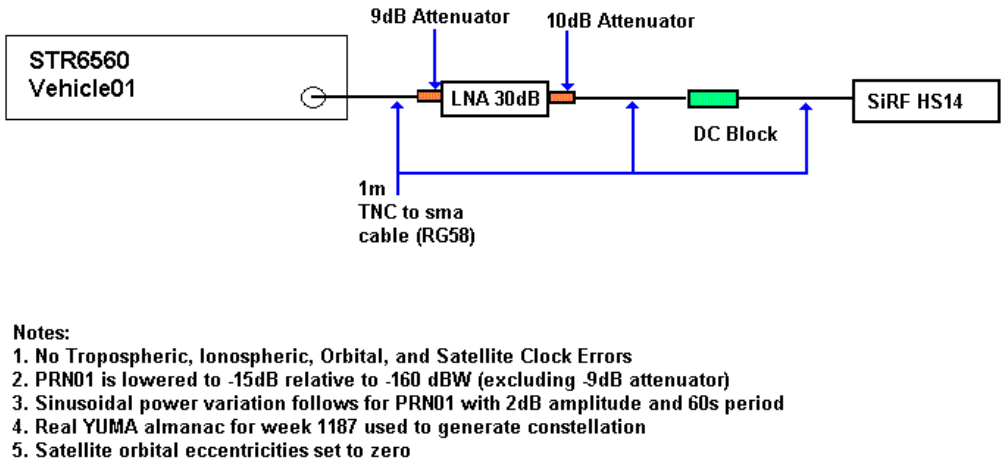

Figure 5.5: Setup Of The Cross-Correlation Hardware Simulation Test

The ratio of the strong signals to the weak signal varied is

$$S/W = 30 + 2 * sin(\frac{2\pi}{60}t)(dB) \tag{5.1}$$

where S/W is the ratio of the strong to weak signal (dB), and t is time (s). The EPE values for all satellite pseudorange measurements were computed and are shown in Figure 5.6. PRN02 shows clear evidence of reacquisition tracking of false correlation peaks due to signal cross correlation.

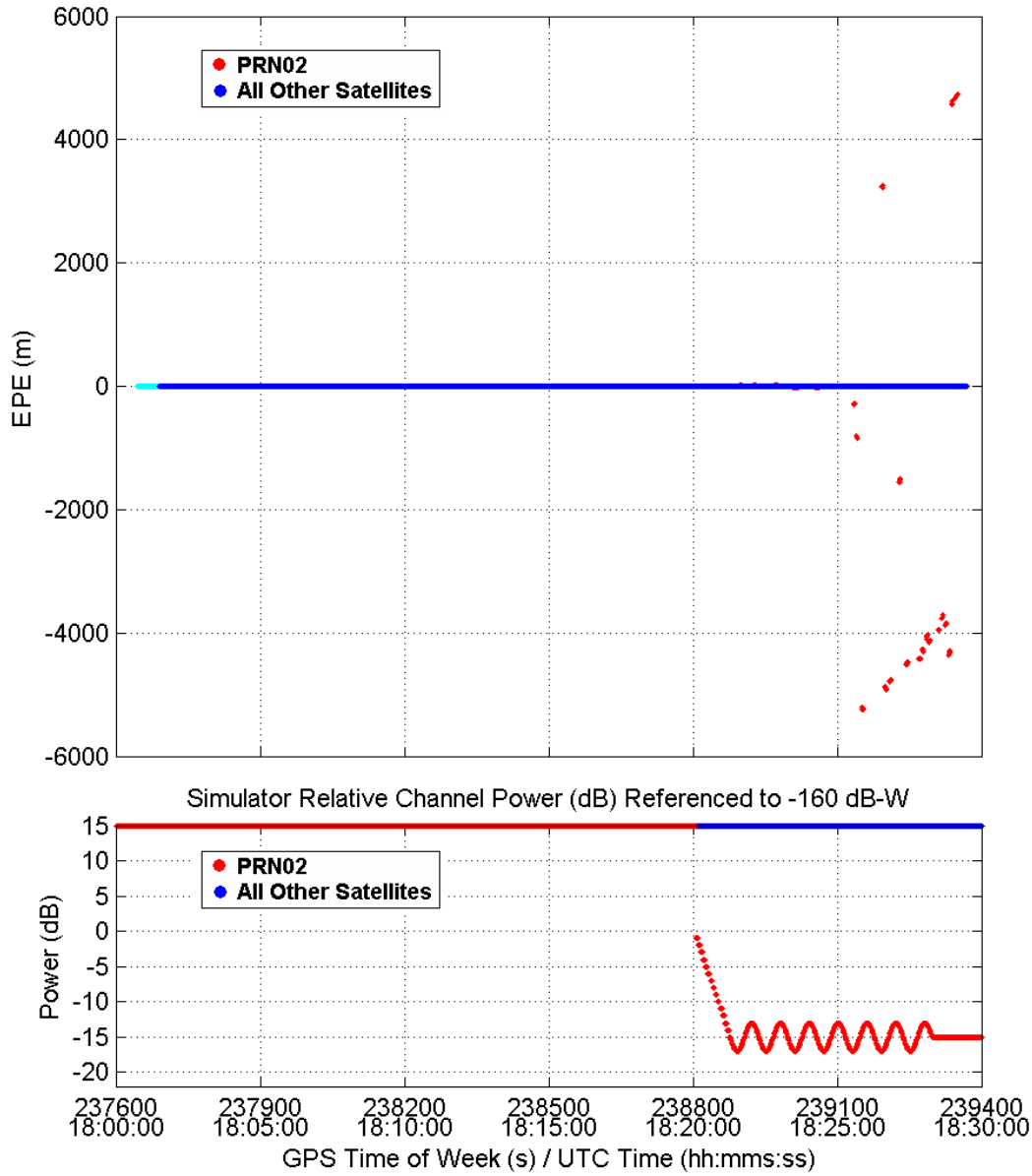

Figure 5.6: Estimated Relative Pseudorange Errors During Cross-Correlation Simulation Test

5.4 Continuous Wave Interference Hardware Simulation

CW interference was identified in Chapter 2 as a significant interference threat to weak signal usage. In order to confirm this susceptibility a hardware GPS simulation test was performed using a Spirent STR-6560 signal simulator. The satellite constellation used for the simulation described in the previous section was also applied in this test. The test setup is shown in Figure 5.7. A coherent CW jamming signal was generated with a 42 kHz offset with respect to PRN01. This offset has been identified as the worst spectral line for the C/A code 1 kHz line spectra. Thus, the CW signal should leak through during the correlation process and jam the receiver if the jammer to signal ratio, J/S, is high enough. In general if the J/S is higher than 21 dB, interference effects due to CW jamming are problematic (Ward, 1996).

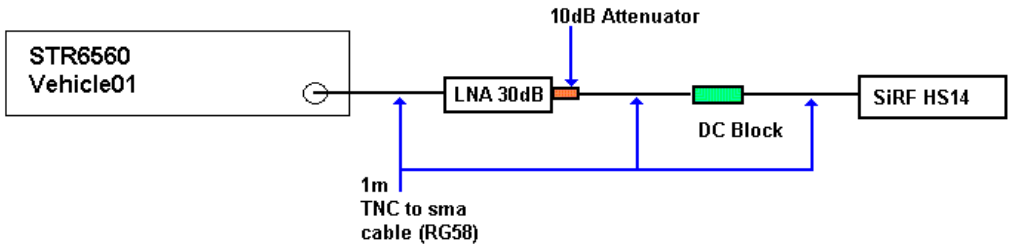

Notes:
1. PRN01 signal power lowered by 1dB steps every 5 s after 20:00 minutes into the run to -15 dB.
2. PRN03, the CW jammer, is slowly raised in power after 21:25 minutes into the run.
3. The jammer has a Doppler offset of 42000 Hz with respect to PRN01 established using a pseudorange ramp
4. PRN01 and PRN03 have exactly the same orbital parameters
5. Nominal atmospheric conditions are simulated

All other satellites are lowered to -9 dB after 20:00 minutes into the run in 1dB steps every 5s.

Figure 5.7: Setup Of The CW Hardware Simulation Test

The signal powers for the CW jammer, PRN01, and all the other satellite channels are shown in Figure 5.8 along with the EPE values for PRN01. The signal powers for all satellites were lowered to eliminate the influence of signal cross-correlation effects

while still providing enough signal power for adequate signal tracking. The CW signal effectively jams PRN01 at a J/S ratio of 16 dB. Some reacquisitions of PRN01 occur for brief periods. A benchmark test with the same constellation, timing, and signal levels without the jammer was performed for comparison purposes. The EPE values for PRN01 and the relative channel powers for PRN01 and the other satellite channels are shown in Figure 5.9. No large errors occurred in the presence of the CW jammer that could be distinguished from noise effects.

The CW jammer power in this case is well below the noise floor. This means that CW jamming may be problematic for weak signal usage. Many devices used indoors may have CW harmonics or radiate CW signals below the noise floor that could interfere with signal tracking.

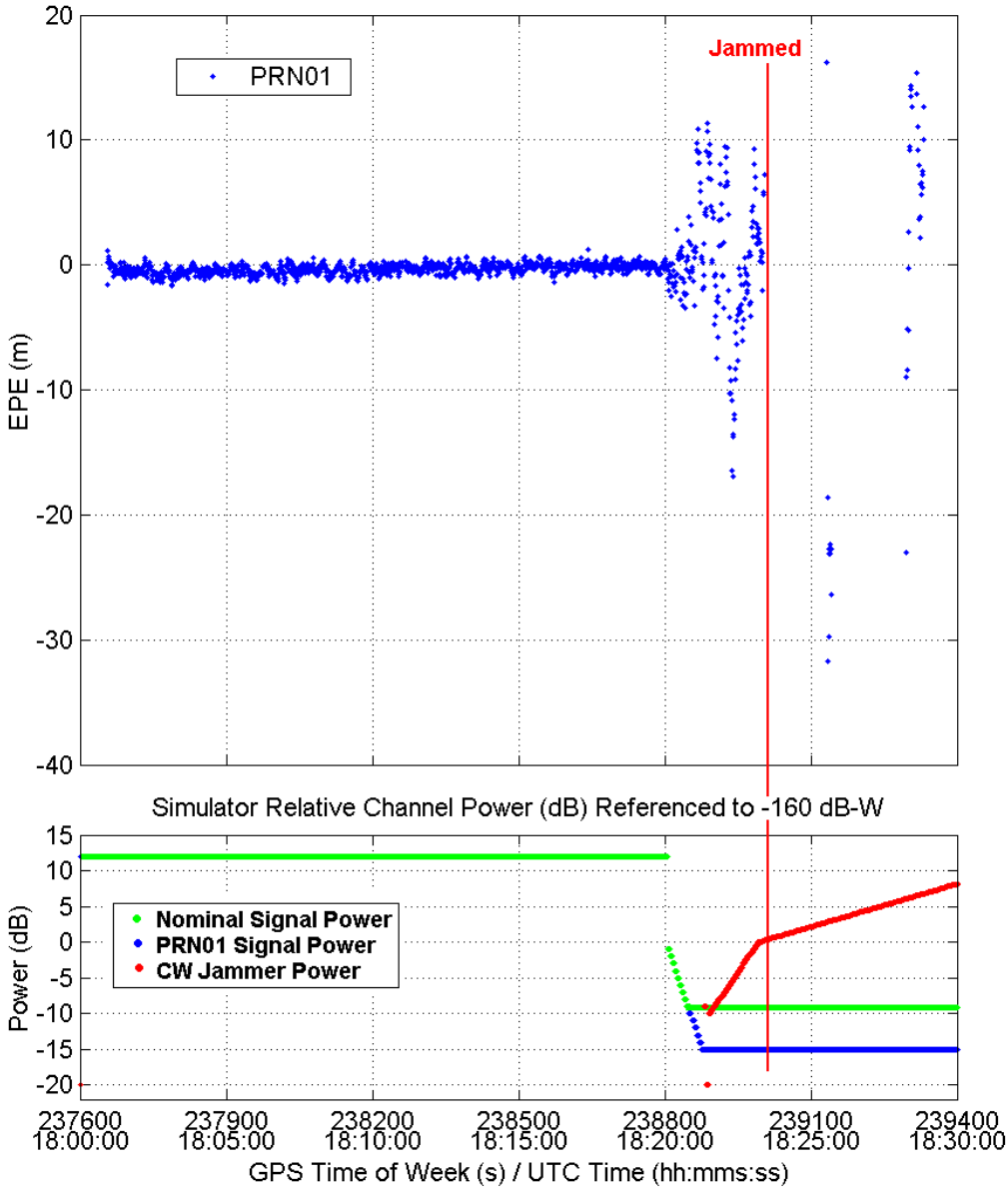

Figure 5.8: Estimated Relative Pseudorange Error For PRN01 During Continuous Wave Interference Hardware Simulation Test

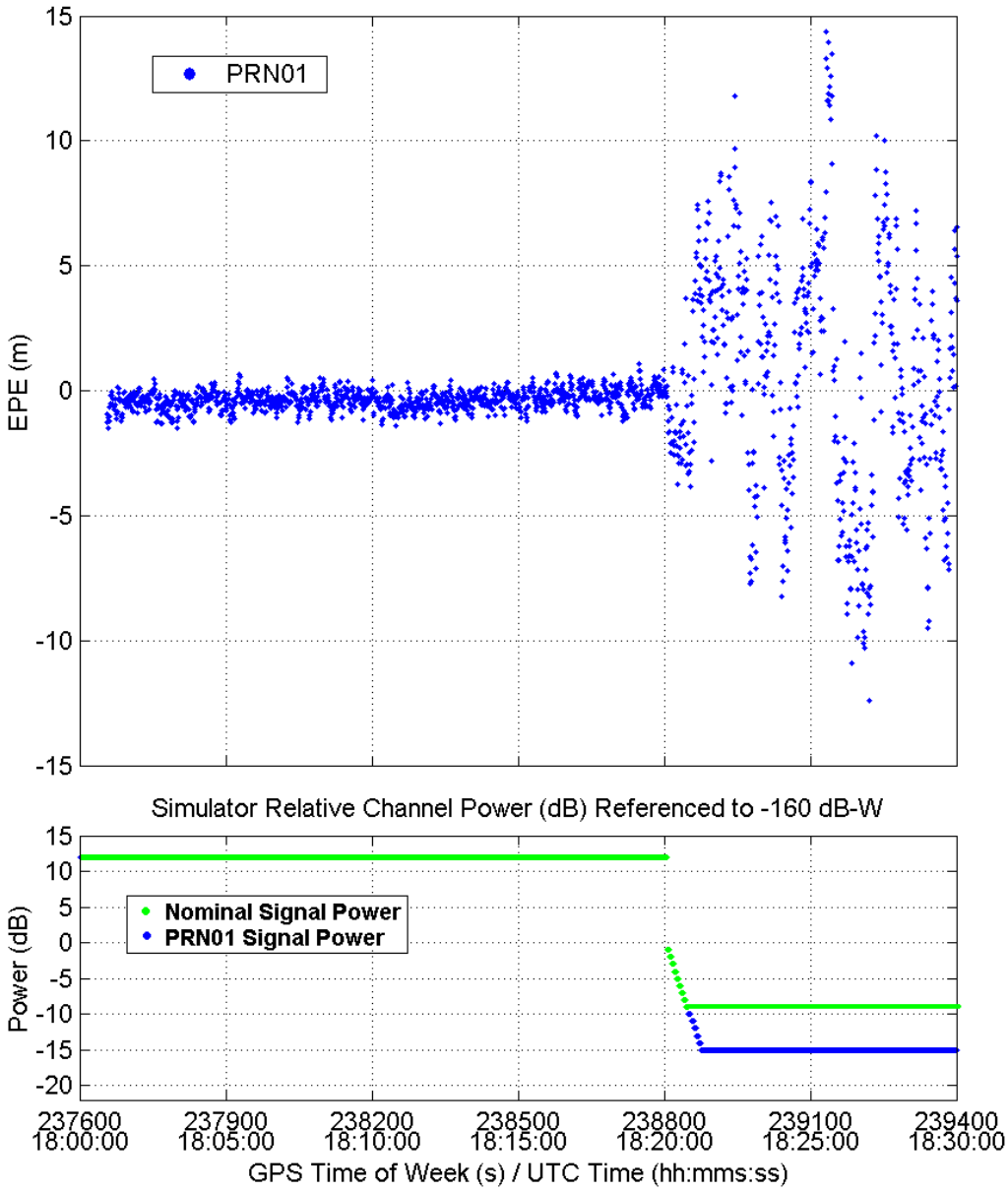

Figure 5.9: Estimated Relative Pseudorange Error For PRN01 During Continuous Wave Interference Hardware Simulation Test With No Jammer Present

5.5 Conclusions

Signal cross-correlation is a significant interference effect when both strong and weak GPS signals are present. However, signal cross-correlation in the line-of-sight case is a deterministic effect in that the cross-correlation peaks can be identified with a-priori knowledge of the Doppler and approximate delay for each satellite signal (i.e. approximate position must be known). Obtaining this information from aiding or if the receiver is already tracking should be fairly trivial. In the case of multipath and echo-only signal tracking, the approximate location of the cross-correlation peaks may also be similar. Thus, high sensitivity receiver manufacturers should use this information to ensure that cross-correlation peaks are not tracked or at least reduce the probability of tracking a false correlation peak.

CW interference has been identified as a probable source of weak signal jamming. Further research as to the prevalence of CW signals in various environments is needed but is beyond the scope of this thesis. The CW signals generated in the simulation testing are worst case in that the CW exactly matches the worst case Doppler offset for PRN01 and the CW signal is produced with phase coherence with respect to the PRN01 signal. Obviously, CW signals of this type are not realistic in most operational environments. However, the tracking weakness of weak GPS signals with CW jamming is significant.

In subsequent chapters EPE values are computed using a method that rejects very large blunders otherwise the error due to the blunder is spread into the other measurements due to the receiver clock offset estimation. The algorithms employed rejects measurements with EPE values larger than 150 m. This value was chosen to allow a certain amount of error to be analyzed while not overly distorting the EPE statistics due to very large error effects.

Chapter 6

Performance in the Forest Environment

The Montréal Morgan Arboretum was selected for testing in a forest environment due to previous knowledge of its characteristics by the Department of Geomatics Engineering. The arboretum is located on the western end of the Island of Montréal in Québec, Canada. A trail and road map for the arboretum are shown in Figure 6.1. The forest consists mainly of deciduous trees including birches, lindens and maples. However, some sections of the forest include numerous coniferous varieties of spruce, pine, and fir.

Both static and kinematic testing was performed at the arboretum. A test loop that follows the road shown as the Orange walking trail in Figure 6.1 was selected for testing. The forest height and density varied as shown in Figure 6.2 throughout the test track with most of the test containing 'medium' density foliage as shown in the figure. Usually the forest canopy obscured the view of the sky directly above the road. Static testing was performed at a point on the road with similar forest characteristics in all directions.

A reference station was established in Vaudrueil, approximately 7 km away, from which two control points were also established at the arboretum. All control points were established using carrier phase differential GPS. The road loop was then conventionally surveyed with respect to the two control points at the arboretum. The estimated accuracy with respect to WGS84 of the road loop points is better than 2 m. This is based on the conventional survey loop closure and the estimated accuracy of the carrier phase differential GPS solutions for the control points.

The surveyed points are shown in a plan view in Figure 6.3. Point G was selected for static testing.

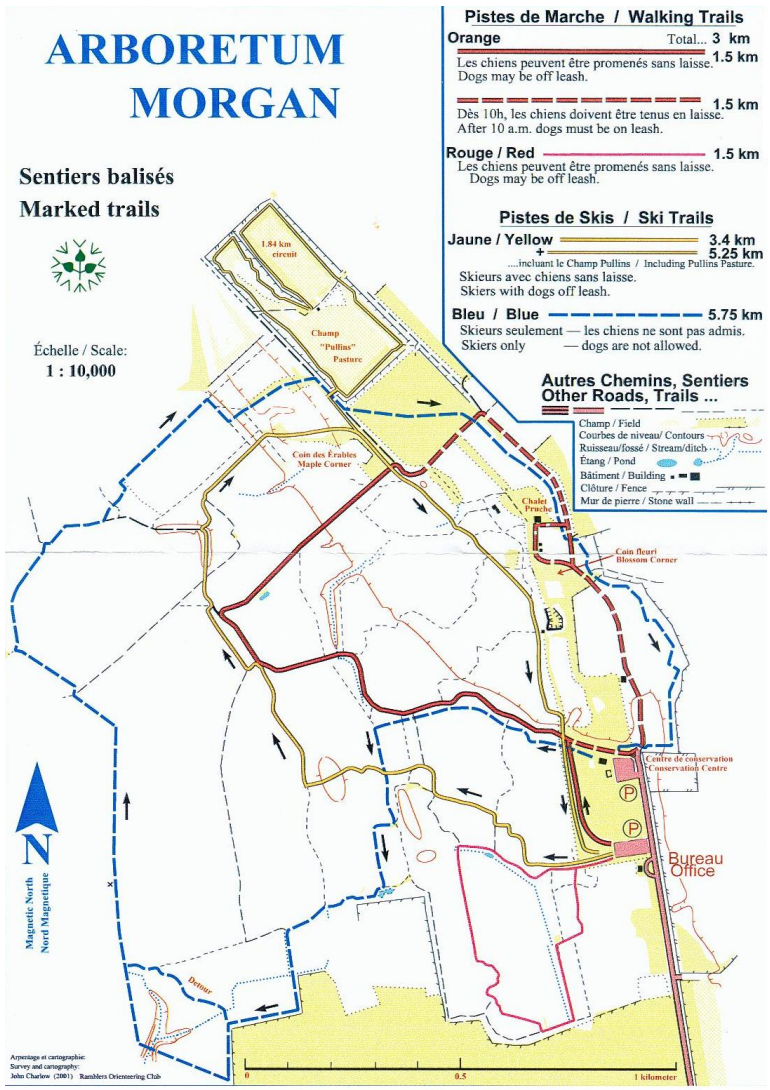

Figure 6.1: Trail Map of the Morgan Arboretum [http://www.total.net/arbo/anglais/arboretum.htm]

Figure 6.2: Photos of the Morgan Arboretum Forest Environment

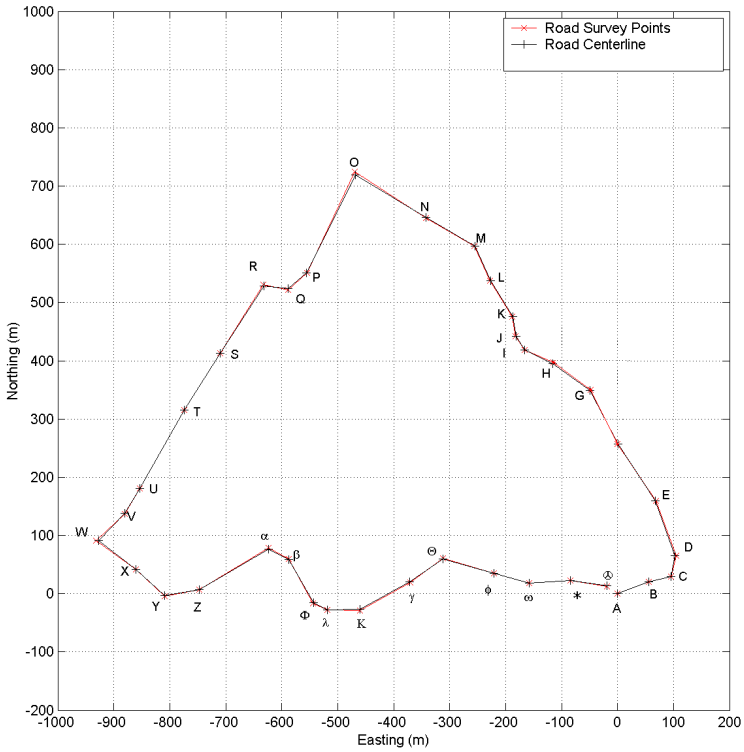

Figure 6.3: Plan View of the Morgan Arboretum Forest Test Loop

6.1 Static Test

6.1.1 Test Details

Point G had similar forest density characteristics for all azimuths except that the canopy density is less along the road's direction of travel (SE to NW). Some photos of the test point and surrounding foliage are shown in Figure 6.4.

The data collected at this point is very useful for analysis of the pseudorange error effects in this forest environment. Static data was collected, following a 20 minute warmup period (at a nearby location with a good view of the sky), using a SiRF HS receiver, a SiRF ST receiver, and a NovAtel OEM4 receiver. Table 6.1 provides the timing details for this static test. Over 5 hours of data were collected.

Figure 6.4: Photos of the Static Forest Test Point

Table 6.1: July 16, 2002, Static Forest Test Details

Test Label	Initialization Time of Week (s)	Start Time Of Week (s)	End Time Of Week (s)	Test Duration (hours)
2300	270200	272200	290630	5.2

6.1.2 Measurement Availability

The number of available measurements as tracked by each test receiver is shown in Figure 6.5. Moving averages using a 2 minute window are also plotted to provide a more intuitive comparison between the receivers. The statistics concerning the number of satellites tracked are shown in Table 6.2. The HS receiver clearly obtains more measurements than the other receivers, although all receivers track a sufficient number of satellites to obtain a full navigation solution during most of the test. The HS receiver typically had 2 more satellites in track during the entire test. The DOP corresponding to the useable measurements is discussed in section 6.1.7.

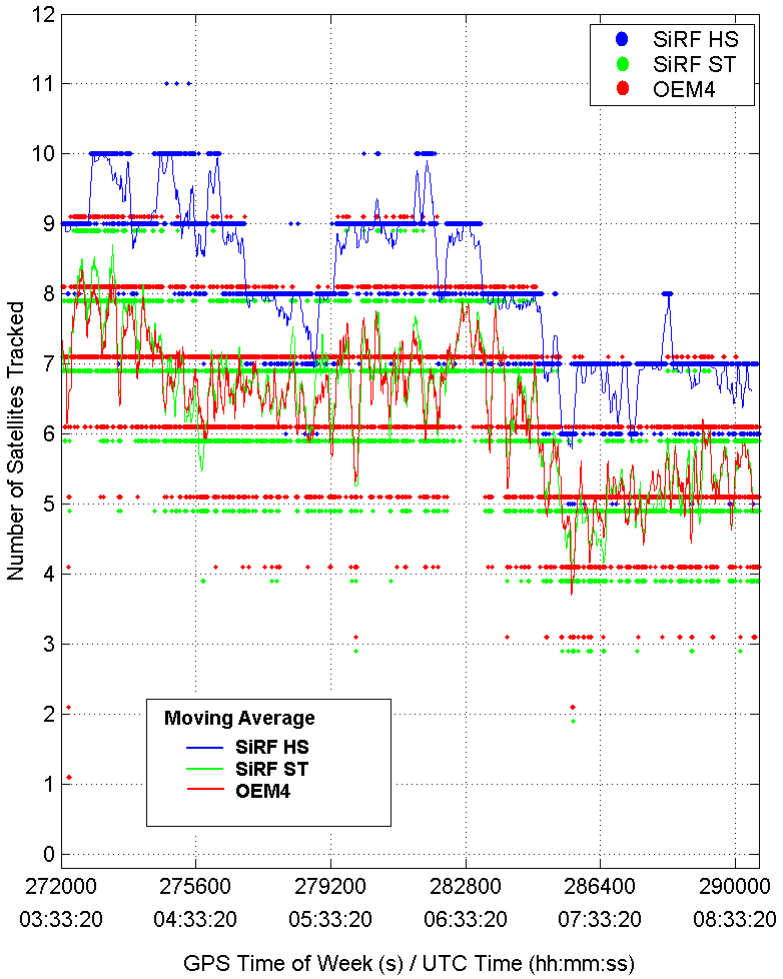

Figure 6.5: Static Forest Test - Measurement Availability

Table 6.2: Static Forest Test - Measurement Availability Statistics

Receiver	SiRF HS	SiRF ST	OEM4
Mean	8.1	6.4	6.3
σ	1.2	1.3	1.3

6.1.3 HS Fading and EPE Time Series Analysis

Fading was computed using C/N_0 differences utilizing the Vaudreuil reference station. The EPE test values, calculated using differential corrections from the Vaudreuil reference station, and the fading values for each satellite along with their corresponding elevation angle are shown in Figures 6.6, 6.7, and 6.8 for the HS receiver. Please note that since the test point coordinates are held fixed to the known value, the DOP values have no affect on the EPE values. The results for the ST and OEM4 receiver are not presented in this section as further sections provide the necessary comparative results. Also included in these figures are the large blunder effects (discussed in Chapter 5), rejected from solution in EPE calculation, shown as red dots on the top of each plot. The number of occurrences for each satellite, NF, and the number of EPE values, N, used in computed statistics are also shown in the figures.

RMS EPE values range from 13 m to close to 30 m. Error effects generally occur more frequently at lower elevation angles but with some exceptions. For example, Satellite 27 shows large error peaks even at around 60^o elevation. Strong signal fades often correspond to peak error effects but some large error effects are not associated with strong signal fades. The very large error spikes are due to signal cross correlation while multipath otherwise contaminates the pseudorange measurements.

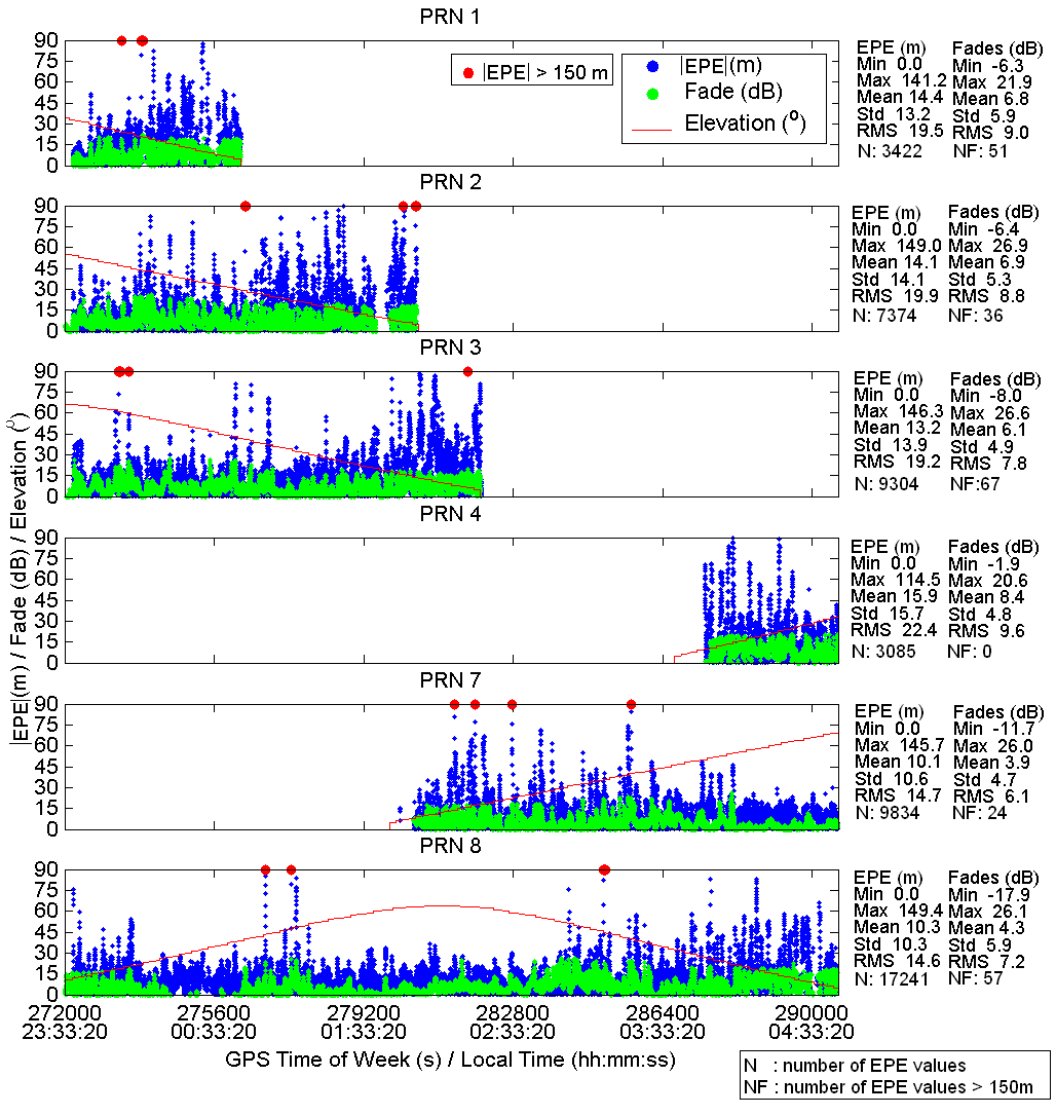

Figure 6.6: Static Forest Test - Time Series Fading and EPE Data for the HS Receiver Part 1 of 3

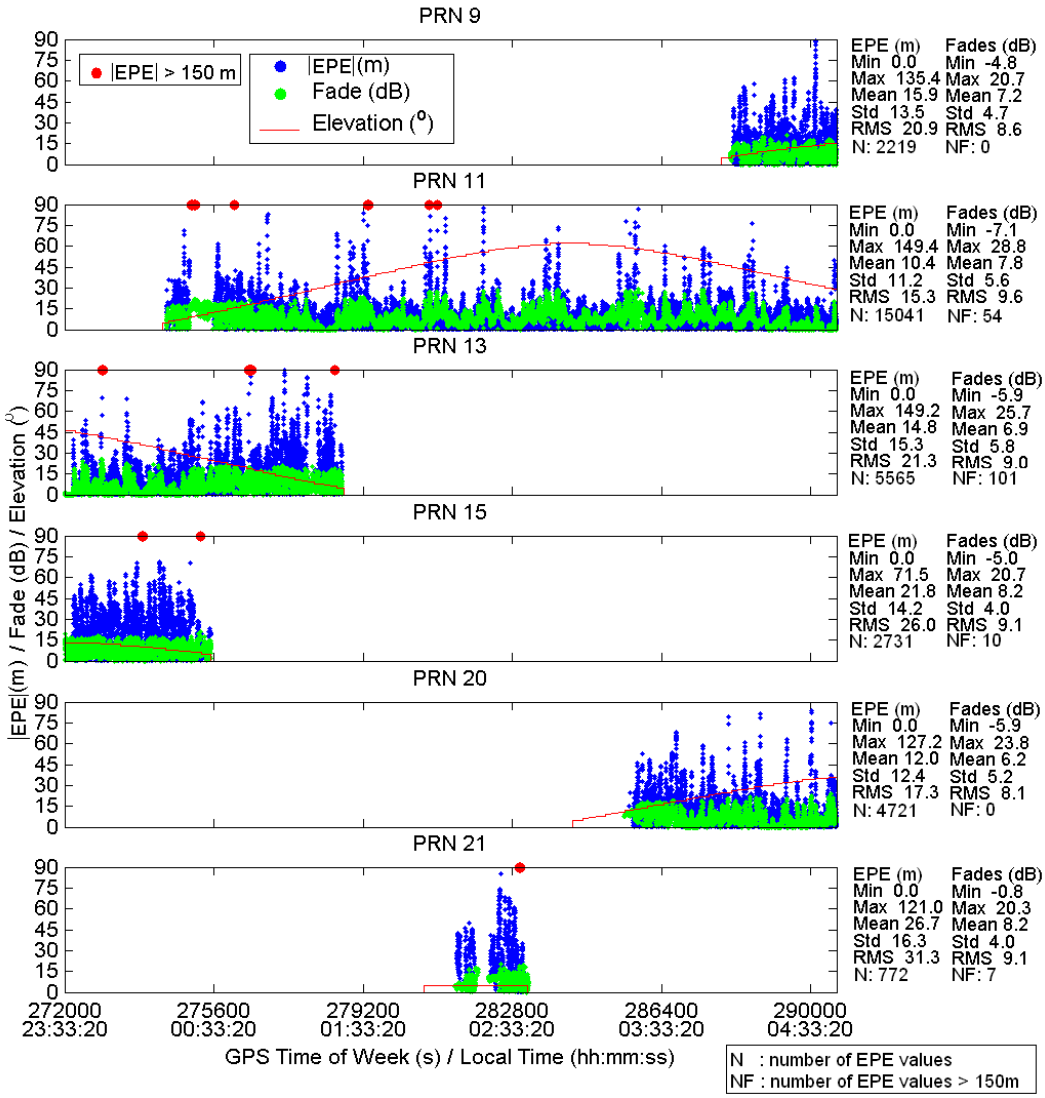

Figure 6.7: Static Forest Test - Time Series Fading and EPE Data for the HS Receiver Part 2 of 3

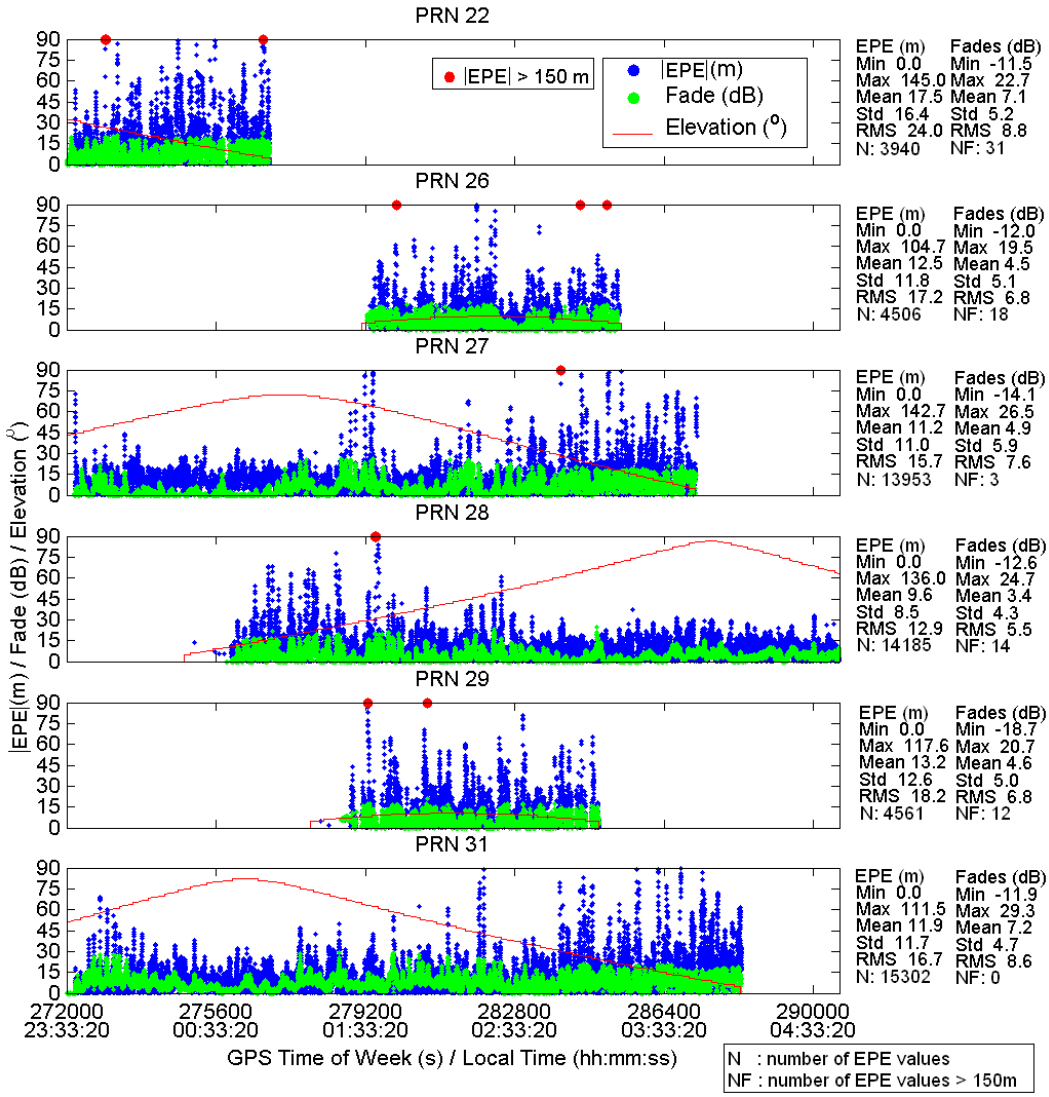

Figure 6.8: Static Forest Test - Time Series Fading and EPE Data for the HS Receiver Part 3 of 3

6.1.4 Fading

The fading data was binned into groups of elevation angle by 15^o. Figures 6.9, 6.10, and 6.11 show the fading histograms for each elevation angle grouping for the SiRF HS, SiRF ST, and OEM4 receivers respectively. Corresponding statistics are given in

Tables 6.3, 6.4, and 6.5, for the SiRF HS, SiRF ST, and OEM4 receivers respectively.

The fading distributions indicate that the availability of measurements at elevation angles less than 45^o is much higher for the HS receiver. This is reflected in the number of samples for the elevation groups and shows that the HS receiver tracks more signals at lower elevation angles and high associated signal fades.

Maximum fading effects range from 22 to 29 dB for the HS receiver, while typical fades of 5 dB at high elevations and 9 dB at low elevations occur. Typical fades for the ST receiver are about 5 dB and 3 to 4 dB for the OEM4. Maximum fades for the ST receiver range from 18 to 28 dB while the maximum fades for the OEM4 are less than 20 dB.

The occurrence of negative fading can be attributed to multiple sources. Constructive interference due to multipath causes some negative fading. A small RF line bias at the base station would cause a slight shift of the fading distributions to the left and result in some negative fading. While the reference station in Vaudreuil had a clear view of the sky, interference due to multipath is still possible at low elevations, and this might cause some reference station C/N_0 values to be lower than those at the test location. In addition, the accuracy of the fading measure in controlled conditions for low elevations is 2.0 to 3.0 dB at 3 sigma.

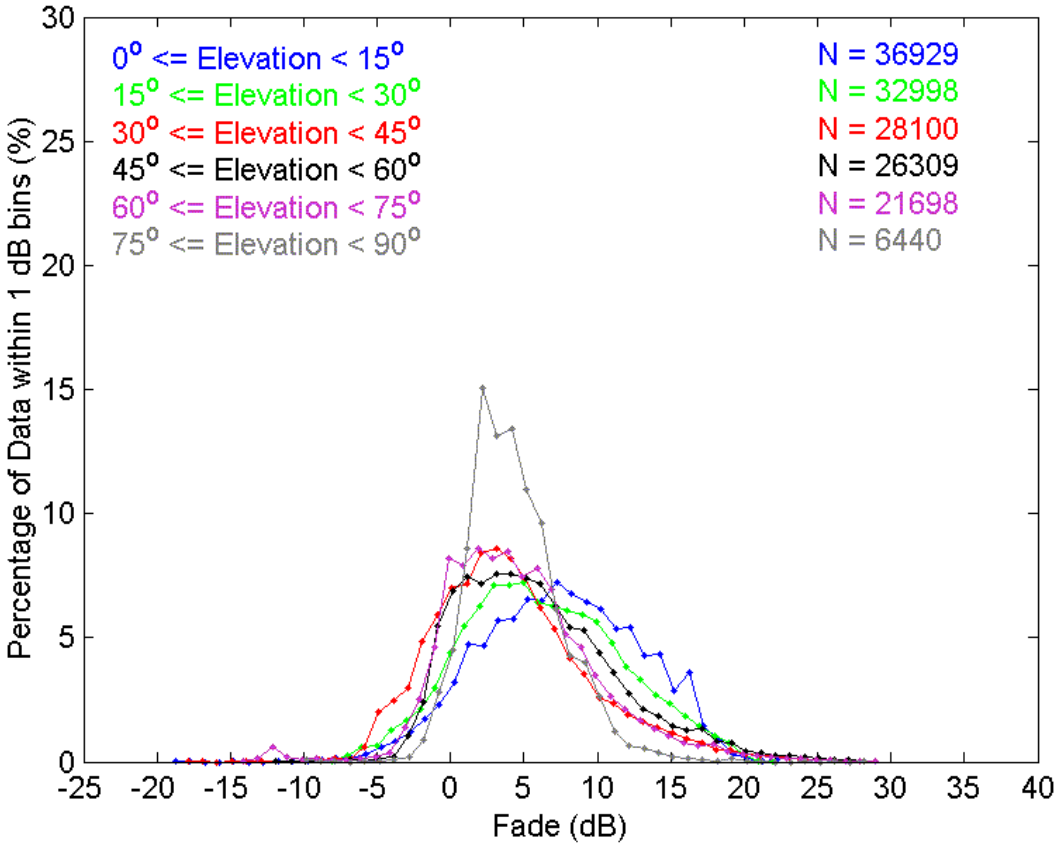

Figure 6.9: Static Forest Test - Fading Histograms for SiRF HS

Table 6.3: Static Forest Test - SiRF HS Receiver Fading Statistics Grouped By Elevation Angle

Elevation Angle Range (°)	Number of Measurements	Max (dB)	Mean (dB)	σ (dB)	RMS (dB)
00-15	36929	22.7	7.5	5.3	9.2
15-30	32998	22.0	6.2	5.4	8.2
30-45	28100	26.0	4.2	5.4	6.8
45-60	26309	28.9	5.9	5.4	8.0
60-75	21698	29.3	4.8	5.3	7.1
75-90	06440	28.6	4.4	3.2	5.5

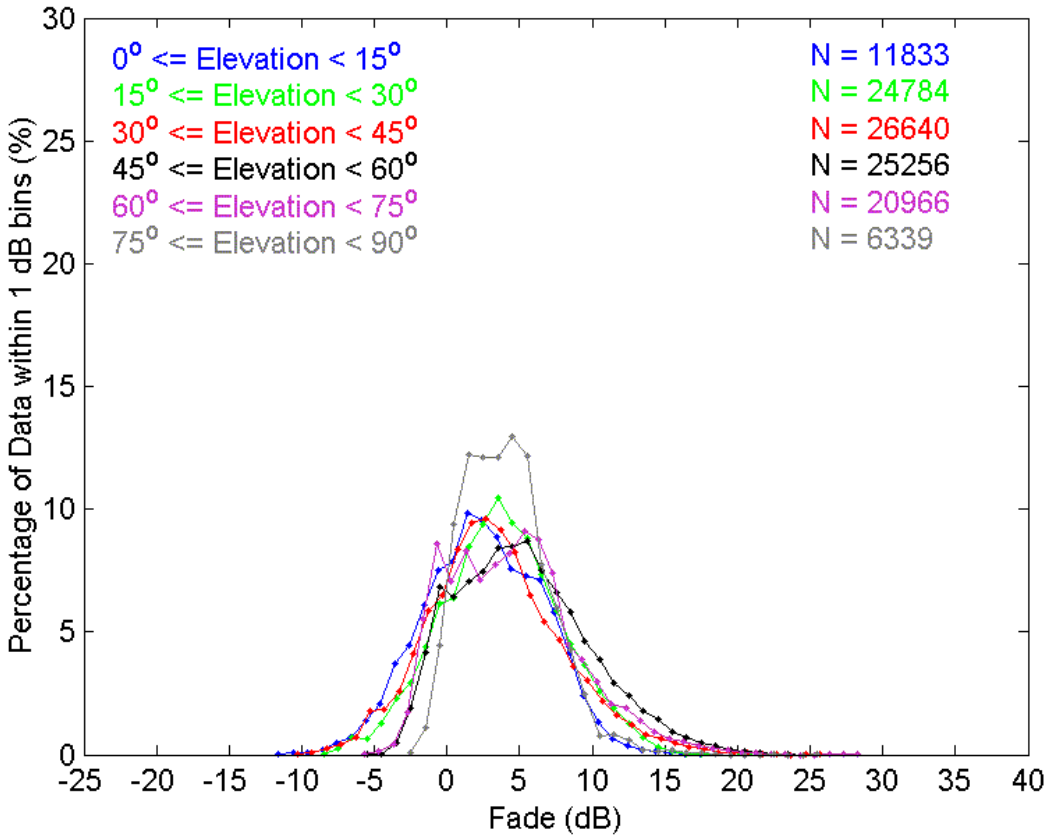

Figure 6.10: Static Forest Test - Fading Histograms for SiRF ST

Table 6.4: Static Forest Test - SiRF ST Receiver Fading Statistics Grouped By Elevation Angle

Elevation Angle Range (°)	Number of Measurements	Max (dB)	Mean (dB)	σ (dB)	RMS (dB)
00-15	11833	18.0	2.5	4.0	4.8
15-30	24784	23.0	3.7	4.1	5.5
30-45	26640	26.0	3.3	4.6	5.7
45-60	25256	25.7	5.2	4.6	6.9
60-75	20966	28.3	4.4	4.4	6.2
75-90	06339	25.5	4.0	3.0	5.0

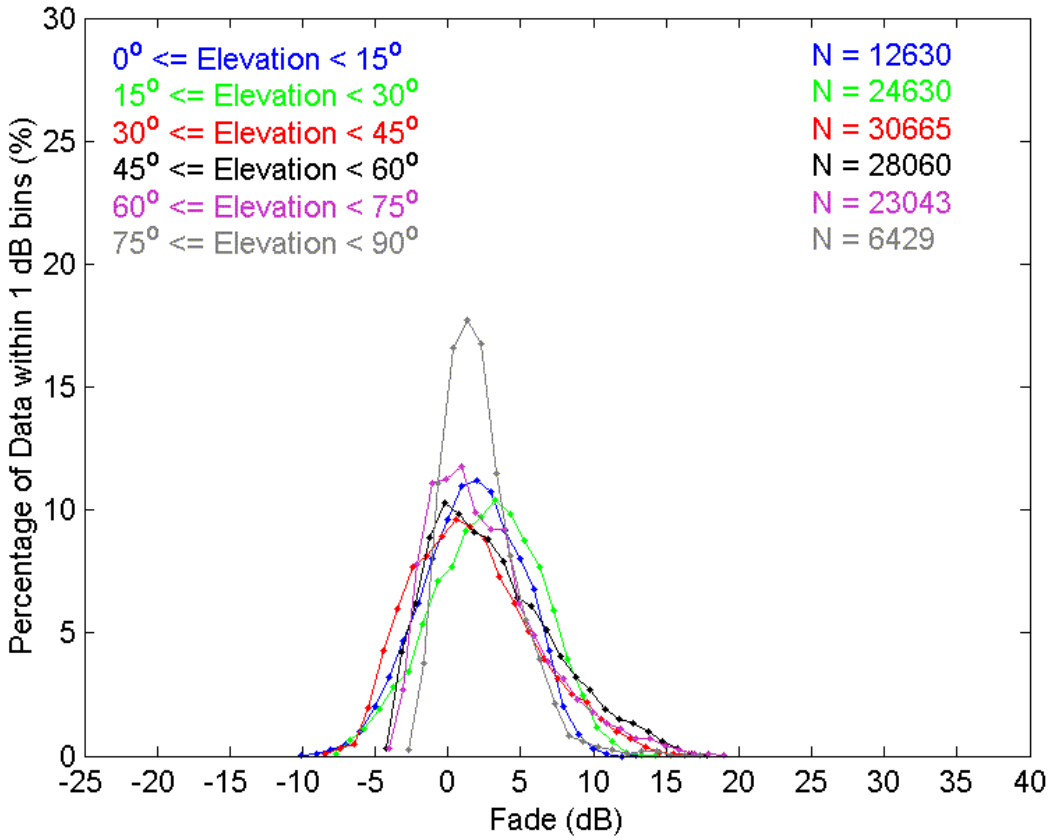

Figure 6.11: Static Forest Test - Fading Histograms for OEM4

Table 6.5: Static Forest Test - OEM4 Receiver Fading Statistics Grouped By Elevation Angle

Elevation Angle Range (°)	Number of Measurements	Max (dB)	Mean (dB)	σ (dB)	RMS (dB)
00-15	12166	13.6	1.6	3.4	3.8
15-30	24630	15.0	2.7	3.8	4.6
30-45	26566	17.5	2.2	4.1	4.7
45-60	25388	18.3	3.6	4.1	5.4
60-75	21245	19.6	2.8	3.9	4.8
75-90	06429	17.8	2.2	2.5	3.4

6.1.5 Estimated Pseudorange Error

The EPE test values were also binned into 15^o elevation groups. The distributions of the EPE values grouped in 15^o bins are shown in Figures 6.12, 6.13, and 6.14 for the SiRF HS, SiRF ST, and OEM4 receivers respectively. The corresponding statistics are shown in Tables 6.6, 6.7, and 6.8.

The variance of the measurements obtained at less than 30^o is 5 to 10 m greater for the HS receiver when compared to the ST and OEM4 receivers. This is also indicated by the shape of the associated distributions for the HS receiver. Measurement availability is higher for the HS receiver for satellite elevations less then 30^o but these measurements are often of poor accuracy. The HS measurement precision for satellites with elevations less than 30^o is close to 20 m at 1-sigma. The OEM4 receiver makes high precision measurements when it tracks satellites but the measurement availability at less than 45^o is much less than the HS receiver. The ST receiver obtains more measurements at lower elevations than the OEM4 and its measurement precision reflects the wide correlation method employed.

The EPE values at elevation angles less than 30 degrees are not zero mean for the OEM4 receiver. They are biased by -3 to -4 m. This effect is more pronounced for the SiRF HS and SiRF ST receivers with a bias of -12 m. Higher elevation satellites have a slight positive bias up to 8 m.

The method used to establish the height of Point G was examined for possible errors. The height of Point G was compared by two different methods. The NovAtel OEM4 data was processed using C^{3}NavG^{2TM} in code differential mode without position constraint and the computed height was compared to that of the surveyed position. The height values were consistent to within 2 m. In addition, a single point solution was carried out using only the NovAtel OEM4 data with pre-

cise orbits and clocks obtains from Natural Resources Canada's Geodetic Survey Division (NRCAN's CACS service), and Klobuchar ionospheric coefficients from CODE, [http://www.cx.unibe.ch/aiub/ionosphere.html]. This position differed by only about 2 m horizontally and 6 m vertically. The limited vertical precision of this method is due to residual ionospheric delays. The conventional survey method of establishing the height of Point G was also compared with a calibrated barometric height determination and these solutions differed by only 1 m.

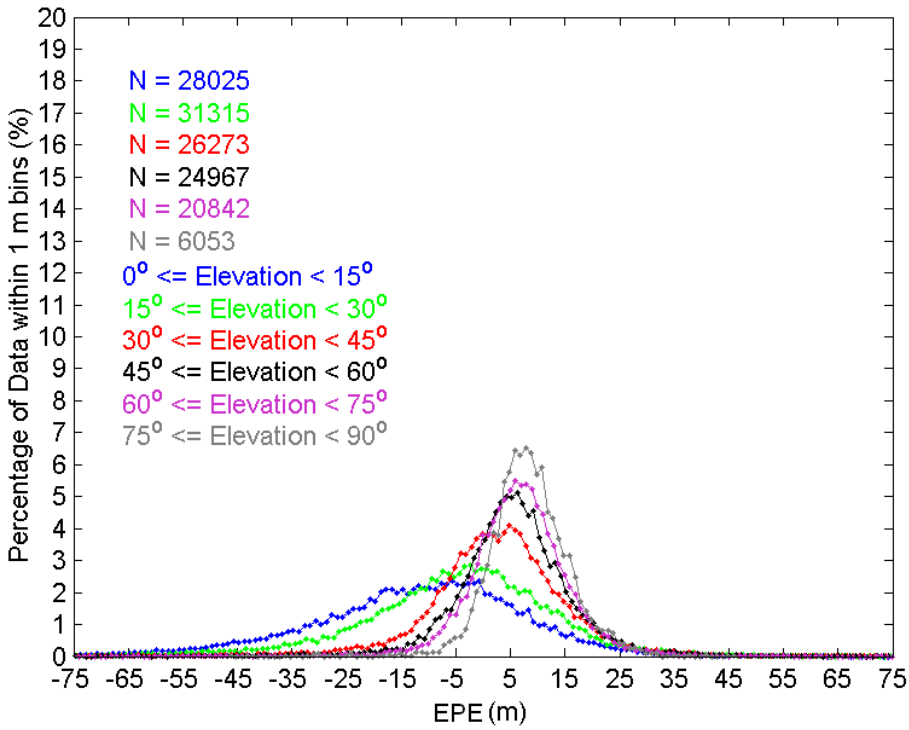

Figure 6.12: Static Forest Test - SiRF HS Distributions of EPE Values

Table 6.6: Static Forest Test - SiRF HS Receiver EPE Statistics Grouped By Elevation Angle

Elevation Angle Range (°)	Number of Measurements	Max (m)	Min (m)	Mean (m)	σ (m)	RMS (m)
00-15	28025	144.5	-139.7	-12.1	20.4	23.7
15-30	31315	147.3	-149.4	-5.3	18.9	19.7
30-45	26273	145.7	-149.2	2.4	13.9	14.1
45-60	24967	149.4	-146.8	5.4	12.0	13.1
60-75	20842	146.3	-121.1	6.5	9.9	11.8
75-90	6053	46.6	-46.2	8.4	7.5	11.2

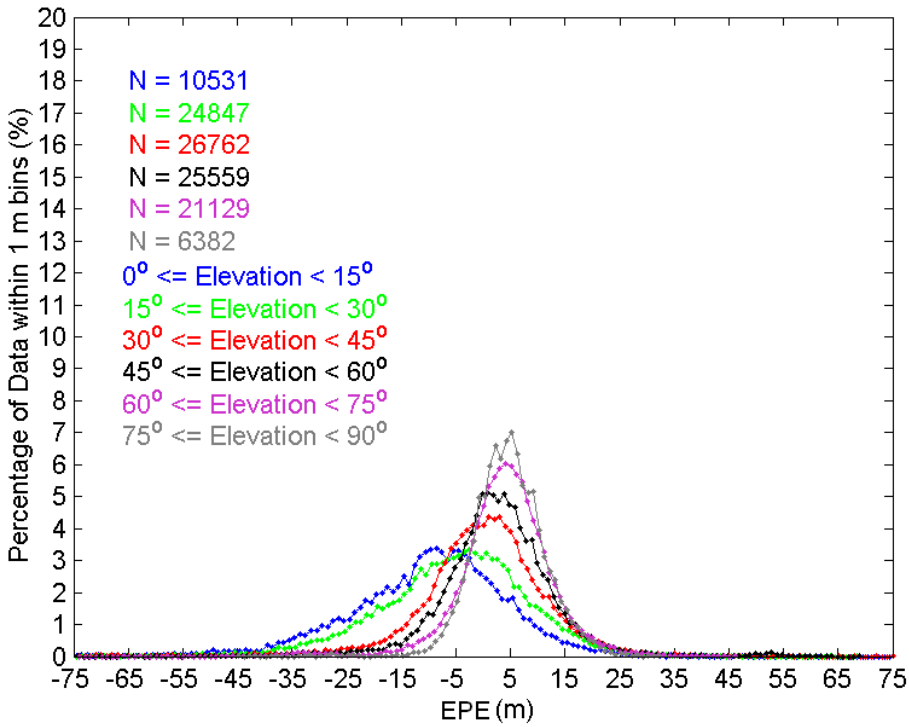

Figure 6.13: Static Forest Test - SiRF ST Distribution of EPE Values

Table 6.7: Static Forest Test - SiRF ST Receiver EPE Statistics Grouped By Elevation Angle

Elevation Angle Range (°)	Number of Measurements	Max (m)	Min (m)	Mean (m)	σ (m)	RMS (m)
00-15	10531	80.1	-92.5	-10.0	14.7	17.8
15-30	24847	69.3	-84.4	-5.4	13.9	14.9
30-45	26762	103.5	-97.9	0.3	15.1	15.1
45-60	25559	68.9	-75.1	2.6	11.0	11.3
60-75	21129	47.1	-98.9	4.0	8.8	9.7
75-90	6382	32.7	-44.7	4.7	6.7	8.2

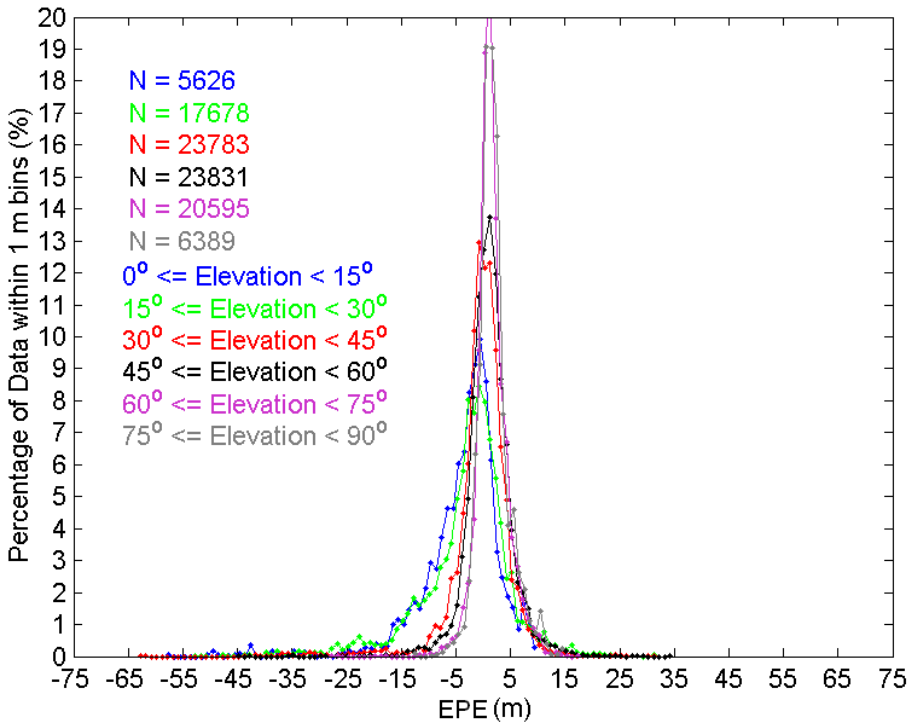

Figure 6.14: Static Forest Test - OEM4 Distributions of EPE Values

Table 6.8: Static Forest Test - OEM4 Receiver EPE Statistics Grouped By Elevation Angle

Elevation Angle Range (°)	Number of Measurements	Max (m)	Min (m)	Mean (m)	σ (m)	RMS (m)
00-15	5626	10.4	-57.5	-4.0	7.7	8.7
15-30	17678	31.8	-52.8	-3.2	8.5	9.1
30-45	23783	31.6	-62.8	-0.3	5.6	5.6
45-60	23831	35.2	-44.8	1.1	4.3	4.4
60-75	20595	17.8	-27.7	1.6	2.9	3.3
75-90	6389	15.3	-12.4	1.9	3.0	3.5

The cumulative distributions of the absolute EPE values are shown in Figures 6.15, 6.16, and 6.17 for the SiRF HS, SiRF ST, and OEM4 units respectively. These figures also show the EPE values for the 50^{th} and 95^{th} percentiles of the sample data. There are clearly correlated increasing pseudorange error effects with decreasing elevation angles. This is due to a combination of increased noise and multipath at lower elevations. These effects cannot be differentiated in this case.

The 50^{th} and 95^{th} percentile EPE values for low elevation satellites, 0 to 15^{o} indicate the general measurement performance of each receiver well. The HS, ST, and OEM4 have 14 m, 10 m, and 4 m 50^{th} percentile EPE values and 48 m, 35 m, and 16 m 95^{th} percentile EPE values.

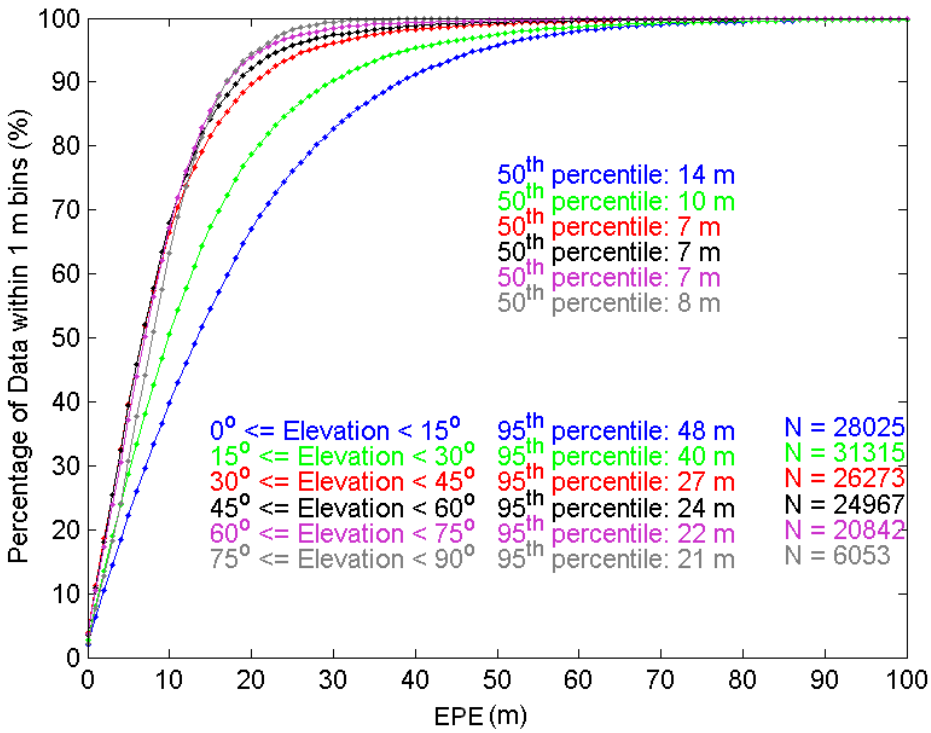

Figure 6.15: Static Forest Test - SiRF HS Cumulative Distributions of Absolute EPE Values

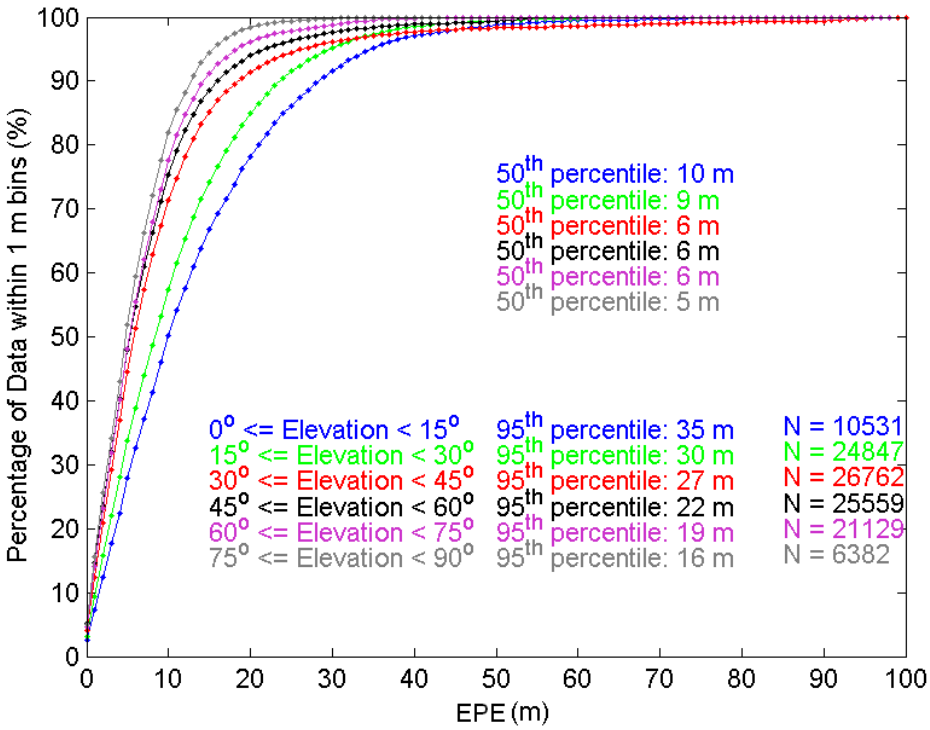

Figure 6.16: Static Forest Test - SiRF ST Cumulative Distributions of Absolute EPE Values

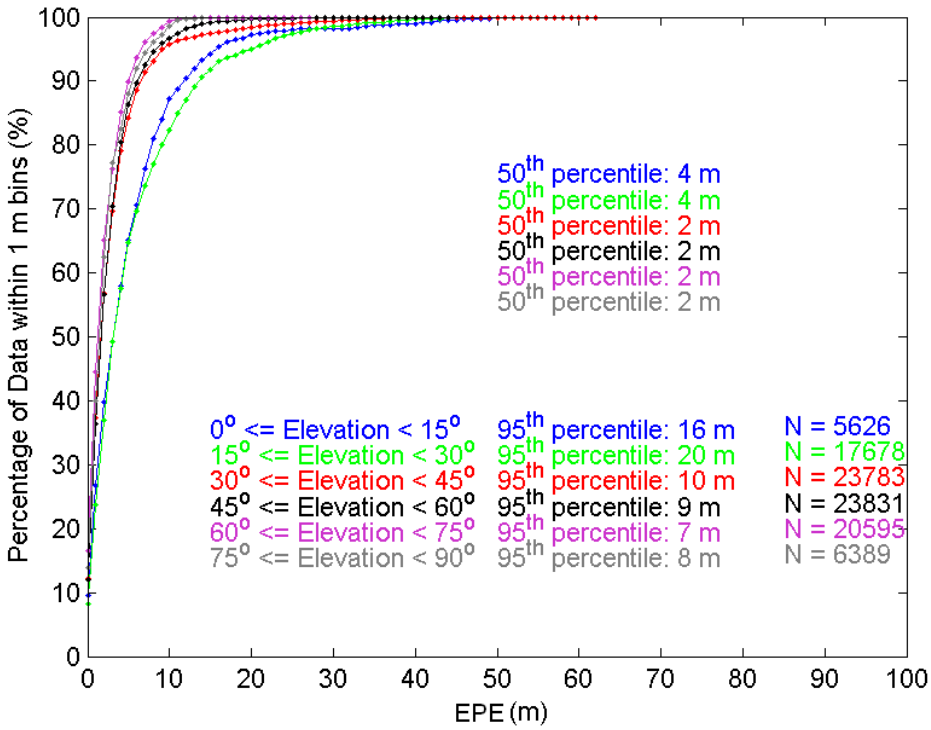

Figure 6.17: Static Forest Test - OEM4 Cumulative Distributions of Absolute EPE Values

6.1.6 Positioning Accuracy, Solution Availability, and Dilution of Precision

In order to assess the impact of the pseudorange errors induced in this environment, it is necessary to examine the positioning accuracy achievable with the available measurements on an epoch by epoch least-squares basis. This means all the measurements must be included in the solution. However, it is known from the EPE analysis that measurement faults do occur and will need to be removed from the solutions if possible. For this reason, epoch by epoch least-squares solutions with fault detection and exclusion enabled are computed as well. Since this static test point is

known, a height fix will be used to improve the ability to detect measurement faults and only the horizontal position domain will be assessed.

The plan view of the horizontal positioning solution and associated accuracy statistics for the HS, ST, and OEM4 receivers for the case with and the case without fault exclusion and as a function of the HDOP are shown in Figure 6.18. There are very large position errors for the HS receiver due to measurements of cross correlation signals. These errors reach the kilometre level. The positioning accuracy and reliability of the HS receiver is much improved when fault exclusion is enabled. This is not the case for the ST and OEM4 receivers as their measurements are less contaminated by faults and due to low measurement availability, the removal of measurements often adversely affects the solution geometry. In fact, the statistics show that the solutions with fault exclusion are worse than without fault exclusion for the ST and OEM4 receivers. Figure 6.18 shows the HDOP of the solution by color coding the points on the plan view. In an effort to show the statistics for the solutions when geometry is good, the statistics were also computed for solutions with HDOP lower than 5. The choice of when to exclude a measurement when redundancy is low and DOP may be adversely affected is difficult.

The RMS horizontal accuracy for the HS, ST, and OEM4 receivers with fault exclusion enabled and a HDOP mask of 5.0 was 25.3 m, 22.8 m and 10.6 m respectively. The performance of the HS and ST receivers is not very different, although the HS has better solution availability and HDOP in general.

The solution availability with height fixing with and without fault exclusion when HDOP is lower than 5 is also given in Table 6.9.

Table 6.9: Static Forest Test - Solution Availability with Height Fixing for HDOP < 5

Receiver	With Fault Exclusion	Without Fault Exclusion
HS	98.8	99.9
ST	96.1	99.2
OEM4	96.6	97.9

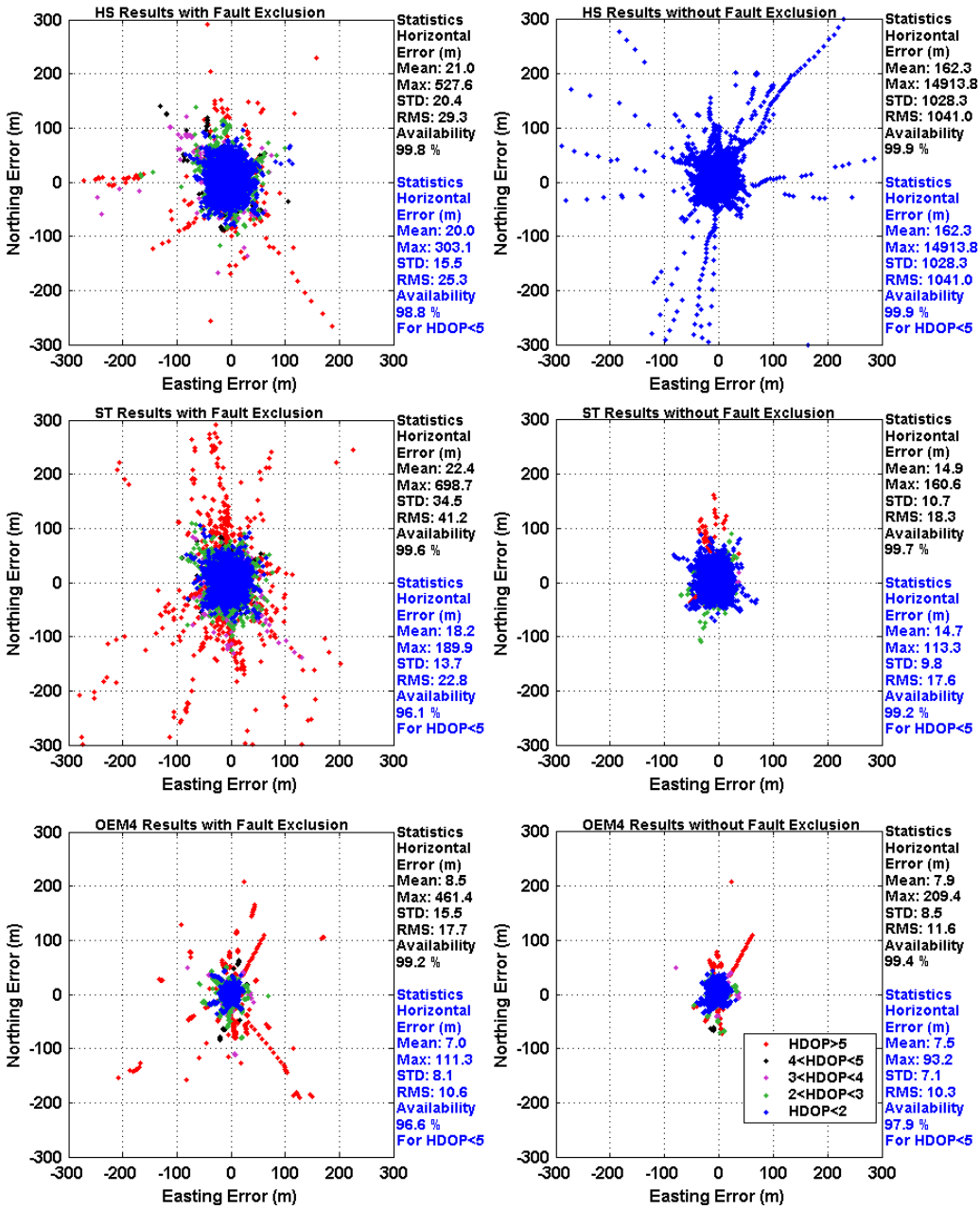

Figure 6.18: Static Forest Test - Plan View of the Horizontal Positioning Solutions for All Receivers with and without Fault Exclusion

6.2 Kinematic Testing

Data was collected using a SiRF HS receiver in parallel with a NovAtel OEM4 using a common NovAtel 600 model antenna. The standard model SiRF (ST) receiver was not available during this test. A comparative analysis is presented for the NovAtel OEM4 and the SiRF HS receiver. Data was also collected at the Vaudrueil reference station using a SiRF HS receiver in parallel with a NovAtel OEM4 using a common NovAtel 600 model antenna.

The test was performed by driving the loop once after a warm-up period. The antenna was mounted on the roof of a Ford Explorer roughly above the area between the driver and front passenger seats. The warm-up period in open sky conditions was followed by a 10 to 20 minute period in which the loop was driven at speeds below 20 km/h. The loop was run 6 times on July 15, 2002. The timing details of each run are listed in Table 6.10. A total of 5964 seconds, 1.7 hours, of test data was collected (excluding warm-up period data).

Adequate truth trajectory information was not available for an EPE analysis of the kinematic data. However, the fading and position domain analysis is still applicable.

Table 6.10: July 15, 2002, Kinematic Loop Tests

Test Label	Initialization Time of Week (s)	Start Time Of Week (s)	End Time Of Week (s)	Test Duration (s)
1100	140400	142340	143100	760
1200	143400	144800	145400	600
1300	147300	148317	150023	1706
1400	151000	151370	152750	1380
1700	161800	162725	163440	715
1730	163624	164560	165363	803

6.2.1 Measurement Availability

The availability of measurements and associated statistics for the satellites tracked by each receiver is shown in Figure 6.19. The figure includes data obtained during the specified test periods (no initialization data included) and shows the data in a contiguous fashion with vertical lines differentiating the different tests. The HS receiver is able to track on average 9.3 satellites while the OEM4 receiver maintains an average of 4.7 satellites. There is a distinct measurement availability difference when comparing the HS receiver to the OEM4 receiver.

The OEM4 receiver experiences fast intermittent signal blockages in kinematic mode while in the forest. The receiver must reacquire the signals often and thus the measurement availability is low. The HS receiver has nearly continuous tracking and demonstrates one of the distinct advantages of the high sensitivity approach.

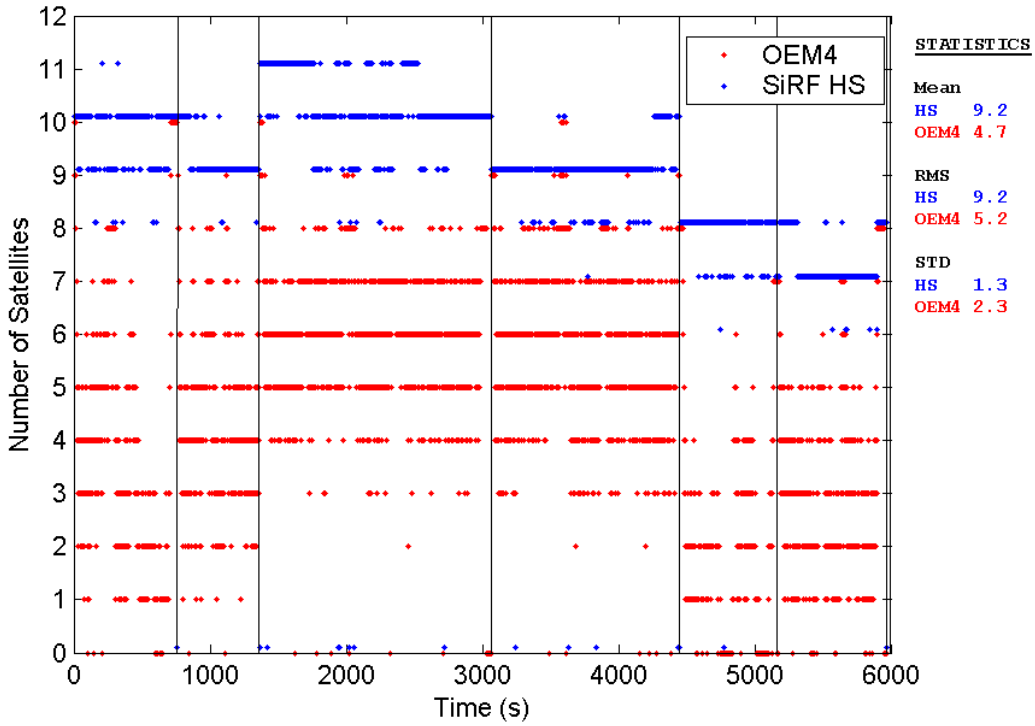

Figure 6.19: Kinematic Forest Test - Measurement Availability

6.2.2 Fading

A direct measure of fading for the HS receiver, using a like type receiver at the base station, did not provide a quality measure of signal fading due to a large line loss to the HS receiver at the base station (most likely due to a lossy cable after the signal splitter).

Signal quality was assessed by analyzing the HS receiver's output C/N_0 values and the differences from their nominal C/N_0 values as computed during the warmup period using Equations 4.3 and 4.4. The nominal C/N_0 value for each satellite was computed using an average of 300 s of its data just prior to the start of the test period while in an open-sky environment. Since the test periods are less than 30 minutes,

it is a fair assumption that the difference between the nominal C/N_0 value during the warmup period and during the test period will be a good estimator of the signal fading. This assumes the C/N_0 values do not change much over less than a 30 minute period. Upon further analysis of the data sets at the start and end of the test periods, it was found that the nominal C/N_0 values did not change by more than 1 dB. It should be noted that this method does not allow analysis of satellites acquired during the test interval.

For consistency in comparison, the same method was used in computing the fading test measure for the OEM4 receiver data.

C/N_0 values for three representative satellites including the warmup period for Run 1100 are shown in Figures 6.20 and 6.21 for the OEM4 and SiRF HS receivers respectively. Some statistics concerning the signal fading during only the test period are also shown on these figures. The OEM4 receiver exhibits tracking of mostly high elevation satellites with high C/N_0 values and low associated fading values as well as decreased tracking ability as elevation angles decrease. Typical fading values observed for the OEM4 receiver in this forest environment range from 3 to 5 dB (RMS). The HS receiver is able to track and make C/N_0 measurements for nearly all satellites while under the forest canopy. Deep fades of 15-20 dB are observed with typical (RMS) fading values ranging from 3 to 8 dB.

Since HS receiver C/N_0 measurements were available on a nearly continuous basis, signal fading can be characterized for this environment. The fading data for the HS receiver was grouped by elevation bins of 15^o and the distributions are shown in Figure 6.22. The corresponding statistics for each are shown in Table 6.11. The analysis was also performed for the OEM4 receiver for comparison purposes. These results are shown in Figure 6.23 and Table 6.12.

The availability of measurements at elevation angles less than 45^o is reflected in the number of samples for the elevation groups and shows that the HS receiver tracks more signals at lower elevation angles and higher associated signal fades.

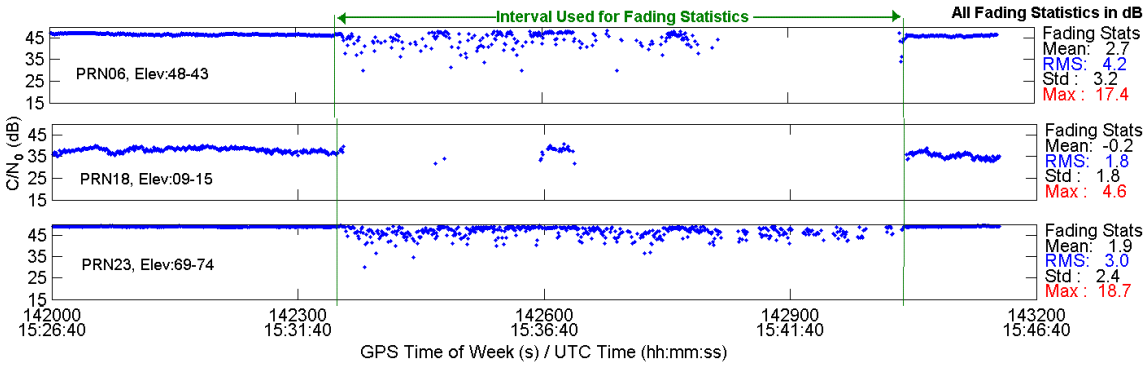

Figure 6.20: Kinematic Forest Test - OEM4 C/N_0 Values During Test 1100

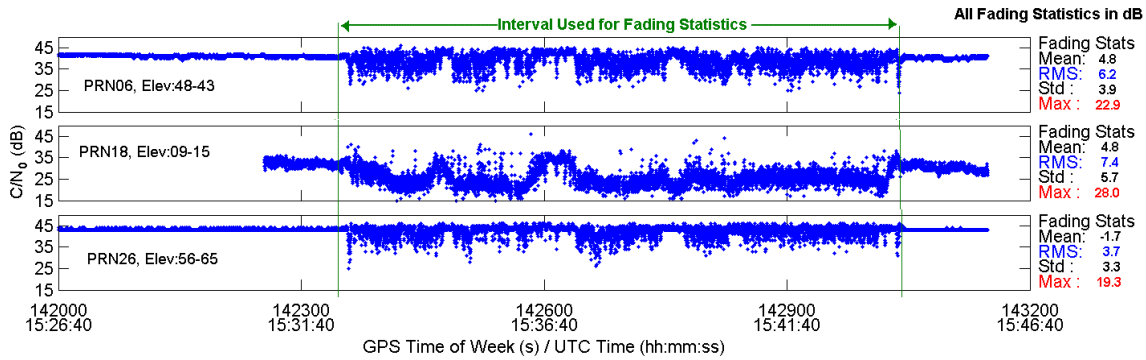

Figure 6.21: Kinematic Forest Test - HS SiRF C/N_0 Values During Test 1100

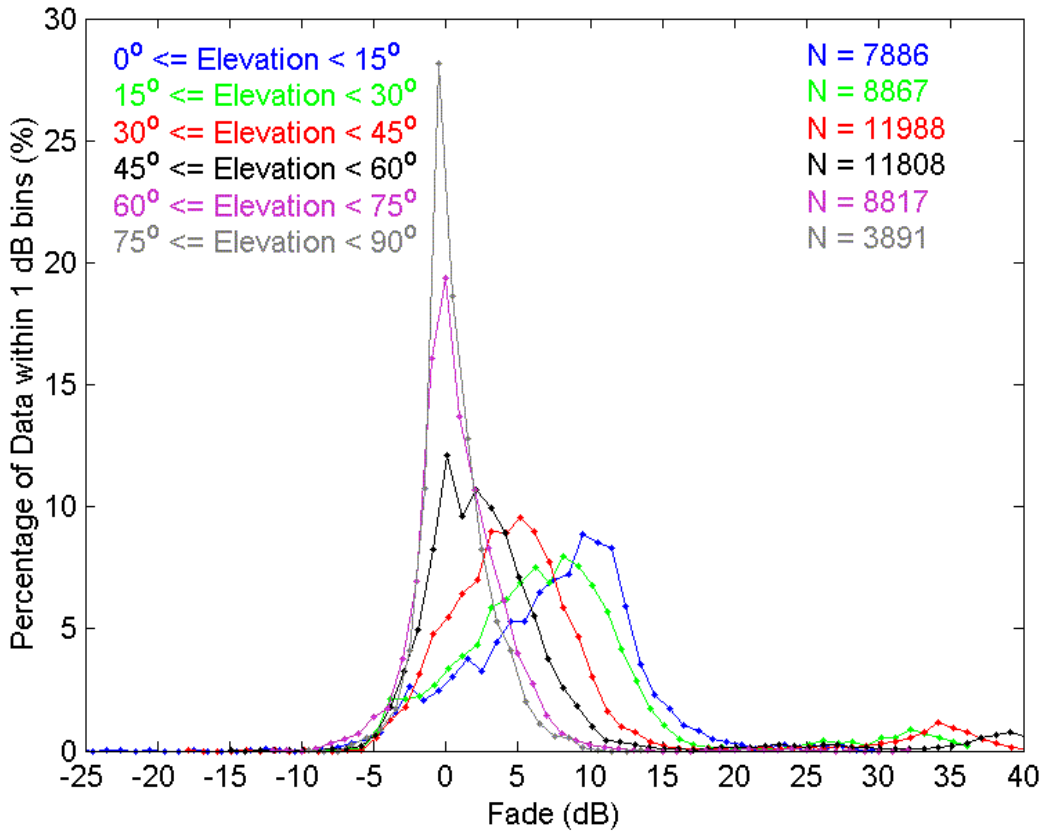

Figure 6.22: Kinematic Forest Test - Histograms of HS SiRF Fading Data

Table 6.11: Kinematic Forest Test - HS Receiver Fading Statistics Grouped By Elevation Angle

Elevation Angle Range (°)	Number of Measurements	Max (dB)	Mean (dB)	σ (dB)	RMS (dB)
00-15	7886	30.4	7.4	5.6	9.3
15-30	8867	36.7	7.6	7.4	10.6
30-45	11988	42.9	6.4	8.4	10.5
45-60	11808	43.0	4.2	8.2	9.3
60-75	8817	32.0	0.9	3.1	3.3
75-90	3891	14.2	0.6	2.3	2.4

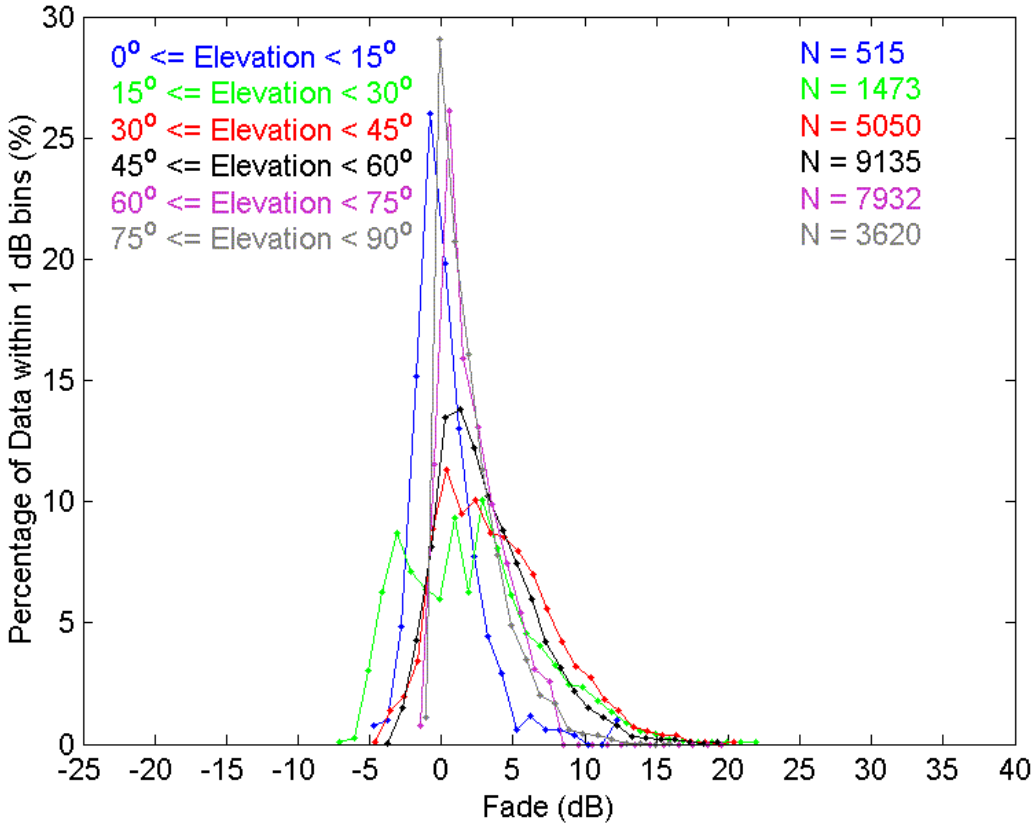

Figure 6.23: Kinematic Forest Test - Histograms of OEM4 Fading Data

Table 6.12: Kinematic Forest Test - OEM4 Receiver Fading Statistics Grouped By Elevation Angle

Elevation Angle Range (°)	Number of Measurements	Max (dB)	Mean (dB)	σ (dB)	RMS (dB)
00-15	515	12.7	0.3	2.4	2.4
15-30	1473	22.0	2.2	4.7	5.1
30-45	5050	20.9	3.8	4.0	5.5
45-60	9135	20.0	3.1	3.4	4.6
60-75	7932	20.2	2.5	2.6	3.6
75-90	3620	16.1	2.0	2.3	3.0

6.2.3 Positioning Accuracy, Solution Availability, and Dilution of Precision

Given the poor measurement availability of the OEM4 receiver during the kinematic tests, poor 3D solution availability is expected. All test data was analyzed using C^3NavG^{2TM} in differential mode and the ability of the receiver to provide a quality 3D navigation solution was challenged. The solution availability for solutions with fault exclusion enabled and a PDOP of lower than 5.0 is given in Table 6.13 for the HS and OEM4 receivers. As the height of the test trajectory did not vary more than 20 m, height fixed solutions with fault exclusion enabled were also computed. Fixing the height in this manner will slightly distort the horizontal solution but given the measurement quality observed in the static analysis, this error is at or less than the level of the noise in the position solution. The solution availability for the height fixed method with fault exclusion is shown in Table 6.14.

There is a distinct advantage when using the HS receiver in this kinematic environment. Since satellite tracking is nearly continuous, the solution availability is well over 90 % for every test. The OEM4 on the other hand requires height fixing to provide better solution availability and still can only provide a solution 30 % of the time.

Figure 6.24 shows a plan view of the horizontal position solutions using the measurements from the HS and OEM4 receivers in a height fixed solution with fault exclusion enabled for Test 1100. The position solutions are color coded to identify when good HDOP is available. The areas of availability for the OEM4 correspond to the regions of the test loop with light forest density and some open sky. The OEM4 often suffers from poor geometry as well. The HS receiver on the other hand has very good HDOP nearly throughout the test and solution availability is again apparent. The across-track accuracy of the HS solution for this test is always better

than 25 m.

However, the accuracy of the HS solution can be severely affected by measurement faults as shown in Figure 6.25 where the horizontal positions from a full position solution with no fault exclusion are shown. Here also, the poor capability of the OEM4 receiver to provide measurements in the forest is observed. The HDOP for the HS solutions is always good but measurement faults must be removed to provide reliable and accurate position solutions.

Table 6.13: Kinematic Forest Testing - Full 3D Solution Availability Given a PDOP Mask of 5.0 and with Fault Exclusion Enabled

Test	HS Solution Availability (%)	OEM4 Solution Availability (%)
1100	99.5	18.7
1200	89.8	03.0
1300	96.7	10.7
1400	94.5	13.2
1700	98.6	09.4
1730	98.9	13.8

Table 6.14: Kinematic Forest Testing - Height Fixed Solution Availability Given a PDOP Mask of 5.0 and with Fault Exclusion Enabled

Test	HS Solution Availability (%)	OEM4 Solution Availability (%)
1100	99.3	21.4
1200	93.8	10.7
1300	96.3	32.8
1400	98.4	32.0
1700	99.0	14.3
1730	99.3	16.7

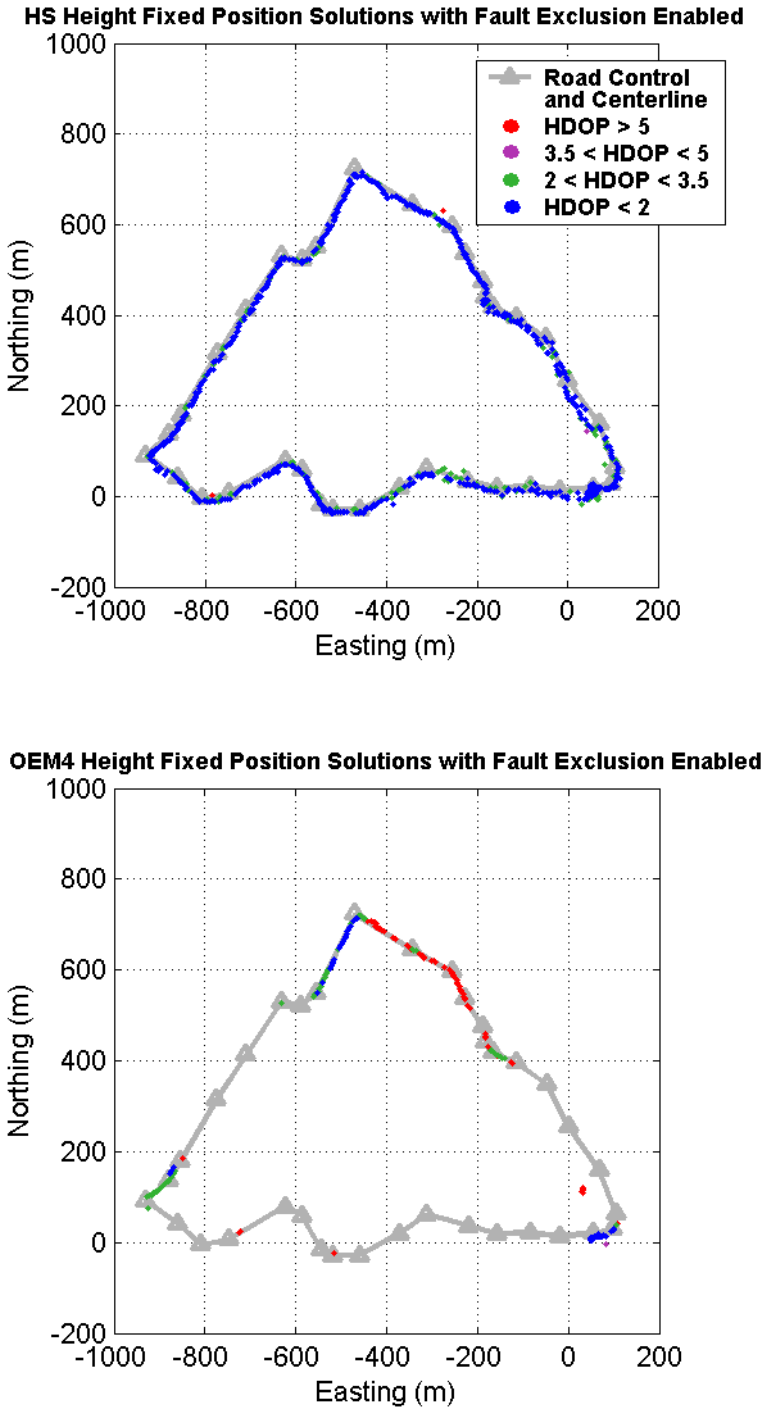

Figure 6.24: Kinematic Forest Test 1100 - Plan View of Height Fixed Solutions with Fault Exclusion Enabled

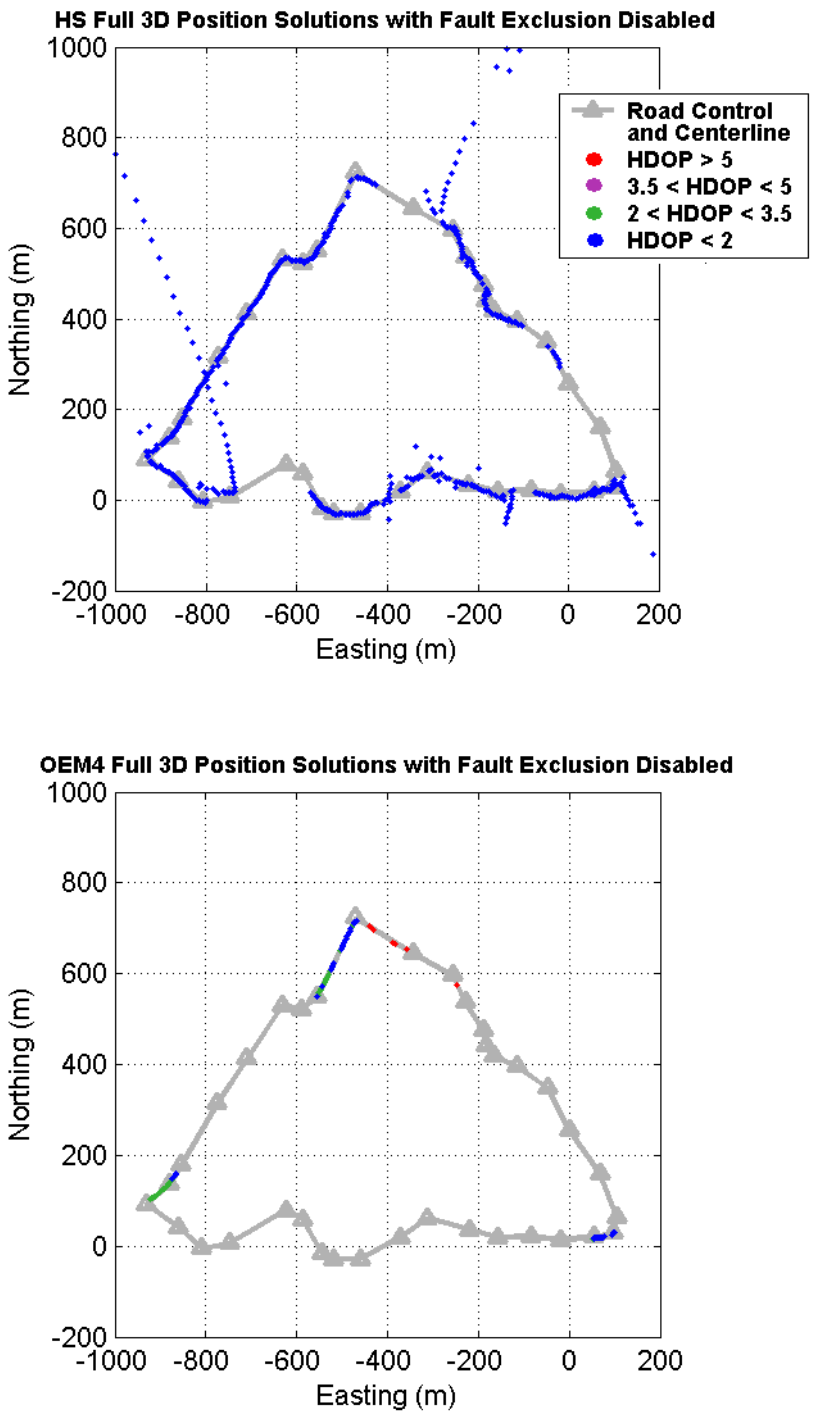

Figure 6.25: Kinematic Forest Test 1100 - Plan View of Full Position Solutions with Fault Exclusion Disabled

Chapter 7

Performance in the Urban Canyon Environment

Multipath and signal masking are severe in the urban canyon environment. Large buildings not only block signals entirely but act as strong specular reflectors that induce large multipath effects and tracking of echo only signals.

The urban canyon environment is of primary interest to possible high sensitivity users as deployment of HS GPS in cellular phones to meet the E-911 mandate is already occurring. Thus, this environment is a primary testing focus for this thesis and as such multiple tests were performed in two cities to provide a large number of sample sets in determining statistics.

A static test was performed at a location on the University of Calgary campus where the surrounding large buildings provide an urban canyon environment. Static testing assesses fading and EPE in terms of the direction of arrival of the GPS signals. In addition, positioning accuracy, dilution of precision, and solution availability can be assessed.

The downtown environments in Calgary, Alberta, and Vancouver, British Columbia, were investigated to determine the signal fading and estimated pseudorange errors while kinematic in an urban canyon. NovAtel's Black Diamond GPS/INS system was used to provide reference trajectories of high accuracy when possible. However, not all tests were successful in terms of obtaining reference navigation data as the system relies upon carrier phase differential GPS to update the system in an environment where carrier phase differential positioning is problematic due to signal masking.

In total, 11 kinematic tests were performed in downtown Calgary and 7 kinematic

tests in downtown Vancouver. All of this data will be used in assessing the fading environment of both city cores. Only tests 7 through 10 in Calgary and all but test 5 in Vancouver were successful in obtaining high accuracy reference trajectories.

Positioning accuracy, solution availability and dilution of precision are presented for a representative test case in downtown Vancouver.

7.1 Static Urban Canyon Test

7.1.1 Test Details

Static data was collected on the University of Calgary campus at a known point chosen to provide a similar signal environment as that experienced in a downtown setting. Buildings obscured the signals on the east and west sides of the location at elevation angles up to 50^o and 30^o, respectively. In addition, a walled walkway obscured signals arriving from the north below about 25^o in elevation. The southern direction was relatively unhindered with some trees contributing to signal masking from the southwest side of the test site. Photos of the test location are shown in Figure 7.1 followed by an azimuth by elevation representation of the signal-masking environment, determined from angles measured using a total station, in Figure 7.2. The building on the east and north side of the test site has a glass and metallic surface and is a probable source of strong specular signal reflection. The building on the west side of the site location has small windows and a rough stone textured exterior and is a probable source of diffuse signal reflection or obscuration.

Six hours of data were collected on July 04, 2002, as shown in Table 7.1, using a SiRF HS and an OEM4 receiver tested in parallel. Receivers of the same type as the test receiver were located at a nearby reference station location with a clear view of

the sky to facilitate differential corrections.

Fading and EPE values were only computed up until GPS time of week 418100 s for comparative purposes between the OEM4 and the HS receivers. This is because the EPE values are not available for the OEM4 receiver after 418100 s due to a lack of measurements. This still allows 3.6 hours of data for comparison.

Figure 7.1: Static Urban Canyon Testing Environment

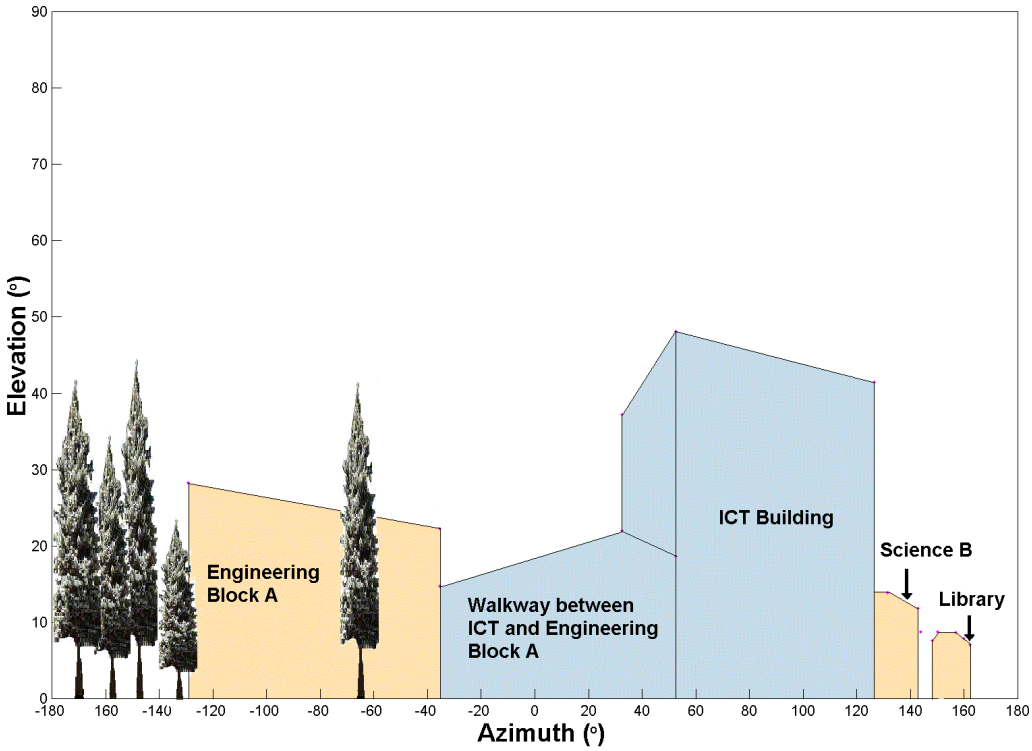

Figure 7.2: Map of Static Urban Canyon Testing Environment

Table 7.1: July 4, 2002, Static Urban Canyon Test Details

Initialization Time of Week (s)	Start Time Of Week (s)	End Time Of Week (s)	Test Duration (hours)
403800	405000	426600	6

7.1.2 Measurement Availability

The measurement availability for the static test is shown in Figure 7.3. A 120 s moving average of the number of measurements obtained is also shown to provide more intuitive comparison between the receivers tested. The HS receiver is able to provide 2 more measurements than the OEM4 receiver during most of the test and 4 more measurements at many epochs. The OEM4 is only able to track 2 or 3 satellites

during the last two hours of testing while the HS receiver is able to track 4 or 5.

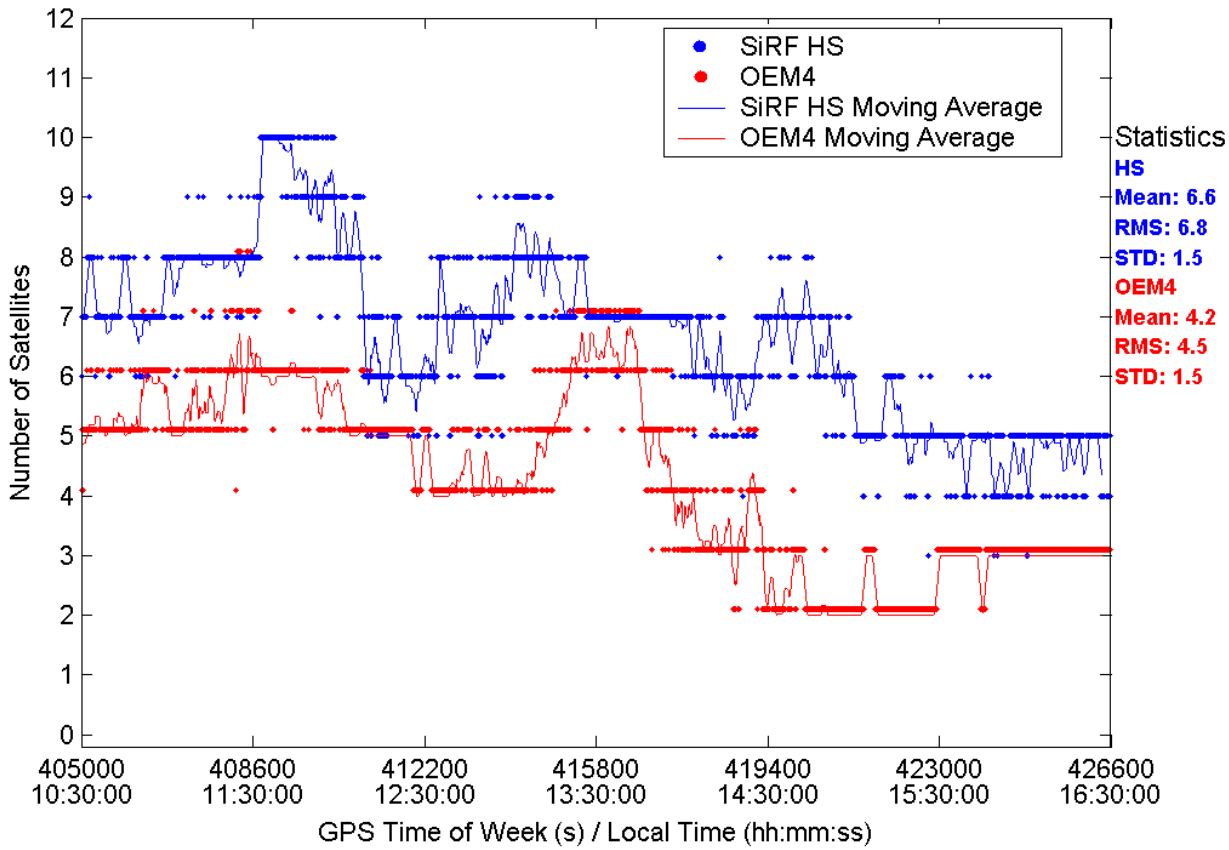

Figure 7.3: Measurement Availability In A Static Urban Canyon Environment (120 s Moving Average Was Used)

7.1.3 Fading

The static fading data from the HS and OEM4 receivers were grouped into azimuth and elevation bins, of 3^o by 3^o, to provide statistical insight into the nature of the test environment. The RMS fading value for each group is shown in Figures 7.4 and 7.5 for the SiRF HS and OEM4 receivers respectively. The sky tracks of the satellites based on the reference station data for the same time are shown in grey in

these figures.

The OEM4 and SiRF HS fading responses differ significantly in terms of which signals are tracked. In general, the OEM4 tracks only line-of-sight signals except for one satellite in particular which is behind the building to the west of the test location. The HS receiver tracks signals from satellites that are clearly located behind buildings. The building to the east of the test location is most likely acting as a strong specular reflector and is providing strong multipath and echo-only signals. This is clearly apparent with strong signals, of 5 to 10 dB fading, arriving from behind the building to the west of the test location as tracked by the HS receiver. The building to the west of the test location is a poor reflector. Signals arriving from behind the the building to the east of the test location are most likely a combination of diffuse reflections, and the attenuated line-of-sight response and thus these signals are highly faded.

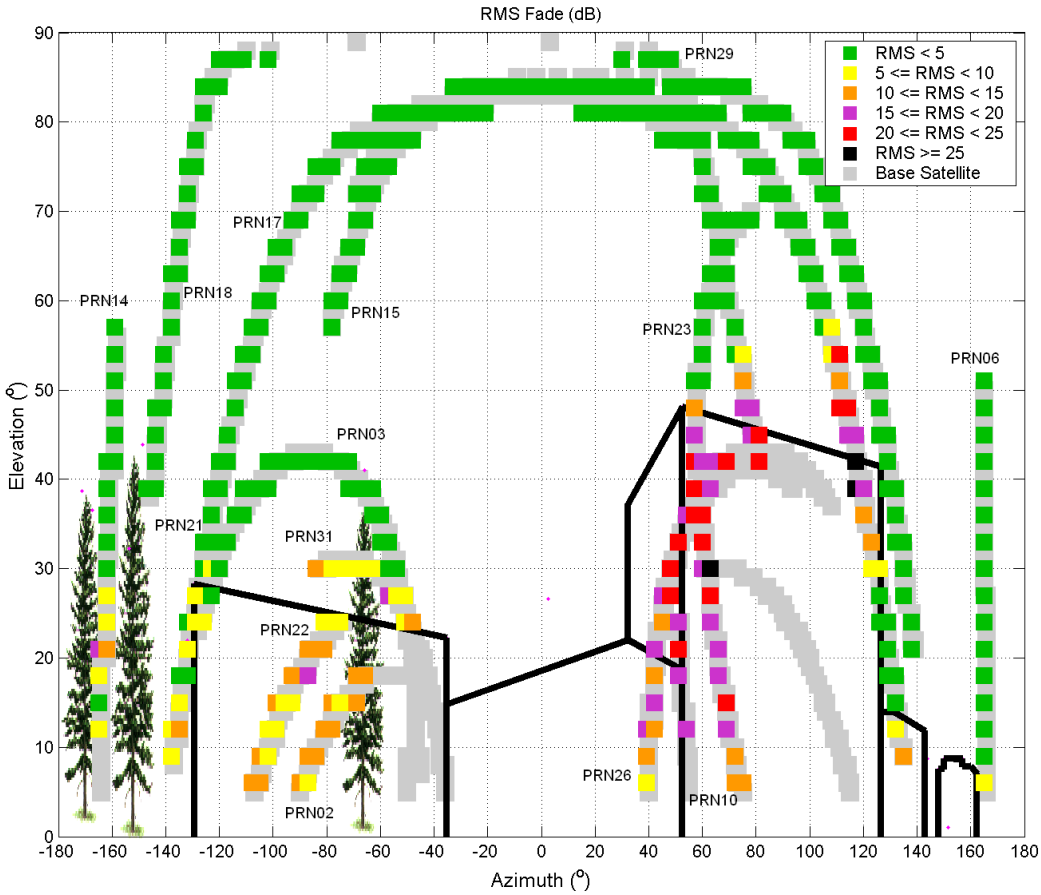

Figure 7.4: Static Urban Canyon - SiRF HS RMS Fading

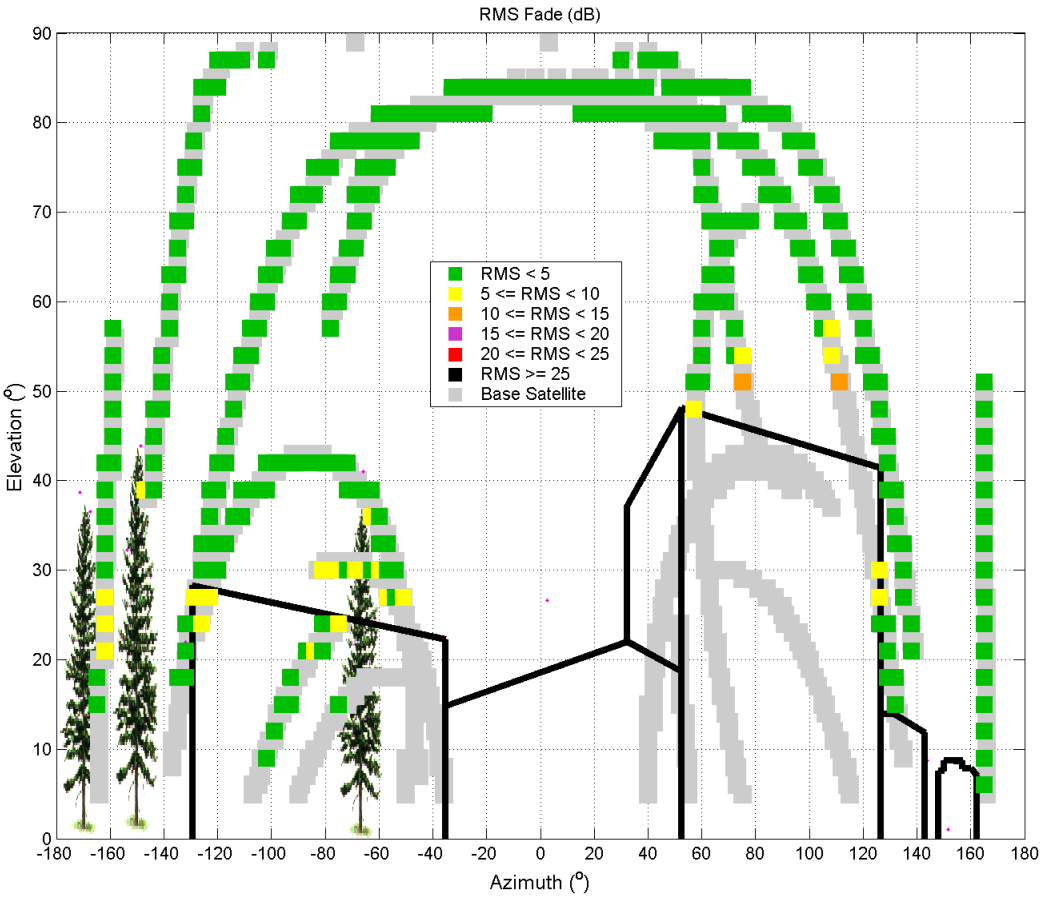

Figure 7.5: Static Urban Canyon - OEM4 RMS Fading

7.1.4 Estimated Pseudorange Errors

The EPE values for the static test were also binned into 3^o by 3^o azimuth and elevation groups and statistics for each group were computed. The RMS EPE value is a very useful measure of the amount of error from one particular group. These values are shown in Figures 7.6 and 7.7 for the SiRF HS and OEM4 receivers respectively.

The signal tracked by the OEM4 receiver that originates behind the building to the west is an echo-only signal. The OEM4 has a well known multipath response that does not include values of this magnitude. Thus, the signal that is tracked must be an

echo-only signal. Furthermore, if echo-only signals are predominantly tracked by the HS receiver for signals behind the building to the west, the magnitude of the RMS EPE values should correspond to approximately twice the distance to the reflecting source or more. The RMS EPE values are typically between 30 and 60 m which supports this reasoning considering that the building to the east is approximately 23 m away from the test point.

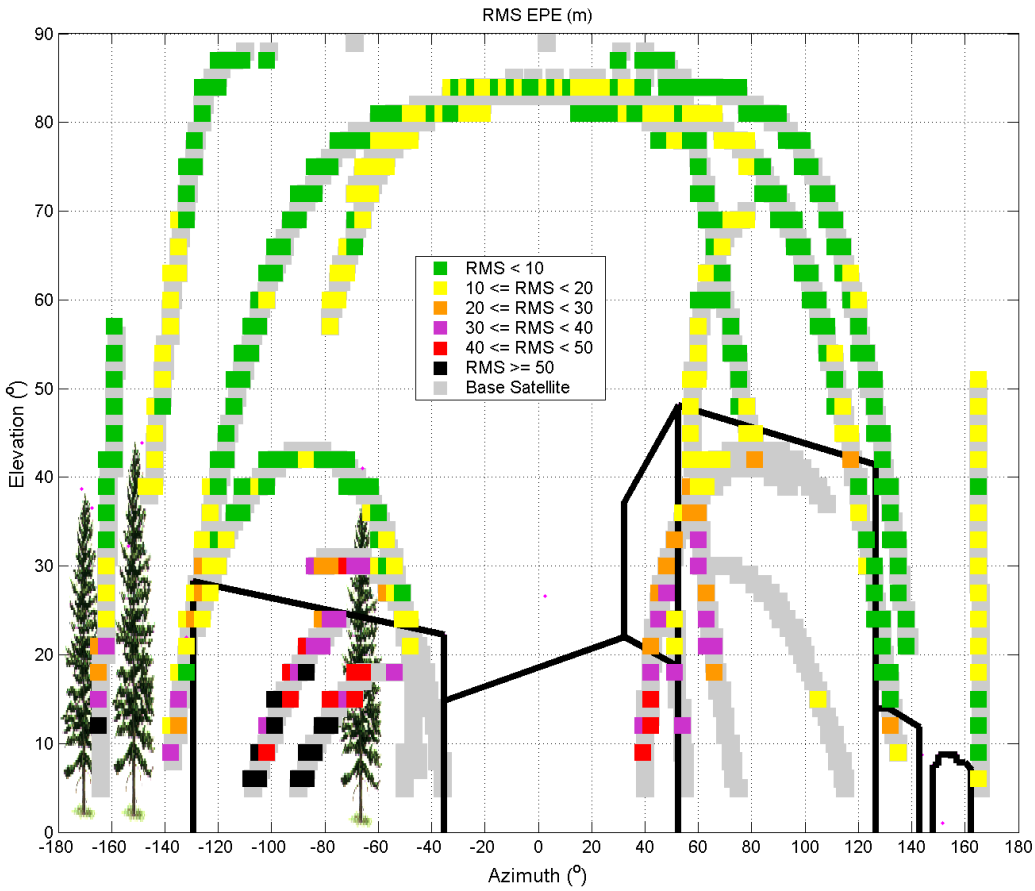

Figure 7.6: Static Urban Canyon - SiRF HS RMS EPE

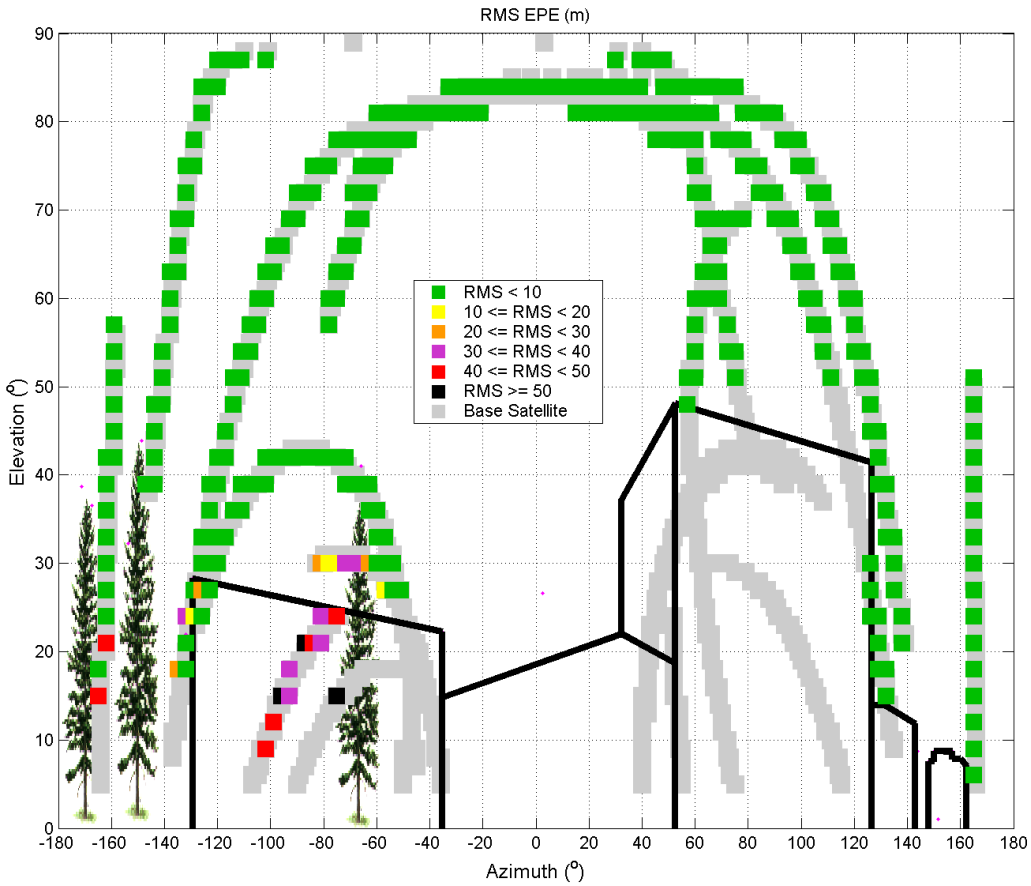

Figure 7.7: Static Urban Canyon - OEM4 RMS EPE

7.1.5 Fading and EPE Time Series Analysis for the HS Receiver

The EPE and fading values for the HS receiver are shown in time series plots in Figures 7.8 and 7.9. Highly faded signals often correspond to large pseudorange measurements errors. The results for PRN23 at GPS time of week of around 412000 s are a clear example of this. However, strong signals also have some large errors. PRN03 at 412200 s shows an error greater than 40 m while the fading value is less than 6 dB. Given that this satellite is positioned such that strong specular reflection off the building to the east is probable, large multipath errors are understandable.

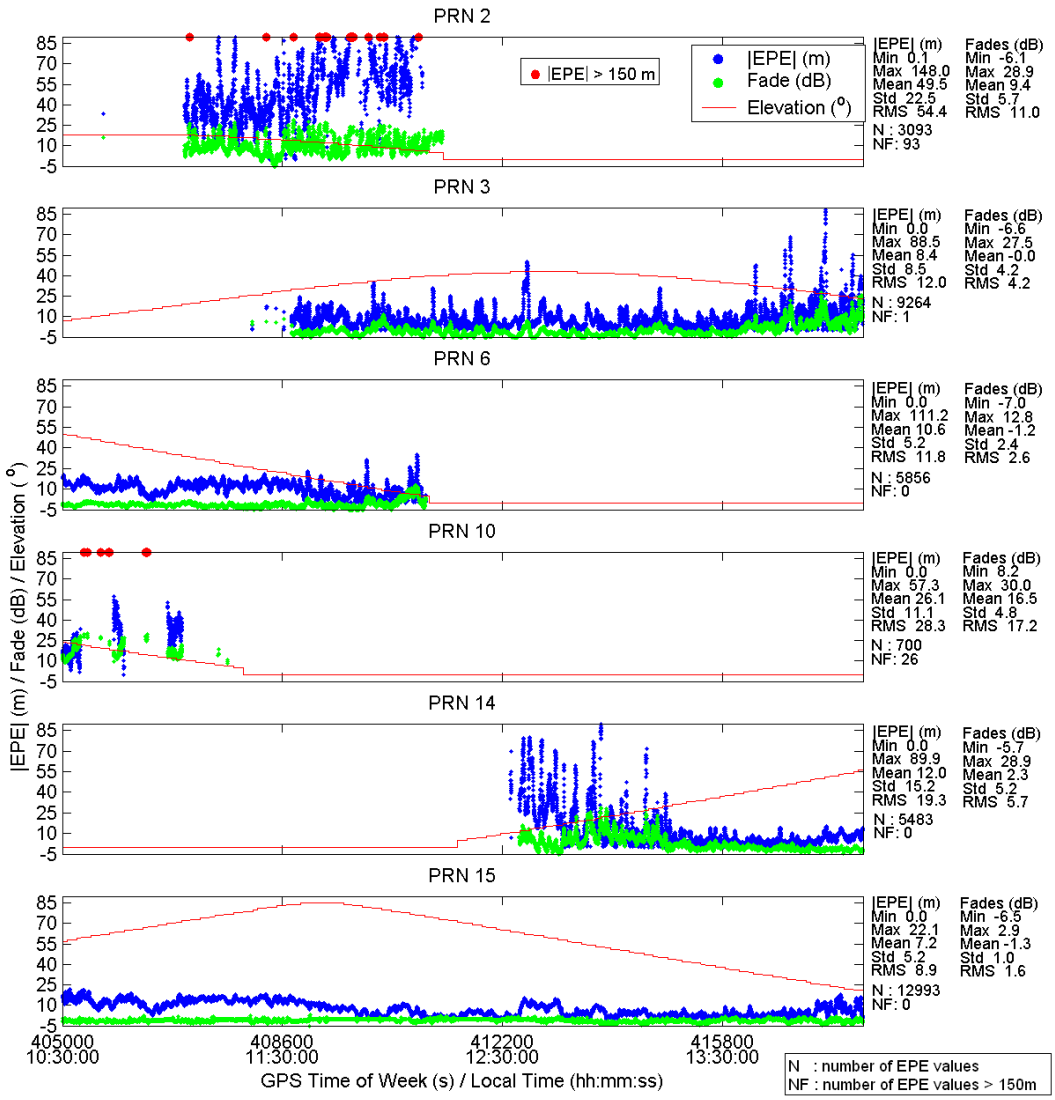

Figure 7.8: Static Urban Canyon - Time Series Fading and EPE Data for the HS receiver Part 1 of 2

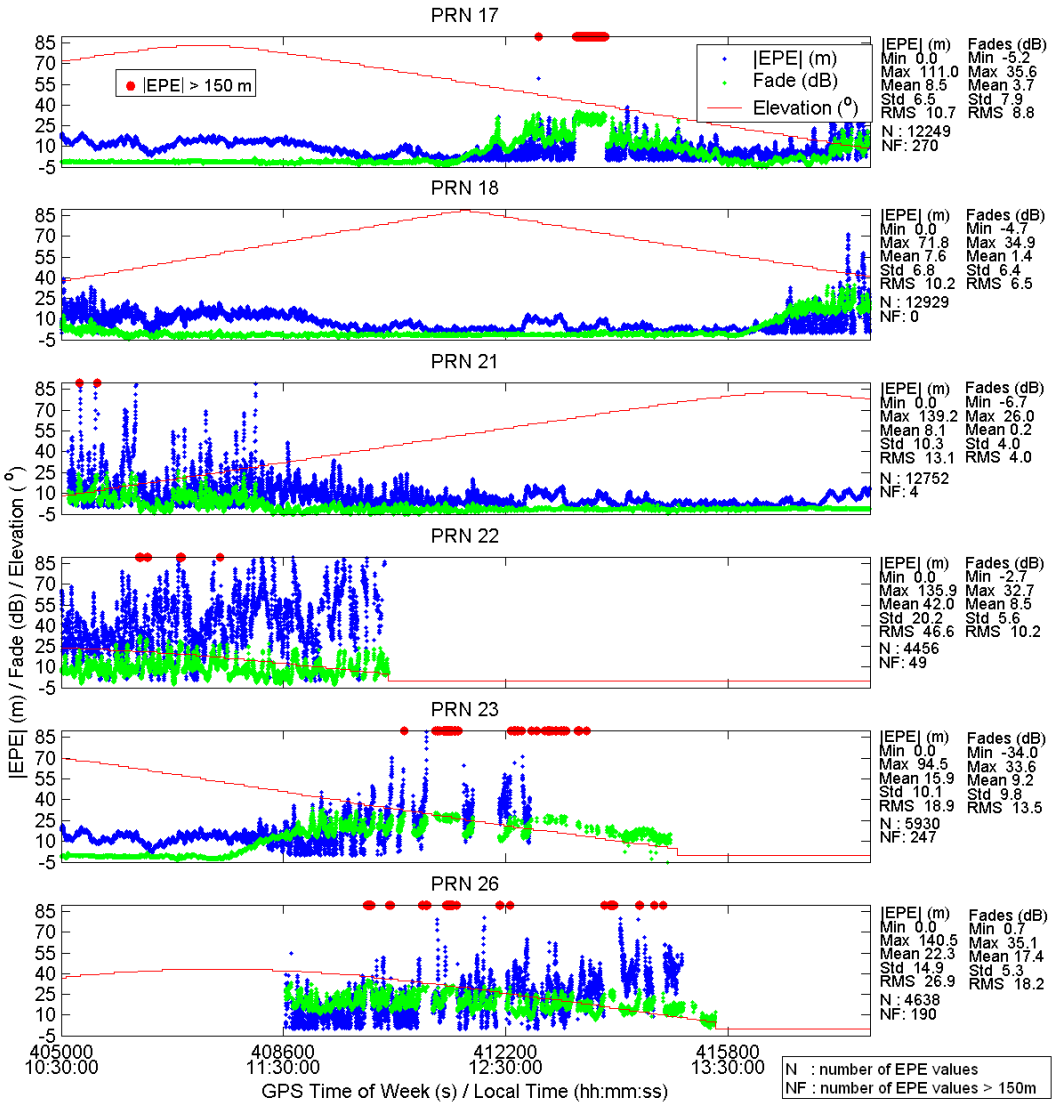

Figure 7.9: Static Urban Canyon - Time Series Fading and EPE Data for the HS receiver Part 2 of 2

7.1.6 Positioning Accuracy, Solution Availability, And Dilution of Precision

The measurements from the OEM4 and HS receivers were processed using the same method discussed in the static forest test.

The plan view of the height-fixed horizontal positioning solution and associated accuracy statistics for the HS and OEM4 receivers for the case with and the case without fault exclusion and as a function of the HDOP is shown in Figure 7.10. There are very large position errors for the HS receiver due to measurements of cross-correlation and echo-only signals. The HS horizontal position errors even reach 389 km at one point. The positioning accuracy and reliability of the HS solution is much improved when fault exclusion is enabled although large position errors are still present. The fault exclusion method used requires redundant measurements. Poor redundancy leads to difficulties identifying which measurement contains a blunder and a good measurement can sometimes be removed leaving the measurement fault to contaminate the solution. This occurs for both the HS and OEM4 solutions. The OEM4 solution with fault exclusion shows large position errors, 260 m, associated with HDOPs larger than 5.0. This occurs when the receiver has only 4 satellites in solution and measurements with large errors due to echo-only signal tracking are not removed while a good measurement is rejected. The resulting geometry is very poor and a 260 m horizontal position error occurs. The error in the case of no fault exclusion does not reach this extent because the HDOP of the solution is still good. This is more clearly understood when examining Figures 7.11 and 7.12 for the HS and OEM4 receivers respectively where the horizontal position error, associated HDOP, and number of satellites used and excluded are shown for the cases with and without fault exclusion.

The solution availability for the height fixed case with fault detection and exclusion enabled when HDOP is lower than 5.0 is 91.6 % for the HS solution and 83.6 % for the OEM4 solution.

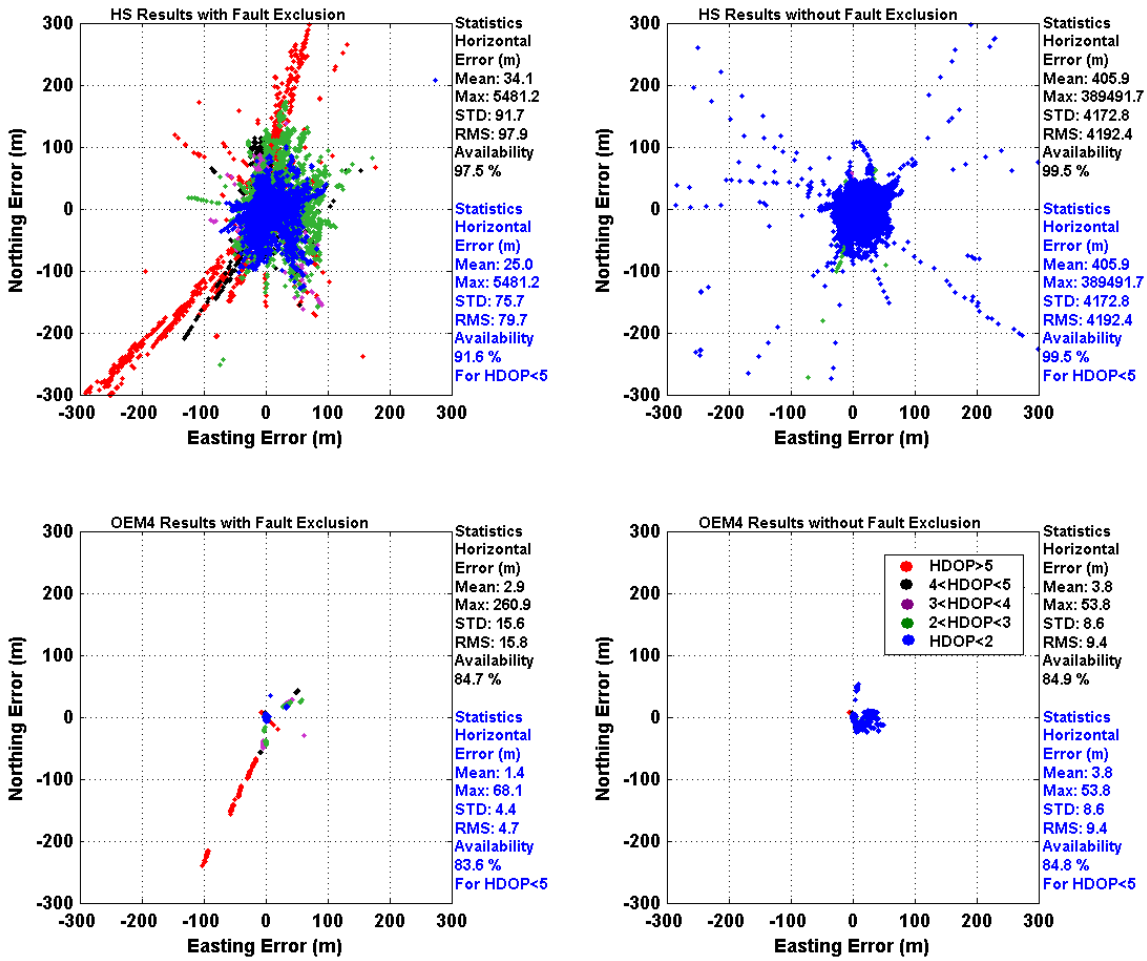

Figure 7.10: Static Urban Canyon - Plan View of Positioning Accuracy, HDOP and Associated Statistics

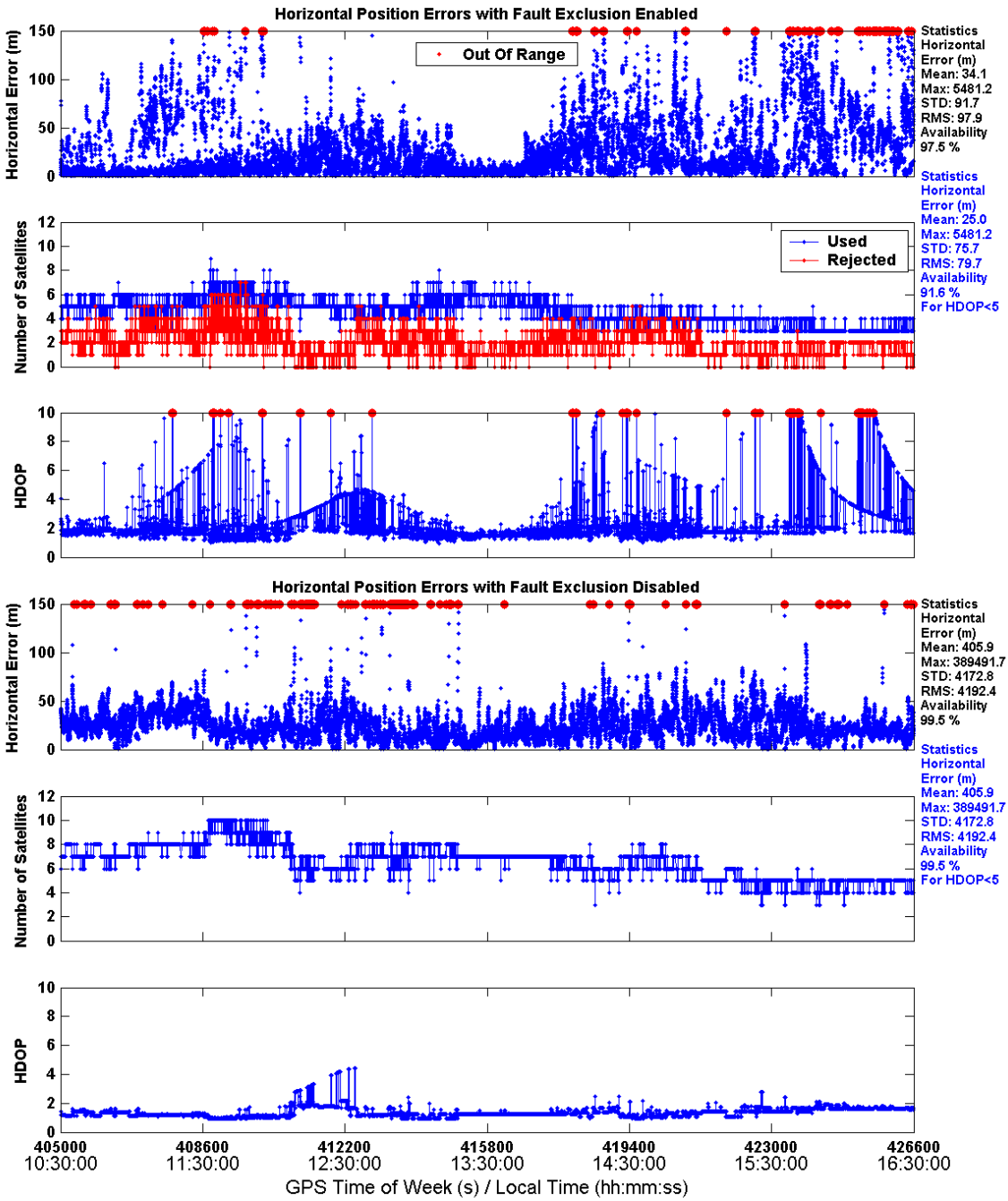

Figure 7.11: Static Urban Canyon - Time Series View of HS Positioning Accuracy, HDOP and Associated Statistics

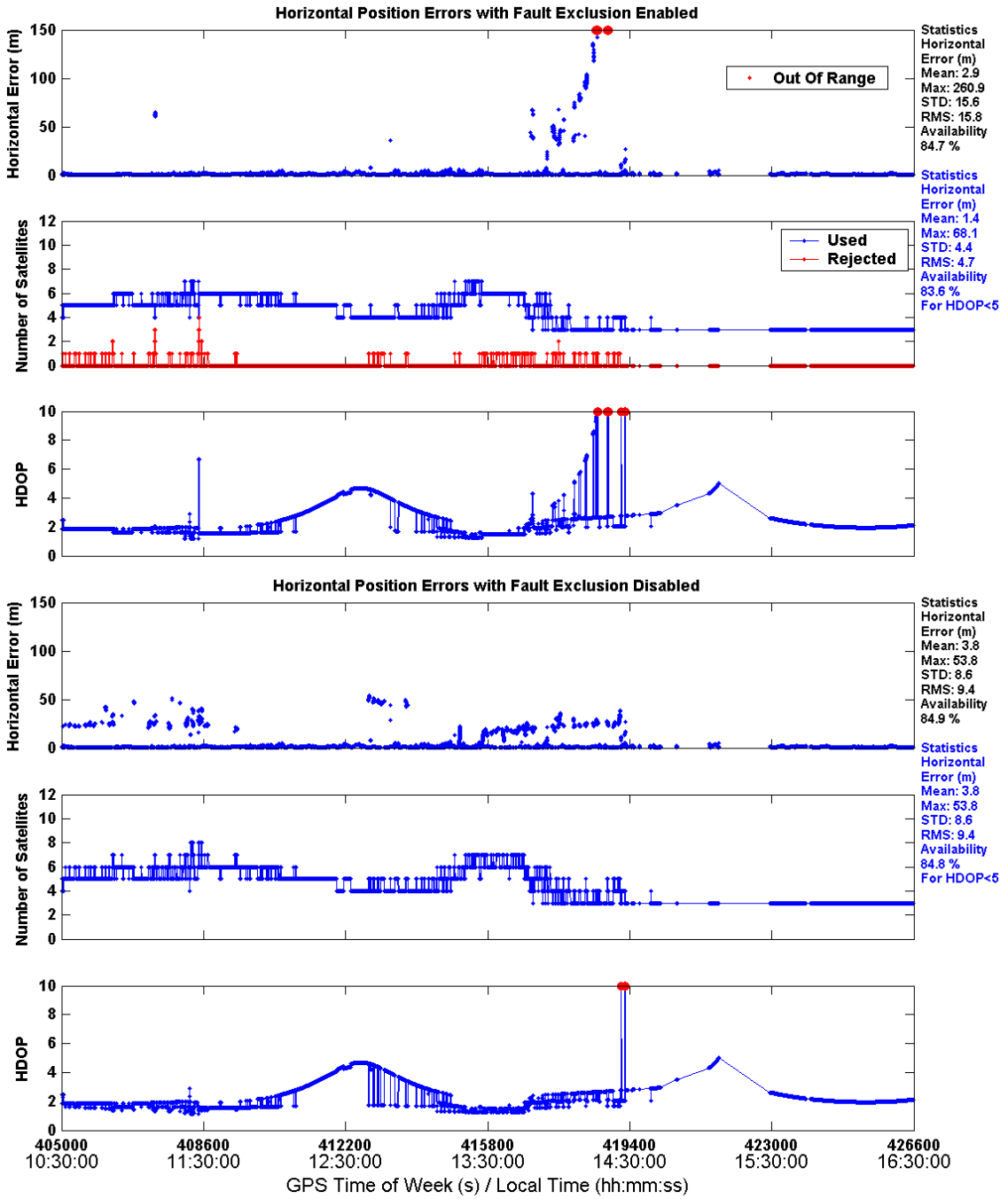

Figure 7.12: Static Urban Canyon - Time Series View of OEM4 Positioning Accuracy, HDOP and Associated Statistics

7.2 Kinematic Urban Canyon Testing

The fading, and EPE results of testing in downtown Calgary and downtown Vancouver will be presented together to facilitate comparison between cities. A representative test from the Vancouver field testing will be presented to discuss position domain issues in urban canyons.

7.2.1 Testing Details

Downtown Calgary

Eleven tests were performed in downtown Calgary, Alberta, Canada. The test trajectory included travel on multiple streets with tall surrounding buildings, typically 100 m to 200 m above the road. Photos of portions of the test trajectories are shown in Figure 7.13. The specific timing details for each test are shown in Table 7.2. Tests 7 through 10 have sufficient reference trajectories to facilitate EPE analysis. In total, 11375 epochs, 3.2 hours, of data are available for fading analysis and 6342 epochs, 1.8 hours, of data are available for EPE analysis.

Data was collected in parallel using a SiRF HS receiver, a SiRF ST receiver, and a NovAtel OEM4. A nearby reference station, with a clear view of the sky, located on the roof of the Engineering Building, Block F, at the University of Calgary, used a SiRF ST, and a NovAtel OEM4 in parallel to collect reference data.

Figure 7.13: Calgary Urban Canyon Testing Environment

Table 7.2: Calgary Downtown - Kinematic Tests

Test Label	GPS Week	Initialization Time of Week (s)	Start Time Of Week (s)	End Time Of Week (s)	Test Duration (s)
1	1127	228800	228980	229615	635
2	1127	229830	230010	230892	882
3	1127	231146	231330	232462	1132
4	1127	232600	232790	233679	889
5	1127	233807	234030	234979	949
6	1127	235067	235300	235846	546
7	1130	236180	237350	238667	1317
8	1130	248380	249700	251839	2139
9	1133	413667	414890	415839	949
10	1133	416576	417800	419023	1223
11	1133	419305	420510	421224	714

Vancouver Downtown

Seven tests were performed in downtown Vancouver, British Columbia, Canada, during the intervals shown in Table 7.3. Vancouver's downtown trajectory included areas with buildings typically less than 100 m tall but taller in some parts of the test trajectory. The reference trajectory and some photos of the typical downtown environment are shown in Figure 7.14. All tests began with a twenty minute warmup period in a location with a clear view of the sky. Tests 1, 2, 3, 4, 6, and 7 have usable high accuracy reference trajectories to facilitate EPE analysis.

Data was collected in parallel using a SiRF HS receiver, a SiRF ST receiver, and a NovAtel OEM4. A nearby reference station, with a clear view of the sky, located on the roof of a two storey house, used a SiRF ST and a NovAtel OEM4 in parallel to collect reference data.

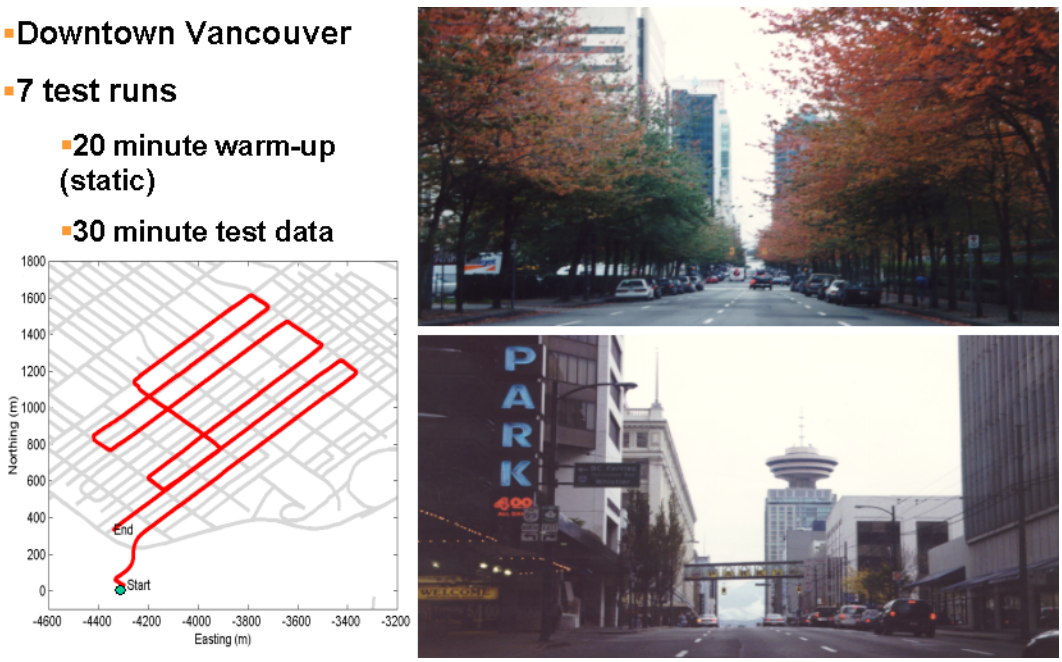

Figure 7.14: Vancouver Urban Canyon Testing Environment

Table 7.3: Vancouver Downtown - Kinematic Tests

Test Label	GPS Week	Initialization Time of Week (s)	Start Time Of Week (s)	End Time Of Week (s)	Test Duration (s)
1	1135	588700	589900	591700	1800
2	1135	591920	593120	595028	1908
3	1135	596090	597290	599106	1816
4	1135	599560	600760	602700	1940
5	1135/1136	603250	604450	1654	2004
6	1136	61700	62900	64556	1656
7	1136	64750	65950	67734	1784

7.2.2 Measurement Availability

The availability of pseudorange measurements for all tests shown in a contiguous fashion for the Calgary and Vancouver urban canyon environments is shown with corresponding statistics in Figures 7.15 and 7.16.

In all tests, the high sensitivity receiver has more available measurements than the standard receivers and less variation in the number of satellites tracked indicating less frequent loss of signal lock.

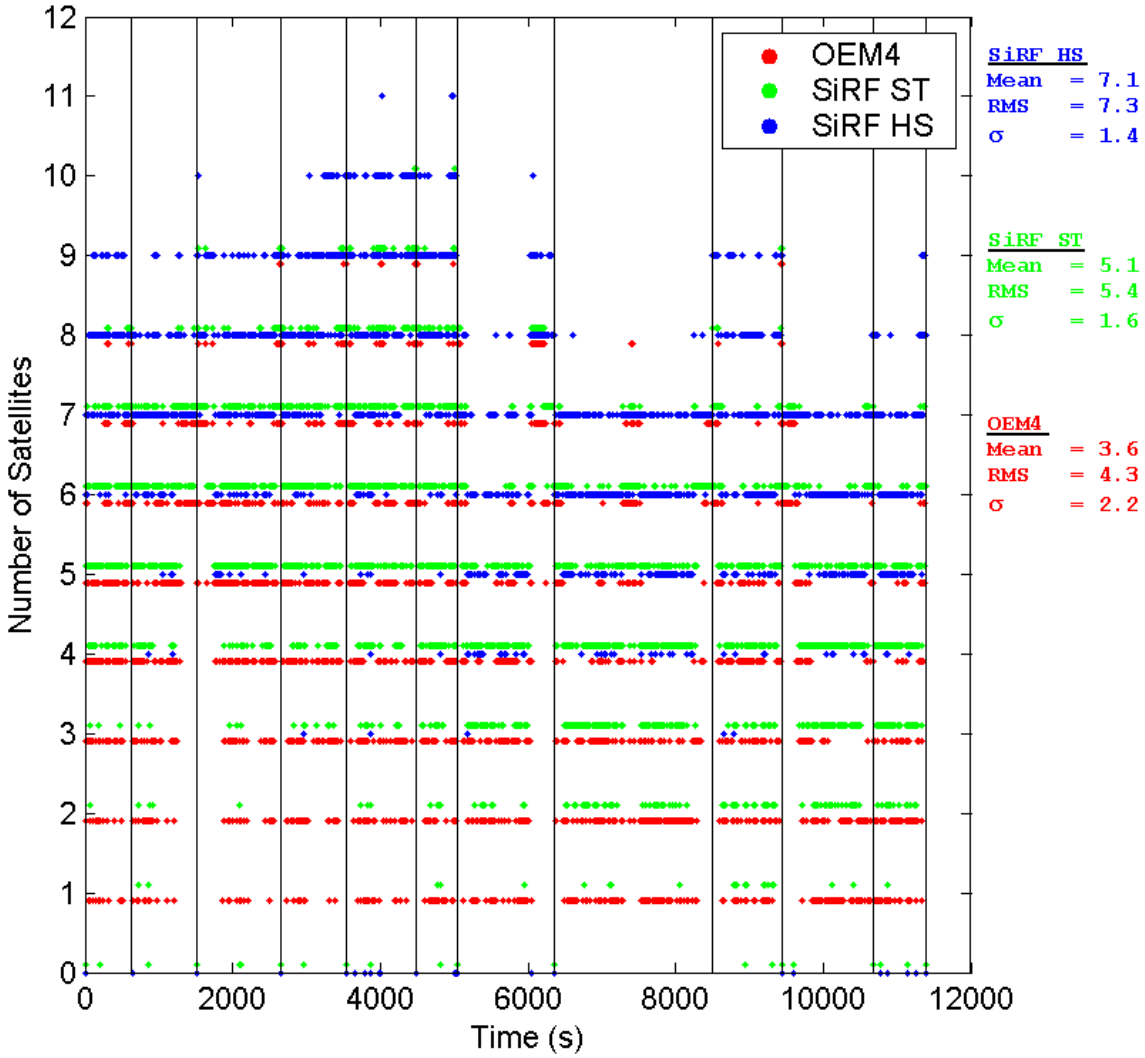

Figure 7.15: Measurement Availability In Downtown Calgary

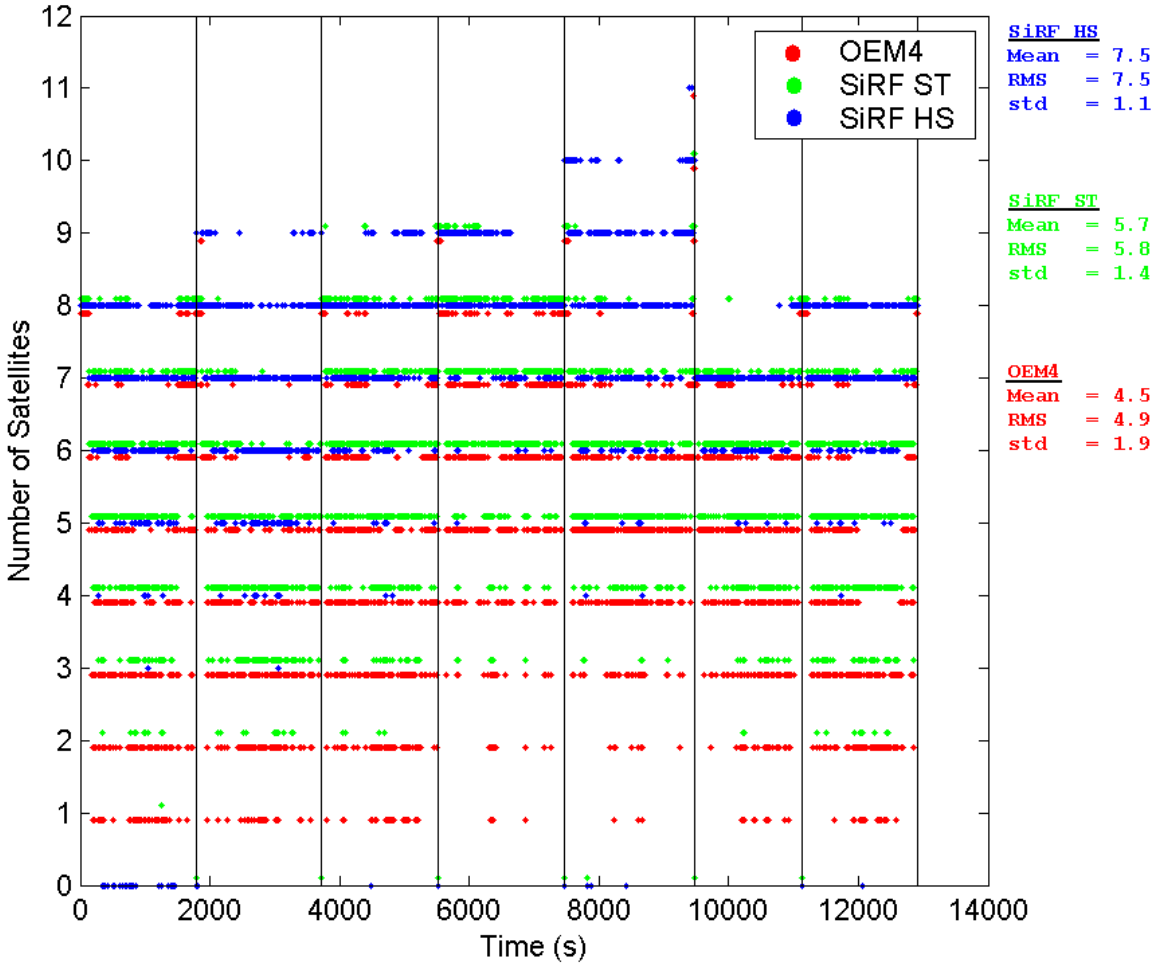

Figure 7.16: Measurement Availability In Downtown Vancouver

7.2.3 Fading

Fading in downtown Calgary and Vancouver was computed using C/N_0 differences with like type receiver-antenna combinations at the reference and test locations. Fading for the SiRF HS receiver was computed using differences with the SiRF ST receiver at the reference station utilizing Equation 4.5. The HS receiver was not available at the base station because at the time it was assumed that the C/N_0

estimator for the SiRF ST and HS receivers was the same and thus no HS data was collected at the base station. As this is not the case, compensation via Equation 4.5 is necessary.

The fading data was binned into 15^o elevation bins and distributions were generated. The fading distributions for the SiRF HS, SiRF ST, and OEM4 receivers are shown in Figures 7.17, 7.18, 7.19, 7.20, 7.21, and 7.22 for the Calgary and Vancouver tests sets respectively. Statistics concerning each elevation bin for the HS, ST, and OEM4 receivers are shown in Tables 7.4, 7.5, 7.6, 7.7, 7.8, 7.9, for the Calgary and Vancouver tests sets respectively.

The OEM4 and SiRF ST use predominantly unfaded signals in these urban canyon environments. The use of multipath or echo only signals which are associated with faded signals are more prevalent with the HS receiver. The HS fading data shows that as elevation angles decrease the influence of line-of-sight signals decreases and a secondary faded signal response increases. The RMS fading values for downtown Calgary and downtown Vancouver range from 7 to 10 dB below 60^o in elevation. Signals above 60^o elevation angle are usually not attenuated.

The fading histograms for Calgary and Vancouver have similar characteristics and statistics. This indicates that the environments have similar signal interference phenomena which is most likely due to signal masking, multipath, and possibly echo only signals.

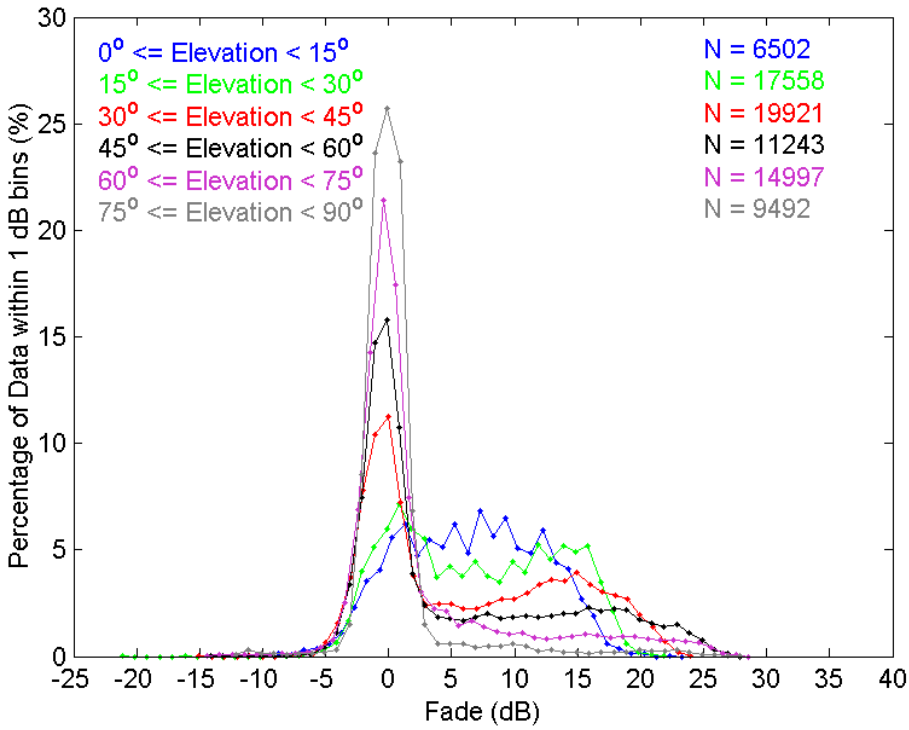

Figure 7.17: Calgary Downtown: SiRF HS Fading Histograms

Table 7.4: Calgary Downtown - HS Receiver Fading Statistics Grouped By Elevation Angle

Elevation Angle Range (°)	Number of Elements	Max (dB)	Mean (dB)	σ (dB)	RMS (dB)
00-15	6502	22.7	6.4	5.5	8.5
15-30	17558	21.5	7.0	6.3	9.4
30-45	19921	23.6	6.2	7.6	9.8
45-60	11243	27.0	5.2	8.1	9.7
60-75	14997	27.9	2.7	6.7	7.2
75-90	9492	27.8	0.7	4.0	4.1

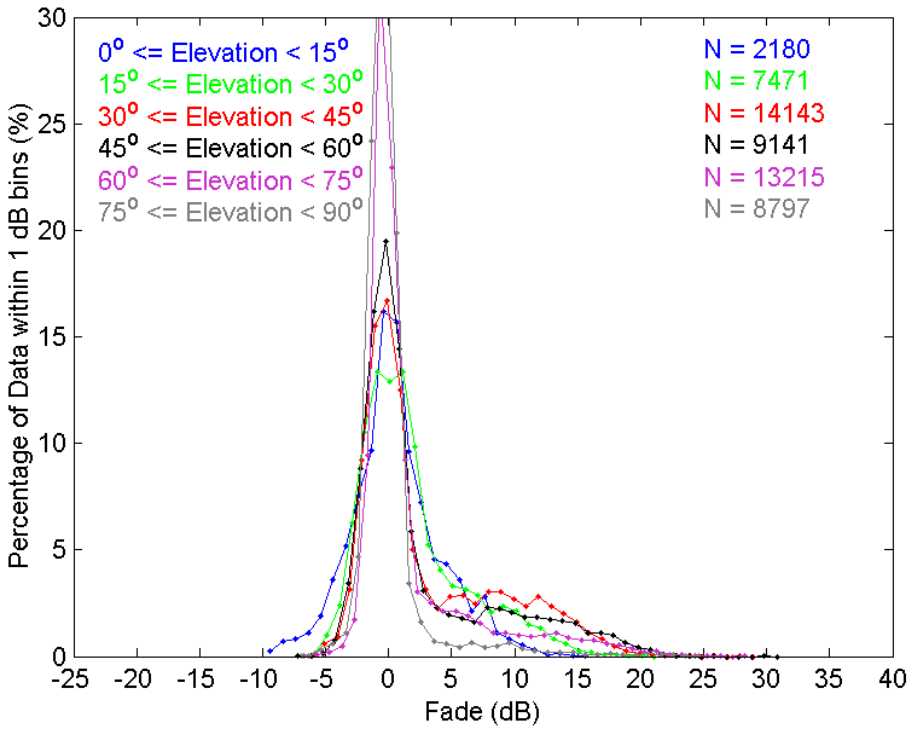

Figure 7.18: Calgary Downtown - SiRF ST Fading Histograms

Table 7.5: Calgary Downtown - ST Receiver Fading Statistics Grouped By Elevation Angle

Elevation Angle Range (°)	Number of Elements	Max (dB)	Mean (dB)	σ (dB)	RMS (dB)
00-15	2180	15.2	0.6	3.6	3.6
15-30	7471	20.1	1.8	4.1	4.5
30-45	14143	28.0	3.0	5.4	6.2
45-60	9141	30.0	2.6	5.6	6.2
60-75	13215	27.9	1.7	4.7	5.0
75-90	8797	24.5	0.0	2.8	2.8

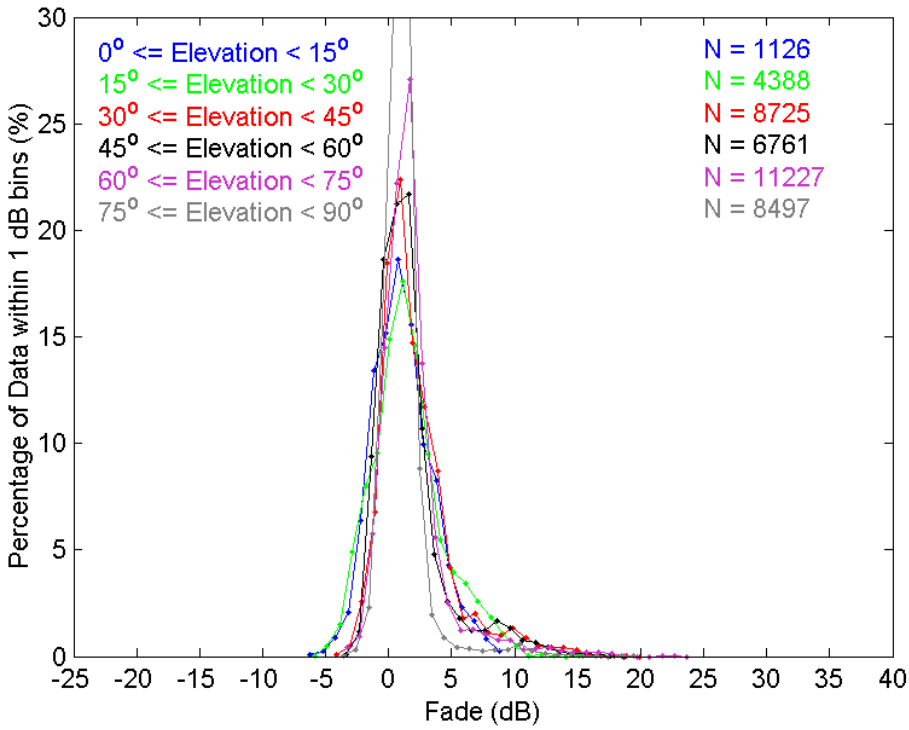

Figure 7.19: Calgary Downtown - OEM4 Fading Histograms

Table 7.6: Calgary Downtown - OEM4 Receiver Fading Statistics Grouped By Elevation Angle

Elevation Angle Range (°)	Number of Elements	Max (dB)	Mean (dB)	σ (dB)	RMS (dB)
00-15	1126	8.7	1.1	2.3	2.6
15-30	4388	14.8	1.5	2.8	3.2
30-45	8725	19.0	2.1	2.9	3.6
45-60	6761	18.0	1.7	2.9	3.3
60-75	11227	22.7	1.8	2.6	3.2
75-90	8497	19.3	1.2	1.8	2.1

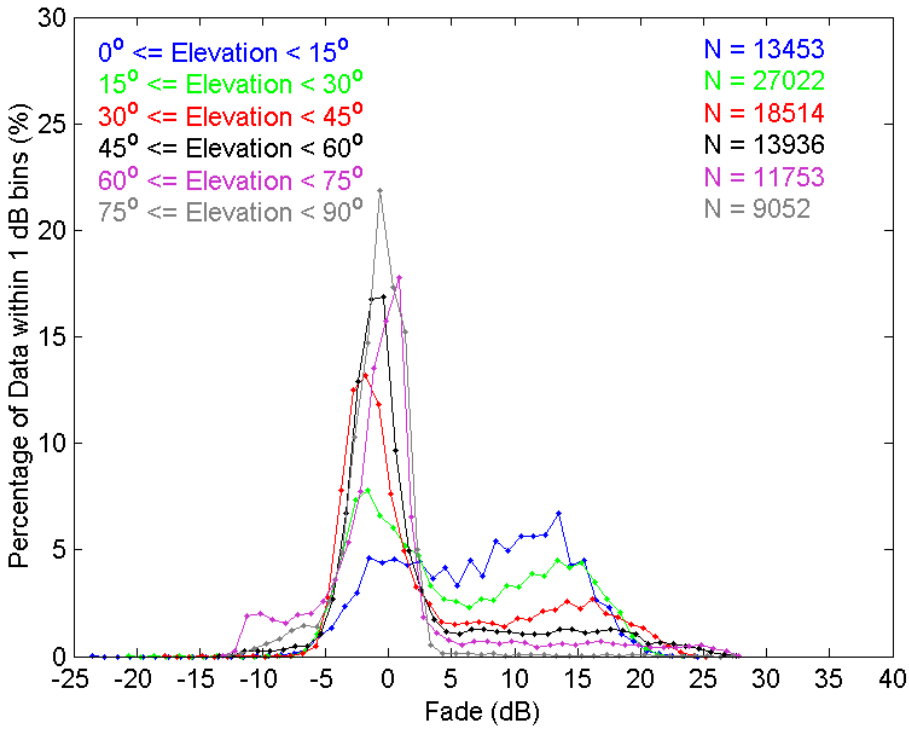

Figure 7.20: Vancouver Downtown - SiRF HS Fading Histograms

Table 7.7: Vancouver Downtown - HS Receiver Fading Statistics Grouped By Elevation Angle

Elevation Angle Range (°)	Number of Elements	Max (dB)	Mean (dB)	σ (dB)	RMS (dB)
00-15	13453	23.6	7.2	6.4	9.7
15-30	27022	23.2	5.5	7.2	9.1
30-45	18514	24.3	3.3	7.5	8.2
45-60	13936	27.1	2.0	6.9	7.2
60-75	11753	27.6	0.4	6.7	6.7
75-90	9052	27.1	-0.8	3.0	3.1

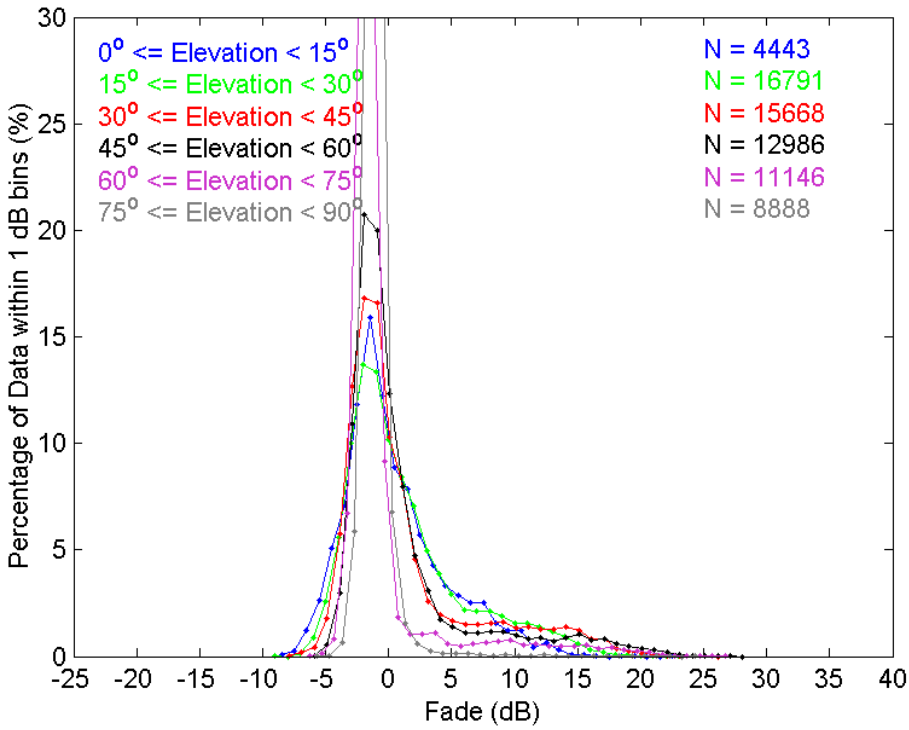

Figure 7.21: Vancouver Downtown - SiRF ST Fading Histograms

Table 7.8: Vancouver Downtown - ST Receiver Fading Statistics Grouped By Elevation Angle

Elevation Angle Range (°)	Number of Elements	Max (dB)	Mean (dB)	σ (dB)	RMS (dB)
00-15	4443	22.0	0.3	4.0	4.0
15-30	16791	22.6	1.1	4.7	4.8
30-45	15668	25.4	1.1	5.3	5.4
45-60	12986	27.5	1.0	5.1	5.3
60-75	11146	26.2	-0.4	4.1	4.1
75-90	8888	24.3	-1.0	1.6	1.9

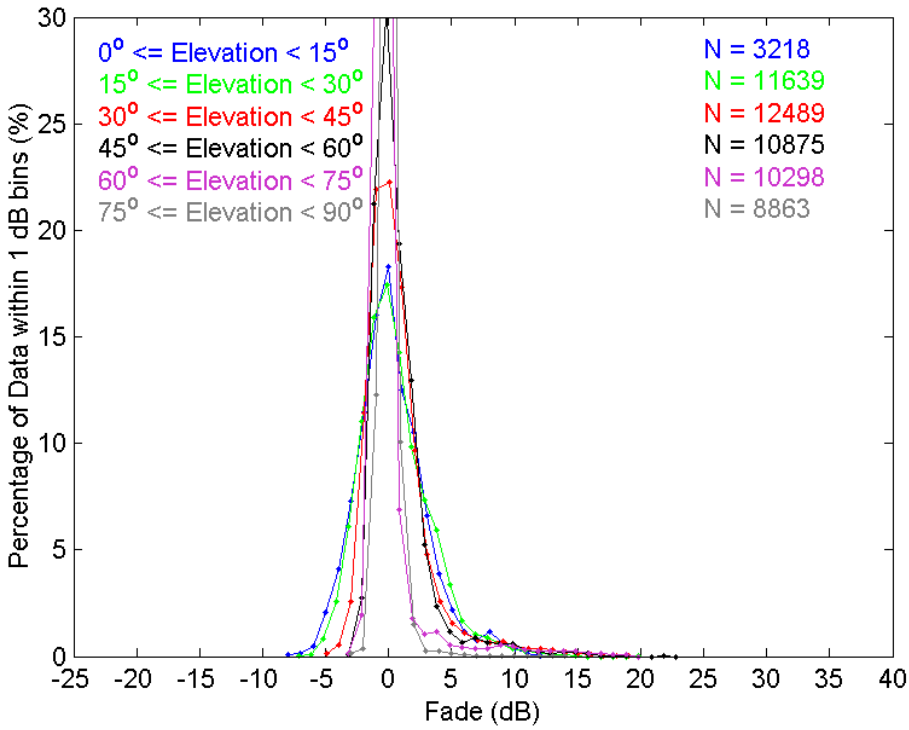

Figure 7.22: Vancouver Downtown - OEM4 Fading Histograms

Table 7.9: Vancouver Downtown - OEM4 Receiver Fading Statistics Grouped By Elevation Angle

Elevation Angle Range (°)	Number of Elements	Max (dB)	Mean (dB)	σ (dB)	RMS (dB)
00-15	3218	11.9	0.2	2.8	2.8
15-30	11639	19.4	0.5	2.8	2.8
30-45	12489	18.9	0.7	2.7	2.7
45-60	10875	22.0	0.8	2.4	2.5
60-75	10298	19.2	0.1	2.4	2.4
75-90	8863	13.5	0.0	0.8	0.8

7.3 Estimated Pseudorange Errors

EPE in downtown Calgary and Vancouver was computed using the least squares method discussed in Section 3.2.3 using a NovAtel Black Diamond GPS/INS system to supply high accuracy reference trajectories. The EPE data was binned into 15^o elevation bins and distributions were generated. The EPE distributions for the SiRF HS, SiRF ST, and OEM4 receivers are shown in Figures 7.23, 7.24, 7.25, 7.26, 7.27, and 7.28 for the Calgary and Vancouver tests sets respectively. Statistics concerning each elevation bin for the SiRF HS, SiRF ST, and OEM4 receivers are shown in Tables 7.10, 7.11, 7.12, 7.13, 7.14, 7.15, for the Calgary and Vancouver tests sets respectively. The cumulative distributions of the absolute value of the EPE data for the SiRF HS, SiRF ST, and OEM4 receivers are shown in Figures 7.29, 7.30, 7.31, 7.32, 7.33, and 7.34 for the Calgary and Vancouver test sets respectively. These figures also include the EPE values corresponding to the 50^{th} and 95^{th} percentiles.

The use of low power signals in the urban canyon environment corresponds to improved measurement availability below 45^o elevation. However, more measurement noise, more multipath errors, echo-only signal tracking errors and cross-correlation signals result and will be shown to be problematic for positioning in the urban canyon environment. The figures showing the cumulative distributions for the HS receiver in both Calgary and Vancouver demonstrate the degraded level of measurements in comparison with the ST receiver. The OEM4 clearly provides very accurate measurements but compromises measurement availability in comparison with HS GPS. Measurement errors are higher for the HS receiver for all elevation groupings in comparison with the ST and OEM4 receivers. The use of narrow correlation techniques would reduce multipath error for both the ST and HS receiver. The performance of the HS receiver in comparison with the ST receiver (both the 50^{th} and 95^{th} percentile values are nearly double in comparison) shows the impact of weak signal usage.

The Calgary results indicate more severe error conditions than experienced in Vancouver. This is best described by the 95^{th} percentile values in the cumulative distributions.

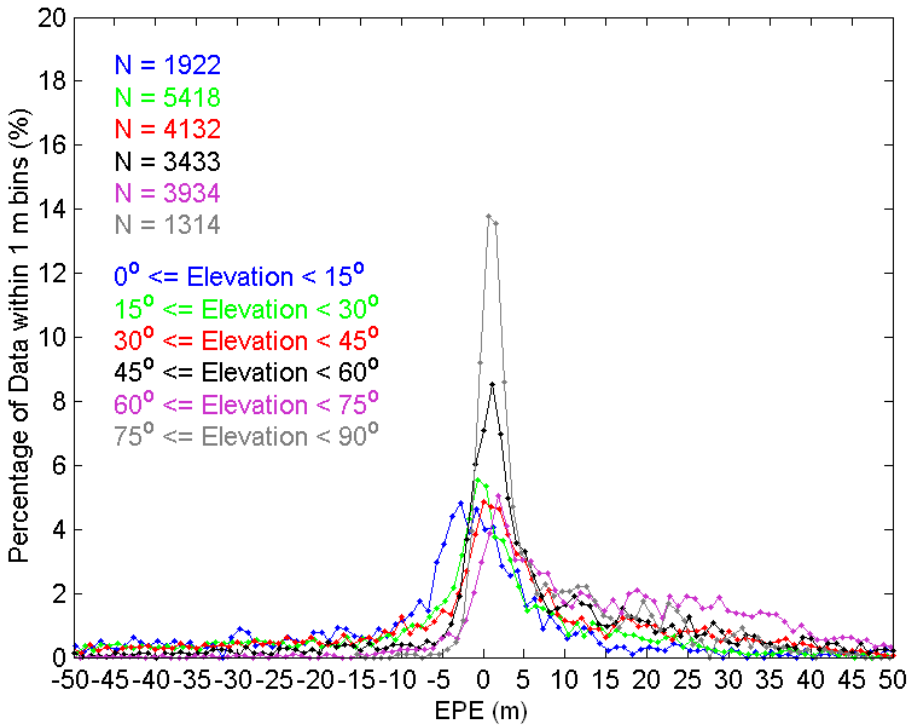

Figure 7.23: Calgary Downtown - SiRF HS EPE Histograms

Table 7.10: Calgary Downtown - SiRF HS Receiver EPE Statistics Grouped By Elevation Angle

Elevation Angle Range (°)	Number of Elements	Max (m)	Min (m)	Mean (m)	σ (m)	RMS (m)
00-15	1922	121.1	-149.7	-14.7	35.0	37.9
15-30	5418	145.3	-149.6	-19.0	42.0	46.1
30-45	4132	148.1	-149.0	-0.7	31.8	31.8
45-60	3433	141.8	-149.9	7.5	23.1	24.3
60-75	3934	149.4	-145.2	18.5	21.7	28.5
75-90	1314	62.8	-15.4	7.8	10.6	13.1

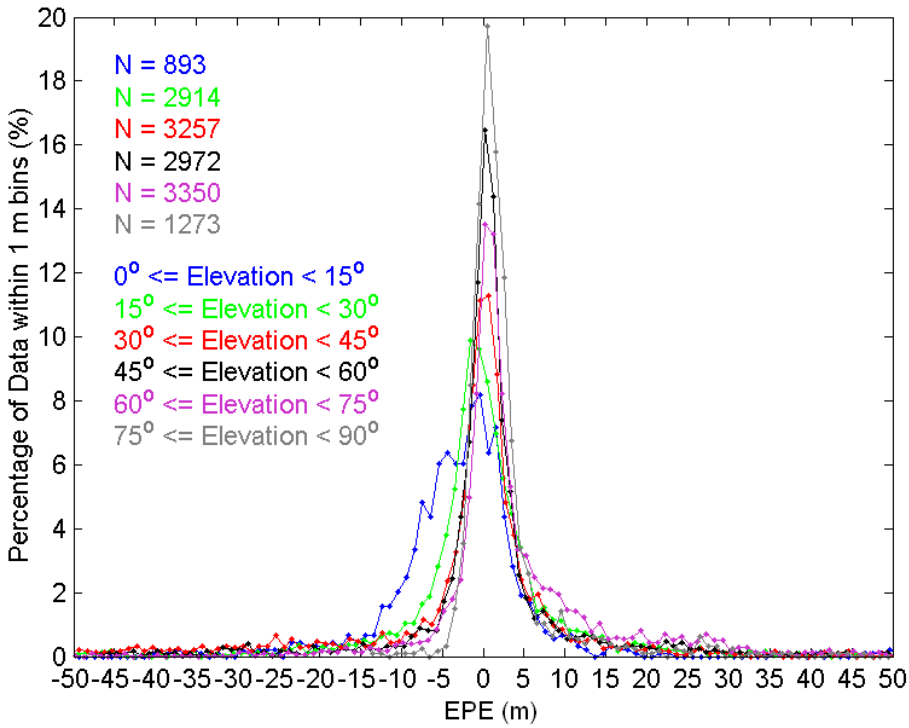

Figure 7.24: Calgary Downtown - SiRF ST EPE Histograms

Table 7.11: Calgary Downtown - SiRF ST Receiver EPE Statistics Grouped By Elevation Angle

Elevation Angle Range (°)	Number of Elements	Max (m)	Min (m)	Mean (m)	σ (m)	RMS (m)
00-15	893	71.8	-83.4	-3.3	11.3	11.7
15-30	2914	119.0	-118.5	-1.2	16.1	16.1
30-45	3257	147.5	-145.3	-4.0	26.8	27.1
45-60	2972	130.7	-147.7	0.3	17.5	17.5
60-75	3350	129.5	-147.7	3.8	17.6	18.0
75-90	1273	62.6	-13.5	2.6	6.4	6.9

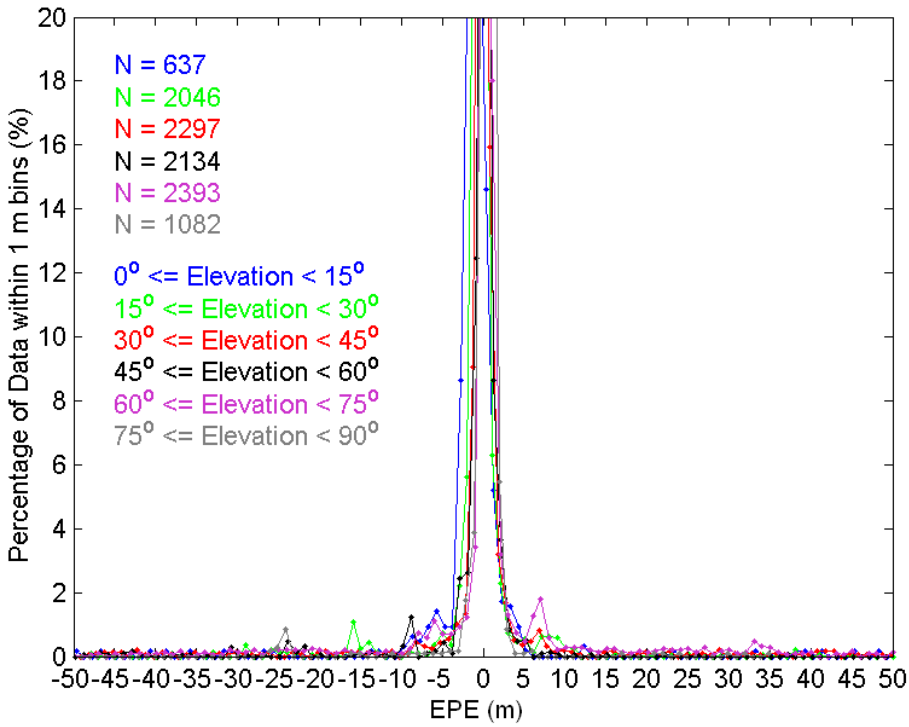

Figure 7.25: Calgary Downtown - OEM4 EPE Histograms

Table 7.12: Calgary Downtown - OEM4 Receiver EPE Statistics Grouped By Elevation Angle

Elevation Angle Range (°)	Number of Elements	Max (m)	Min (m)	Mean (m)	σ (m)	RMS (m)
00-15	637	137.9	-70.7	0.5	16.2	16.2
15-30	2046	94.1	-62.9	-0.5	7.9	8.0
30-45	2297	148.3	-149.2	-0.3	27.2	27.2
45-60	2134	149.8	-111.8	2.3	21.2	21.3
60-75	2393	145.3	-137.9	0.0	20.1	20.1
75-90	1082	34.5	-105.1	-3.3	19.3	19.5

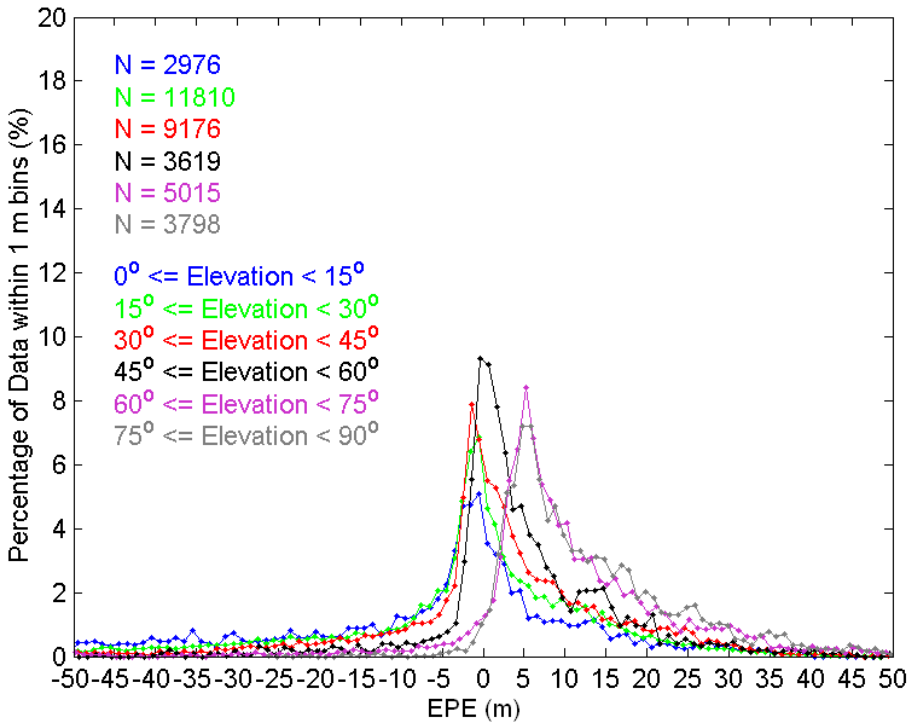

Figure 7.26: Vancouver Downtown - SiRF HS EPE Histograms

Table 7.13: Vancouver Downtown - SiRF HS Receiver EPE Statistics Grouped By Elevation Angle

Elevation Angle Range (°)	Number of Elements	Max (m)	Min (m)	Mean (m)	σ (m)	RMS (m)
00-15	2976	146.0	-149.5	-15.8	34.6	38.0
15-30	11810	149.5	-149.5	-8.2	30.0	31.1
30-45	9176	148.3	-148.4	-0.2	21.1	21.1
45-60	3619	143.0	-148.3	4.1	17.9	18.4
60-75	5015	106.1	-141.8	10.6	14.5	17.9
75-90	3798	108.7	-26.2	13.7	12.3	18.5

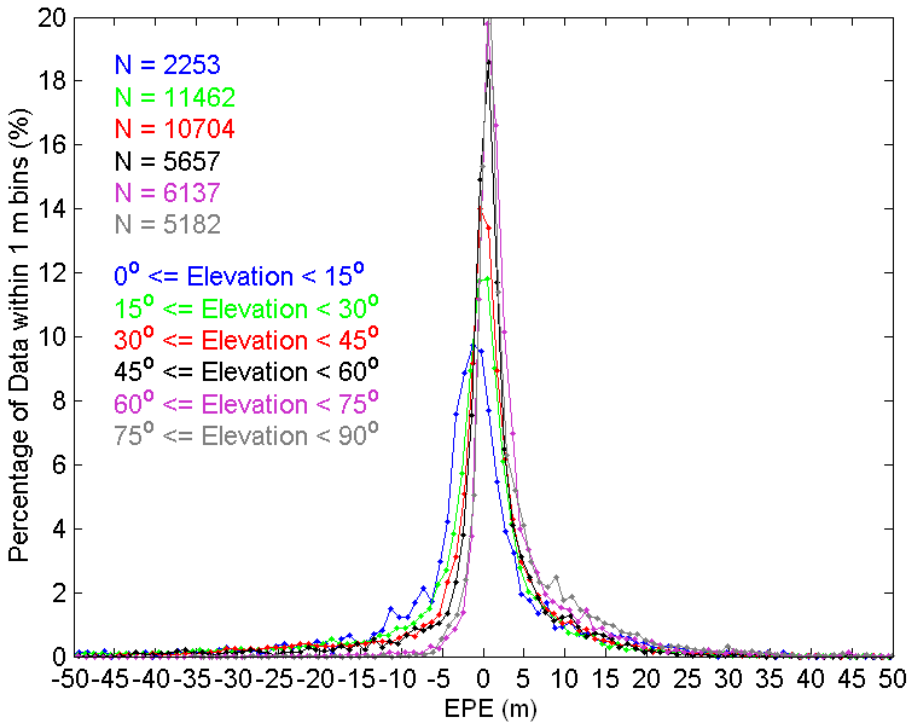

Figure 7.27: Vancouver Downtown - SiRF ST EPE Histograms

Table 7.14: Vancouver Downtown - SiRF ST Receiver EPE Statistics Grouped By Elevation Angle

Elevation Angle Range (°)	Number of Elements	Max (m)	Min (m)	Mean (m)	σ (m)	RMS (m)
00-15	2253	128.0	-107.3	-1.2	13.9	13.9
15-30	11462	84.2	-149.5	-2.9	16.4	16.6
30-45	10704	90.1	-147.3	-1.3	13.5	13.6
45-60	5657	92.9	-98.4	0.2	9.2	9.2
60-75	6137	61.0	-105.5	3.4	7.8	8.5
75-90	5182	61.6	-35.1	4.2	7.2	8.3

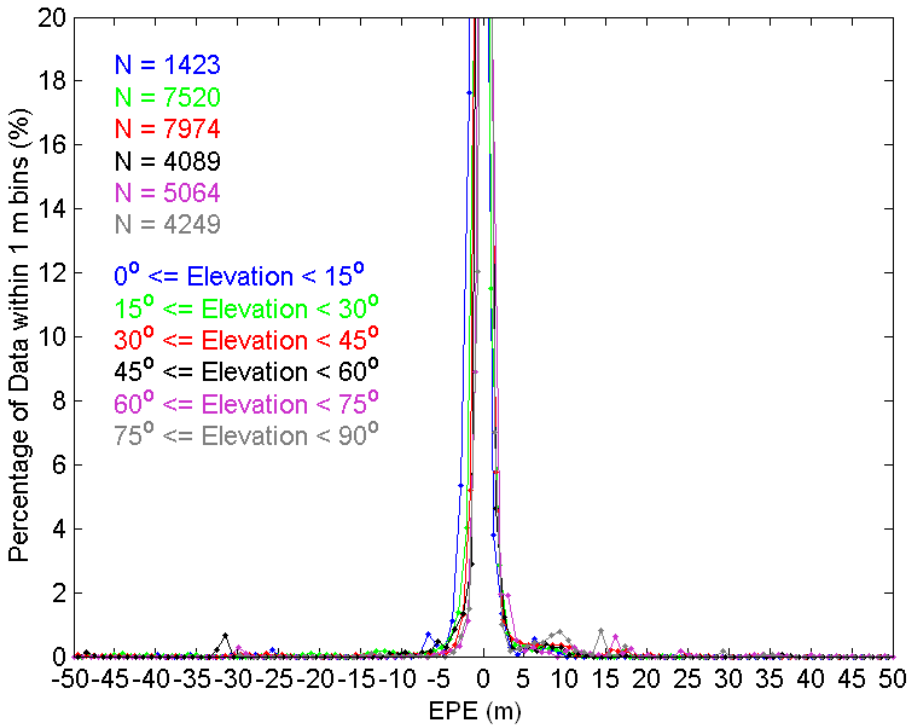

Figure 7.28: Vancouver Downtown - OEM4 EPE Histograms

Table 7.15: Vancouver Downtown - OEM4 Receiver EPE Statistics Grouped By Elevation Angle

Elevation Angle Range (°)	Number of Elements	Max (m)	Min (m)	Mean (m)	σ (m)	RMS (m)
00-15	1423	105.2	-39.7	-0.7	3.8	3.9
15-30	7520	26.4	-81.0	-0.5	4.2	4.2
30-45	7974	71.3	-116.5	-0.3	7.9	7.9
45-60	4089	147.7	-114.5	-0.1	6.8	6.8
60-75	5064	53.9	-53.9	0.7	4.3	4.4
75-90	4249	75.8	-29.7	0.8	3.4	3.5

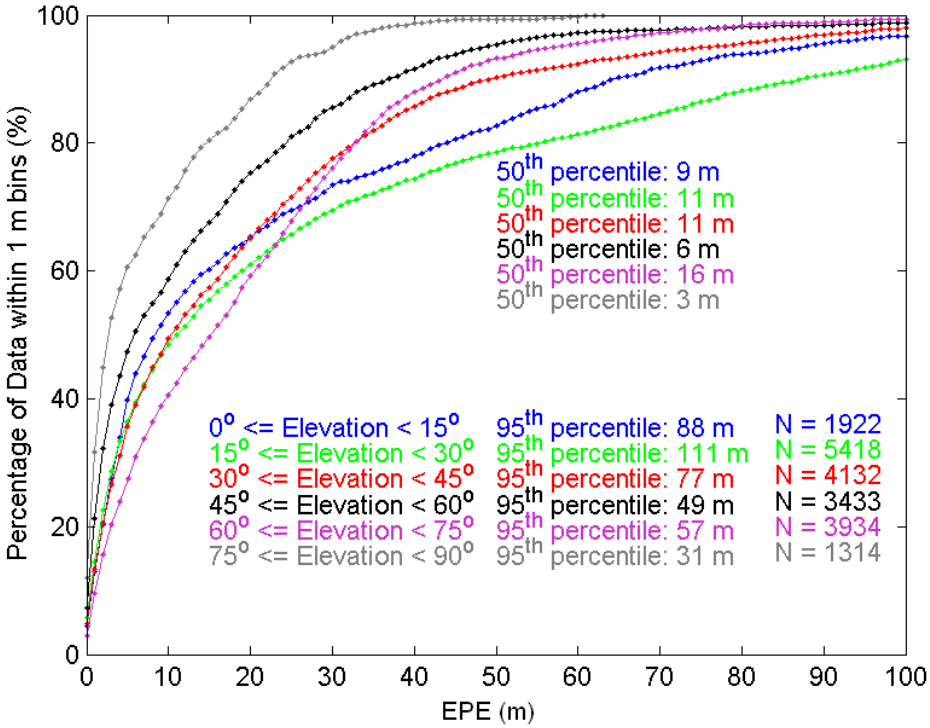

Figure 7.29: Calgary Downtown - SiRF HS EPE Cumulative Distributions

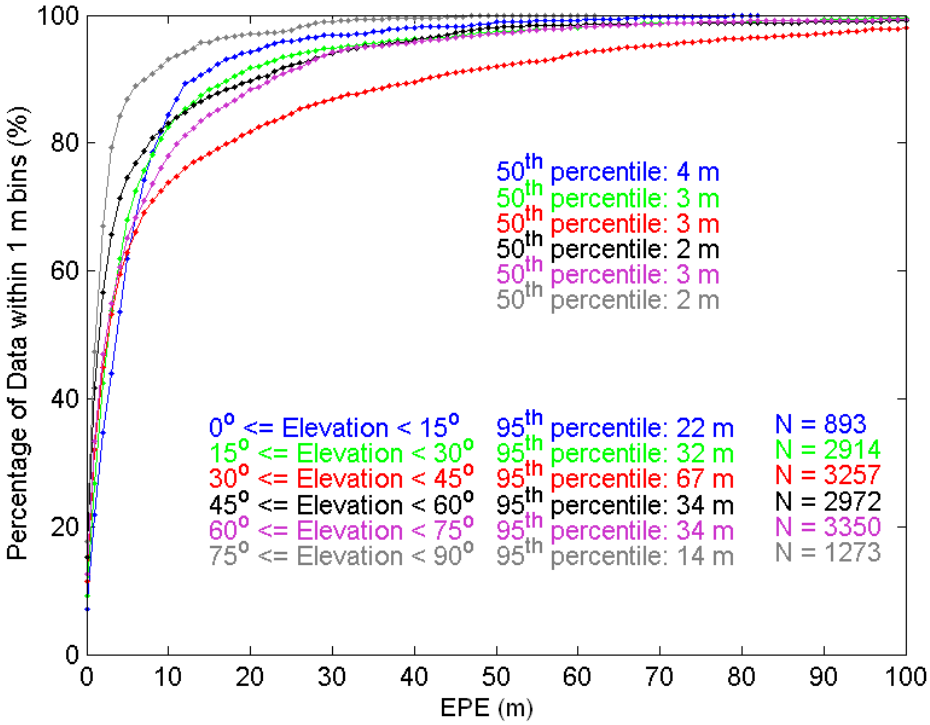

Figure 7.30: Calgary Downtown - SiRF ST EPE Cumulative Distributions

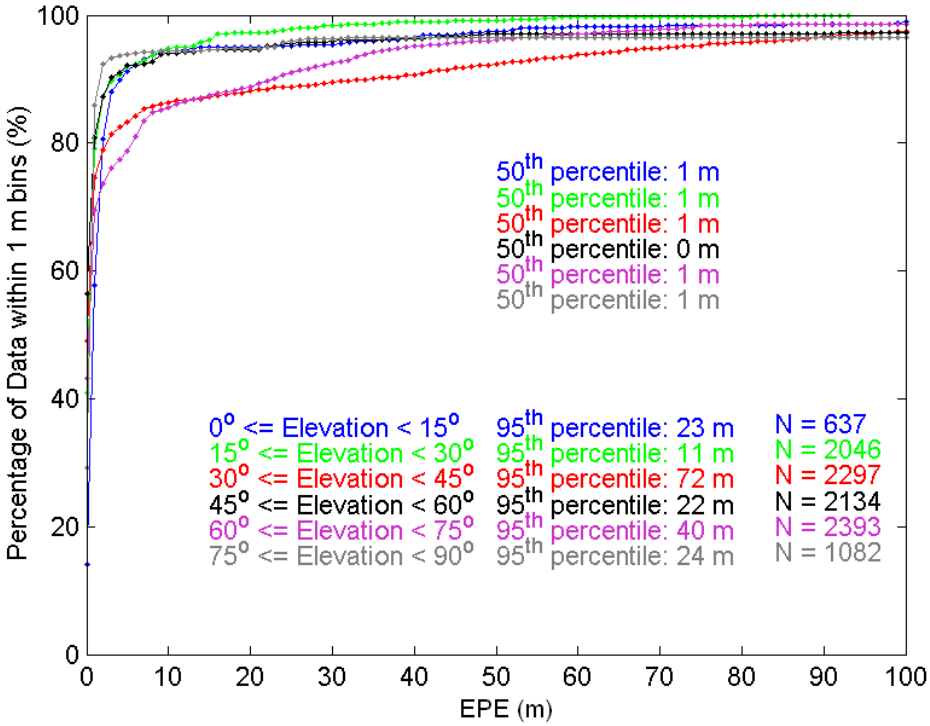

Figure 7.31: Calgary Downtown - OEM4 EPE Cumulative Distributions

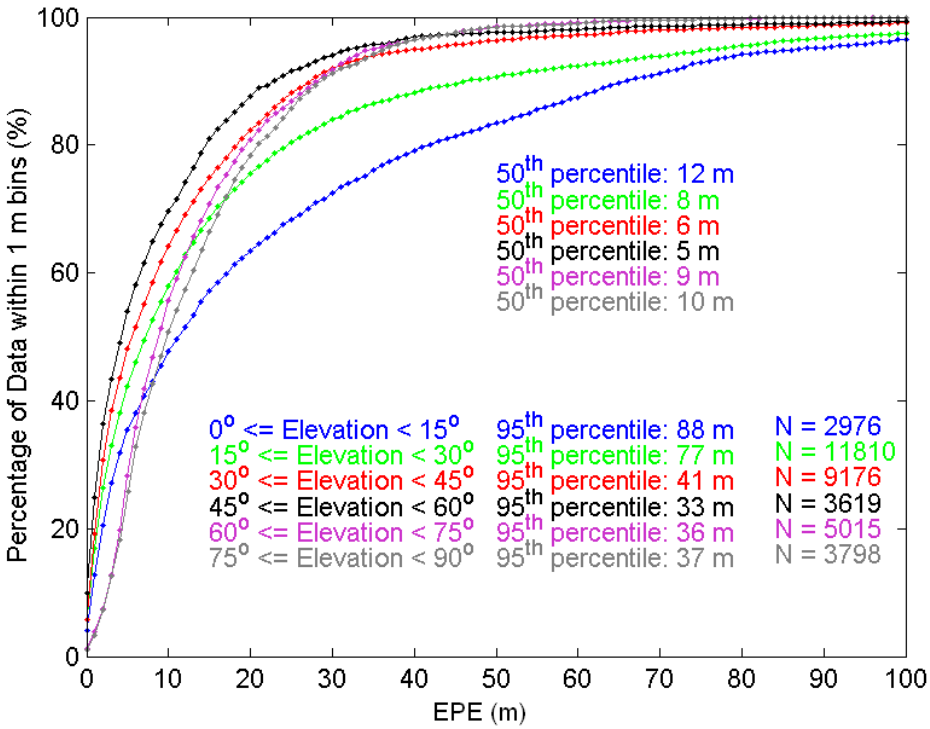

Figure 7.32: Vancouver Downtown - SiRF HS EPE Cumulative Distributions

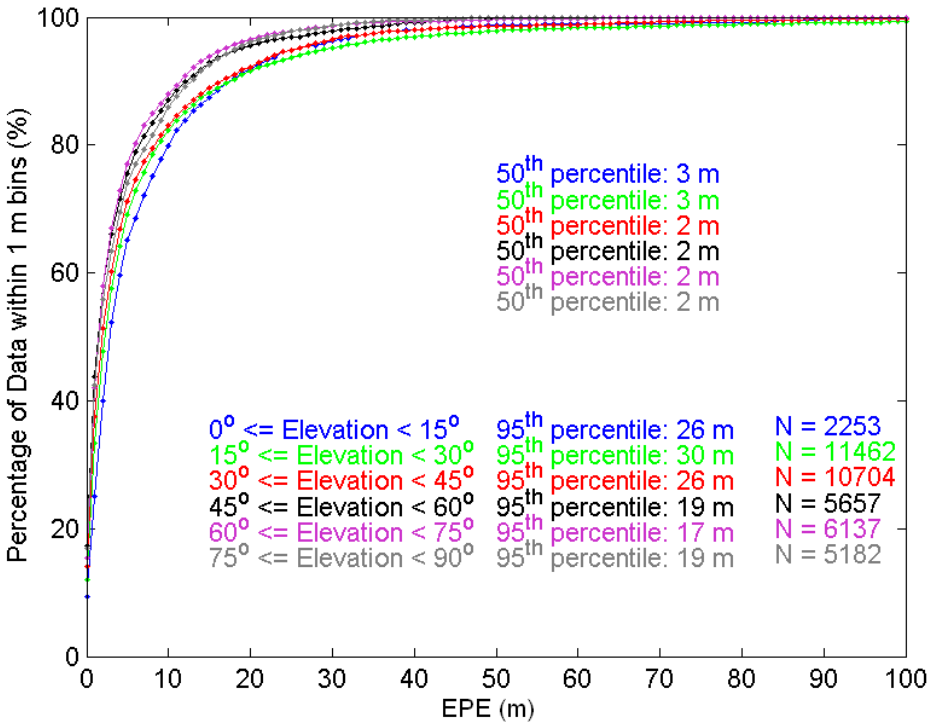

Figure 7.33: Vancouver Downtown - SiRF ST EPE Cumulative Distributions

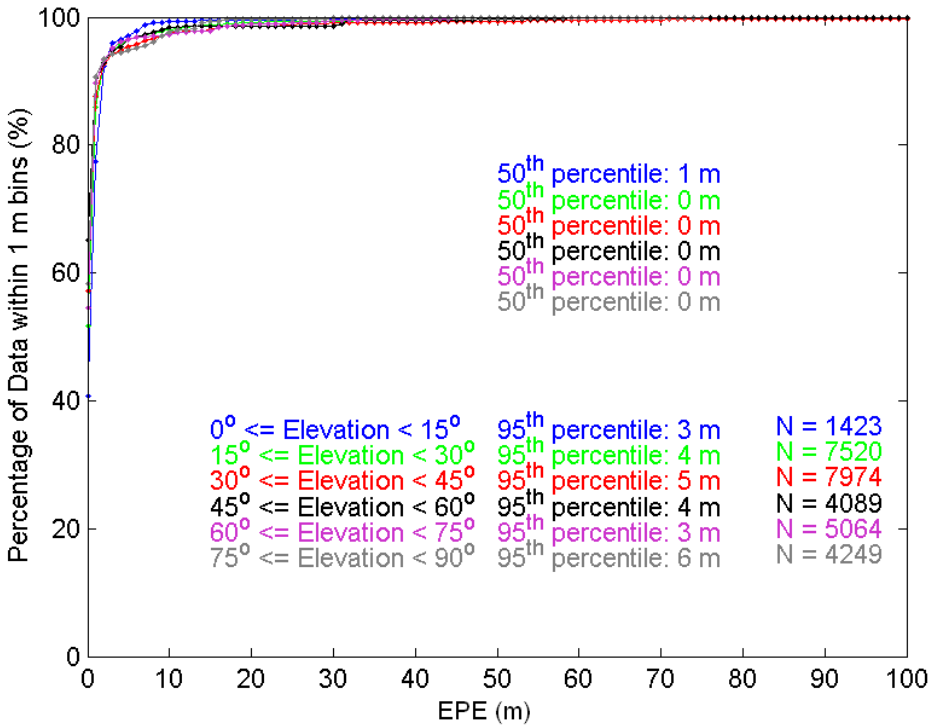

Figure 7.34: Vancouver Downtown - OEM4 EPE Cumulative Distributions

7.4 HS Fading and EPE Time Series Analysis

The SiRF HS time series data for each satellite for EPE and fading along with the corresponding elevation angle are shown in Figures 7.35, 7.35, 7.37 and 7.38 for the Calgary and Vancouver test sets respectively. All tests are shown by making the data contiguous. Also included in these figures are the large blunder effects (discussed in Chapter 5), rejected from solution in EPE calculation, shown as red dots on the top of each plot. The number of large blunder occurrences for each satellite, NF, and the number of EPE values, N, used in computed statistics are also shown in the

figure. Large errors due to signal cross-correlation are a significant problem in this test environment.

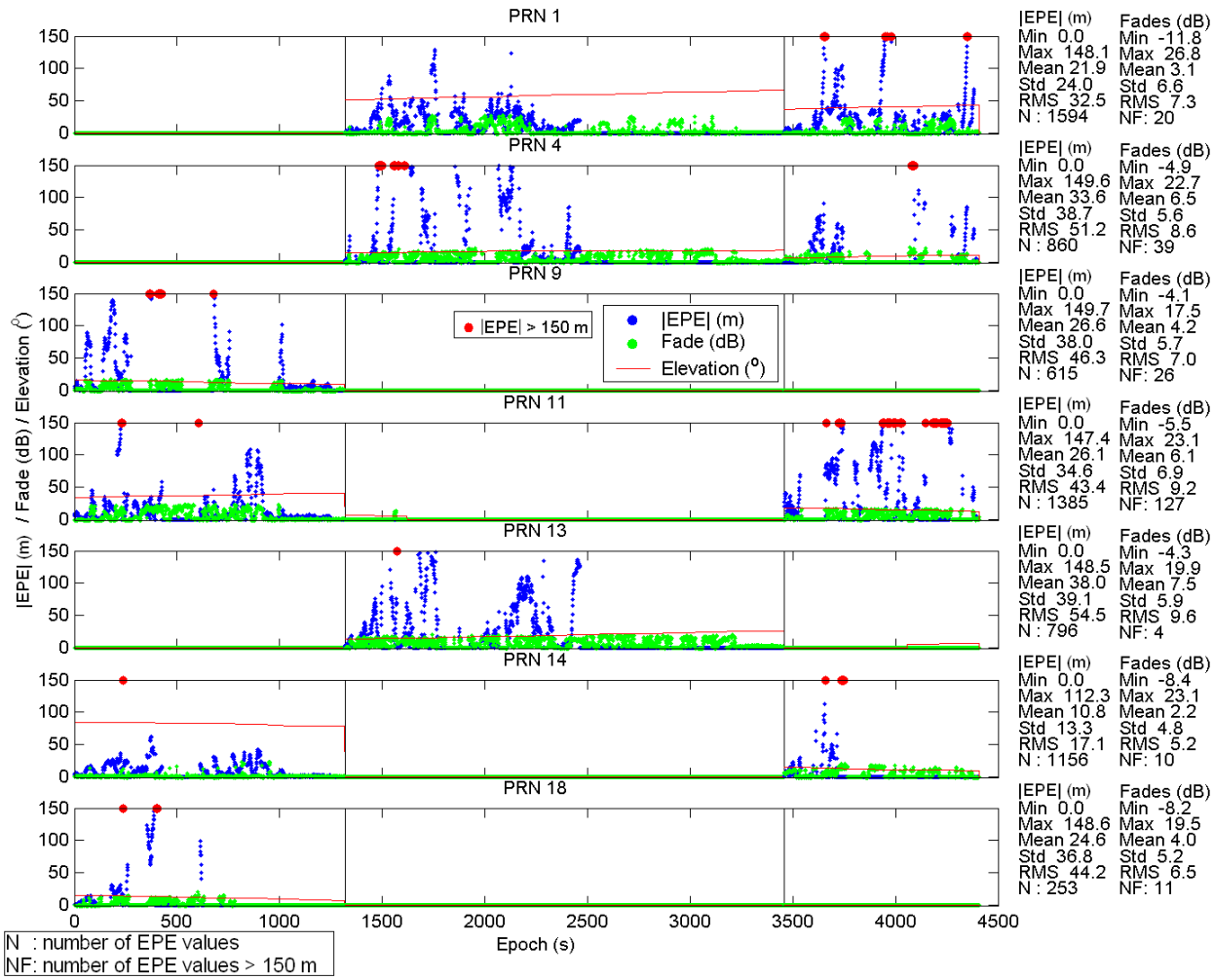

Figure 7.35: Calgary Downtown - Time Series Representation Of Fading, EPE, and Satellite Elevation Part 1 of 2

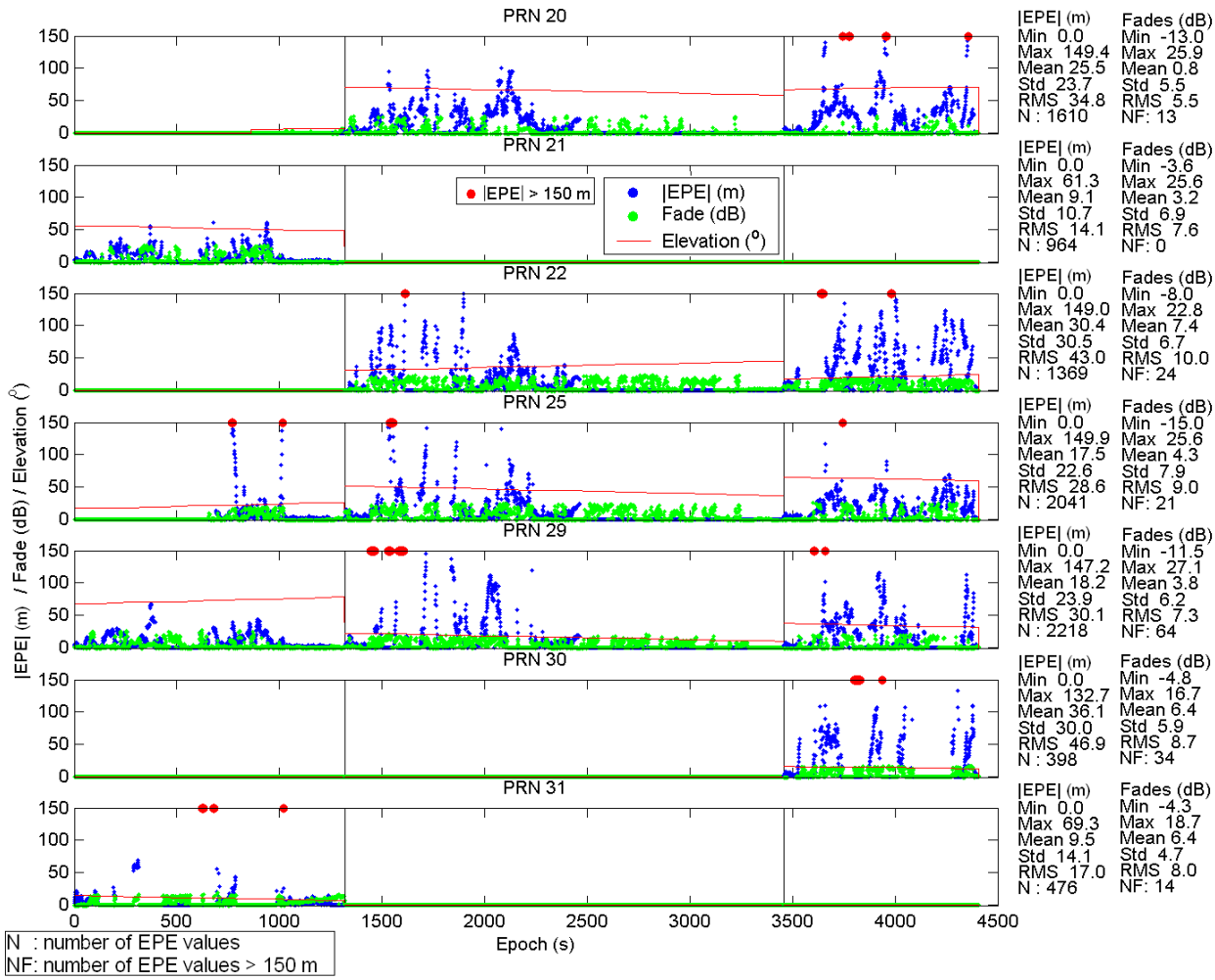

Figure 7.36: Calgary Downtown - Time Series Representation Of Fading, EPE, and Satellite Elevation Part 2 of 2

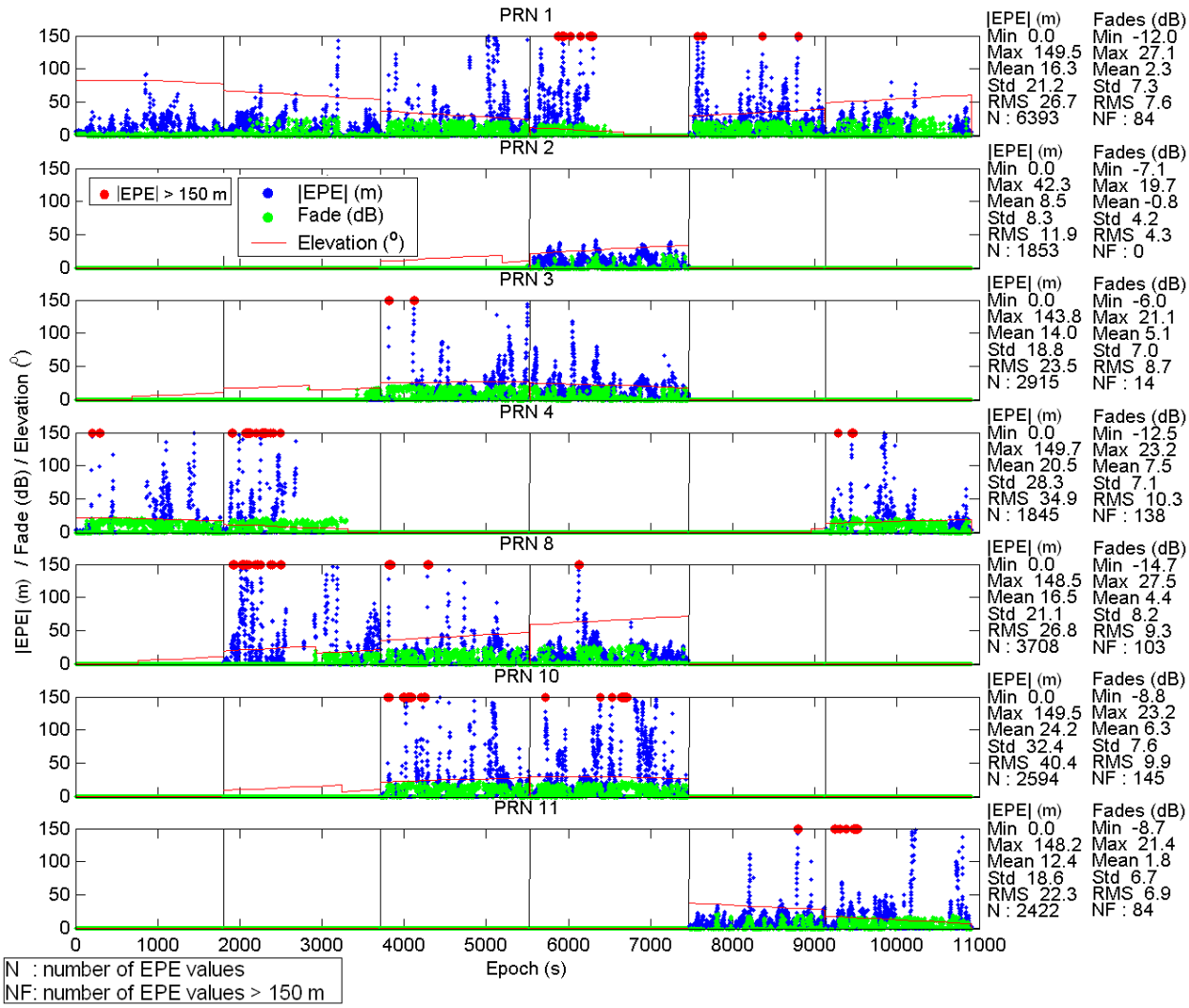

Figure 7.37: Vancouver Downtown - Time Series Representation Of Fading, EPE, and Satellite Elevation Part 1 of 2

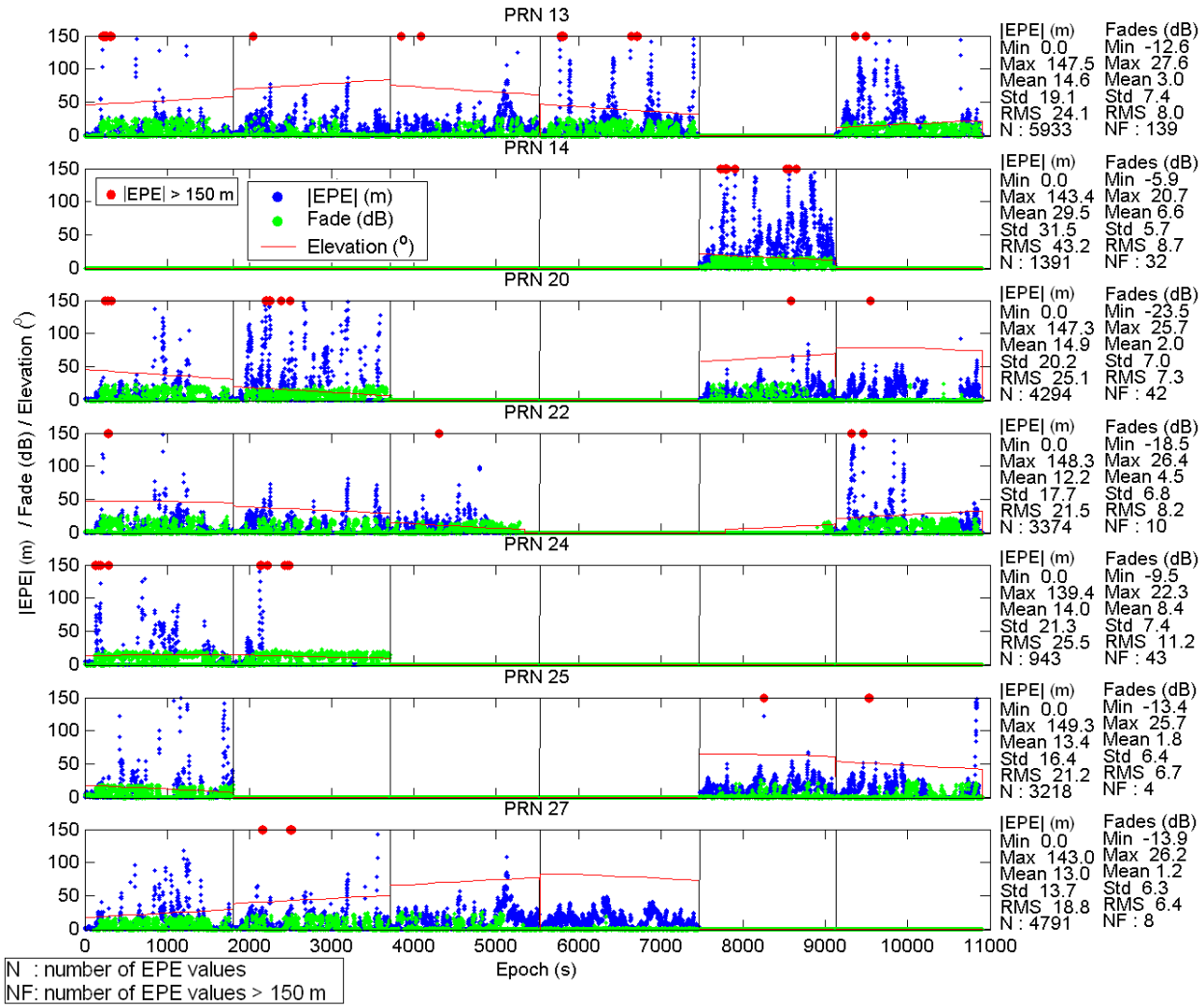

Figure 7.38: Vancouver Downtown - Time Series Representation Of Fading, EPE, and Satellite Elevation Part 2 of 2

7.4.1 Positioning Accuracy, Solution Availability, and Dilution of Precision

Test Run 4 in downtown Vancouver is a good representative example of positioning accuracy and solution availability while kinematic positioning in an urban canyon

environment. Very good truth trajectory information was available for this test. The urban canyon environment in downtown Calgary is more severe than Vancouver in terms of signal masking but this made obtaining complete accurate truth trajectories difficult and thus some Vancouver results are presented.

Height fixed solutions were computed with and without fault detection and exclusion for the HS, ST, and OEM4 receivers. The height of the Vancouver test trajectory varied about a mean height by only 15 m maximum. Thus, using a height fix provides little distortion in horizontal position. These results are presented with the solutions with fault exclusion followed by the solutions without fault exclusion in plan views in Figures 7.39, 7.40, 7.41, 7.42, 7.43, and 7.44 for the HS, ST, and OEM4 receivers respectively. Included in these figures are statistics concerning the entire datasets and for solutions where HDOP was lower than 5.0. The truth trajectory is shown in these figures as the light blue line in the background. In addition, a digital map of Vancouver allowed the centerlines of the city streets to be plotted in the background. The truth trajectory has very good correspondence with the city map.

The solution availability concerning horizontal positions with good geometry, HDOP lower than 5, and with fault exclusion enabled is 97.7 %, 97.8 %, and 88.5 % for the HS, ST, and OEM4 receivers respectively. There is little availability performance difference when comparing the HS and ST receivers in this case. In fact, the ST solution statistics indicate more accurate positioning for this test. This was often the case in urban canyon field testing for Calgary and Vancouver. However, the solution availability is less in general by about 5 % and decreases if height fixing cannot be used. Applications that will use HS GPS must balance solution availability with positioning accuracy.

The HS, and to a lesser extent the ST, position solutions are corrupted by very large measurement faults which lead to multiple kilometre level positioning error

effects. This is much improved by fault exclusion but not all faults can be removed and some very large, 500 to 1700 m, position errors remain. The OEM4 receiver performs well in terms of measurement accuracy; however, even good measurements can be adversely affected by poor geometry. This is clearly seen in Figure 7.43 where measurement errors of 50 m result when HDOP is larger than 5.0.

The urban canyon environment is severe in terms of the measurement errors induced by multipath, echo-only signal tracking, and, as mentioned in Chapter 5, signal cross-correlation effects. For conventional GPS and HS GPS to be useful in such an environment, errors due to cross-correlation tracking of echo-only signals must be removed or deweighted in the estimator used. However, this task is very difficult given the results presented.

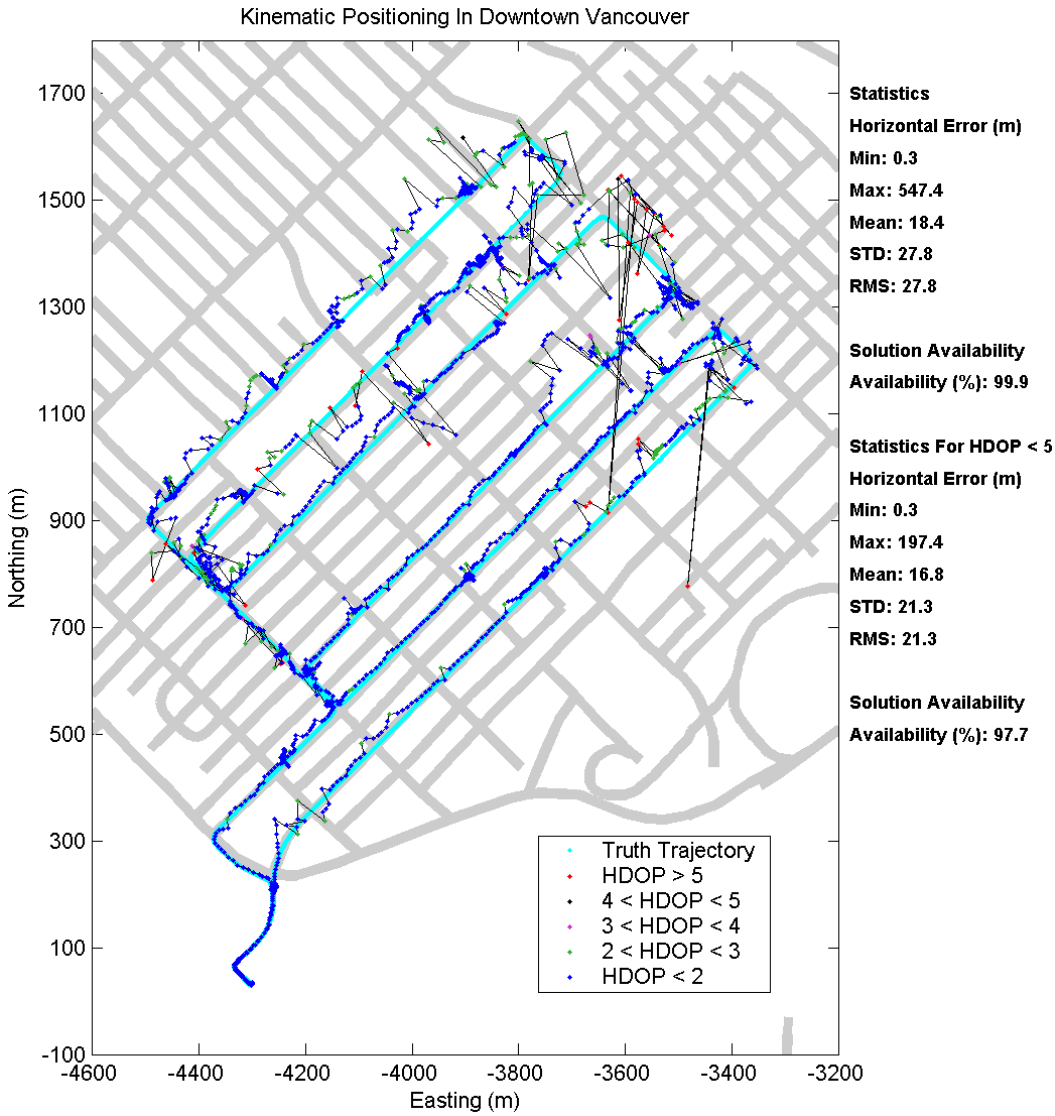

Figure 7.39: Vancouver Downtown - Plan View of HS Position Solutions With Fault Exclusion Enabled Using C^{3}NavG^{2TM}

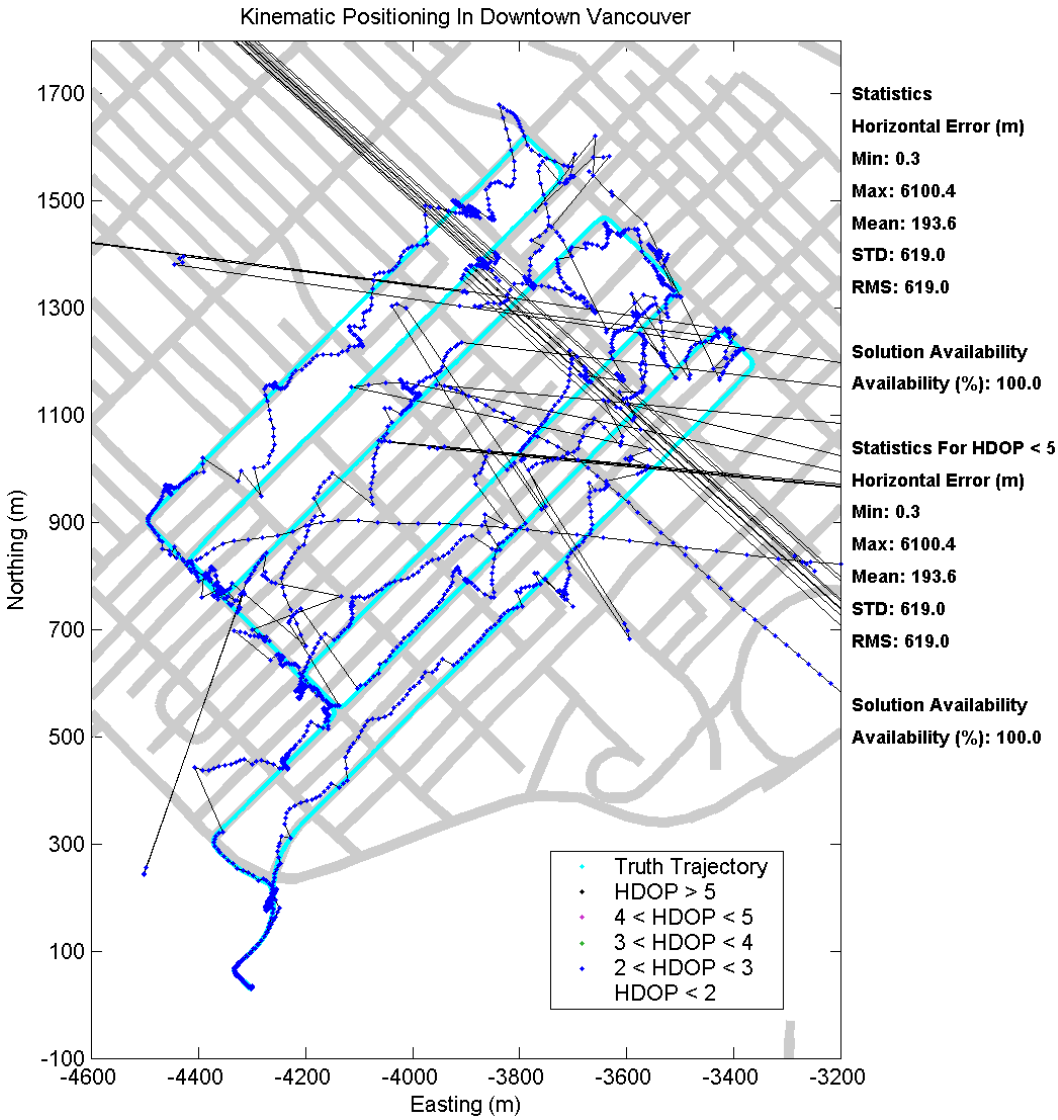

Figure 7.40: Vancouver Downtown - Plan View of HS Position Solutions With Fault Exclusion Disabled Using C^{3}NavG^{2TM}

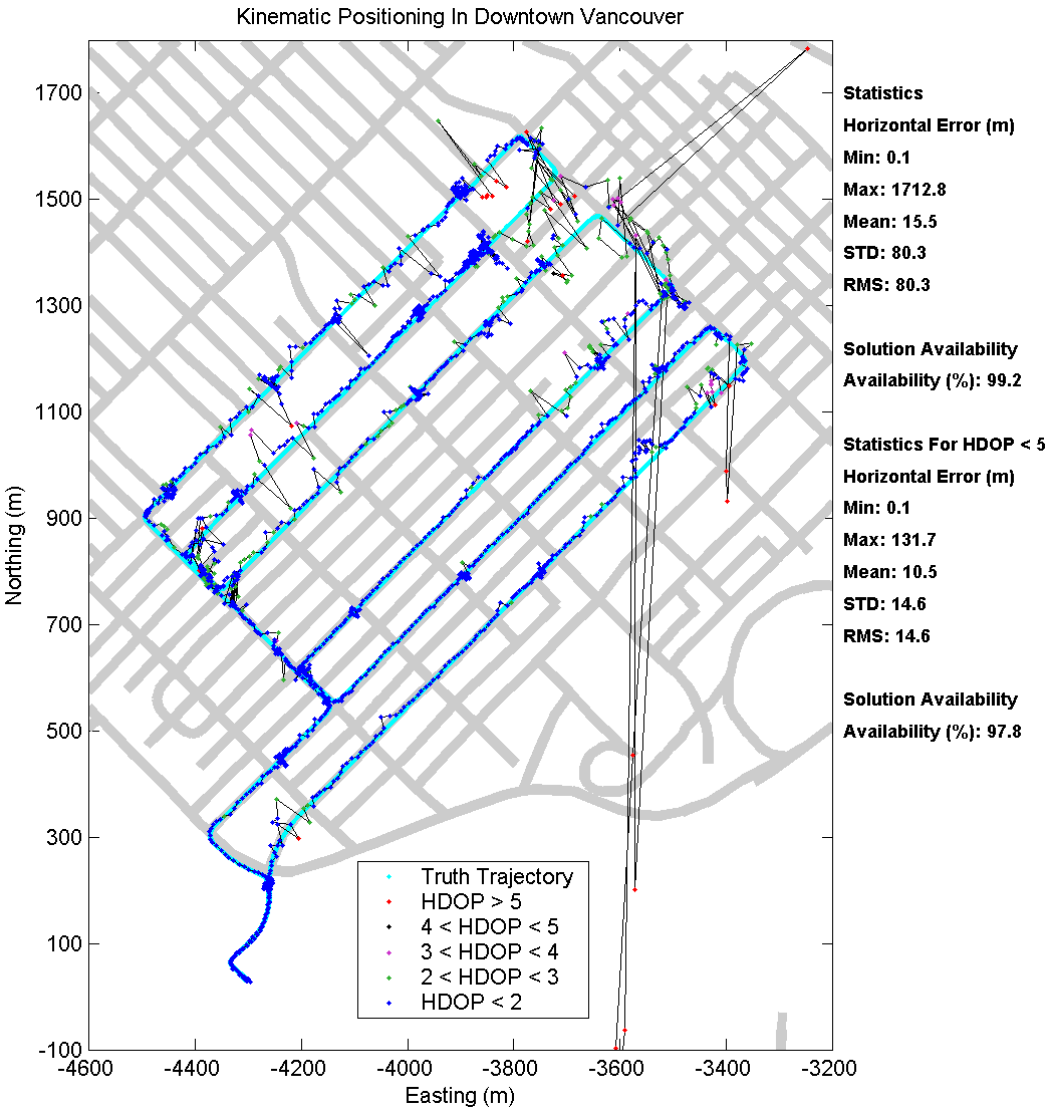

Figure 7.41: Vancouver Downtown - Plan View of ST Position Solutions With Fault Exclusion Enabled Using C^{3}NavG^{2TM}

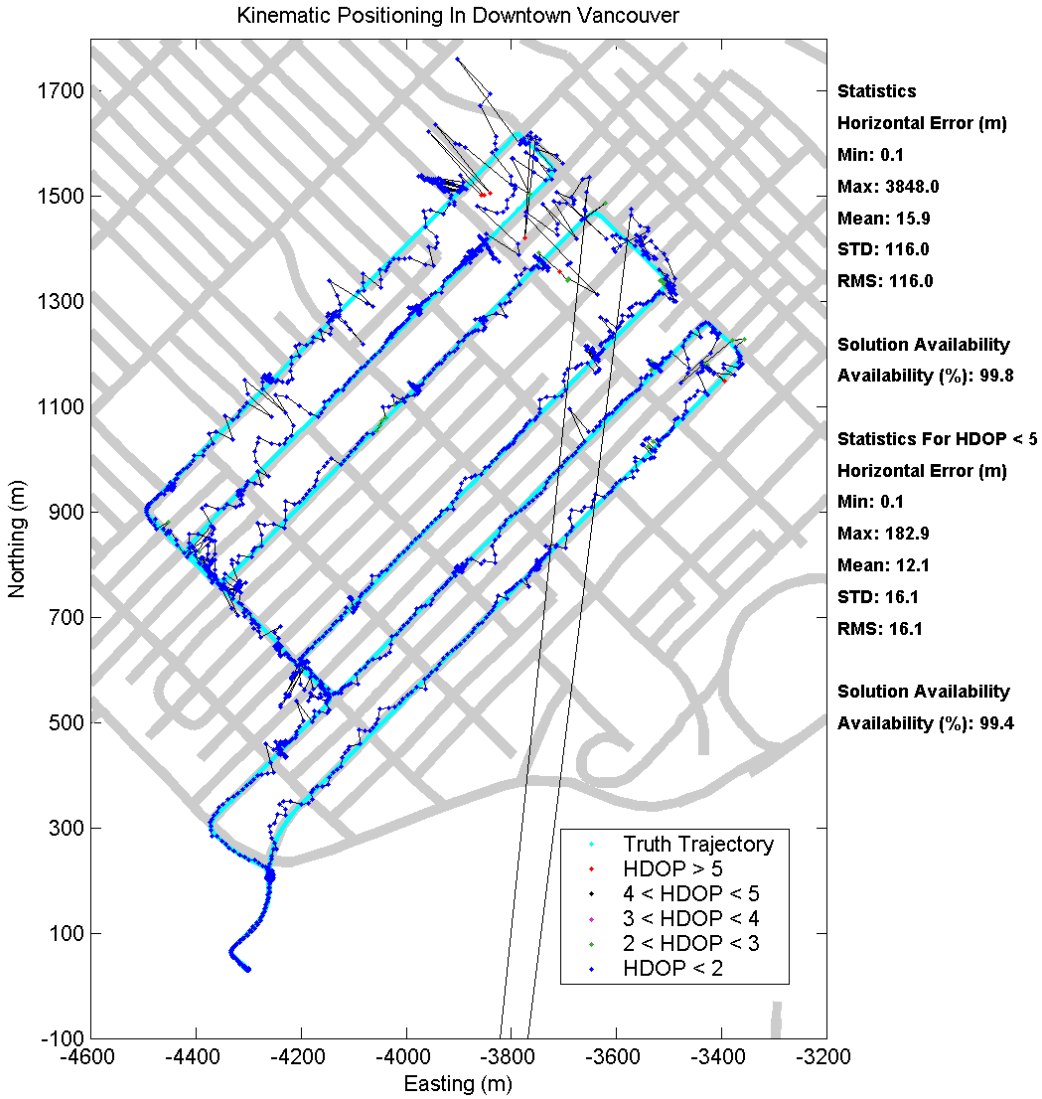

Figure 7.42: Vancouver Downtown - Plan View of ST Position Solutions With Fault Exclusion Disabled Using C^{3}NavG^{2TM}

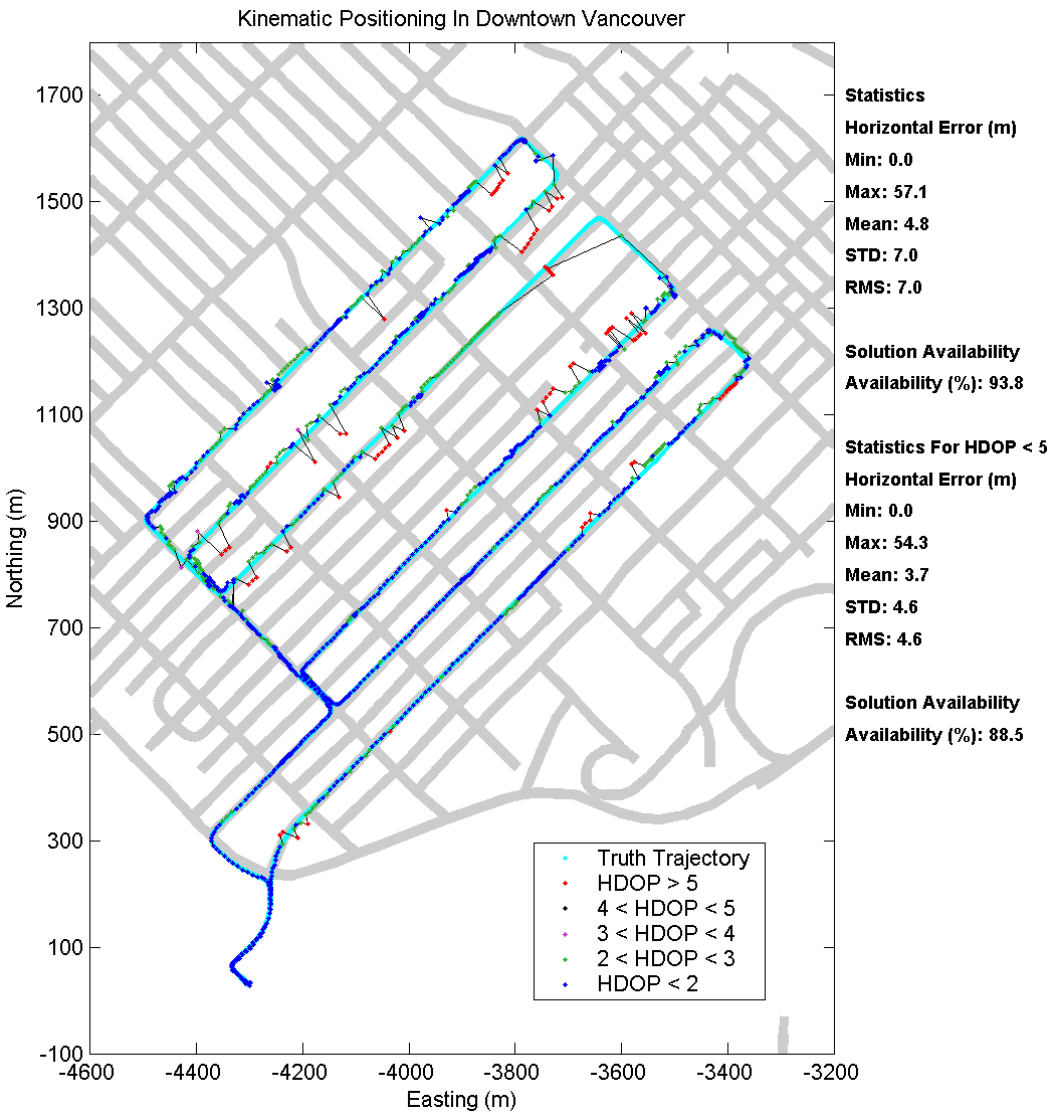

Figure 7.43: Vancouver Downtown - Plan View of OEM4 Position Solutions With Fault Exclusion Enabled Using C^{3}NavG^{2TM}

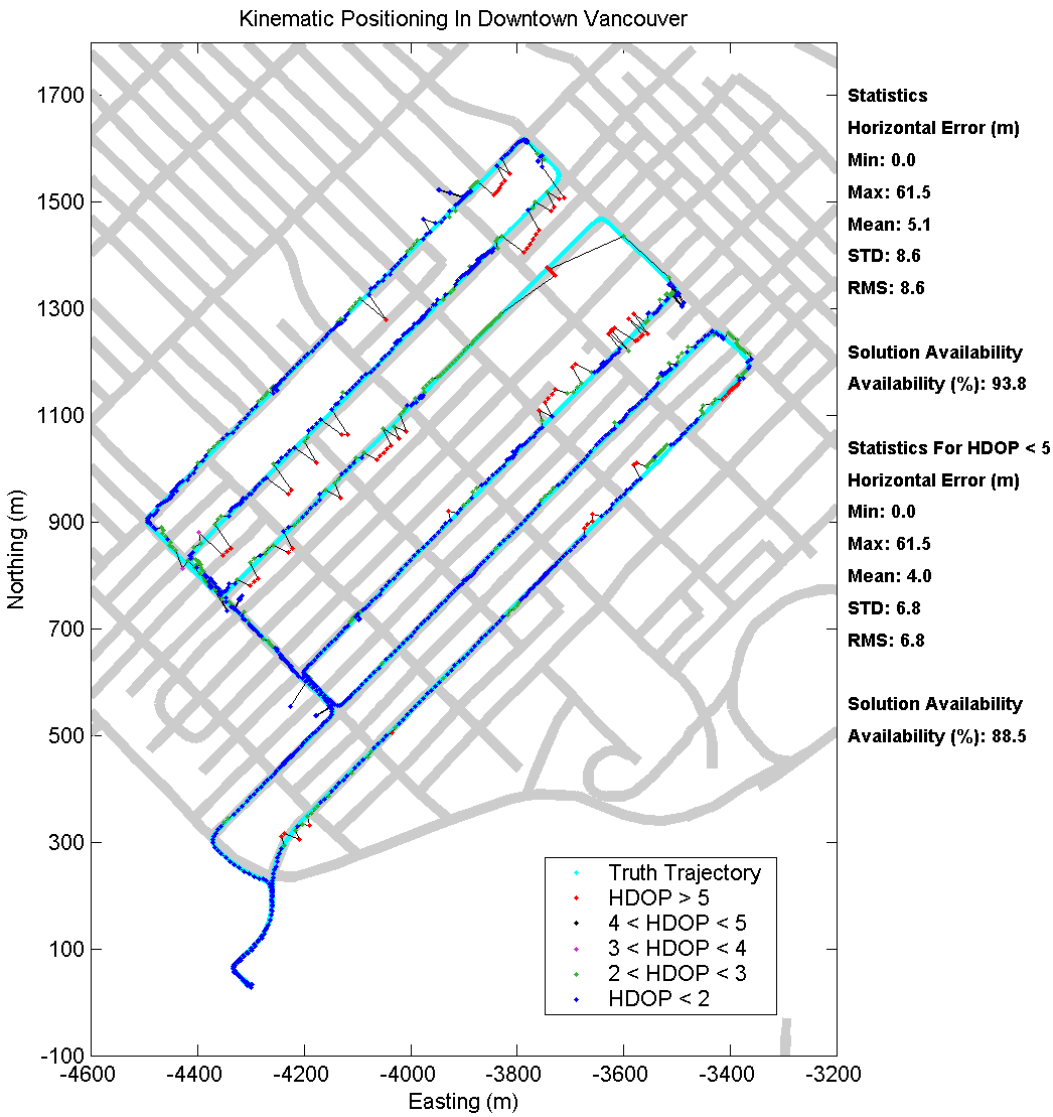

Figure 7.44: Vancouver Downtown - Plan View of OEM4 Position Solutions With Fault Exclusion Disabled Using C^{3}NavG^{2TM}

Chapter 8

Performance In An Indoor Residential Environment

Indoor GPS signal reception is difficult due to almost complete line-of-sight signal masking by various material. The amount of signal attenuation depends on the building materials used, the roof structure, and the number of walls and floors encountered. In addition, reception of reflected signals may be far more likely in an indoor environment.

Testing was performed in a residential garage with a concrete wall structure and a living room above was tested. The house is primarily wood frame construction with brick exterior on the garage, stucco exterior for the living room above, and a concrete tiled roof.

8.1 Details of Testing

The garage tested and a photo of the exterior of the house are shown in Figures 8.1 and 8.2.

A surveyed test point was established inside the garage by establishing two points outside using carrier-phase differential GPS and classically surveying the point inside with respect to these two points using a total station.

Two tests, one hour each, were performed inside the garage with the door closed following a 20-minute warm-up period outside. The antenna was moved from a

surveyed point outside the garage to a surveyed point inside the garage and the door was closed. The timing details for both tests are shown in Table 8.1

Data was collected in parallel using a SiRF HS receiver, a SiRF ST receiver, and a NovAtel OEM4. A nearby reference station, with a clear view of the sky, located on the roof of the Engineering Building, Block F, at the University of Calgary, used a SiRF ST, and a NovAtel OEM4 in parallel to collect reference data.

Figure 8.1: Residential Garage Test Environment

Figure 8.2: Residential Garage Exterior

Table 8.1: Inside A Residential Garage: Static Test Timing Details

Test Label	GPS Week	Initialization Time of Week (s)	Start Time Of Week (s)	End Time Of Week (s)	Test Duration (s)
1	1134	238241	239660	243240	3580
2	1134	243581	244960	248578	3618

8.2 Measurement Availability

Signal availability for the high sensitivity receiver was good for both hour long tests. The conventional GPS receivers on the other hand were not functional inside the garage. The number of satellites tracked by the SiRF HS, SiRF ST, and the OEM4 receivers is shown in Figure 8.3 for both tests showing only the test period data in a contiguous fashion with the warmup period removed. The number of satellites tracked by the SiRF HS receiver did not change significantly during the move from outside to inside. The high sensitivity receiver was able to track satellite signals indoors without frequent loss of signal tracking. Some signals were tracked by the

SiRF ST receiver but typically less than 3 satellites. The SiRF HS receiver tracked 5 to 9 satellites while inside.

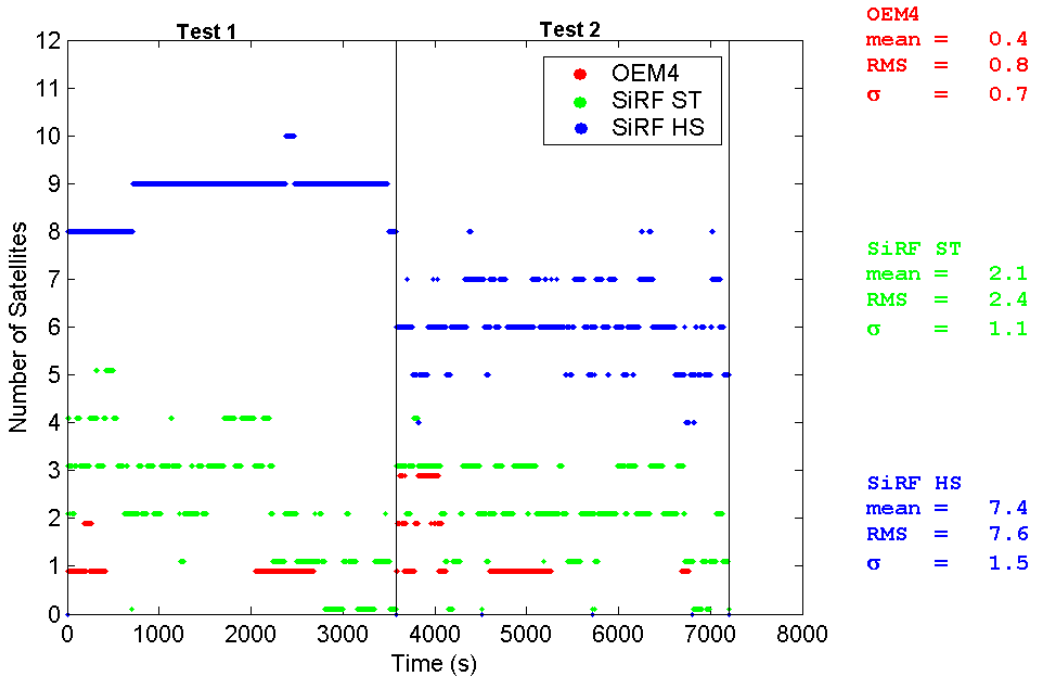

Figure 8.3: Residential Garage Signal Availability

8.3 Fading

Fading in the garage tests was computed using C/N_0 differences with like type receiver-antenna combinations at the reference and test locations. Fading for the SiRF HS receiver was computed using differences with the SiRF ST receiver at the reference station utilizing Equation 4.5. The HS receiver was not available at the base station because at the time it was assumed that the C/N_0 estimator for the SiRF ST and HS receivers was the same and thus no HS data was collected at the base station. As this is not the case, compensation via Equation 4.5 is necessary. Basically no data is available for the SiRF ST and OEM4 receivers and thus analysis

is limited to the SiRF HS receiver.

The fading during Test 1 for one satellite, PRN25, as it travels in azimuth from 130^o to 60^o and in elevation from 50^o to 30^o is shown in Figure 8.4. The approximate satellite track is shown as the green line in the photo on the right side of the figure. The signal fading is between 16 to 25 dB with some short periods of strong signal tracking. Whether the attenuated direct signal or a reflected signal is tracked cannot be ascertained although the fading behavior exhibits constructive and destructive oscillation consistent with multipath.

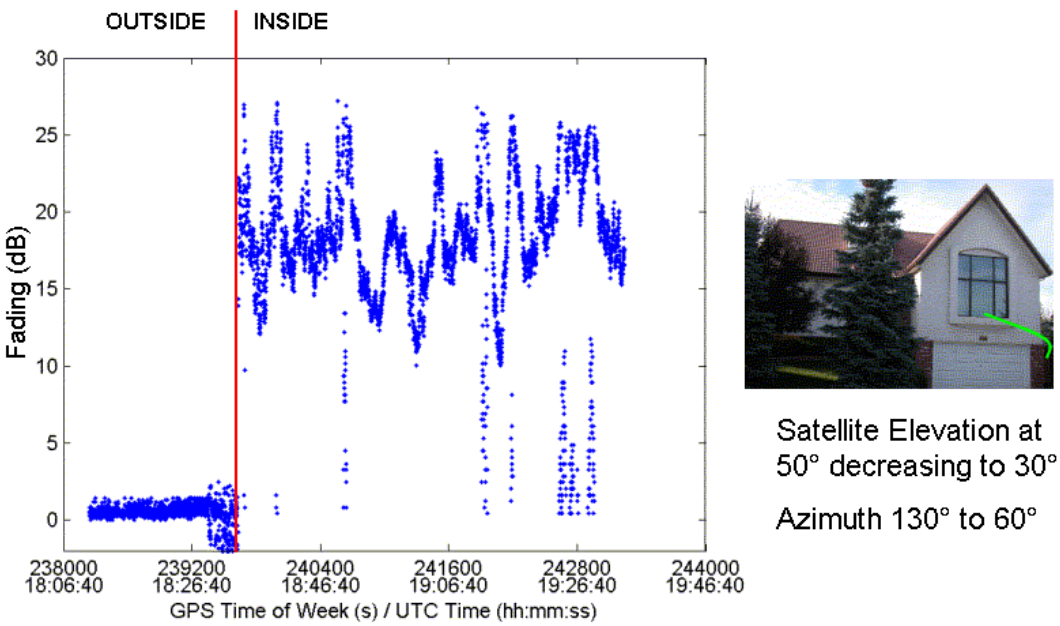

Figure 8.4: Fading For PRN25 During Test 1 Inside A Residential Garage

The fading data was binned into 15^o elevation bins and distribution were generated. These distributions are shown in Figure 8.5 for the HS receiver data. The associated statistics for each elevation bin are shown in Table 8.2. The mean fade is very similar for most elevation groupings between 13 and 17 dB. At lower elevation angles, signals propagating through the garage door are likely the cause of the prevalence of strong

signals below 30^o elevation.

The fading distributions indicate that some line-of-sight-like signals were tracked through the wooden garage door but higher elevation angle signals exhibited RMS signal fades of 11 to 17 dB with increasing signal fading as elevation increases.

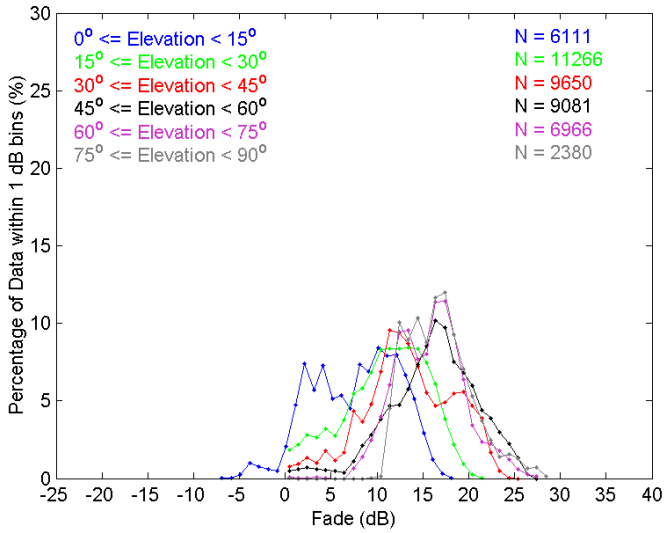

Figure 8.5: Fading Histogram For Tests Inside A Residential Garage

Table 8.2: Fading Statistics Grouped By Elevation Angle For Testing Inside A Residential Garage

Elevation Angle Range (°)	Number of Elements	Max (dB)	Mean (dB)	σ (dB)	RMS (dB)
00-15	6111	17.9	7.7	4.7	9.0
15-30	11266	21.0	10.9	4.5	11.8
30-45	9650	24.6	13.4	4.9	14.3
45-60	9081	26.8	16.1	4.8	16.8
60-75	6966	27.3	15.8	3.7	16.2
75-90	2380	28.2	16.8	3.5	17.1

8.4 Estimated Pseudorange Error

EPE values were computed for the SiRF HS receiver pseudorange measurements based on the surveyed points inside the garage. Two different points about 1 m apart were tested.

The EPE values during Test 1 for PRN25 along with the fading as shown in Figure 8.4 are shown in Figure 8.6. Measurement errors are due to multipath and increased noise. It is interesting to note that during some periods where the signal power increases, for a brief period of time, the estimated pseudorange error also increases. This may be due to tracking of a strong reflected signal through the garage door.

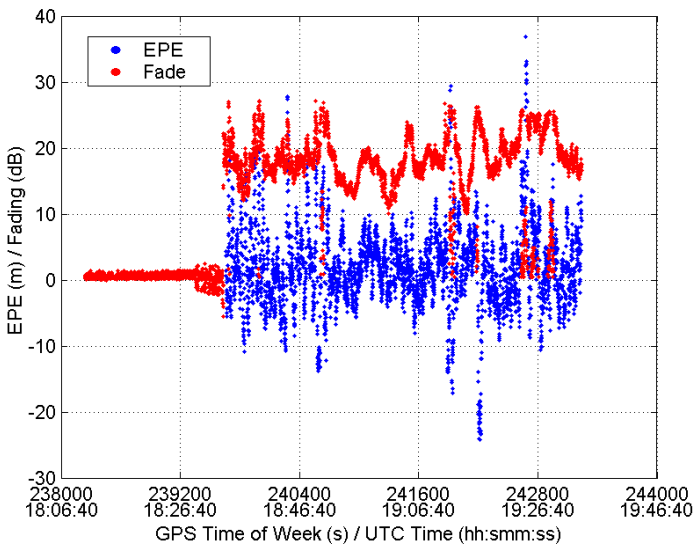

Figure 8.6: Fading and EPE for PRN25 During Test 1 Inside a Residential Garage

The EPE values were binned into 15^o elevation bins and the distributions for the data from both tests are shown in Figure 8.7. The associated statistics are shown in Table 8.3. The cumulative distribution of the absolute value of EPE is shown in

Figure 8.8.

This indoor environment is relatively benign in comparison to the forest or urban canyon static testing environments. Less than 20 m EPE values occur for 95% of the data indicating measurement noise and short delay multipath are the primary sources of error in this environment. In addition, as the ratio of strong to weak signals was never very high, no cross-correlation errors occurred while inside the garage.

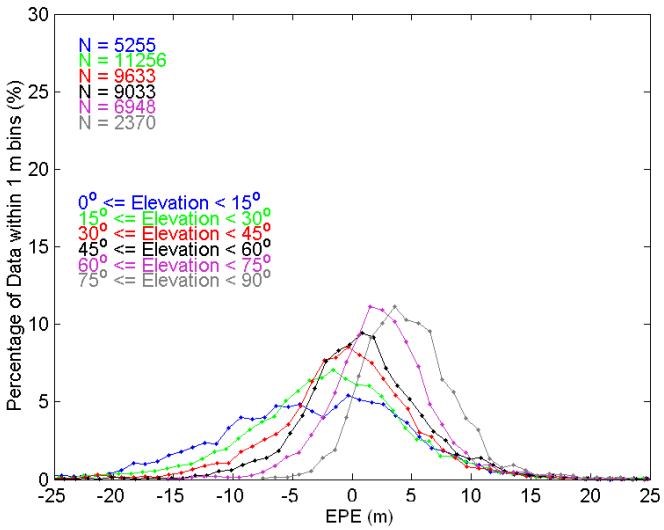

Figure 8.7: EPE Distributions By Elevation Angle Inside A Residential Garage

Table 8.3: HS Receiver EPE Statistics Grouped By Elevation Angle Inside A Residential Garage

Elevation Angle Range (°)	Number of Elements	Max (m)	Min (m)	Mean (m)	σ (m)	RMS (m)
00-15	5255	46.7	-46.4	-3.4	8.3	9.0
15-30	11256	34.7	-42.6	-2.0	7.1	7.4
30-45	9633	35.4	-44.4	-0.7	6.6	6.6
45-60	9033	39.1	-32.2	1.0	5.6	5.7
60-75	6948	27.8	-15.5	2.5	4.3	5.0
75-90	2370	23.2	-7.5	4.8	3.9	6.2

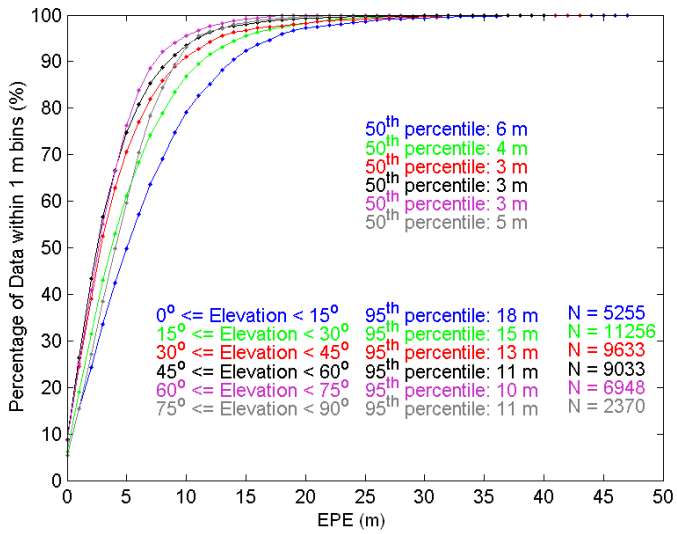

Figure 8.8: Cumulative Absolute EPE Distribution Inside A Residential Garage

8.5 HS Fading and EPE Time Series Analysis

The SiRF HS time series data for each satellite for EPE and fading along with the corresponding elevation angle are shown in Figures 8.9 and 8.10. This environment was interesting in that no large blunder effects were observed during the test intervals.

The lack of strong LOS signals (all signals are typically faded by 4 dB or more) to interfere with the faded signals lead to no cross correlation signal tracking.

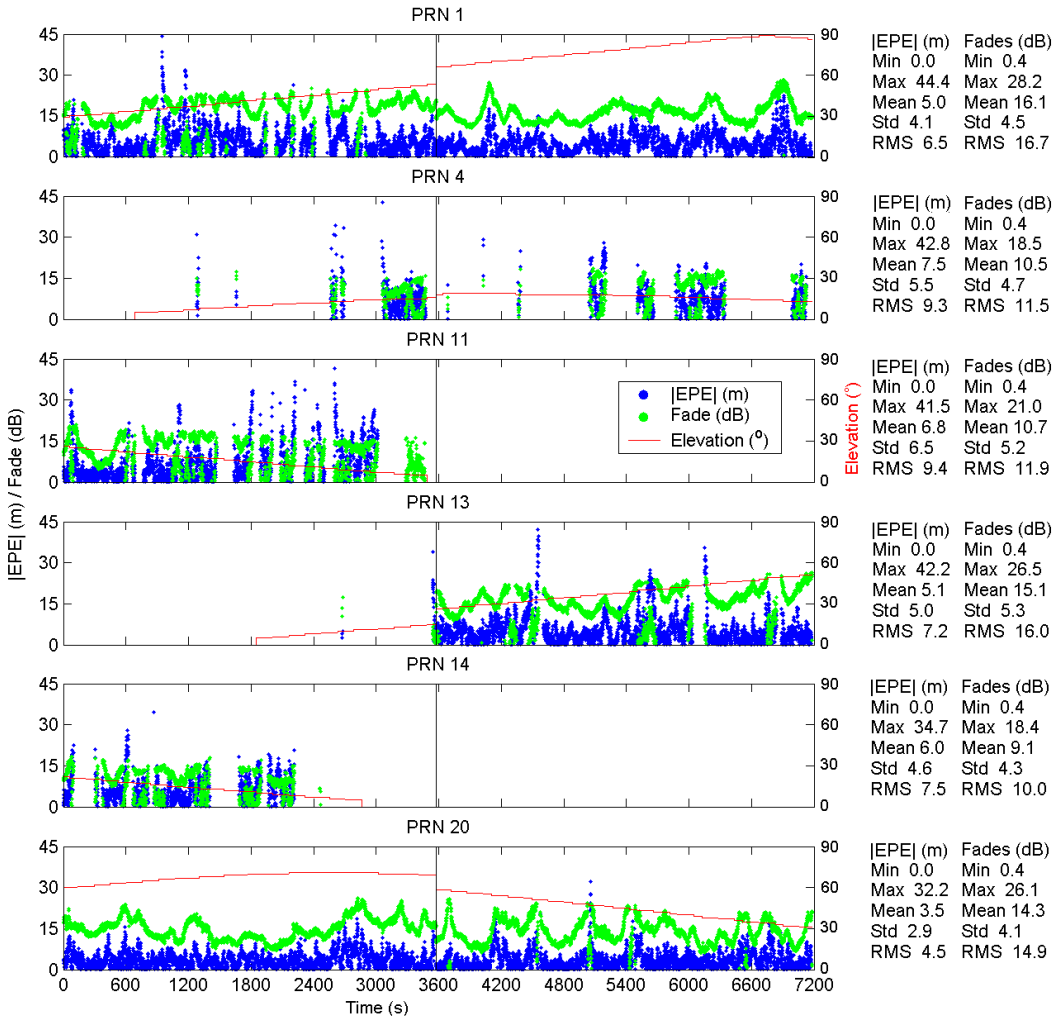

Figure 8.9: Fading, EPE, And Corresponding Elevation Angle Inside A Residential Garage Part 1 of 2

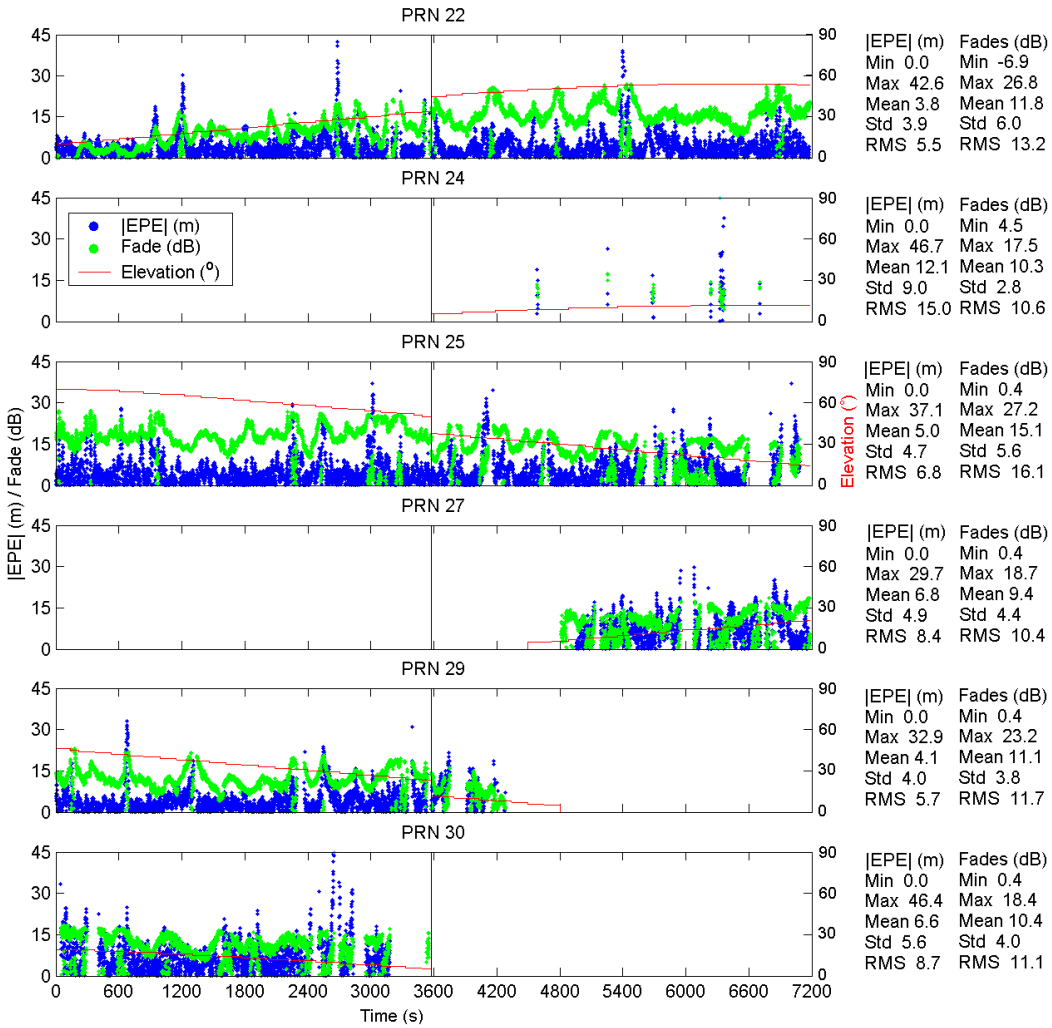

Figure 8.10: Fading, EPE, And Corresponding Elevation Angle Inside A Residential Garage Part 1 of 2

8.6 Positioning Accuracy, Solution Availability, and Dilution of Precision

Given the lack of measurement availability for the ST and OEM4 receivers while inside the garage only the HS positioning results are presented. One representative

test, Test 2, is presented as an example of the positioning accuracy and solution availability achievable with the HS receiver while inside the garage.

Just as in the static forest testing and the static urban canyon testing, only height fixed positions were computed using C^{3}NavG^{2TM} with and without fault detection and exclusion. Figure 8.11 shows a plan view of the horizontal positioning accuracy for the two cases with associated statistics and HDOP color encoding of the positioning results. Figure 8.12 shows a time series representation of the results in Figure 8.11 along with the number of satellites used and rejected in solution and the corresponding HDOP. Statistics concerning the entire test period and for solutions when HDOP is lower than 5.0 are given in the two figures. The solution availability while indoors was very good in all tests. In this case a solution availability for HDOP lower than 5.0 of 98.2 % was achieved.

The lack of cross-correlation errors in this testing environment is reflected in the position domain results in that in the example case presented, no very large position errors occurred. Fewer large measurement faults occurred in this environment as the ratio of strong to weak signals was never very high.

The implementation of fault exclusion does not improve the horizontal positioning results in this indoor case. In fact, the removal of some measurements adversely affects the HDOP and poorer solution accuracy results. RMS horizontal errors of 10 to 14 m are typical for this testing case when HDOP is lower than 5.0.

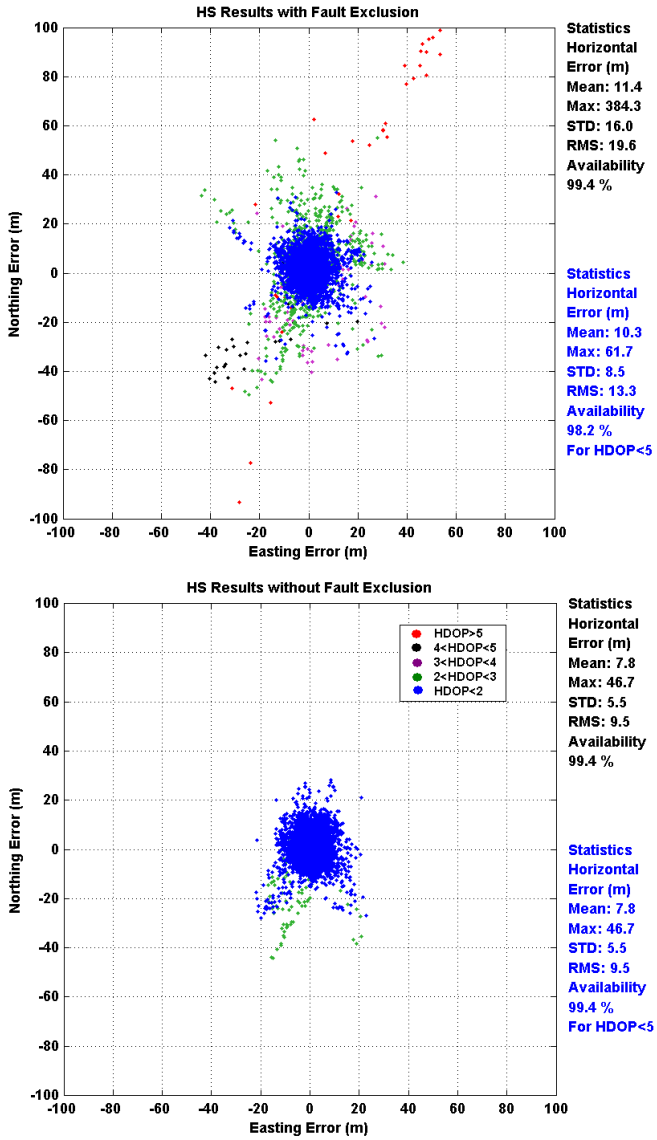

Figure 8.11: Plan View of the HS Horizontal Positioning Solutions with and without Fault Exclusion during Test 2 Inside A Residential Garage

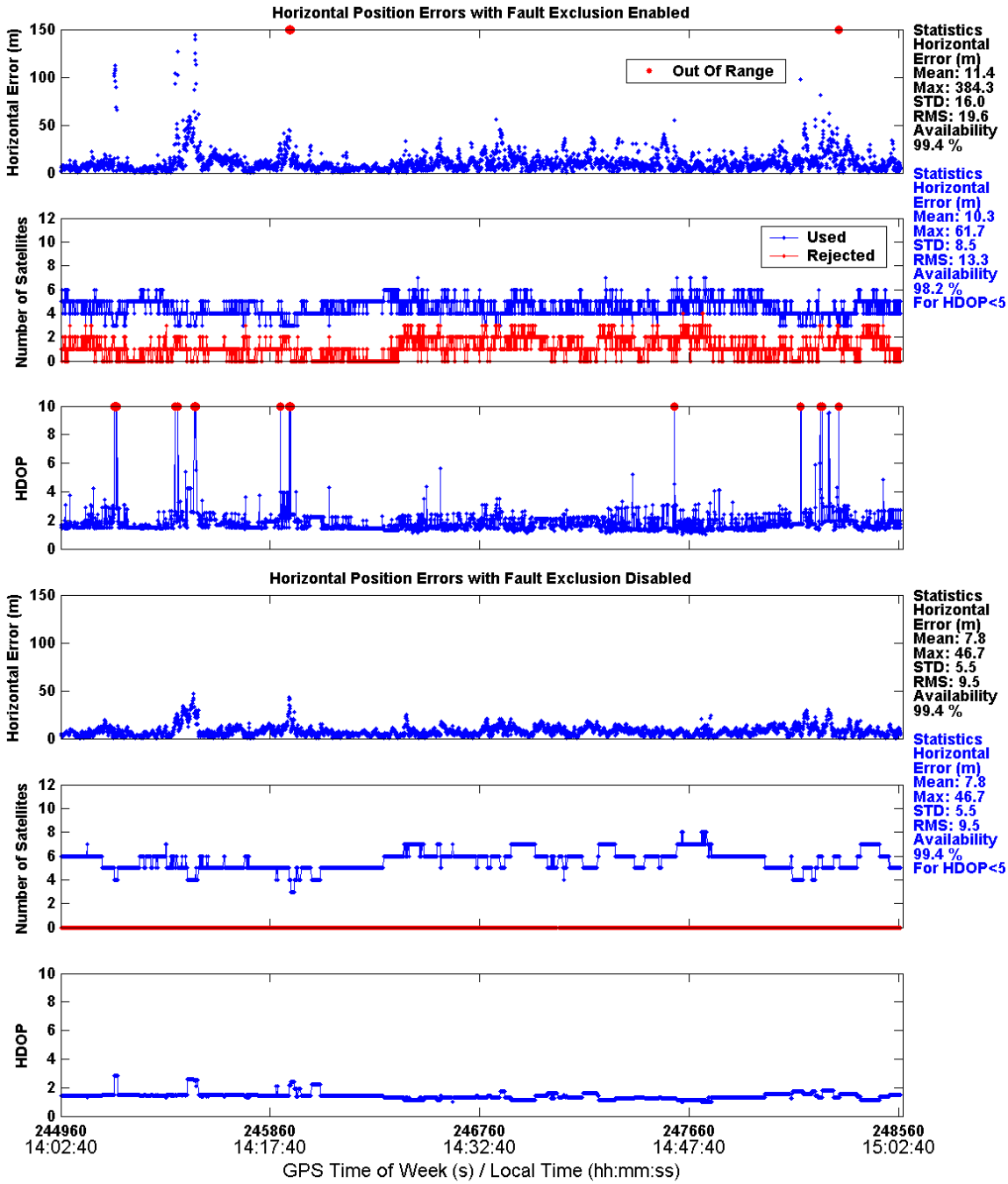

Figure 8.12: Time Series Analysis of the HS Horizontal Positioning Solutions with and without Fault Exclusion during Test 2 Inside A Residential Garage

Chapter 9

Conclusions And Recommendations

9.1 Conclusions

Using a Spirent STR6560 hardware GPS simulator, the signal tracking capability of the SiRF unaided high sensitivity GPS receiver was assessed. Signals with a C/N_0 as low as 18 dB-Hz as measured by the HS receiver were tracked. This corresponds to tracking signals down to about -186 dB-W or 25 to 30 dB weaker than outdoor line-of-sight signals in a test environment with more noise as a hardware simulator was used. In addition, the pseudorange measurements taken close to the tracking threshold of the HS receiver are clearly corrupted by noise effects. Typical maximum EPE values due to noise of around 10 to 25 m were observed and a 54 m maximum noise effect was observed for one satellite during weak signal tracking.

The newly available High Sensitivity (HS) GPS receivers provide a capability to take measurements in degraded mode GPS environments where standard mode GPS receivers typically exhibit frequent loss of signal tracking and or signal acquisition failure. These receivers were taken into the following degraded mode environments: a forest, in urban canyons, and an indoor residential garage. In most of the field testing performed, large pseudorange error effects were observed. Effects greater than 150 m and even at the kilometre level occurred. Hardware GPS simulation tests identified signal-cross correlation as a primary cause of the large pseudorange error effects. These errors occurred when strong and weak signals were tracked and the ratio of strong signal power to weak signal power was greater than 24 dB.

The high sensitivity receiver tested was susceptible to interference effects when utilizing weak signals. Field tests and hardware simulation tests demonstrated the problem of signal-cross correlation. In addition, CW jamming was identified, using hardware simulation, as a significant jamming threat as weak signals are jammed by CW signals with signal strengths well below the noise floor.

In the forested environment tested, the high sensitivity receiver was better able to track signals less than 45^o in elevation angle than the conventional receivers tested. These signals were faded by 6 to 11 dB (RMS). Higher pseudorange degradation at elevation angles less than 30^o is prevalent with HS measurements with an increase in the standard deviation of about 6 m when compared to the ST receiver. Pseudorange degradation above 30^o was similar to the ST receiver. The ST receiver is not capable of making as many measurements at low ($< 30^o$) elevation angles but when it does, the associated errors are lower than the HS receiver. Errors of 10 to 50 m occur at low elevation angles in the forested environment. Dominant sources of measurement errors include measurement noise, multipath, and tracking of false correlation peaks. The positioning accuracy and solution availability achieved using the HS receiver in the forest environment demonstrates clear advantages in comparison with conventional GPS. The HS receiver is clearly suited to this environment as it provided across-track position accuracies better than 25 m with 99% or greater solution availability during kinematic testing.

The unaided high sensitivity receiver is capable of providing 2 to 3 more satellite measurements than conventional GPS in urban canyon settings with less frequent loss of signal tracking. However, the measurements obtained are degraded in comparison with the conventional GPS measurements. More signals are tracked at lower elevation angles than by the conventional receivers and these signals are highly faded in general. There is a fair amount of consistency between the Vancouver and Calgary

fading and EPE distributions indicating common effects in downtown environments. High sensitivity GPS measurements in urban canyons are typically faded by as much as 10 dB below 60^o in elevation angle. The EPE statistics for both Calgary and Vancouver indicate RMS EPE values of 18 to 40 m, increasing in magnitude as elevation angles decrease. The HS pseudorange measurements are highly corrupted by multipath and proven echo-only signals when compared to the conventional GPS receivers; although, the conventional receivers suffer from the same effects but to a lesser extent. The urban canyon environment is severe in terms of the measurement errors induced by multipath, echo-only signal tracking, and signal cross-correlation effects and this is reflected in the least-squares positioning accuracy results for the HS receiver.

The high sensitivity receiver was the only receiver tested that was able to track satellite signals inside a concrete residential garage without frequent loss of signal tracking or no tracking at all. Some signals were tracked by the SiRF ST receiver but typically less than 3 satellites. The SiRF HS receiver continuously tracked 5 to 9 satellites while inside. The indoor environment tested exhibits an interesting fading profile that lacks the line-of-sight signal response in general. The fading distributions indicate that some line-of-sight-like signals were tracked through the wooden garage door but higher elevation angle signals exhibited RMS signal fades of 11 to 17 dB with increasing signal fading as elevation increases. The HS horizontal positioning accuracy from a height fixed least-squares solution was 10 to 20 m RMS.

In all environments tested, the high sensitivity receiver proved to have better signal tracking capabilities based on measurement availability than the conventional GPS receivers tested. This corresponds to better least-squares positioning solution availability for almost all field tests. However, a degraded level of positioning accuracy performance was observed when comparison was possible between the HS receiver

and ST and OEM4 receivers. This is due to increased measurement noise associated with the use of low power signals, increased influence of multipath signals as more signals at lower elevations were tracked, errors due to echo-only signal tracking, and in some cases very large errors due to tracking of false correlation peaks caused by signal cross-correlation. Clearly, with such large measurement faults, fault detection and exclusion is absolutely essential for reliable navigation. This is exemplified by the results of the least squares positioning analysis for each field test.

9.2 Recommendations

High sensitivity GPS provides availability where conventional GPS methods falter. However, reliable navigation is a primary concern when using measurements based on weak signals as interference effects lead to large measurement errors. Augmentation, constraints, and using a-priori information about the user's dynamics provide additional information that could significantly aid reliable navigation.

High sensitivity GPS by itself is not robust enough to be used in degraded signal environments. The variance-covariance matrix of the measurements is important in determining which measurement is faulty, especially in the case of low redundancy. Noise on the pseudorange and Doppler measurements should be characterized in relation to C/N_0 by further hardware simulation testing. In addition, multipath and noise could be characterized by detecting the operational environment of the user and applying a measurement variance model based on empirical testing. Lastly, as a simple method to remove very large measurement errors, data screening methods using a Doppler predicted pseudorange from the previous epoch may help to identify tracking of false correlation peaks.

Further environmental testing is required to characterize the indoor GPS signal envi-

ronment as the unaided high sensitivity receiver tested was limited in terms of indoor use. In other words, testing was limited to relatively benign indoor environments. Signal propagation through different building materials needs to be characterized to develop an understanding of indoor signal degradation and signal paths indoors.

Echo-only signal tracking was identified as a probable source of large measurement errors especially in urban canyons. Little research has looked at echo-only signal tracking and further study is warranted. Ray tracing techniques based on digital elevation models of urban canyons could possibly be used to identify signals that are completely blocked and identify the echo-only measurements.

Bibliography

Akos, D. M., P. Normark, J. Lee, K. G. Gromov, J. B. Y. Tsui, and J. Schamus (2000). Low Power Global Navigation Satellite System (GNSS) Signal Detection And Processing. In Proceedings of the Institute of Navigation ION GPS-2001 (September 19-22, 2000, Salt Lake, Utah), pages 784–791.

Black, H. D. and A. Eisner (1984). Correcting Satellite Doppler Data for Tropospheric Effects. Journal of Geophysical Research, 89.

Braasch, M. S. (1996). Multipath Effects, Global Positioning System Theory and Applications Volumn 1, chapter 14, pages 547–569. American Institute of Aeronautics and Astronautics, Inc., Washinton D.C.

Cannon, M. E. (1999). Course Notes: ENGO 561, Satellite Positioning, Winter 2001, Geomatics Engineering, University of Calgary.

Chansarkar, M. and L. J. Garin (2000). Acquisition of GPS Signals at Very Low Signal to Noise Ratio. In Proceedings of the Institute of Navigation ION National Technical Meeting-2000 (January 26-28, 2000, Anaheim, California), pages 731–737.

Enge, P., R. Fan, A. Tiwari, A. Chou, W. Mann, A. Sahai, J. Stone, and B. Roy (2001). Improving GPS Coverage and Continuity: Indoors and Downtown. In Proceedings of the Institute of Navigation ION GPS-2001 (September 11-14, 2001, Salt Lake, Utah), pages 3067–3076.

FCC (2000). Federal Communications Commision, USA, OET BULLETIN No. 71, Guidelines for Testing and Verifying the Accuracy of Wireless E911 Location Systems, www.fcc.gov/Bureaus/Engineering_Technology/Documents/bulletins/oet71/oet71.pdf.

Ford, T. (1998). Lead Discussion on NovAtel's Narrow Correlators, ENGO 625 Course Seminar, Geomatics Engineering, University of Calgary.

Garin, L. J., M. Chansarkar, S. Miocinovic, C. Norman, and D. Hilgenberg (1999). Wireless Assisted GPS-SiRF Architecture and Field Test Results. In Proceedings of the Institute of Navigation ION GPS-99 (September 14-17, 1999, Nashville, Tennessee), pages 489–497.

Gelb, A. (1974). Applied Optimal Estimation. Analytical Sciences Corporation.

Haddrell, T. and A. R. Pratt (2001). Understanding The Indoor GPS Signal. In Proceedings of the Institute of Navigation ION GPS-2001 (September 11-14, 2001, Salt Lake, Utah), pages 1487–1499.

Hopfield, H. S. (1963). The Effect of Tropospheric Refraction on the Doppler Shift of Satellite Data. Journal of Geophysical Research, 68(13), pages 5157–5168.

ICD200C (2000). GPS Interface Control Document, ARINC Research Corporation, NAVSTAR GPS Space Segment / Navigation User Interfaces, IRN-200C-004.

Jahn, A. (2001). Propagation Considerations and Fading Countermeasures for Mobile Multimedia Services. International Journal of Satellite Communications, 19, pages 223–250.

Kaplan, E. (1996). GPS Satellite Signal Characteristics, Understanding GPS Signal Characteristics. Artech House, Inc., 685 Canton Street, Norwood, MA 0206.

Klobuchar, J. A. (1996). Ionospheric Effects on GPS, Global Positioning System Theory and Applications Volumn 1, chapter 12, pages 485–513. American Institute of Aeronautics and Astronautics, Inc., Washinton D.C.

Krakiwsky, E. and M. A. Abousalem (1995). Course Notes: Number 10015, ENGO 361, Adjustment of Observations, Winter 1997, Geomatics Engineering, University of Calgary.

Lachapelle, G. (1998). GPS Theory and Applications, ENGO 625 Course Lecture Notes, Department of Geomatics Engineering, University of Calgary.

Lachapelle, G. (1999). Hydrography, ENGO 545 Course Lecture Notes 10016, Department of Geomatics Engineering, University of Calgary.

Lachapelle, G., M. E. Cannon, R. Klukas, L. Dong, and O. Julien (2002). Additional Performance Testing Of UHF/CDMA Technologies For A Tactical Indoor Positioning System (TIPS), Project Report 70-6425.

Ma, C., G. Jee, G. MacGougan, G. Lachapelle, S. Bloebaum, G. Cox, L. Garin, and J. Shewfelt (2001). GPS Signal Degradation Modeling. In Proceedings of the Institute of Navigation ION GPS-2001 (September 11-14, 2001, Salt Lake, Utah), pages 882–893.

Misra, P. and P. Enge (2001). Global Positioning System Signals, Measurements, and Performance. Ganga-Jamuna Press, Lincoln, Massachusetts, 01773.

Moeglein, M. and N. Krasner (1998). An Introduction to SnapTrack Server-Aided GPS Technology. In Proceedings of the Institute of Navigation ION GPS-98 (September 15-18, 1998, Nashville, Tennessee), pages 333–342.

Parkinson, B. and J. J. Spilker (1996). Global Positioning System: Theory And Applications Volume 1. American Institute of Aeronautics and Astronautics, Inc., Washinton D.C.

Peterson, B., D. Bruckner, and S. Heye (1997). Measuring GPS Signals Indoors. In Proceedings of the Institute of Navigation ION GPS-97 (September 16-19, 1997, Kansas City, Missouri), pages 615–624.

Rash, G. D. (1997). GPS Jamming In A Laboratory Environment. In Proceedings of the Institute of Navigation ION GPS-97 (September 16-19, 1997, Kansas City, Missouri), pages 389–398.

Ray, J. (2000). Mitigation of GPS Code and Carrier Phase Multipath Effects Using a Multi-antenna System, UCGE Report No. 20136, Department of Geomatics Engineering, University of Calgary, www.geomatics.ucalgary.ca/links/GradTheses.html.

Ray, J. (2002). Course Notes: ENGO 699.73, Advanced GPS Receiver Technology, August 05-16, 2002, Geomatics Engineering, University of Calgary.

Saastamoinen, J. (1972). Atmospheric Correction for the Troposphere and Stratosphere in Radio Ranging of Satellites. Geophysical Monograph 15, American Geophysical Union.

Shewfelt, J. L., R. Nishikawa, C. Norman, and G. F. Cox (2001). Enhanced Sensitivity For Acquisition In Weak Signal Environments Through The Use Of Extended Dwell Times. In Proceedings of the Institute of Navigation ION GPS-2001 (September 11-14, 2001, Salt Lake, Utah), pages 155–162.

Spilker, J. J. (1996a). Foliage Attenuation for Land Mobile Users, Global Positioning System Theory and Applications Volumn 1, chapter 15, pages 569–582. American Institute of Aeronautics and Astronautics, Inc., Washinton D.C.

Spilker, J. J. (1996b). Signal Structure and Theoretical Performance, Global Positioning System Theory and Applications Volumn 1, chapter 3, pages 89–21. American Institute of Aeronautics and Astronautics, Inc., Washinton D.C.

Spilker, J. J. (1996c). Tropospheric Effects on GPS, Global Positioning System Theory and Applications Volumn 1, chapter 13, pages 517–545. American Institute of Aeronautics and Astronautics, Inc., Washinton D.C.

Sudhir, N. S., C. Vimala, and J. K. Ray (2001). Receiver Sensitivity Analysis and Results. In Proceedings of the Institute of Navigation ION GPS-2001 (September 11-14, 2001, Salt Lake, Utah), pages 1420–1426.

Syrjärinne, J. (2001). Studies of Modern Techniques for Personal Positioning, Publications 319. Phd, Tampere University of Technology, Tampere, Finland.

Townsend, B. and P. Fenton (1994). A Practical Approach to the Reduction of Pseudorange Multipath Errors in a L1 GPS Receiver. In Proceedings of the Institute of Navigation ION GPS-1994 (September 20-23, 1994, Salt Lake, Utah), pages 143–148.

van Dierendonck, A. J. (1996). GPS Receivers, Global Positioning System Theory and Applications Volumn 1, chapter 8, pages 343–345. American Institute of Aeronautics and Astronautics, Inc., Washinton D.C.

van Dierendonck, A. J., R. Erlandson, G. McGraw, and R. Coker (2002). Determination of C/A Code Self-Interference Using Cross-Correlation Simulations And Receiver Bench Tests. In Proceedings of the Institute of Navigation ION GPS-2002 (September 24-27, 2002, Portland, Oregon), IN PRESS.

van Dierendonck, A. J., P. Fenton, and T. Ford (1992). Theory and Performance of Narrow Correlator Spacing in a GPS receiver. NAVIGATION: Journal of The Institute of Navigation, 39(3), pages 265–283.

van Diggelen, F. (2001). Indoor GPS: Wireless Aiding And Low Signal Strength Detection, NAVTECH Seminar Course Notes, (March 22, 2001, San Diego, CA).

van Diggelen, F. and C. Abraham (2001). Indoor GPS, The No-Chip Challange. GPS World, 12(9), pages 50–58.

van Nee, R. D. J., J. Siereveld, P. Fenton, and B. Townsend (1994). The Multipath Estimating Delay Lock Loop: Approaching Theoretical Accuracy Limits. In Proceedings IEEE Position, Location and Navigation Symposium, pages 246–251.

Vogel, W. J., G. W. Torrence, and H. P. Lin (1995). Into Building Fading at L- and S-Band For Satellite PCS. In Proceedings of the 19th NASA Propagation Experimenters Meeting and the Seventh Advanced Communications Technology Satellite Propagation Studies Workshop, JPL Publication 95-15 (Fort Collins, Colorado, June 14-16).

Ward, P. (1996). GPS Satellite Signal Characteristics, Understanding GPS Signal Characteristics, chapter 4, pages 83–116. Artech House, Inc., 685 Canton Street, Norwood, MA 02062.